DISSERTATION

SOLUBLE AND INSOLUBLE POLYMER DELIVERY SYSTEMS FOR CELLULAR TARGETING AND REMOTE DRUG DELIVERY

Submitted by

R. James Christie

Department of Chemistry

In partial fulfillment of the requirements

For the Degree of Doctor of Philosophy

Colorado State University

Fort Collins, Colorado

Summer 2006

COLORADO STATE UNIVERSITY

July 10, 2006

WE HEREBY RECOMMEND THAT THE DISSERTATION PREPARED UNDER OUR SUPERVISION BY R. JAMES CHRISTIE ENTITLED SOLUBLE AND INSOLUBLE POLYMER DELIVERY SYSTEMS FOR CELLULAR TARGETING AND REMOTE DRUG DELIVERY BE ACCEPTED AS FULFILLING IN PART REQUIREMENTS FOR THE DEGREE OF DOCTOR OF PHILOSOPHY.

Committee on Graduate Work

George B. Barisas

Alan Van Orden

Richard G. Finke

Kenneth F. Reardon

David W. Grainger, Advisor

Ellen R. Fisher/ Acting Department Head

ABSTRACT OF DISSERTATION

SOLUBLE AND INSOLUBLE POLYMER DELIVERY SYSTEMS FOR CELLULAR TARGETING AND REMOTE DRUG DELIVERY

This dissertation is divided into two distinct parts connected by the theme of polymer-based drug delivery. Part 1 focuses on a series of studies aimed at improving polymer drug delivery systems prepared with poly[N-(2-hydroxy propyl) methacrylamide] aimed to deliver large therapeutics into the cytoplasm; part 1 also provides insight into the currently unknown mechanism of membrane translocation with cell-penetrating peptides. Specifically, the ability to synthesize poly(HPMA) conjugates, with the Tat cell-penetrating peptide, and subsequent cellular trafficking of the construct were investigated. This novel bioconjugate was designed and synthesized to mask the Tat peptide between two macromolecules (i.e., poly(HPMA)-Tat-poly(ethylene glycol)) minimizing non-specific cell-surface interactions resulting from free Tat peptide, allowing traditional endocytotic trafficking of internalized conjugate. Programmed release points (hydrazones) within the polymer carrier, allowing degradation and release of exposed free Tat peptide to interact with lysosome membrane components. Subcellular trafficking studies of fluorescent labeled conjugates indicates endocytotic uptake of poly(HPMA)-Tat-PEG conjugate at early time points and the Tat-PEG component gains cytoplasmic entry after extended incubations, while the poly(HPMA)

carrier remains mostly entrapped within lysosomes. This suggests a mechanism involving active or selective transport of compounds covalently attached to Tat peptide.

More detailed studies of specific chemistries required for polymer hydrazone chemistries were performed to delineate the requirements needed for forming hydrazones stable in circulation (pH 7.4), but which degrade at the pH of the target site (pH 5.0). It was found that stability was affected by the chemistries contained on the imine carbon, with hydrazones formed from π-conjugated methyl ketone groups showing the best combination of stability and pH 7.4 and lability at pH 5.0.

Part 2 demonstrates practical application of PEG hydrogels for delivery of live *Brucella abortus* strain RB51 vaccine ballistically to bison in Yellowstone National Park. Hydrogels loaded into the payload of hydroxypropyl cellulose degradable biobullets showed similar ballistic properties compared to commercially available counterparts when fired out of an air-rifle. The live vaccine showed excellent viability in both hydrated and lyophilized gels and generates the desired immune response when administered to bison. These results are currently being considered by the National Parks Service in for long-term strategies to eradicate brucellosis in wild bison herds.

R. James Christie
Department of Chemistry
Colorado State University
Fort Collins, CO 80523
Summer 2006

ACKNOWLEDGMENTS

First and foremost I thank my wife, Asako for her love, support, and patience during my whole graduate school journey. I also thank my parents for their support and words of encouragement. I thank all of my fishing buddies (Adam Steidler, Dave Grainger, Rick Finke, Peng Wu, Lu Yunfeng, Joe Kremer) here in Colorado for making my stay a memorable one. I thank my friends back in Oregon (Dustin and Kim Clark, Daniel Menasco) for their support and maintaining strong ties while I was away.

I thank my advisor Dave Grainger for showing unusual patience during my development as a scientist, teaching me how to think critically and creatively, and for his continuous encouragement.

I thank the entire Grainger Research Group (Ping Gong, Peng Wu, Colleene Santoro, Lisa Chamberlain, Shaun Bevers, Marisha Godek and Greg Harbers) for their support and willingness to discuss and understand my work. I especially thank Greg Harbers for proofreading sections of this dissertation and providing many helpful suggestions.

PREFACE

This dissertation is written in the "journals-format" style. It is based on: three publications written in the format appropriate for each, three manuscripts in development for submission after completion of this dissertation, plus one chapter not intended for publication. A brief overview of each chapter is presented below. Although the two sections are distinctly different, they are tied together by the common theme of employing polymers to overcome drug delivery barriers.

The most important hypothesis tested in this dissertation are: (i) cell-penetrating peptides enhance cytoplasmic entry of attached cargo after lysosome escape; (ii) the effect of chemistries involved with hydrazone formation on stability; and (iii) PEG hydrogel matrixes provide a benign environment for ballistic delivery of live vaccine.

Specific details of the chapters and sections are as follows: Section 1 presents studies of poly[N-(2-hydroxypropyl) methacrylamide] (HPMA) conjugates for subcellular drug delivery. Chapter I of this section is a review of the literature of current macromolecular-based drug delivery strategies. This chapter identifies the current limitations of this approach and mechanisms to overcome them.

Chapter II provides a detailed description of the methods used for synthesizing and characterizing HPMA copolymers that are crucial to the studies performed in

Chapters III-V. An improved trinitrobenzene sulfonic acid assay for amine content analysis is described.

Chapter III presents the design, synthesis and preliminary *in vitro* tracking results of a poly(HPMA)-Tat-PEG model drug delivery construct. The construct showed initial trafficking to lysosomes, with cytoplasmic entry of Tat-PEG observed after degradation and release from the poly(HPMA) carrier. The crosslinker used to couple Tat-PEG to poly(HPMA) hydrazone bond was found to be more stable than desired. This result led to the experiments described in Chapter V investigating the effects of carbonyl functionality on hydrazone stability.

Chapter IV describes preparation of a novel thiol-containing tetramethylrhodamine dye. This dye was prepared as an inexpensive thiol-containing model compound to quantify hydrazone degradation studies in Chapter V. In addition to its intended use as a reactive dye, the disulfide dimer formed between two dye molecules exhibited several interesting optic properties including a hypsochromic shift in absorbance and fluorescence quenching upon dimer formation. An isosbestic point was found between the oxidized and reduced forms.

Chapter V assesses the stability of hydrazone bonds formed with heterobifunctional crosslinkers containing carbonyl and maleimide functionality. Specifically, requirements to form hydrazone linkages that are stable at pH 7.4 (physiological) and degrade at pH 5.0 (lysosome) were investigated. The results provide insight for future design of highly reactive crosslinkers with desired stability.

Chapter VI presents a summary of this section and proposed future work. Potential chemistries for formation of hydrazones with desired stability, experiments aimed at confirming subcellular trafficking of HPMA-Tat-PEG using metabolic inhibitors, and future design of functional Tat conjugates are discussed.

Section 2 includes studies of poly(ethylene glycol) hydrogels as live vaccine carriers for remote delivery. Chapter I in section 2 presents initial assessment of photopolymerized poly(ethylene glycol) hydrogels for use as an encapsulation matrix for ballistic administration of live SRB51 vaccine to bison. Release of bacteria-sized particles is controlled by incorporating degradable lactide or glycolide endgroup chemistries into the gel matrix. Ballistic properties of hydrogel-loaded biobullets and excellent vaccine post-processing vaccine viability show the potential for practical application of this remote delivery method.

Chapter II investigated the practical application of hydrogel-encapsulated vaccine to bison. Serological tests show that the desired immune response to the vaccine is persistent and comparable to hand-vaccination.

Chapter III describes production of lyophilized PEG hydrogels for encapsulation of live SRB51 vaccine for ballistic delivery to bison. This approach is an improvement upon the "wet" hydrogels investigated in Chapters I and II since the lyophilized payload does not soften the biobullet casing. Excellent ballistic performance and vaccine viability warrant future assessment of this approach for *in vivo* testing.

Chapter IV contains a summary for this dissertation section and proposed future work. Future work presented involves additional RB51 viability assessments, approaches

to anchor lyophilized hydrogels into the payload chamber of biobullets, and utilization of microspheres for development of a two-stage Rb51 vaccine delivery system.

TABLE OF CONTENTS

PART 1

WATER SOLUBLE POLYMER CONJUGATES FOR ENHANCED SUBCELLULAR TRAFFICKING

CHAPTER I

DESIGN STRATEGIES TO IMPROVE SOLUBLE MACROMOLECULAR DELIVERY CONSTRUCTS

This dissertation chapter contains a literature review of current macromolecular drug delivery constructs. Specifically, current limitations and solutions to overcome them are presented. This chapter is reprinted with permission from: R. James Christie, D.W. Grainger, Advanced Drug Delivery Reviews, 2003, *55(3)*, 421-437.

Contents

Abstract

Macromolecular therapeutics provide numerous benefits for the delivery of cytotoxic or poorly soluble drugs in vivo. However, these constructs often encounter barriers for drug delivery on both the systemic and subcellular level. Many soluble polymer carriers have been designed to surmount specific physiological barriers individually, but less work has been dedicated to designing an all-encompassing construct that addresses multiple therapeutic barriers at once. Incorporation of multiple agents already individually known to increase effectiveness into one carrier could further improve current drug delivery technology. Recent developments in subcellular delivery of therapeutic agents in soluble macromolecular carriers will be discussed in the context of the future possibility for the design of an all-encompassing soluble multi-functional drug delivery vehicle.

1. Introduction

Motivation for designing new macromolecular drug delivery constructs continues to arise from barriers associated with the serum of a host, limited circulation half-life, insoluble drugs, or undesirable side affects associated with a given therapeutic agent. Many drugs in systemic dosage forms are toxic at minimal doses, immunogenic, insoluble, or degraded in the serum. Some candidate drugs are not bio-available in parenteral formulations or systemic doses, rendering the drug useless, regardless of its therapuetic potential. Additionally, serum is a favorable environment for drug binding and modification: enzyme degradation, hydrolysis, and oxidation or reduction can leave the therapeutic agent ineffective. Even if the drug remains unaltered in serum, a

bioavailable drug must escape rapid elimination by the reticuloendothelial system (RES) – the complex organ-based filtration system for serum. Drug may also be enzymatically modified upon first pass or subsequent exposure in the liver by glucuronyl, sulfate, acetyl, glutathione, or glycine conjugation. In order for a drug to be effective, it must exhibit sufficient stability and circulation half-life to allow it to reach its target at doses effective to produce the desired therapeutic effect without toxicity.

Drug targeting and delivery challenges have been addressed with the design of soluble polymer-based drug delivery constructs. These vehicles attempt to facilitate more effective delivery to desired targets while shielding the body from harmful side effects through attachment of a drug to a water-soluble macromolecular scaffold. Polymer scaffolds can be designed for direct covalent conjugation of drug, association of therapeutic agents by electrostatic interactions, or drug encapsulation by aggregation as in micro- and nano-particles. Many papers discuss the current design strategies and benefits of various soluble drug delivery vehicles [1-14].

In addition to systemic barriers precluding effective drug delivery, subcellular barriers must also be overcome before many drugs can become effective. Barriers associated with macromolecular drug delivery are shown in Figure 1.1.1 [3]. In general, non-specific cellular entry of soluble drug delivery constructs occurs primarily through the endocytotic pathway. Membrane-bound specifically or non-specifically outside the cell, soluble species can enter the cell by encapsulation and internalization within a cell membrane-derived vesicle (the endosome). In the cytosol, this endosomal vesicle then fuses with a cell vesicle organelle, the lysosome, where the compartment environment is favorable for drug degradation. Here, drug must be released from the compartment into

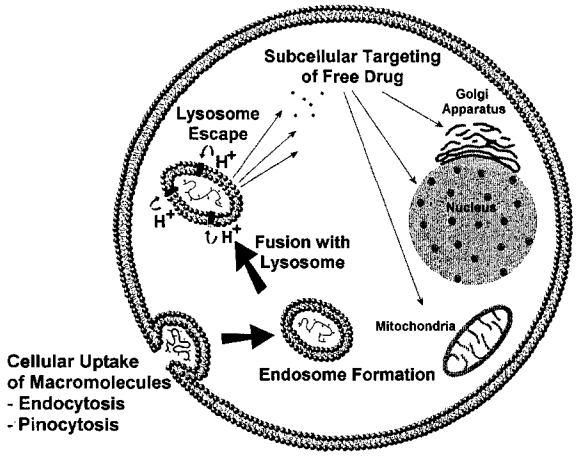

Figure 1.1.1. Subcellular trafficking of macromolecular drug carriers.

the cytosol before excessive degradation or cell re-expulsion (exocytosis) occurs. Attached drug can be cleaved from the polymer scaffold in the lysosomal environment by enzymatic degradation or pH-sensitive hydrolysis. Even after drug is cleaved from the carrier, it must diffuse through the lysosome membrane to enter the cytosol. Finally, because many drugs act on molecular targets in the cytosol or inside membrane-bound cellular organelles, untargeted pharmacons require that released drug find its therapeutic target by random diffusion and statistical encounters with molecules inside the cell. While chances for this targeted success and subsequent therapeutic benefit scale with drug dose, so do adverse toxic effects.

Advances in the design of macromolecular drug delivery constructs, and identification of targetable subcellular features both facilitate increased opportunities for drug delivery. These include improvements in the design of spacers for covalently attached drugs, natural and synthetic endosomolytic polymers, and nuclear targeting

peptides. In addition to the therapeutic agent, carefully designed conjugation features to enhance subcellular delivery can also be incorporated into the vehicle to enhance the overall effectiveness of delivery and therapeutic value. Such design elements transform polymer-based drug delivery from a passive to an active and directed process. In this sense, macromolecular drug delivery vehicles can be designed as molecularly engineered devices containing multiple, specific functionalities with spatial and temporal components.

While some aspects of this polymer carrier targeting discussed here are already subjects of their own reviews (citations can be found in corresponding sections of this paper) it is timely and appropriate to address multiple, coupled aspects and advances in the delivery of macromolecular constructs in relation to each other in a single review. This contribution discusses recent advances that attempt to overcome previously identified cellular barriers, specifically lysosome escape and nuclear targeting, as well as identify new components useful in the development of a novel all-encompassing macromolecular drug delivery vehicle.

2. Cellular Uptake of Macromolecules

While clever construction of macromolecular drug carriers provides increased systemic stability and circulation half-life, these synthetic additions can produce a delivery vehicle often too large and too polar for rapid passive transmembrane diffusion into the cell. Unlike small apolar molecules that readily permeate through the cell lipid bilayer membrane, soluble macromolecular uptake occurs primarily through the endocytotic pathway. This pathway can be specifically targeted via polymer attachment

of a ligand that binds specific cell-surface receptors to trigger internalization of membrane-attached macromolecules. Cell surface receptors can vary depending on the type of cell, are frequently recycled by internalization, and thus provide a means for uptake of drug conjugates by specific cell types. The available ligands/membrane receptors used for drug targeting have recently been summarized in several recent papers [15, 16].

Alternatively, macromolecules can be efficiently internalized without targeting specific cell-surface receptors in cells of certain types of cancers. This is partially a result of the enhanced permeability and retention (EPR) effect resulting from leaky capillary vasculature that characterizes cancerous tissue [17,18]. This increased tumor site vascular permeability results from architectural defects, high vascular density due to rapid tumor angiogenesis, impaired lymphatic drainage, and generation of permeability-enhancing factors [18]. Rapidly dividing cancerous cells also constantly ingest nutrients from their surroundings by macropinocytosis, or random gulping of extracellular fluid. Since macromolecules and polymeric drugs are retained in tumor tissues at much higher concentrations than in plasma due to EPR, therapeutic macromolecules are internalized by cancerous cells at higher concentrations than normal non-cancerous tissue. A recent and promising area of research in this area is aimed at targeting tumor lymphatic structures using the cyclic 9-amino acid peptide LyP-1 [19]. Targeting this tissue structure instead of specific cell-surface receptors could perhaps increase the efficacy of cancer-targeted therapeutics by removing the drug carriers from circulation while retaining localization in cancerous tissue, thus reducing the clearance rate.

In either case, soluble macromolecules are captured and internalized by a cell membrane invagination event that forms a membrane-bound vesicle, which then undergoes a series of fusion events to mature into an endosome, and finally a lysosome, where the compartment pH is ~ 5.0. The lysosome environment is often hostile to drug delivery systems. In addition to the low compartment pH, the lysosome is also host to degrading enzymes such as proteases, esterases, glycosidases, phosphatases, and nucleases.

3. Lysosomal Release of Drug

The lysosomal compartment represents the second cellular membrane barrier limiting the effectiveness of macromolecular drug delivery constructs [20]. It also represents a unique opportunity to design a linker between the polymer carrier and drug that will degrade and release drug in an environment distinctly different from serum. These drug/polymer linkers have often been designed based on naturally occurring peptide spacers that are cleaved by specific lysosome enzymes, or synthetic systems that utilize a pH drop to induce pH-dependent release locally in that subcellular organelle [21-38].

3.1. Peptide Linkers

The most developed peptide linker for triggered release of covalently attached drug is the glycylphenylalanylleucylglycine (GFLG) tetra-peptide spacer. This spacer is often employed in published polymer anti-cancer conjugates based on N-(2-hydroxypropyl)methacrylamide (HPMA). The HPMA-doxorubicin (DOX) anticancer

drug PKI is now in phase I/II clinical trials [21]. This peptide spacer is not a natural substrate for serum enzymes, leading to high stability in serum, and is not cleaved until the polymer is internalized into an endocytotic vesicle containing the cysteine protease, cathepsin-B, that recognizes and cleaves the GFLG peptide sequence [23]. Cathepsin concentration in lysosomes can well exceed 1 mM [23]. Release profiles in vitro show that this linker can release 100% of bound DOX in ~ 30 hr when incubated in a mixture of rat liver lysosomal enzymes (tritosomes). Quantitative release studies of DOX from PKI in cells however, show that only ~ 21% of DOX is released after 48 hrs [24]. Other drugs bound to HPMA by this type of linkage include paclitaxel, camptothesin and ellipticine [25]. Direct comparison of this type of drug releasing construct vs. pH triggered release constructs is shown in Figure 1.1.2.

Structure	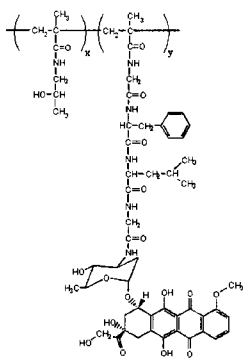	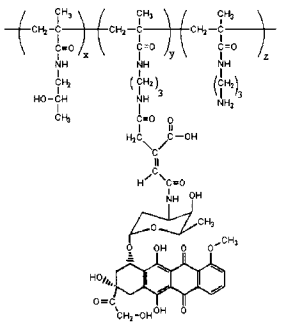	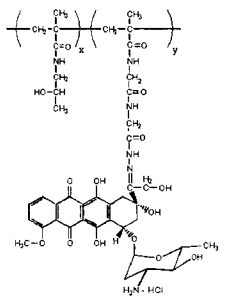
Linkage	GFLG	cis-aconityl	hydrazone
Polymer Carrier/Drug	HPMA/DOX	HPMA-APMA/ADR	HPMA/DOX
IC_{50}	19 μg DOX/ml	1.3 μM ADR/ml	0.08 μg Dox/ml
IC_{50} Free Drug	~ 0.1 μg DOX/ml	0.1 μM ADR/ml	~ 0.1 μg Dox/ml
Reference	[21]	[38]	[30]

Figure 1.1.2. Reduced cytotoxicity of drugs covalently attached to soluble polymer carriers

The efficacy of HPMA-drug constructs utilizing the GFLG spacer may not be attributed to the release of free drug. Ulbrich and coworkers have recently investigated the cytotoxixity of HPMA-bound DOX [24]. Upon cell internalization of an HPMA-DOX conjugate, HPLC analysis shows that only ~ 30% of the total DOX concentration is released from the polymer after 90 minutes, with no more released after 48 hrs. Also, the observed mechanism of cell death was different between free DOX and HPMA-DOX conjugates. In the case of DOX-induced cell death, DOX intercalates into DNA, causing single and double strand breakage, leading to a signal cascade resulting in cell death by apoptosis. In the case of HPMA-DOX conjugates, the observed mechanism of cell death was necrosis. The authors suggest that the cytotoxicity of HPMA-DOX conjugates can possibly be attributed to a different mechanism, such as directly acting on cell membranes as a result of increased polymer hydrophobicity due to bound DOX.

3.2. Acid-Labile Linkers

The acidic environment of the lysosome makes pH-sensitive conjugation of drug to polymer an appropriate strategy [26]. Although lysosomal pH can vary between individual cells and cell types, it is generally accepted that the lysosomal pH is approximately 5.0. For example, recent studies utilizing pH-sensitive fluorophores show an average pH of axon cell lysosomes to be 5.1 (with a range of 4.4-5.6), and macrophage lysosomes to be 5.7 [27, 28]. Acid-labile linkers have the inherent advantage of simpler reaction kinetics by utilizing the inherent pH gradient, and not relying on enzymatic activity. Many pH-sensitive linkers have been explored and are recently reviewed [29]. Two acid-sensitive linkers, cis-aconitic acid and hydrazone, have recently been compared

to the classical GFLG spacer in releasing the anticancer drugs, DOX or adriamycin (ADR) from HPMA polymers (Fig.2).

3.2.1. The Hydrazone Linkage

The hydrazone linkage has been investigated as a pH-labile linker located between polymeric HPMA, hyaluronan, antibodies and DOX, as well as linkages between DOX and antibody conjugates [30-32]. These studies showed that HPMA copolymers containing DOX bound via hydrazone linkers showed anti-proliferative activity on T-cell EL4 lymphoma cells 234 times greater than the traditional GFLG spacer described above. In fact, the cytotoxic effect of HPMA-DOX resulting from the hydrazone linkage alone was greater than that of DOX linked to the polymer by a GLFG/hydrazone linkage [30]. However, another recent study showed that the HPMA-DOX conjugate containing the GFLG spacer was more cytotoxic than a hyaluronan construct carrying DOX via a hydrazone linkage [33]. This linkage has also been used to incorporate DOX into a biodegradable PEG polymer [34]. The polymer was shown to release the bound DOX, remaining highly cytotoxic to EL4 lymphoma cells in vitro. After release of bound DOX, Gly/Leu/Gly peptide spacers within the polymer backbone allow degradation to PEG 2000 by lysosomal peptidases. This linkage is also under investigation for the conjugation of norfloxacine, a fluoroquinolin with DNA inhibiting activity used for treatment of tuberculosis, to poly [N^5-(2-hydroxyethyl-L-glutamine)] [35].

3.2.2. The Cis-aconityl Linkage

The cis-aconityl acid linkage was first investigated by Shen and Ryser, and has since been used for conjugation of drug to aminoethyl polyacrylamide beads, soluble HPMA, monoclonal antibodies, as well as degradable PEG constructs [36-39]. This linker is stable at physiological pH, with only trace degradation resulting from hydrolysis detected after 96 hrs [36]. The inherent disadvantage for this type of linkage is preservation of the pendant cis-carboxylic moiety. Conjugation reactions to form a cis-aconityl moiety typically involve ring opening of cis-aconitic anhydride, resulting in two free carboxylic acid functional groups. A carbodiimide-mediated condensation reaction is then employed to complete drug conjugation through the terminal carboxylic acid. Although the reaction has been optimized to preserve the cis-carboxylic acid moiety, side products result in the loss of the cis-carboxylic acid [39]. Typically, this linker produces an initial burst of drug release from conjugates that retain the cis-acidic moiety, followed by slow release of conjugates in which the cis-moiety was not preserved. Release of ADR from an HPMA/APMA copolymer bound by the cis-aconitic acid vs. the peptide GFLG spacer was directly compared [38]. As with the hydrazone linkage, ADR bound via the pH-labile bond was more toxic than that with the enzymatically cleavable linker, and even as toxic as free ADR in multidrug resistant human ovarian carcinoma cell cultures. However, the authors suggested that this increased cytotoxicity could be attributed to an increased number of amino groups inherent in the polymer construct from incomplete cis-aconityl/ ADR conjugation to the polymer backbone, leading to increased basicity and positive charge, and increased interaction with the negatively charged cell surface, thus increased cellular uptake. Secondly, it was hypothesized that free ADR may

be released very slowly from the conjugate with long incubation times, increasing the concentration of free drug outside of cells. However, Shen and coworkers have shown the cis-aconityl linker to be stable at pH 7.0 up to 96 hr. More in-depth analysis and *in vivo* work is needed to verify the efficacy and release mechanism of this type of conjugation.

4. Lysosome Escape

Lysosome permeability is inherently attributed to hydrogen bonding capability of a penetrant molecule, and to a lesser extent, the size of the molecule. Therapeutic agents must diffuse through this vesicle membrane, or the membrane itself must be disrupted, to allow entry into the cytosol where drugs might reach their therapeutic target. Lysosome membranes have permeability properties typical of phospholipid membranes, whether natural or synthetic [40]. Naturally occurring metabolic by-products must diffuse through the lysosome membrane during metabolism of naturally occurring macromolecules. These metabolite products are typically smaller hydrophilic molecules such as glucose, glucuronic acid, N-acetylhexosamines, amino acids, nucleosides and other end products. However, the lysosome contains many substrate-specific porters to efflux these types of molecules [41]. Transport of molecules with low membrane permeability is facilitated by formation of non-discriminating membrane pores. Large polar therapeutic molecules, such as proteins or DNA, must rely on a different mechanism for endosomal escape since diffusion through the vesicle membrane is very slow. For example, endosomal escape has been shown to be the rate-limiting step for

DNA delivery [42]. Therefore, lysosomal membranes must be disrupted in order to permit rapid escape of these types of macromolecular therapeutic agents.

4.1 Release of Agents by pH-Sensitive Pore-Forming Peptides

Drug delivery constructs can exploit non-discriminating membrane pores or channels to facilitate release into the cytosol. Pore-forming proteins are used by both viruses and bacteria to facilitate lysosome escape of their contents to host cells to avoid destruction. Peptides promoting membrane fusion are used by viruses to enter host cells. Both natural and synthetic peptides with membrane activity have been identified and recently reviewed [43, 44]. The most extensively studied natural fusion protein is the influenza virus hemagglutin (HA) and its pH-sensitive action has just been reviewed [45]. Analogous peptides have been synthetically developed to exploit this pH-dependent activity for the release of agents from liposomes. These types of peptides have also been designed to increase membrane disruption efficiency, as well as serving as DNA condensing agents. These include the JTS1, GALA, KALA, and the yet-unnamed "29-mer" peptides designed to change conformation as a function of pH, while the DNA-binding KALA peptide remains more stable over a broad pH range [46-48]. KALA, GALA, and the "29mer"are all α-helical structures at pH ~ 5.0. These peptides have been designed to exhibit random coil structures at physiological pH 7.4, transforming back to a membrane-active, penetrating helix to prompt liposome membrane leakage in the acidic lysosomal environment. Their direct effect on biologically based membranes has not been extensively studied nor mechanistically verified.

The GALA peptide is a 30-amino acid peptide rationally designed to facilitate membrane disruption at lysosomal pH. The peptide sequence contains repeat glutamic acid residues, which at physiological pH are anionic, resulting in charge repulsion that prevents the formation of secondary structure. Upon acidification, and protonation of glutamic acid residues, an α-helix conformation is obtained and this peptide then forms multi-mer aggregates, which can then insert into lipid bilayers, forming pores of 10 +/- 2 monomers [47]. Unlike KALA, GALA α-helicity occurs only at acid pH. GALA-induced leakage of the self-quenching dye, calcein, from liposomes revealed no adverse side affects such as change in liposome size or fusion, micelle formation or other catastrophic changes in liposome structure resulting from GALA- formed pores [49]. These GALA membrane pores are approximately 5-10 Å in diameter [47]. However, the pore size is dependent on the GALA/lipid content ratio [50]. Complete calcein dye leakage is observed with 100:1 lipid:GALA ratio in POPC and OBPC liposomes. At this concentration, leakage of 3000 MW dextran was also observed. Increasing the ratio of GALA content 4-10 times above that required for 100% leakage of 3000 MW dextran allows release of 10,000 MW dextran, implying that pore size is tunable to allow passage/exclusion of specific molecules. Additionally, GALA pores were formed with conjugation to the macromolecule OKT9, a transferrin receptor ligand. This study showed that GALA pore-forming activity was retained after conjugation. Liposome membrane composition has also been shown to affect GALA-induced pore formation [51]. Membrane surface association, but not pore formation, is favored in membranes containing cis-unsaturated acyl chains (e.g., POPG, POPC), as well as membranes containing phosphatidylethanolamine (PE) lipids. The activity of GALA towards the

biologically based egg phosphatidylcholine liposomes has been confirmed to produce leakage of small molecules [47], making GALA a candidate for conjugation to non-liposomal delivery constructs to facilitate their leakage from lysosome membranes by direct association of GALA with this membrane. Also, the use of GALA to increase the transfection efficiency of a cationic liposome gene delivery construct has been observed [52]. Increased transfection efficiency has also been observed for neutral dendrimer-based transfection agents as well [53]. The increase in transfection efficiency of these constructs was attributed to endosome membrane disruption, providing preliminary evidence for the utility of this peptide in delivery to real biological systems. The effectiveness of this type of construct may be limited for GALA due to the dependence of pore formation on biomembrane composition, as well as this peptide's susceptibility to serum or lysosomal protease degradation. Protease degradation could be overcome with the development of D-amino acid designed analogous GALA-like peptides.

The KALA peptide was synthetically designed as a cationic version of GALA to encapsulate DNA, and facilitate DNA release from the lysosomal compartment. The α-helical content decreases with increasing pH (pH: 8-4.5, α-helicity: 45-24%). Membrane leakage efficiency for fluorophores, ANTX and DPX, from POPC/POPG negatively charged liposomes seems to be more dependent on lipid/peptide ratios than pH. Complete leakage is observed from negatively charged POPC/POPG liposomes at 50:1 lipid:peptide ratios over the pH range of 4.5-8.5 [54].

New work shows that the hydrophilic amino acid residue secondary structure arrangement on post α-helical peptide conformation dictates the types of pores formed in membranes by these peptides. Peptides with a high angle of hydrophilic residues on

helicity wheel diagrams were compared to a newly designed peptide (un-named "29mer") with a smaller angle of hydrophilic residues. High angle peptides such as GALA require more peptides to aggregate and form pores. The new peptide was designed with a smaller hydrophilic face, leading to more rapid pore formation in limiting amounts of peptide. The leakage of the pH-insensitive membrane impermeable dye, PI, that fluoresces only when bound to DNA, into a solution containing calf thymus DNA and ~10,000 and ~ 40,000 MW dextrans was considerably different, with PI leakage occurring at a much higher rate. Thus, pores formed with the 29-mer must on average be smaller, while larger pores are formed when sufficient peptide is present, consistent with findings from GALA studies [48].

4.2. Synthetic Endosomolytic Polymers

Chloroquine, the antimalarial drug, is a classical endosomolytic agent that prevents the acidification of endosomes, promotes swelling of the endosomal vesicle, and is membrane destabilizing. This molecule can diffuse through the endosome membrane in its uncharged state, but upon acidification in the endosome, becomes charged and can no longer diffuse back out into the cytosol, becoming trapped inside this compartment. Another similar type of molecule, tamoxifen, the clinically applied breast cancer drug, has been shown to promote lysosome escape of ADR in ADR-resistant cells [55]. ADR is sequestered primarily in the acidic compartments of ADR-resistant cells, rendering the drug ineffective. Administration of tamoxifen to cells in concentrations as low as 0.5μM facilitated lysosome release of ADR and subsequent localization of the drug into the cytosol and nucleus. Although these drugs in their free form have shown efficacy *in*

vitro, this approach is impractical for *in vivo* use to facilitate intracellular delivery. Adverse side effects of tamoxifen treatment including increased risks of liver disease, as well as treatment of certain types of refractory cancers (uteral, liver, endometrial), might be better addressed by polymer conjugation as well.

Other synthetic constructs have also been designed to act as proton sponges to prevent endosomal acidification, and promote rupture of this compartment through a mechanism similar to that of chloroquine. Examples of these types of polymer constructs can be seen back in Figure 1.1.2. Most chemistries based on polycations are designed for DNA delivery, but short fragments of these polymers are incorporated into carrier polymer backbones, or as pendant side chains in soluble macromolecular delivery constructs to achieve the desired proton sponge effect. Polymers containing carboxylic acid groups facilitate direct lipid membrane disruption upon protonation of these functional groups. Several synthetic polymers designed for pH-dependent lipid membrane destabilization are shown in Figure 1.1.3.

Polymer Structure	Polymer Name	Proven Utility	Ref.
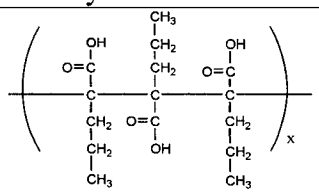	Poly(propylacrylic acid) PPAAc	Red blood cell homolysis DOTAP mediated DNA delivery	[73] [74] [75]
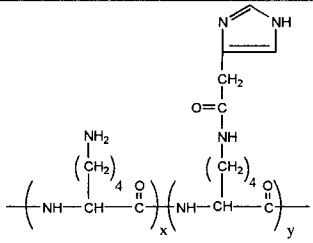	Polylysine-graft-imidizole acetic acid	DNA delivery by polymer complexation Antisence Oligonucleotide delivery	[67] [65] [66]
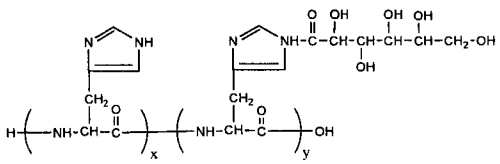	Gluconic acid modified polyhistidine G-pHis	DNA delivery in PLL construct	[68]

Figure 1.1.3. Endosomolytic Polymer Constructs

Additionally, recent studies have shown that gene delivery *in vivo* requires minimization of positive charge at physiological pH [56]. These synthetic polycation constructs can then be tailored for charge based on protonation and deprotonation of basic amino groups; at physiological pH only one of six primary amino nitrogens on lysine residues are protonated [57]. Unprotonated amino groups can thus serve as a proton sponge at acidic pH, triggering osmotic swelling and destabilization in the endosome/lysosome compartment. This acidic neutralization effect has been observed to differ in various cell types [58]. Endosome disruption is observed upon internalization of cationic polyethyleneimine (PEI)/DNA complexes in EA.hy 926 cells. However, no evidence for endosome disruption and delivery of DNA into the cytoplasm of L929 cells

was observed, implying that this type of neutralization mechanism promoting endosomal lysis by sequestered basic polymers may be cell-specific, depending on the types of proton pumps present in different cells [58]. This approach would be of limited value for constructs that utilize pH-dependent or enzymatic release, since lysosomal enzymes are inactive in non-acidic environments.

The synthetic polycation, polyethylenimine (PEI), has been observed to be detrimental to several cell types, and is rapidly cleared (24 hrs in rats). A more biocompatible system is required for *in vivo* use [59, 60]. Polycations are generally believed to disrupt biological membranes. A recent study illustrates that the polycation, poly-(N-ethyl-4-vinylpryidinium bromide) binds to stearoylated chymotripsin in proteoliposomes, leading to protein clustering. This complex also increased membrane permeability to the non-ionic drug DOX, but did not increase permeability to Na^+ ions [61]. Cytotoxicity studies for highly branched cationic poly(amidoamine) (PAMAM) dendrimers, high MW poly-L-lysine (PLL), and PEI showed that these basic synthetic polymers are responsible for elevated activity of the blood complement cascade [62]. Recent studies comparing polycationic and polyanionic dendrimers demonstrate that anionic dendrimers are neither lytic, nor cytotoxic over a broad concentration range. Coating a dendrimer surface with a hydrophilic PEG corona also reduced cytotoxicity [63]. This evidence provides incentive to create soluble macromolecular carriers that reduce the amount of positive charge in the delivery to permit controlled, effective and reliable membrane lysis without associated toxicity.

Polymers have been developed that incorporate basic imidazole groups into polymer vehicles, acting as a proton sponge to mediate endosomal escape without the

cytotoxic effects of basic polylysine or PEI [64]. Polymers with imidazole content of 86.5% allowed for gene expression comparable to PEI, but with little cytotoxicity [65]. Similar results were obtained for oligolysine (DP=19) polymers with histidyl residues. This study showed that a 20-fold enhancement of biological activity of antisense oligonucleotides towards the inhibition of transient as well as constitutive gene expression [66]. This study also showed that acidification of the endosome is necessary for the activity of this polymer, since its effectiveness was reversed with the addition of bafilomycin A, an inhibitor of the proton pump involved in endosome acidification. This effect was first realized with a histidylated polylysine polymer (DP=190) containing ~ 38% histidylated groups [67]. This polymer was able to increase polyfection of plasmid DNA containing the β-galactosidase gene up to 104 times more effectively than poly-L-lysine alone. Other polymers based on polyhistidine have also been investigated for gene delivery and endosome escape [68]. Poly-L-lysine/poly-L-histidine (PLL/PLH) comb polymers have been developed to deliver DNA through the endosome [69]. This polymer was constructed of ~8000 Da PLL, with 25% of ε-amine groups tethered with a polyhistidine side chain (DP=17). This construct also led to increased transfection of DNA containing the β-galactosidase gene in 293T cells. However, transfection efficiency in the presence of chloroquine was further enhanced, indicating that maximum transfection capability with the PLL/PLH construct was not achieved, and that delivery mechanism requires elucidation.

Polymers utilizing weakly acidic side chains have also been investigated for their ability to destabilize lipid membranes [70]. Specifically, poly(ethylacrylic acid) (PEAAc), and poly(propylacrylic acid) (PPAAc) have been compared for their

membrane destabilizing properties. PEAAc was the first synthetic construct of this type, designed to disrupt liposomal membranes and facilitate the release of their contents in a pH-dependent fashion [71, 72]. The PPAAc polymer is designed with shorter hydrophobic pendant side chain monomer units relative to PEAAc, resulting in membrane association that is more sensitive to pH. Both polymers show an increased level of hemolysis of red blood cells with increasing pH, with PPAAc showing hemolytic activity at higher pH. The authors attribute this to a pKa shift of the carboxylate group in lower dielectric biomembrane microenvironment. Polymers belonging to the alkyl acrylic acid family have exhibited higher membrane disruption capability than PEAAc [73]. PPAAc has shown membrane-lytic activity in a pH-dependant fashion [74]. This polymer exhibits minimum lytic activity towards red blood cells at physiological pH, with lytic activity increasing to a maximum at ~ pH 6.4 at ca. of 15μg/10^8 red blood cells ($4.5x10^6$ molecules of PPAc/red blood cell). The cytotoxicity of this polymer is minimal, with no cytotoxic effects observed in mouse fibroblasts at concentrations up to at least 100 μg/mL. Incorporation of PPAAc into novel cationic lipid DOTAP/DNA delivery constructs has been shown to substantially increase transfection rates [75]. Similar results are also obtained with gluconic acid-modified polyhistidine polymers (G-pHis) [69]. Incorporation of gluconic acid-modified polyhistidine to a transferrin-conjugated polylysine-DNA delivery construct was found to achieve transfection efficiencies similar to that of chloroquine at a DNA/G-pHIS/Tf-pLys ratio of 1:3:4.5. Cytotoxicity studies showed that G-pHis was not cytotoxic at polymer concentrations of 20 μg/ml.

4.3. Cell Membrane Penetrating Peptides

Cell penetrating peptides (CPPs), also known as protein transduction domains (PTDs), have been extensively studied for their ability to ferry cargo across cell membranes. Delivery systems utilizing CPPs can promote delivery of therapeutic proteins, bioactive peptides, small molecules, as well as nucleic acids across cell membranes. A recent list of peptides used for cellular targeting is available, and current reviews on the topic are published [76-80]. Most extensively studied of these CPP peptides are the sequences derived from HIV-1 Tat, antennapedia, and VP22 proteins. In addition to membrane translocating potential, Tat CPPs also have inherent nuclear translocating properties as well [81, 82]. The peptide sequences used range in size from the 11-peptide Tat sequence to the 46-residue K15RGD peptide. Three major categories of CPPs are identified: hydrophobic sequences, amphipathic sequences, and cationic sequences [83]. These peptides are typically truncated versions of naturally occurring membrane translocating peptide sequences, but new synthetic PTDs have been designed based on the known natural templates. Short oligomers of arginine have been found to be up to 100 times more efficient than the Tat sequence in delivering fluorescein into cells [84]. Internalization efficiency of these arginine oligomers is further enhanced with the addition of methylene groups between the peptide backbone and side chain guanidine groups. The increased flexibility and reduced steric hinderence of the arginine guanidine group could allow for improved cell-surface interactions [84].

The ability of these peptides to translocate large molecules across cell membranes is quite remarkable, with cargo translocated to date including β-galactosidase, horseradish peroxidase, Fab antibody fragment, 26 kDa HPMA and 45nm

magnetic iron particles (~1/10 the size of a cell) [85-88]. While the success of these peptides to translocate cargo across cell membranes is generally the rule, conjugation of the Tat or VP22 CPP peptides to the diphtheria toxin A-fragment promoted cell surface binding of the protein, but not internalization [89]. Although the exact mechanism for membrane translocation is not known, it has been hypothesized that interaction of the positively charged peptide with the negatively charged cell membrane interface induces local invagination of a single-layer of the lipid bilayer, creating an inverted micelle with peptide and lipid which then translocates peptide and cargo through the destabilized local membrane region where the cargo is then released intracellularly [90]. Another hypothesis describes a "membrane-thinning' effect, claiming that the basic peptides carpet the membrane surface, causing a localized electrostatic perturbation in the outer leaflet, resulting in a lateral rearrangement of the cell membrane lipids and localized membrane thinning. Aggregation of surface-bound peptides results in reduced local surface tension, allowing the peptides to intercalate the membrane [91]. Although the exact mechanism is unknown, structural analysis of some peptides during membrane translocation demonstrates that a common internalization mechanism is not likely [92]. Tat peptide requires cell surface proteoglycans in order to be effective [93]. Proteoglycans are generally acidic, carrying a net negative charge at physiological pH, thus facilitating peptide interaction. A more recent study involving cell lines deficient of surface proteoglycans demonstrated that Tat conjugates were internalized as efficiently as the corresponding wild-type cells, once again clouding the understanding of a specific requirement for membrane translocation [94]. All experimental data to date overwhelmingly support a cellular internalization mechanism independent of

endocytosis: CPP membrane transduction occurs at similar efficiency at 4° C, and in the presence of metabolic inhibitors [81, 95]. It can be speculated, however, that a cell surface component is necessary for internalization, since efflux of internalized cargo is not observed for Tat conjugates, even at dose concentrations of 20 μM [96]. It is interesting to note that the CPP's MAP (KLAL) and transportan did demonstrate an efflux of internalized cargo. These peptides have a higher hydrophobic moment, μ, which leads to membrane destabilization, suggesting that μ should be minimized for practical applications. Studies have also shown that non-native D-amino acid forms of membrane active peptides retain translocation characteristics [97, 98]. The D-form peptides would result in increased efficacy in vivo, since enzymatic degradation would be minimized.

The use of these CPP peptides *in vivo* to enhance the cellular internalization of macromolecules will most likely not be practical when specific cell types must be targeted, since they generally trigger internalization in many cell types. Conjugation of Tat peptide to the tumor-specific antibody scFv (L19) abolished tumor targeting activity, with the Tat conjugated antibody accumulating in the liver and spleen [98]. However, these types of peptides present a unique opportunity for enhancing delivery of molecules across the lysosome membrane. In spite of the extensive investigation of these peptides to transport cargo across the cell membrane, no work has reported their utility for lysosomal membrane transduction. Clever attachment of these types of basic peptides to therapeutic agents using polymers could facilitate the transport of cargo through the endosomal compartment into the cytosol. Although the endosome/lysosome environment is different from the extracellular environment where CPP transport effectiveness has

already been proven, the lower pH of this lysosomal compartment would increase the net positive charge of these peptides on which their activity is based, preserving their effectiveness and membrane activity. Also, the exterior cell surface becomes the interior surface of an endosome upon invagination, where CPP activity has been demonstrated. Burying the cell penetrating peptide inside the polymer delivery construct could prevent the polymer carrier from entering all cells *in vivo*. However, a linker designed to selectively degrade in the endosome/lysosome to release or expose these peptides only in that compartment, allowing them to then transport cargo across that membrane into the cytosol, would be novel and potentially useful.

5. Import into the Nucleus

After drug is released from the lysosome, it must randomly diffuse through the cytosol in order to reach its therapeutic target, often a protein, enzyme or DNA. The stochastic nature of this transport often limits drug efficacy, particularly if the target lies within yet another subcellular compartment (e.g., nucleus). Improvement can be achieved by covalently linking the therapeutic agent to a subcellular localization moiety. Such signals have been identified for import into the nucleus, mitochondria and Golgi apparatus [99]. These signals typically comprise a short peptide sequence that cells naturally incorporate into newly synthesized proteins to target them from the site of protein packaging (Golgi apparatus) to their effective end-location within the cell.

Import of macromolecules into the nuclear envelope is known to involve transport through the nuclear pore complex (NPC). While the exact structure of the NPC varies with cell type, they typically comprise about 50-100 proteins, forming a pore that

selectively allows transport of molecules through the membrane complex. This complex import machine has been extensively reviewed [100-104]. The pore channel size allows for passive diffusion of macromolecules smaller than about 40 kD, but molecules above this threshold must be actively transported into the nucleus [103]. The maximum NPC diameter during active transport is 25 nm, while the diffusion channel size is 9 nm [105].

In order to be actively transported through the NPC, the cargo must carry a nuclear localization sequence (NLS). Typically, an NLS is a short 3-5 basic amino acid peptide sequence, or sequence containing two basic regions separated by spacers of various lengths (bipartite). Many NLS peptide sequences discovered to date and tabulation of these sequences can be found in recent reviews, with the most widely used being the sequence derived from the SV40 large T antigen [106-108]. While an NLS is required for protein transport into the nucleus, it has been shown that an NLS is not required for DNA entry [109]. Kinetic measurements carried out using the cell-free nuclear reconstructive system based on extracts from *Xenopus laevis* showed that nuclear import of NLS-labeled double stranded (ds) DNA was uninhibited by ATP depletion and incubation at 4°C, while protein import was inhibited. The width of dsDNA is approximately 2-3 nm, which is smaller than the diffusion pore channel size. The authors suggested that the linear dsDNA is imported by passive reptation or ratchet dynamics, governed by linear diffusion through the NPC followed by irreversible retention in the nucleus. Actual cell cytoplasm is much more complex than model buffer milieu, and it is possible that random diffusion through the pore is inhibited in live cells by resistance due to cytosolic factors. In normal cell lines, it has been shown that an NLS sequence does in fact increase nuclear import efficiency. Zanta and coworkers showed that DNA

transfection is enhanced up to a factor of 1000 in 3T3 cells with a single NLS sequence [110]. Additionally, an NLS sequence was found to increase nuclear transport and expression of a 1kb sized DNA in microinjected HeLa cells [111]. Alternatively, NLS conjugation to the site-specific recombinase, Cre, did not increase the recombination efficiency when compared to a non-NLS labeled Cre recombinase enzyme [112]. Nuclear delivery of a non-DNA/peptide therapeutic agent utilizing an NLS sequence has also been investigated. The chemical nuclease, metalloporphyrin (manganese (III) porphyrin), has been coupled to an amphipathic peptide/NLS signal to mediate cellular uptake and nuclear localization [113]. Cellular uptake of free metalloporphyrin occurred at a much lower frequency, and final subcellular localization was cytoplasmic, not nuclear.

While the linkage of an NLS to large nuclear cargo has shown mixed results for therapeutic potential, linkage of NLS sequences to small molecule nuclear targeted therapeutics has not been completely assessed. A study by Salman showed that an NLS is not required for 732 bp dsDNA entry into the nucleus [109]. However, other studies show that NLS sequences conjugated to DNA do in fact increase their nuclear import. Although an NLS is not required for transport of small molecules into the nucleus that are smaller in size than the diffusion channel of the NPC, could nuclear uptake be further enhanced utilizing these peptides that activate the nuclear import machinery? Coupling an NLS sequence to a small molecule could possibly further enhance the efficacy of current nuclear-targeted drugs (e.g., DOX) by the following mechanisms: 1) binding of NLS-drug to the NPC to enhance diffusion rates by actively shuttling the molecule across the NPC; 2) NLS transport-enhanced nuclear loading beyond equilibrium concentrations,

driven by chemical potential; or 3) binding of NLS-labeled drugs to enhance the diffusion rate of molecules not binding to the NPC receptor by activating dilation of the NPC diameter from 9 nm to 25 nm. NLS-coupling could, however, also serve to hinder nuclear delivery of small molecules. The increased size (reduced diffusion coefficient) of the small molecule resulting from attachment of the NLS sequence could hinder passive diffusion through the cytosol to reach the nucleus. This utility must be assessed to determine what actual effects NLS conjugation might have on nuclear import of different sized molecules.

6. Other Targetable Cellular Organelles

Other cell organelles also present potential for drug targeting with similar barriers. Mitochondria contain numerous protein and nucleic acid therapeutic targets, and possess characteristics such as a high membrane potential, as well as protein import machinery [114]. Most mitochondrial proteins are synthesized outside of this organelle, and specific protein translocating pathways and peptides are utilized for their natural import. Various aspects involved in mitochondrial drug delivery have been recently reviewed [115], and is the theme of *Advanced Drug Delivery Reviews, volume 49, issue 1-2, July 2000.* Peroxisome, endoplasmic reticulum, Golgi apparatus targeting can also be achieved and suitable targets have been identified [99].

7. Conclusions

Improved efficacy by delivering therapeutic agents utilizing soluble macromolecular vehicles has been realized for over a decade. Bioavailability is enhanced

while toxicity is reduced. The task now at hand is to optimize these systems to increase both specificity and delivery efficiency. The anticancer drug, PK1, shows the most advanced promise as a clinically useful polymer conjugate with DOX, but studies comparing its efficacy to constructs utilizing acid labile linkers demonstrate the possibility that this delivery system can be improved. More efficient targeting utilizing multi-functional polymer vehicles with capabilities for endosome disruption and nuclear targeting remain to prove two objectives: 1) that such carriers can exploit multiple functional components to improve delivery; 2) that such delivery, using more sophisticated vehicle designs with serial functions triggered spatially and temporally within a cell transport pathway truly improves drug therapy. Efforts will tap more advances in molecular and cell biology, adoption of endogenous cell signaling mechanisms into polymer constructs, and creative conjugation architectures to sew the pieces together with sufficient drug loading. It is not unreasonable to conceive of new polymer carriers that increase the efficacy of toxic, insoluble drugs such as DOX by combining above-mentioned targeting strategies to create anticancer drug carriers potentially more effective than free DOX. Generalizing these architectures to multiple tissue and cell types in physiologically complex milieu, many other drug candidates, and new in vitro-in vivo correlations presents a daunting amount of new work and associated challenges. Pioneering work reviewed here presents a sound basis on which to proceed with more complex macromolecular designs. Realization of new effective molecular constructs will depend on innovative chemical architectures that permit selective component function in multi-functional vehicles at appropriate locations and times at desired targets within the host.

Acknowledgements

The Authors graciously acknowledge partial support from NIH R01 GM56751.

References

[1] R. Duncan, J. Kopecek, Soluble synthetic polymers as potential drug carriers, Adv. Polym. Sci. 57 (1984) 53-90.
[2] C. Monfardini, F .C. Veronese, Stabilization of substances in circulation, Bioconj. Chem. 9 (1998) 418-450.
[3] S. Brocchini, R. Duncan, Pendant drugs, release from polymers, in: E. Mathiowitz (Ed.), Encyclopedia of Controlled Drug Delivery, Vol 1, John Wiley and Sons, NY., 1999, pp. 786-816.
[4] G. Storm, D. Crommelin, Liposomes:quo vadis? Pharm. Sci. Technol. Today 1(1) (1998) 19-31.
[5] K. Uhrich, S. Cannizzaro, R. Langer, K. Shakesheff, Polymeric systems for controlled drug release, Chem. Rev. 99 (1999) 3181-3198.
[6] J. Jagur-Grodzinski, Biomedical application of functional polymers, React. Funct. Polym. 39 (1999) 99-138.
[7] A. Nagarsekar, H. Ghanehari, Genetically engineered polymers for drug delivery, J. Drug Target. 7(1) (1999) 11-32.
[8] M. Kumar, Nano and microparticles as controlled drug delivery devices, J. Pharm. Sci. (2000), 3(2) 234-258.
[9] K. Ulbrich, V. Subr, M. Pechar, J. Strohalm, M. Jelinkova, B. Rihova, Hydrophilic polymers for drug delivery, Macromol. Symp. 152 (2000) 151-162.
[10] R. Brokx, S. K. Bisland, J. Gariepy, Designing peptide-based scaffolds as drug delivery vehicles, J. Controll. Rel. 78 (2002) 115-123.
[11] Z. R. Lu, J. G. Shia, S. Sakuma, P. Kopeckova, J. Kopecek, Design of novel bioconjugates for targeted drug delivery, J. Control. Rel. 78 2002 165-173.
[12] J. Kopecek, P Kopeckova, T. Minko, Z.R. Lu, HPMA copolymer-anticancer drug conjugates: design, activity, and mechanism of action, Eur. J. Pharm. Biopharm. 50 (2000) 61-81.
[13] J. Kopecek, P. Kopeckova, T. Minko, Z-R. Lu, C.M. Peterson, Water soluble polymers in tumor targeted delivery, J. Control. Rel. 74 (2001) 147-158.
[14] D. Putnam, J. Kopecek, Polymer conjugates with anticancer activity, Adv. Polym. Sci. 122 (1995) 55-123.
[15] S. P. Vyas, V. Sihorkar, Endogenous carriers and ligands in non-immunogenic site-specific drug delivery, Adv. Drug Deliv. Rev. 43 (2000) 101-164.
[16] S. P. Vyas, A. Singh, V. Sihorkar, Ligand-receptor-mediated drug delivery: an emerging paradigm in cellular drug targeting, Crit. Rev. Ther. Drug Carrier Syst. 18(1) (2001) 1-76
[17] D.F. Baban, L.W. Seymore, Control of tumor vascular permeability, Adv. Drug Deliv. Rev. 34 (1998) 109-119.

[18] H. Maeda, J. Wu, T. Sawa, Y. Matsumura, K. Hori, Tumor vascular permeability and the EPR effect in macromolecular therapeutics: a review, J. Control. Rel. 65 (2000) 271-278.
[19] P. Laakkonen, K. Porkka, J. A. Hoffman, E. Ruoslahti, A tumor-homing peptide with a targeting specificity related to lymphatic vessels, Nature Med. 8(7) (2002) 751-755.
[20] R. Wattiaux, N. Laurent, S. Wattiaux-De Connick, M. Jadot, Endosomes, lysosomes: their implication in gene transfer, Adv. Drug Deliv. Rev. 41 (2000) 201-208.
[21] P.A. Vasey, S.B. Kaye, R. Morrison, C. Twelves, P. Wilson, R. Duncan, A.H. Thompson, L. S. Murray, T. E. Hilditch, T. Murray, S. Burtles, D. Fraier, E. Frigerio, J. Cassidy, Phase I clinical and pharmacokinetic study of PK1[N-(2-Hydroxypropyl)methacrylamine copolymer doxorubicin]: first member of a new class of chemotherapeutic agents-drug-polymer conjugates, Clin. Cancer Res. 5 (1999) 83-94.
[22] P. Rejmanova, J. Pohl, M. Baudya, V. Kostka, J. Kopecek, Polymers containing enzymatically degradable bonds. 8. degradation of oligopeptide sequences in N-(2-hydroxypropyl)methacrylamide copolymers by bovine spleen cathepsin B, Makromol Chem. 184 (1983) 2009-2020.
[23] V. Turk, B. Turk, D. Turk, Lysosomal cysteine proteases: facts and opportunities, EMBO J. 20 (2001) 4629-4633.
[24] O. Hovorka, M. St'astny, T. Etrych, V. Subr, J. Strohalm, K. Ulbrich, B. Rihova, Differences in the intracellular fate of free and polymer-bound doxorubicin, J. Control. Rel. 80 (2002) 101-117.
[25] R. Duncan, S. Gac-Breton, R. Keane, R. Musila, Y.N. Sat, R. Satchi, F. Searle, Polymer-drug conjugates, PDEPT and PELT: basic principles for design and transfer from the laboratory to clinic, J. Control. Rel. 74 (2001) 135-146.
[26] A. Asokan, M.J. Cho, Exploitation of intracellular pH gradients in the cellular delivery of macromolecules, J. Pharm. Sci. 91(4) (2002) 903-913.
[27] C. C. Overly, K. D. Lee, E. Berthiaume, P. J. Hollenbeck, Quantitiative measurement of intraorganelle pH in the endosomal-lysosomal pathway in neurons by using ratiometric imaging with pyranine, Proc. Natl. Acad. Sci. USA 92 (1995) 3156-3160.
[28] K. P. McNamara, T. Nguyen, G. Dumitrascu, J. Ji, N. Rosenzweig, Z. Rosenzweig, Synthesis, characterization, and appication of fluorescence sensing lipobeads for intracellular pH Measurements, Anal. Chem. 73 (2001) 3240-3246.
[29] F. Kratz, U. Beyer, M. T. Schutte, Drug-polymer conjugates containing acid cleavable bonds. Critical Rev. in Ther. Drug Carrier Sys. 16(3) (1999) 245-288.
[30] T. Etrych, M. Jelinkova, B. Rihova, K. Ulbrich , New HPMA copolymers containing doxorubicin bound via ph-sensitive linkage: synthesis and preliminary in vitro and in vivo biological properties, J. Control. Rel. 73 (2001) 89-102.
[31] T. Etrych, P. Chytil, M. Jelinkova, B. Rihova, K. Ulbrich, Synthesis of HPMA copolymers containing doxorubicin bound via a hydrazone linkage. Effect of spacer on drug release and in vitro cytotoxicity, Macromol. Biosci. 2 (2002) 43-52.
[32] H.D. King, D. Yurgaitis, D. Willner, R.A. Firestone, M.B. Yang, S.J. Lasch, K.E. Hellstrom, P.A. Trail, Monoclonal antibody conjugates of doxorubicin prepared with branched linkers: a novel method for increasing the potency of doxorubicin immunoconjugates, Bioconj. Chem. 10 (1999) 279-288.

[34] Y. Luo, N. Bernshaw, Z. Lu, J. Kopecek, G.D. Prestwich, Targeted delivery of doxorubicin by HPMA copolymer hyaluronan bioconjugates, Pharm. Res. 19(4) (2002) 396-402.
[34] M. Pechar, K. Ulbrich, M. Jelinkova, B. Rihova, Enzymatically degradable PEG multiblock copolymers with hydrazone attached doxorubicin in cancer therapy, J. Control. Rel. 72 (2001) 225-309.
[35] E. Roseeuw, E. H. Schacht, B. Paesen, Modified poly[N^5-(2-Hydroxyethyl-L-Glutamine)] as carrier for macromolecular prodrugs, J. Control. Rel. 72 (2001) 257.
[36] W. C. Shen, H. J. P. Ryser, Cis-aconityl spacer between daunomycin and macromolecular carriers: a model of pH-sensitive linkage releasing from a lysosomotropic conjugate, Biochem. Biophys. Res. Comm. 102(3) (1981) 1048-1054.
[37] H. S. Yang, R. A. Reisfeld, Doxorubicin conjugated with a monoclonal antibody directed to a human melanoma-associated proteoglycan suppresses the growth of established tumor xenografts in nude mice, Proc. Natl. Acad. Sci. USA. 85 (1988) 1189-1193.
[38] W. M. Choi, P. Kopeckova, T. Minko, J. Kopecek, Synthesis of HPMA copolymer containing adriamycin bound via an acid-labile spacer and its activity toward human ovarian carcinoma cells, J. Bioact. Comp. Polym. 14 (1999) 447-456.
[39] M. C. D. Clochard, S. Rankin, S. Brocchini, Synthesis of soluble polymers for medicine that degrade by intramolecular acid catalysis, Macromol. Rapid Commun. 21 (2000) 853-859.
[40] J.B. Lloyd,The Lysosome/endosome membrane: a barrier to polymer-based drug delivery? Macromol. Symp. 172 (2001) 29-34.
[41] J. B. Lloyd, Lysosome membrane permeability: implications for drug delivery, Adv. Drug Deliv. Rev. 41 (2000) 189-200.
[42] A. Kichler, K. Mechtler, J. P. Behr, E. Wagner, Influence of membrane-active peptides on lipospermine/DNA complex mediated gene transfer, Bioconj. Chem. 8 (1997) 213-221.
[43] C. J. Povoda, K. D. Lee, Bacterial pore-forming hemolysins and their use in the cytosolic delivery of macromolecules, Adv. Drug Deliv. Rev. 41 (2000) 209-221.
[44] E. Wagner, Application of membrane-active peptides for nonviral gene delivery Adv. Drug Del. Rev. 1999, 38, 279-289.
[45] J. Skehel, D. C. Wiley, Receptor binding and membrane fusion in virus entry: the influenza hemagglutinin, Annu. Rev. Biochem. 69 (2000) 531-69.
[46] S. Gottschalk, J. T. Sparrow, J. Hauer, M. P. Mims, F. E. Leland, S. L. C. Woo, L. C. Smith, A novel DNA-peptide complex for efficient gene transfer and expression in mammalian cells, Gene Ther. 3 (1996) 448-457.
[47] R.A. Parente, S. Nir., F. C. Szoka, Mechanism of leakage of phospholipid vesicle contents induced by the peptide GALA, Biochemistry 29 (1990) 8720-8728.
[48] M. J. Turk, J .A. Reddy, J. A. Chmielewski, P. S. Low, Characterization of a novel pH-sensitive peptide that enhances drug release from folate-targeted liposomes at endosomal pHs, Biochim. Biophys. Acta 1559 (2002) 56-58.
[49] J. Kuehne, M. Murphy, Synthesis and characterization of membrane-active GALA-OKT9 conjugates, Bioconj. Chem. 12 (2001) 742-749.
[50] F. Nicol, S. Nir, F. C. Szoka, Effect of cholesterol and charge on pore formation in bilayer vesicles by a pH-sensitive peptide, Biophys. J. 71 (1996) 3288-3301.

[51] F. Nicol, S. Nir, F. C. Szoka, Effect of phospholipid composition on an amphipathic peptide-mediated pore formation in bilayer vesicles, Biophys. J. 78 (2000) 818-829.
[52] S. Simoes, V. Slepushkin, E. Pretzer, P. Dazin, R. Gaspar, M. C. Pedroso de Lima, N. Duzgunes, Transfection of human macrophages by lipoplexes via the combined use of transferrin and pH-sensitive peptides, J. Leukocyte Biol. 65(2) (2002) 270-279.
[53] J. Haensler, F. C. Szoka, Polyamidoamine cascade polymers mediate efficient transfection of cells in culture, Bioconj. Chem. 4 (1993) 372-379.
[54] T. B. Wyman, F. Nicol, O. Zelphati, P. V. Scaria, C. Plank, F. C. Szoka, Design, synthesis, and characterization of a cationic peptide that binds to nucleic acids and permeabilizes bilayers, Biochemistry 36 (1997) 3008-3017.
[55] N. Altan, Y. Chen, M. Schindler, S. M. Simon, Tamoxifen inhibits acidification in cells independent of the estrogen receptor, Proc. Natl. Acad. Sci. USA 96 (1999) 4432-4437.
[56] A. Prokop, E. Kozlov, W. Moore, J. M. Davidson, Maximizing the in vivo efficiency of gene transfer by means of nonviral polymeric gene delivery vehicles, J. Pharm. Sci. 91 (2002) 67-76.
[57] E. Wagner, Effects of membrane-active agents in gene delivery, J. Control. Rel. 53 (1998) 155-158.
[58] A. Remey-Kristensen, J. P. Clamme, C. Vuilleumier, J. G. Kuhry, Y. Mely, Role of endocytosis in the transfection of L929 fibroblasts by polyethylenimine/DNA complexes, Biochim. Biophys. Acta 1514 (2001) 21-32.
[59] W. T. Godbey, A. G. Mikos, Recent progress in gene delivery using non-viral transfer complexes, J. Control. Rel. 72 (2001) 115-125.
[60] C. A. Nichol, D. Yang, W. Humphrey, S. Ilgan, W. Tansey, T. Higuchi, F. Zareneyrizi, S. Wallace, D.A. Podoloff, Biodistribution and imaging of polyethyleneimine – a gene delivery agent, Drug Deliv. 6 (1999) 187-194.
[61] N. O. Kozlova, I. B. Bruskovskaya, I. B. Okuneva, N. S. Melik-Nubarov, A. A. Yaroslavov, V. A. Kabanov, F. M. Menger, Interaction of a cationic polymer with negatively charge proteoliposomes, Biochim. Biophys. Acta 1514 (2001) 139-151.
[62] C. Plank, K. Mechtler, F. C . Szoka, E. Wagner, Activation of the complement system by synthetic DNA complexes: a Potential barrier for intravenous gene delivery, Hum. Gene Ther. 7 (1996) 1437-1446.
[63] N. Malik, R. Wiwattanapatapee, R. Klopsch, K. Lorenz, H. Frey, J. W. Weener, E. W. Meijer, W. Paulus, R. Duncan, Dendrimers: relationship between structure and biocompatibility in vitro, and preliminary studies on the biodistribution of ^{125}I-labelled polyamidoamine dendrimers in vivo, J. Control. Rel. 65 (2000) 133-148.
[64] C. Pichon, C. Goncalves, P. Midoux, Histidine-rich peptides and polymers for nucleic acids delivery, Adv. Drug Deliv. Rev. 53 (2001) 75-94.
[65] D. Putnam, C. A. Gentry, D. W. Pack, R. Langer, Polymer-based gene delivery with low cytotoxicity by a unique balance of side chain termini, Proc. Natl. Acad. Sci. USA 98(3) (2001) 1200-1205.
[66] C. Pichon, M. B. Roufai, M. Monsigny, P. Midoux, Histidylated oligolysines increase the transmembrane passage and the biological activity of antisense oligonucleotides, Nucl. Acids Res. 28(2) (2000) 504-512.

[67] P. Midoux, M. Monsigny, Efficient gene transfer by hystidylated polylysine/pDNA complexes, Bioconj. Chem. 10 (1999) 406-411.
[68] D. W. Pack, D. Putnam, R. Langer, Design of imidizole-containing endosomolytic biopolymers for gene delivery, Biotechnol. Bioeng. 67 (2000) 217-223.
[69] J. M. Benns, J. S. Choi, R. I. Mahato, J. S. Park, S. W. Kim, pH-sensitive cationic polymer gene delivery vehicle: N-Ac-poly(L-histidine)-graft-poly(L-lysine) comb shaped polymer, Bioconj. Chem.11 (2000) 637-645.
[70] N. Murthy, J. Robichaud, P. S. Stayton, O. W. Press, A. Hoffman, D. A. Tirrell, Design of polymers to increase the efficiency of endosomal release of drugs, Proceed. Int'l Symp. Control. Rel. Bioact. Mater. 25 (1998) 224-225.
[71] J. L. Thomas, D. A. Tirrell, Polyelectrolyte-sensitized phospholipid vesicles, Acc. Chem. Res. 25 (1992) 336-342.
[72] J. L. Thoms, S. W. Barton, D.A. Tirrell, Membrane solubilization by a hydrophobic polyelectrolyte: surface activity and membrane binding, Biophys. J. 67 (1994) 1101-1106.
[73] N. Murthy, J. R. Robichaud, D. A. Tirrell, P. S. Stayton, A. S. Hoffman, The design and synthesis of polymers for eukaryotic membrane disruption, J. Control. Rel. 61 (1999) 137-143.
[74] C. A. Lackey, N. Murthy, O. W. Press, D. A. Tirrell, A. S. Hoffman, P. S. Stayton, Hemolytic activity of pH-responsive polymer-streptavidin bioconjugates, Bioconj. Chem. 10 (1999) 401-405.
[75] C. Y. Cheung, N. Murthy, P. S. Stayton, A. Hoffman, A pH-sensitive polymer that enhances cationic lipid-mediated gene transfer, Bioconj. Chem. 12 (2001) 906-910.
[76] J. Schwartz, S. Zhang, Peptide mediated cellular delivery, Curr. Opin. Molec. Ther. 2 (2000) 162-167.
[77] M. Morris, L. Chaloin, F. Heitz, G. Divita, Translocating peptides and proteins and their use for gene delivery, Curr. Opin. Biotechnol. 11 (2000) 461-466.
[78] S. R. Schwarze, K. A. Hruska, S. F. Dowdy, Protein transduction: unrestricted delivery into all cells? Trends in Cell Biol. 10 (2000) 290-295.
[79] E. L. Snyder, S. F. Dowdy, Protein/peptide transduction domains: potential to deliver large DNA molecules into cells, Curr. Opin. Molec. Ther. 3(2) (2001) 147-152.
[80] P. M. Fischer, E. Krausz, D. P. Lane, Cellular delivery of impermeable effector molecules in the form of conjugates with peptides capable of mediating membrane translocation, Bioconj, Chem. 12(6) (2001) 825-841.
[81] E. Vives, P. Brodin, B. Lebleu, A truncated HIV-1 Tat protein basic domain rapidly translocates through the plasma membrane and accumulates in the cell nucleus, J. Biol. Chem. 272(25) (1997) 16010-16017.
[82] A. Efthymiadas, L. J. Briggs, D. A. Jans, The HIV-1 Tat nuclear localization sequence confers novel nuclear import properties, J. Biol. Chem. 273(3) (1998) 1623-1628.
[83] J. Gariepy, K. Kawamura, Vectorial delivery of macromolecules into cells using peptide-based vehicles, Trends Biotechnol. 19(1) (2001) 21-28.
[84] P. A. Wender, D. J. Mitchell, K. Pattabiramin, E. T. Pelkey, L. Steinman, J. B. Rothbard, The design, synthesis, and evaluation of molecules that enable or enhance cellular uptake: peptoid molecular transporters, Proc. Natl. Acad. Sci USA 97 (2000) 13003-13008.

[85] D. C. Anderson, E. Nochols, R, Manger, D. Woodle, M. Barry, A. R. Fritzberg, Tumor cell retention of antibody Fab fragments is enhanced by an attached HIV TAT protein-derived peptide, Biochem. Biophys. Res. Commun. 194 (1993) 876-884.
[86] S. Fawell, J. Seery, Y. Daikh, C. Moore, L. L. Chen, B. Pepinsky, J. Barsoum, Tat-mediated delivery of heterologous proteins into cells, Proc. Natl. Acad. Sci. USA. 91 (1994) 664-668.
[87] M. Lewin, N. Carlesso, C. H. Tung, X. W. Tang, D. Cory, D. T. Scadden, R. Weissleder, Tat peptide-derivatized magnetic nanoparticles allow in vivo tracking and recovery of progenitor cells, Nature Biotechnol. 18 (2000) 410-414.
[88] A. Nori, K. D. Jensen, P. Kopeckova, J. Kopecek, Cytoplasmic delivery and nuclear targeting of HPMA copolymer-Tat conjugates to ovarian carcinoma cells Proceed. Int'l. Symp. Control. Rel. Bioact. Mater. 28 (2001) 854-855.
[89] P. O. Falnes, J. Wesche, S. Olsnes, Ability of the Tat basic domain and VP22 to mediate cell binding, but not membrane translocation of the diphtheria toxin A-fragment, Biochemistry 40 (2001) 4349-4385.
[90] D. Derossi, G. Chassaing, A. Prochiantz, Trojan peptides: the penetratin system for intracellular delivery, Trends Cell Biol. 8 (1998) 84-87.
[91] M. Magzoub, L. E. Goran Eriksson, A. Graslund, Conformational states of the cell-penetrating peptide penetratin when interacting with phospholipid vesicles: effects on surface charge and peptide concentration, Biochim. Biophys. Acta In Press 2002.
[92] M. Magzoub, K. Kilk, L. E. Goran Eriksson, U. Langel, A. Graslund, Interaction and structure induction of cell-penetrating peptides in the presence of phospholipid vesicles, Biochim. Biophys. Acta. 1512 (2001) 77-89.
[93] M. Tyagi, M. Rusnati, M. Presta, M. Giacca, Internalization of HIV-1 Tat requires cell surface heparin sulfate proteoglycans, J. Biol. Chem. 276(5) (2001) 3254-3261.
[94] M. Silhol, M. Tyagi, M. Giacca, B. Lebleu, E. Vives, Different mechanisms for cellular internalization of the HIV-1 Tat-derived cell penetrating peptide and recombinant proteins fused to Tat, Eur. J. Biochem. 269 (2002) 494-501.
[95] D. Derossi, S. Calvet, A. Trembleau, A. Brunissen, G. Chassaing, A. Prochiantz, Cell internalization of the third helix of the antennapedia homeodomain is receptor-independent, J. Biol. Chem. 271 (1996) 18188-18193.
[96] M. Hallbrink, A. Floren, A. Elmquist, M. Pooga, T. Bartfai, U. Langel, Cargo delivery kinetics of cell-penetrating peptides, Biochim. Biophys. Acta 1515 (2001) 101-109.
[97] S. Futaki, T. Suzuki, W. Ohashi, T. Yagami, S. Tanaka, K. Ueda, Y. Sugiura, Arginine-rich peptides. An abundant source of membrane-permeable peptides having potential as carriers for intracellular protein delivery, J. Biol. Chem. 276 (2001) 5836-5840.
[98] U. Niesner, C. Halin, L. Lozzi, M. Gunthert, P. Neri, H. Wunderli-Allenspach, L. Zardi, D. Neri, Quantitation of the tumor-targeting properties of antibody fragments conjugated to cell-Permeating HIV-1 Tat peptides, Bioconj. Chem. 13 (2002) 729-736.
[99] G. A. Keller, W. Li, R. J. Mrsny, Targeting macromolecular therapeutics to specific cell organelles, ACS Symp. Series, 752 (2000) 168-192.
[100] C. Feldherr, Macromolecular exchanges between the nucleus and cytoplasm, J. Cell. Biochem.Supp. 30/31 (1998) 214-219.

[101] D. Gorlich, U. Kutay, Transport between the cell nucleus and the cytoplasm, Annu. Rev. Cell. Dev. Biol. 15 (1999) 607-660.
[102] J. Moroianu, Nuclear import and export pathways, J.Cell. Biochem. Supp. 32/33 (1999) 76-83.
[103] M. Stewart, R. P. Baker, R. Bayliss, L. Clayton, R. P. Grant, T. Littlewood, Y. Matsuura, Molecular mechanism of translocation through nuclear pore complexes during nuclear protein import, FEBS Lett. 498 (2001) 145-149.
[104] C. W. Pouton, Nuclear import of polypeptides, polynucleotides and supramolecular complexes, Adv. Drug Deliv. Rev. 34 (1998) 51-64.
[105] I. Mattaj, L. Englmeier, Nucleocytoplasmic transport: the soluble phase, Ann. Rev. Biochem. 123 (1998) 265-306.
[106] T. Boulikas, Nuclear localization signals (NLS), Crit. Rev. Euk. Gene Exp. 3(3) (1993) 193-227.
[107] D. Christophe, C. Christophe-Hobertus, B. Pichon, Nuclear targeting of proteins: how many different signals? Cell. Signal. 12 (2000) 337-341.
[108] M. R. Hodel, A. H. Corbett, A. E. Hodel, Dissection of a nuclear localization signal, J. Biol. Chem. 276 (2001) 1317-1325.
[109] H. Salman, D. Zbaida, Y. Rabin, D. Chatenay, M. Elbaum, Kinetics and mechanism of DNA uptake into the cell nucleus, Proc. Natl. Acad. Sci USA 98(13) (2001) 7247-7252.
[110] M. A. Zanta, P. Belguise-Valladier, J. P. Behr, Gene delivery: a single nuclear localization signal peptide is sufficient to carry DNA to the cell nucleus, Proc. Natl. Acad. Sci. USA 96 (1999) 91-96.
[111] J. J. Ludtke, G. Zhang, M. G. Sebestyen, J. A. Wolff , A nuclear localization signal can enhance both the nuclear transport and expression of 1 kb DNA, J. Cell. Sci 112 (1999) 2033-2041.
[112] M. Peitz, K. Pfannkuche, K. Rajewsky, F. Edenhofer, Ability of the hydrophobic FGF and basic TAT peptides to promote cellular uptake of recombinant Cre recombinase: a tool for efficient genetic engineering of mammalian genomes, Proc. Natl. Acad. Sci. USA 99(7) (2002) 4489-4494.
[113] L. Chaloin, P. Bigey, C. Loup, M. Marin, N. Galeotti, M. Piechaczyk, F. Heitz, B. Meuner, Improvement of porphyrin cellular delivery and activity by conjugation to a carrier peptide, Bioconj. Chem. 12 (2001) 691-700.
[114] S. M. Moghimi, A. R. Rajabi-Siahboomi, Recent advances in cellular, sub-cellular and molecular targeting, Adv. Drug Deliv. Rev. 41 (2000) 129-133.
[115] M. P. Murthy, R. A. J. Smith Drug delivery to mitochondria; the key to mitochondrial medicine, Adv. Drug Deliv. Rev. 41 (2000) 235-250.

CHAPTER II

SYNTHESIS AND CHARACTERIZATION OF POLY[N-(HYDROXYPROPYL) METHACRYLAMIDE] COPOLYMERS

This dissertation chapter describes the preparation, derivatization, characterization, and other results obtained for HPMA copolymers prepared for studies described in later chapters. Detailed information regarding the general processing of HPMA copolymers is typically omitted from works in this dissertation intended for publication since it has already been broadly described in the literature. However, this detailed presentation is deemed necessary for the dissertation since HPMA copolymers are a primary component in studies presented in Chapters III, IV, and IV of this dissertation section.

Contents

1 Introduction

1.1 HPMA Copolymers as Drug Carriers

Applications of water-soluble polymers as multi-functional drug carriers was first proposed by Helmut Ringsdorf in 1975, a vision that has since resulted in substantial efforts to produce polymer-drug conjugates with high pharmacological activity.[1] The rapidly emerging field of polymer-based drug delivery has resulted in development of a host of macromolecular constructs including linear polymers, dendrimers, micelles, and nanoparticles.[2-5] Drug delivery systems based on linear copolymers of N-(2-hydroxypropyl) methacrylamide (HPMA) have received considerable attention for use as drug delivery vehicles due to their high water solubility, low toxicity, and ease of derivatization for attachment of therapeutic cargo. This developing drug delivery platform utilizes HPMA copolymers to covalently attach therapeutic agents in a reversible fashion, resulting in a polymer-drug conjugate both stable in circulation and able to release drug at specific sites of desired activity. These HPMA copolymer-drug conjugates exhibit long circulation times and reduced non-target toxicity typical to polymer drug delivery systems as outlined in Chapter II of this dissertation.

The basic polymer structure generally comprises a large fraction of non-reactive, water-soluble HPMA monomer units (> 80%) and a small number of reactive side chains for attachment of therapeutic agents, as shown in Figure 1.2.1. High water-soluble HPMA monomer facilitates increased solubility of hydrophobic drugs as attached side chains. For example, the solubility of the anticancer drug doxorubicin (DOX), increases 10-fold after covalent attachment to poly(HPMA), with similar effects observed with other attached hydrophobic drugs.[6-8] This is important to therapeutic formulations as

many drugs are often intrinsically too insoluble for effective bioavailability when administered alone.

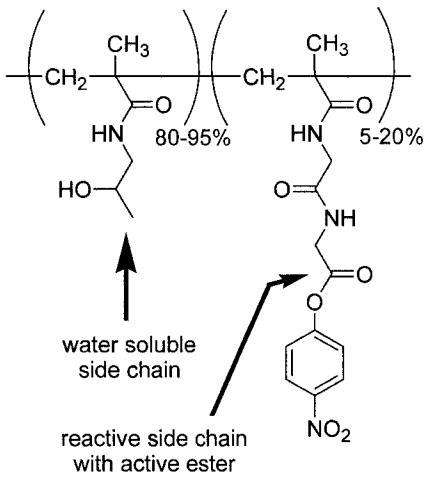

Figure 1.2.1. Structure of reactive HPMA copolymers for attachment of therapeutics. The copolymer comprises HPMA monomer (80-95%) with water soluble side chains and 5-20% of derivatized methacryloyl glycylgycine monomer containing 4-nitrophenol ester-terminated side chains capable of covalent attachment to therapeutic agents.

The reactive side chains in the methacryloyl glycylglycine copolymer units are designed to allow covalent attachment of therapeutics, often exploiting nucleophilic functional groups on the therapeutic agent for reaction with terminal ester moieties. Furthermore, these pendant side chains can be designed to degrade at the desired site of activity and release free drug by mechanisms such as enzymatic cleavage or pH-dependent hydrolysis after cellular internalization and trafficking to internal organelles. Release of covalent poly(HPMA)-bound drug from side chains containing peptide sequences specific to the enzymes cathepsin B, trypsin, and chymotrypsin has been shown.[9-13] Alternatively, hydrazide-containing polymer side chains have been synthesized that allow reversible covalent attachment of therapeutics by condensation with carbonyl groups present within some drug molecules, forming a pH-labile

hydrazone bond that hydrolyzes at acidic pH (< 5.0).[14, 15] Recently, semi-telechelic HPMA polymers with terminal carboxyl, methyl ester, hydrazide and amino chemistries have been described for single-point drug-polymer attachment to be used for protein modification, similar to PEGylation.[16]

Much of the pioneering work for developing HPMA copolymers as therapeutic carriers has been performed by Kopecek, dating to the early 1970's.[17] Since the advent of this technology, a large number of therapeutic agents have been attached to poly(HPMA) including the anti-cancer drugs, doxorubicin (adriamycin) and daunomycin, paclitaxil, platinate, calichemicin, NMR contrast agents and therapeutic siRNAs.[18-22] Additionally, two-component drug delivery systems have been described using HPMA copolymers, in true accordance with the original multi-dimensional drug delivery platform envisioned by Ringsdorf. These advanced drug delivery systems have been synthesized to contain both cell-surface receptor ligands for enhanced targeting of polymer conjugates to specific cell types and small molecule therapeutics. Targeting ligands used to date on HPMA systems include lectins, the Epstein-Barr virus binding epitope, galactose, lactose, OV-TL16 antibody, and the Tat peptide.[23-29] Thorough reviews of therapeutic HPMA copolymer-drug conjugates and their efficacy have been published.[6, 19, 30, 31]

1.2 Synthesis of HPMA Copolymers

HPMA copolymers are typically generated using free-radical polymerization of monomer methacrylamide groups initiated with 2,2'-azobisisobutyronitrile (AIBN). Figure 1.2.2 shows the polymerization process in the context of this work; namely classic free radical generation, initiation, propagation and termination.

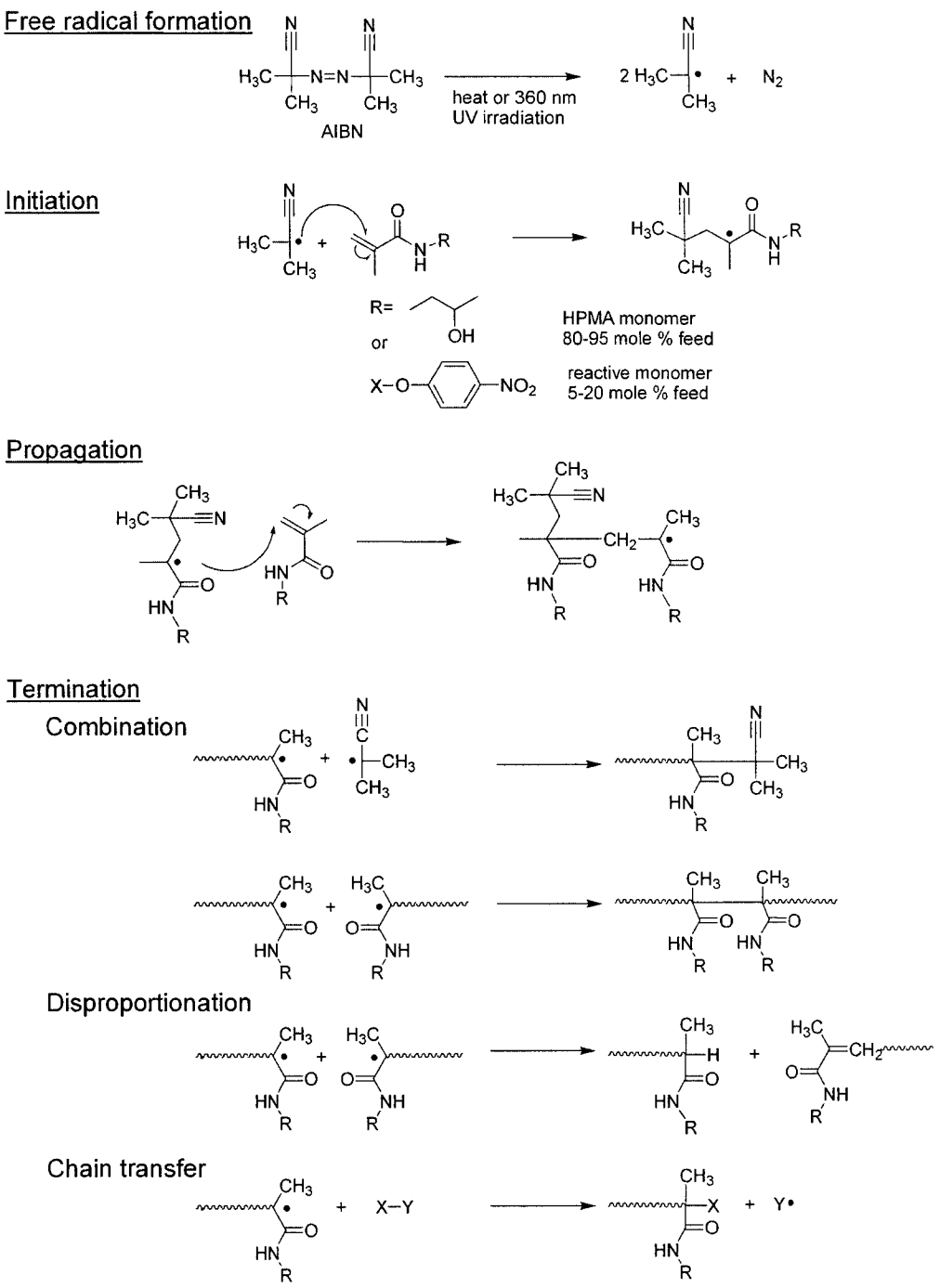

Figure 1.2.2. Free radical-initiated polymerization of HPMA copolymers.

Decomposition of AIBN occurs at relatively low temperatures (half-life = 1.3 hr at 80 °C), with the driving force for decomposition being formation of nitrogen and the resonance-stabilized cyanopropyl radical.[32] The resultant free radicals then react with π electrons contained in the electrophilic methacrylamide double bonds. One π electron in the double bond can spin pair with the free radical electron present on decomposed AIBN initiator to form a new carbon-carbon bond. The other π electron in the reacted double bond is transferred to the most substituted carbon on the monomer, generating another reactive free radical. Repeat of this process (propagation) continues to elongate the polymer chain in a stepwise fashion.

Chain propagation is in continuous competition with other processes that destroy free radical reactivity and terminate the growing polymer chain. Reactive radicals can simply pair with other radicals present in the polymerization milieu to form unreactive carbon bonds by combination. Paramagnetic species such as O_2 present in the reaction mixture have unpaired electrons that can also combine with free radicals to terminate chain growth or quench activated initiator. Additionally, atom transfer (usually hydrogen) between two radical containing species can lead to deactivation of one of the polymer chains involved in the transfer, a process called disproportionation. Finally, chain transfer of free radicals from a growing polymer chain to other species in the reaction mileu (initiator, monomer, polymer or solvent molecules) in combination with atom extraction (usually hydrogen) also terminates polymerization. However, because a free radical remains after a chain transfer event, initiation can occur with unreacted monomer remaining in solution, thus the presence of excess chain-transfer agent reduces the

molecular weight of polymer product, but also adds to the breadth of the molecular weight distribution which results.

The most utilized polymerization procedure to produce poly(HPMA) entails dissolving monomers (12.5 w/v%) and AIBN (0.06 wt %) in acetone or an acetone/DMSO mixture and heating to 60 °C for 24 hrs. Polymerization in acetone is convenient as polymer product precipitates and is easily isolated by filtration. Recovery of polymer from polymerization in acetone/DMSO mixtures is accomplished by precipitation of the reaction mixture into excess acetone. Polymers produced in this fashion typically have molecular weight (Mw) values from ~ 13,000 - 30,000 and polydispersities of 1.3-2.3.[14, 15, 19, 23, 33] If lower polydispersity is desired, polymerization of monomers utilizing an atom transfer radical polymerization (ATRP) method has been described resulting in polydispersities less than 1.15.[34] Reactive monomer units are incorporated into the polymer backbone by adding monomers with desired side-chain reactivity into the polymerization solution, with final reactive group content in the copolymer product achieved by controlling the ratio within the monomer feed. The most common reactive monomers used are those containing short peptide units (2-4 amino acids) with C-terminus carboxylic acid groups modified with 4-nitrophenyl esters.

1.3 Purification of HPMA Copolymers using Size Exclusion Chromatography

Size exclusion chromatography (SEC) is a convenient and useful technique to purify polymer samples and determine size or molecular weight after appropriate calibration. SEC is a unique form of chromatography since analytes are not separated by chemical interactions with the column material, but rather by their differential ability to

diffuse through pores in the column matrix. A variety of resin materials are available as pre-packed columns for use in pump-driven systems, or as loose resins for homemade columns. The basic principle of SEC is shown in Figure 1.2.3. Common HPLC systems are easily adapted to SEC by changing the type of column with preparative scale columns available for bulk purifications.

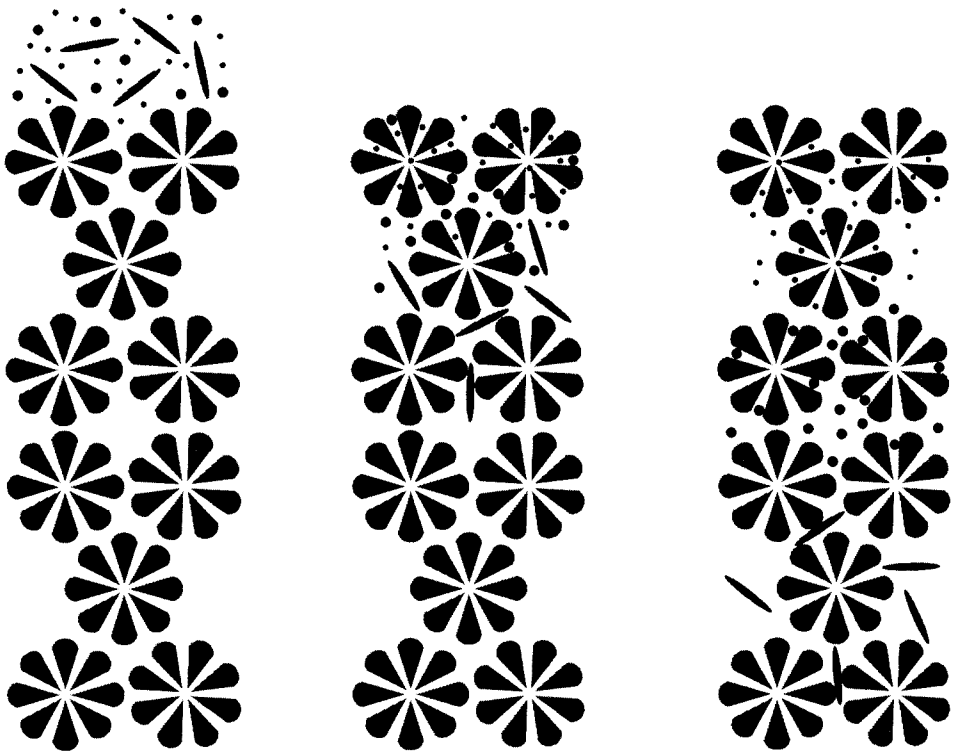

1) Sample loaded onto column.

2) As mobile phase and sample pass through the column, small molecules partition into the column matrix.

3) As mobile phase continually passes through the column, large molecules unable to diffuse into the column matrix elute first, while small molecules are retained within the column.

Figure 1.2.3. Schematic: Illustration of the Principles of size exclusion chromatography (SEC).

SEC packing material consists of small particles (~ 5-50 μm) of a crosslinked polymer (usually dextran or agarose) containing pores of a defined size distribution.

These pores act as molecular sieves, requiring molecules smaller than the pore size to partition within the pore and travel a more tortuous path prior to eluting at the end of the column. This relationship is shown in the equation:

$$\mathbf{V_e = V_o + KV_i}$$

where V_e is the elution volume, V_o = is the free volume outside of gel particles, K is the distribution constant for molecules into the matrix pores and V_i is the volume within gel particles.[35] For molecules too large to enter gel pores, K = 0 and the elution volume equals V_o, or the void volume of the column. Molecules that can partially enter the column have K values between 0 and 1 and fractionation occurs. Molecules that can freely disperse within the gel pores have a K value of 1 and elute from the column last with the greatest elution volume.

Slow flow rates (< 0.5 mL/min) are generally used to maximize small molecule diffusion into the pores resulting in greater sample fractionation. Additionally, slow flow rates protect the column material since SEC resin materials are fragile and high flow rates and increased pressure can crush the pores, rendering the column useless. Since this separation is not based on chemical interactions with the column matrix, SEC experiments can be conducted in a wide range of solvents or buffers to match the properties of the sample (i.e. solubility, stability, etc.).

SEC purification strategies offer a much faster alternative to other methods such as dialysis, which can require days, and provides some ability to fractionate samples into different, multiple populations based on elution volume dicrimination. A variety of SEC resin materials have been developed with defined exclusion limits (where K = 0) allowing easy separation of high molecular weight polymer product from lower

molecular weight reactants or buffer salts resulting in bimodal separation between high and low molecular weigh components.

1.4 Measuring Copolymer Reactive Ester Side Chain Content

As described above, reactive side chains in the HPMA copolymers used in this work were designed to contain 4-nitrophenol active esters. After copolymerization with various HPMA and co-monomer feed ratios, reactive side chain content in the polymer product is easily determined by incubating the sample in basic solutions containing NaOH (0.05 M) to cleave the active ester site and release the bright yellow-colored 4-nitrophenolate anion which strongly absorbs at 400 nm ($\varepsilon = 1.74x10^4\ M^{-1}cm^{-1}$) (Figure 1.2.4). This assay is used to estimate the mole % of the reactive side chain component by knowing the mass of the polymer sample and incubating in a known volume of NaOH solution.

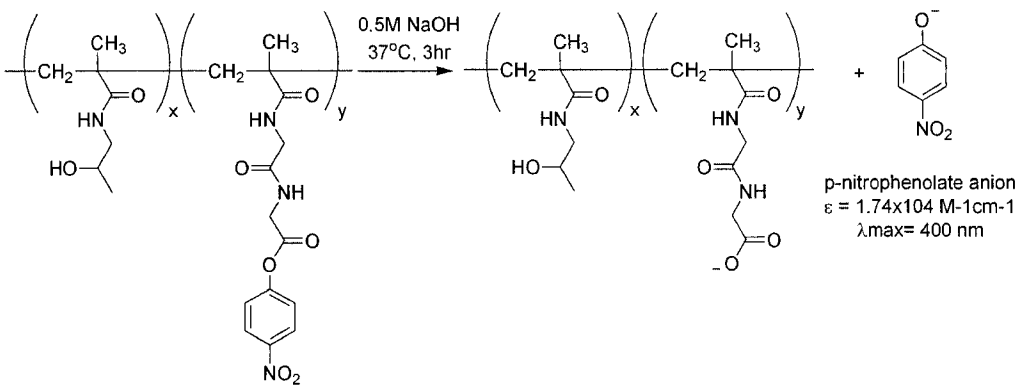

Figure 1.2.4. Base (NaOH) cleavage assay used to estimate active ester content in HPMA copolymers.

1.5 Measuring Copolymer Hydrazide Content

As described above, reactive ester side chains within HPMA copolymers were modified to contain hydrazide functionality to allow subsequent attachment of

ketone/aldehyde containing heterobifunctional crosslinkers via a hydrazone bond (Chapters IV and VI of this dissertation). Determination of hydrazide content in derivatized HPMA copolymers was determined using a trinitrobenzene sulfonic acid (TNBSA) assay. The TNBSA assay is a well-known assay for quantification of primary amines and hydrazide groups.[36-41] This colorimetric assay is based on the bathochromic shift resulting from extended conjugation of the π system with the nonbonding electrons present on reacted amine groups as shown in Figure 1.2.5. The lightly colored TNBSA starting material turns bright orange/red upon reaction with amines, allowing copolymer hydrazide content to be estimated using standard solutions prepared with a known hydrazide containing molecule.

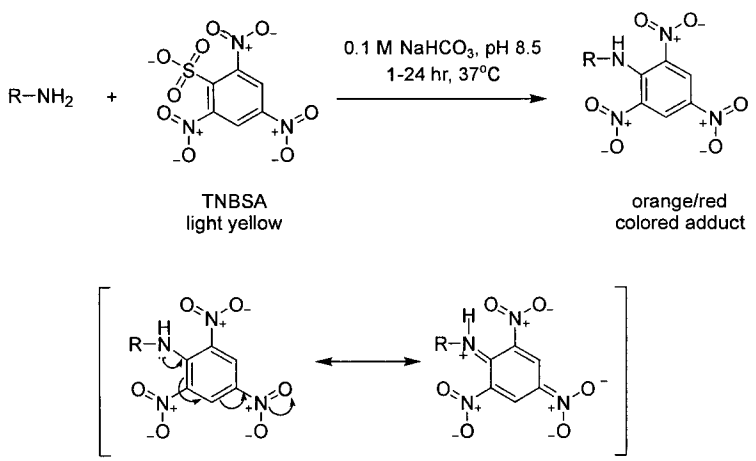

Figure 1.2.5. The TNBSA assay for determination of primary amine content.

2. Experimental

Materials

Glycylglycine (99+%), DL-1-amino-2-propanol (99+%), 4-nitrophenol (99+%), and dicyclohexyl carbodiimide (DCC, 99%) were obtained from Acros Organics (Geel,

Belgium). Methacryloyl chloride (97%), 2,2'-azobisisobutyronitrile (98%), hydrazine monohydrate (97%), and trinitrobenzene sulfonic acid (5% w/v solution in methanol) (TNBSA) were purchased from Sigma Aldrich (St. Louis, MO). All solvents were ACS grade and were purchased from Fisher Scientific (Fair Lawn, NJ). Dimethyl sulfoxide-d_6 containing 0.05% w/v tetramethylsilane was purchased from Cambridge Isotope Laboratories, Inc. (Andover, MA). Spectra/Por 1, 6-8 kDa molecular weight cutt-off dialysis tubing was obtained from Spectrum Laboratories, Inc. (Rancho Dominguez, CA). Poly(HPMA) molecular weight standards were a gift from Dr. P. Kopeckova at the Univ. of Utah. All NMR spectra were recordered on a Magnex Scientific Inova 400 MHz instrument in dimethyl sulfoxide-d_6 containing 0.05% w/v tetramethylsilane as an internal standard. Absorbance measurements were obtained using a Varian Carey 500 Scan instrument.

2.1 Synthesis of Copolymer Components

2.1.1 Synthesis of HPMA monomers

N-(2-hydroxypropyl)methacrylamide (HPMA) was synthesized using a previously published proceedure by reaction of DL-1-amino-2-propanol with methacryloyl chloride as shown in Scheme 1.2.1.[42]

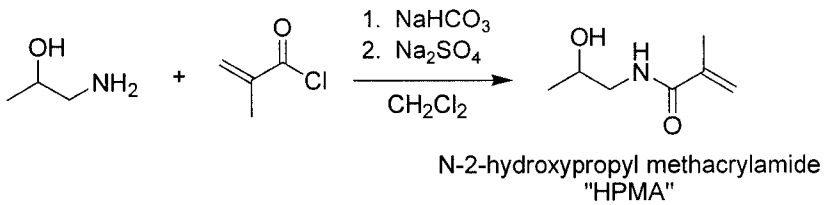

Scheme 1.2.1. Synthesis of HPMA monomer with water-soluble side chain.

1-amino-2-propanol (24.3 mL, 0.311 mol, 1 eq) and sodium bicarbonate (33.6 g, 0.40 mol, 1.3 eq) was added to CH_2Cl_2 (85 mL) and the suspension was purged with N_2, capped, and placed in an ice bath. A second solution containing methacryloyl chloride (29.5 mL, 0.304 mol, 0.98 eq) in CH_2Cl_2 (40 mL) was prepared and cooled to –20 °C. Next, the methacryloyl chloride solution was slowly added to the 1-amino-2-propanol solution under N_2 with vigorous stirring. After complete addition the reaction was stirred for 15 min at 25 °C, and anhydrous Na_2SO_4 (10 g) was added. The solution was manually stirred for an additional 10 minutes and the solution was filtered through paper. Solids were washed twice with 20 mL CH_2Cl_2 and the filtrates were combined. The combined filtrates were concentrated under vacuum to ~ 50% of the original volume then placed in a –20 °C freezer overnight. HPMA crystals were collected by filtration and washed with cold acetone. Product was purified by repeated crystallization from acetone. Typical yield: ~15.0 g, 30%, semi-transparent white crystals. ^{1}H NMR, δ ppm: 1.008 (d, 3H), 1.848 (s, 3H), 3.041 (t, 2H), 3.678 (m, 1H), 4.693 (s, 1H), 5.483 (d, 2H), 7.820 (s, 1H). Mp = 72 °C (sharp).

2.1.2 N-methacryloyl glycylglycine 4-nitrophenyl ester with reactive side chain

N-methacryloyl glycylglycine 4-nitrophenyl ester (MAGGONP) was prepared according to previous work.[43, 44] Synthesis began with preparation of methacryloyl glycylglycine (MAGG) using the Schotten-Baumann procedure in aqueous alkaline medium as shown in Scheme 1.2.2.

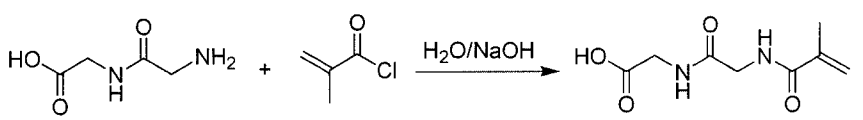

methacryloyl glycylglycine
"MAGG"

Scheme 1.2.2. Synthesis of methcryloyl glycylglycine (MAGG).

Glycylglycine (10 g, 76 mmol, 1 eq) was dissolved in 0.5 M NaOH (15.1 mL, 76 mmol, 1 eq) over 30 minutes then cooled to 0 °C. Methacryloyl chloride (7.5 mL, 77 mmol, 1eq) and 5.0 M NaOH (15.1 mL, 76 mmol, 1 eq) were added dropwise and simultaneously to the glycylglycine solution while stirring at 0 °C. After complete addition, the reaction was stirred for an additional hour at room temperature, then concentrated HCl was added until a dense white precipitate formed. Solids were collected by filtration and washed with cold water until the filtrate was neutral. Crude solid product was dried under vacuum and further purified by repeat crystallization from 50/50 (v/v) ethanol/water. Typical yield: ~5.0 g, 30%, small white crystals. ^{1}H NMR: (400 MHz, DMSO-d_6) δ ppm: 1.876 (s, 3H), 3.766 (d, 4H), 5.561 (d, 2H), 8.132 (t, 1H), 8.190 (t, 1H), 12.594 (s, 1H). Mp = 175-205°C.

Methacryloyl glycylglycine (MAGG) was esterified with 4-nitrophenol using carbodiimide chemistry to yield methacryloyl glycylglycine 4-nitrophenyl ester as shown in Scheme 1.2.3.

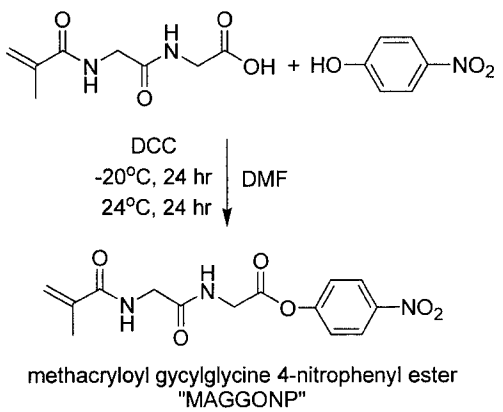

Scheme 1.2.3. Synthesis of methacryloyl glycylglycine 4-nitrophenyl ester (MAGGONP).

MAGG (5.23 g, 26.1 mmol, 1 eq) was dissolved in dry dimethyl formamide (DMF, 50 mL) and cooled to –15 °C. 4-nitrophenol (4.0 g, 28.71 mmol, 1.1 eq) and dicyclohexylcarbodiimide (DCC) (5.39 g, 26.1 mmol, 1.0 eq) were each dissolved in DMF (26 mL) in separate flasks and cooled to –15 °C. After all solutions were cooled, the 4-nitrophenol and DCC solutions were added dropwise to the MAGG solution sequentially while stirring. The reaction was stirred for 4 hr at –15 °C followed by 24 hr at –20 °C. Upon complete reaction, dicyclohexyl urea (DCU) byproduct was removed by filtration. The filtrate was collected and allowed to sit at room temperature for 24 hrs under N_2 and then cooled to –20 °C. The solution was again filtered to remove DCU crystals. The filtrate was retained and 100 mL cold water was added. This mixture was placed on ice for 1 hr. The pale-yellow solids were collected by filtration and dried under vacuum. Hot 50/50 water/ethanol was added to the dried solids until ~ 80% dissolved. The solution was boiled for an additional 10 minutes then filtered. Small, pale-yellow, fish-scale crystals formed slowly in the filtrate over a 3 hr period at room temperature. Solids were collected by filtration and dried under vacuum. Typical yield ~ 2.0 g, 22%, yellow crystals. ^{1}H NMR, δ ppm: 1.884 (s, 3H), 3.809 (d, 2H), 4.176 (d, 2H), 5.577 (d, 2H), 7.435 (m,2H), 8.267 (t, 1H), 8.326 (m, 2H), 8.479 (t, 1H). Mp = 143-160°C.

2.2 Synthesis of HPMA copolymers:

HPMA copolymer was prepared by free radical initiated polymerization as previously described using 12.5% (w/v) monomer and 0.6% initiator (AIBN) in freshly distilled acetone (Scheme 1.2.4).

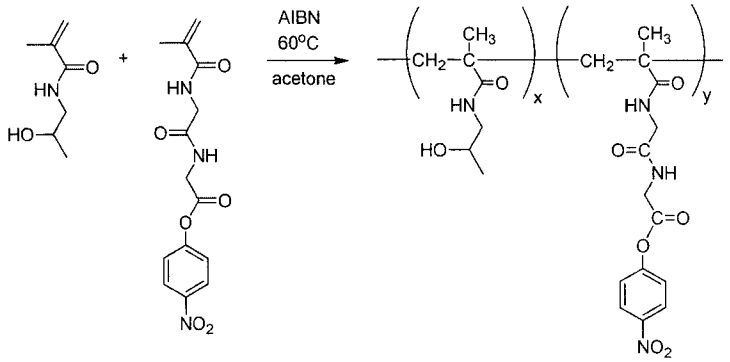

Scheme 1.2.4. Synthesis of poly(HPMA). Values for x and y are typically 80-95 mol% and 5-20 mol% respectively.

Reactive side chain content in the polymer product was controlled by feed ratio of MAGGONP. The following is a typical procedure to produce an HPMA copolymer with 95 mole % HPMA units and 5 mole % MAGGONP units. HPMA monomer (3.35 g, 23.4 mmol, 1 eq), MAGGONP (0.40 g, 1.2 mmol, 0.05 eq), and AIBN (0.18 g, 1.1 mmol, 0.05 eq) were added to acetone (26 mL) in a Chemglass 50 mL pressure flask containing a magnetic stirbar. The solution was degassed by sonication under N_2 flow for 5 minutes and then capped. This solution was stirred until all solids dissolved (~ 30 minutes) and placed in a hot water bath and stirred at 60 °C for 24 hrs. After complete reaction, solids were collected by filtration, washed with cold acetone, and dried under vacuum. Solids were further purified by repeat precipitation from 90/10 CH_2Cl_2/MeOH (v/v) into a 10-fold excess of cold acetone. Typical yield: ~ 2.2 g, 56%, cream colored powder.

2.3 Detemination of Active Ester Content in HPMA Copolymers.

HPMA copolymer product was dissolved in 0.05 M NaOH at concentrations of 0.08-0.1 mg/mL then stirred at 37 °C for 3 hrs. The absorbance of the resulting bright-

yellow solutions was measured at 400 nm and ester content was estimated using the molar extinction coefficient ($\varepsilon = 1.74 \times 10^4\ M^{-1}cm^{-1}$) of the released p-nitrophenolate anion and the original mass of the polymer sample. The molar extinction coefficient was determined by serial dilution of a p-nitrophenol solution in 0.05 M NaOH. No increase in absorbance after incubation for 3 hr at 37 °C was observed, showing complete cleavage p-nitrophenol esters.

2.4 Hydrazide Dramatization of HPMA Copolymers

Hydrazide groups were generated on HPMA copolymers by reaction of hydrazine with active esters present on MAGGONP side chains as previously described (Scheme 1.2.5).[14]

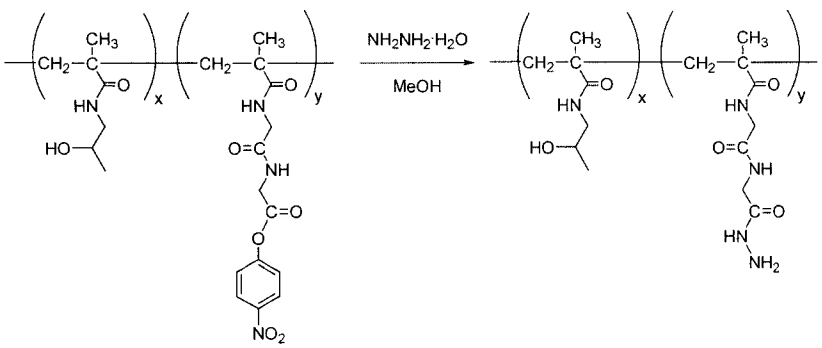

Scheme 1.2.5. Incorporation of hydrazide groups into poly(HPMA).

A representative procedure follows: HPMA/MAGGONP copolymer (5 mole % MAGGONP, 2.0 g, 0.51 mmol active esters, 1 eq) was dissolved in methanol (25 mL). Hydrazine monohydrate (267 uL, 5.1 mmol, 10 eq) was added to 25 mL methanol in a separate flask. The HPMA copolymer solution was added to the hydrazine monohydrate solution dropwise while stirring over ~ 30 minutes then purged with N_2, capped, and stirred for 3 hr at room temperature. After complete reaction, the mixture was slowly

added to 75 mL cold water while stirring, then transferred to dialysis tubing (SpectraPore 7, 6-8 kDa MWCO) and dialyzed against water for 3 days with frequent changing of the dialysis water. Polymer product was isolated by lyophilization. Typical yield: ~ 1.2 g, 60%, white powder.

2.5 Analysis of HPMA Copolymer Hydrazide Content

Hydrazide content in HPMA copolymers was estimated using a modified trinitrobenzene sulfonic acid (TNBSA) assay. TNBSA assay compared ethyl carbazate and methacryloyl glycylglycine hydrazide (MAGGH) as standards. MAGGH was synthesized by reaction of MAGGONP with hydrazine monohydrate. MAGGONP (750 mg, 2.33 mmol, 1 eq) was dissolved in methanol (90 mL) and then slowly added to a solution of hydrazine monohydrate (567 μL, 11.7 mmol, 5 eq) in 10 mL methanol. The reaction was stirred for 5 hr at room temperature under N_2. After complete reaction, solvent was removed under vacuum to yield crude solids. The resulting solids were dissolved in 90/10 CH_2Cl_2/methanol (40 mL), filtered and loaded onto a silica gel column (2.5 x 17.5 cm) equilibrated with 90/10 CH_2Cl_2/MeOH. After the sample was loaded onto the column, the elution solvent was changed to MeOH. MAGGH eluted after the visible yellow 4-nitrophenol band. Yield: 0.156 g, 31%, white powder. ^{1}H NMR, δ ppm: 1.836 (s, 1H), 3.619 (d, 2H), 3.712 (d, 2H), 4.165 (d, 2H), 5.341 (d, 1H), 5.698 (d, 1H), 8.048 (t, 1H), 8.131 (t, 1H), 8.907 (s, 1H). ^{13}C NMR, δ ppm: 18.479, 40.779, 42.402, 119.752, 139.356, 167.597, 168.011, 169.204. MS-FAB m/z = 215.1147 $[M+H]^+$(calculated m/z = 215.1144 $[M+H]^+$)

For each poly(HPMA) hydrazide content analysis, stock solutions of 0.1% w/v TNBSA, ~ 2 x 10^{-4} M MAGGH, and ~ 2 x10^{-4} M ethyl carbazate were prepared in 0.1 M $NaHCO_3$, pH 8.5. MAGGH and ethyl carbazate solutions were further diluted with 0.1 M $NaHCO_3$ to generate standards in the range of ~0.3 - 2 x 10^{-4} M. Next, hydrazide-derivatized HPMA copolymers were dissolved in 0.1 M $NaHCO_3$ at a concentration of 0.2-0.4 mg/mL. Sample or standard solutions (1.0 mL) were combined with 0.5 mL TNBSA stock solution and stirred for 1.5 – 48 hr at 37 °C. After incubation, sample absorbance was measured at 505 nm and hydrazide content was estimated from the equation of the line fit to MAGGH or ethyl carbazate standards plotted as concentration vs. absorbance.

2.6 Molecular Weight Estimation of HPMA Copolymers

Molecular weight of synthesized poly(HPMA) copolymer was estimated following displacement of reactive ester groups with 1-amino-2-propanol by size exclusion chromatography using an HP1050 HPLC system equipped with an HP1040A refractive index detector and Biosil 125 column. The instrument was calibrated with poly(HPMA) samples of known molecular weight. For each characterization, sodium phosphate buffer (0.05 M, pH 7.4) was used as the mobile phase with a 100 μL sample injection and a 0.5 mL/min flow rate.

3 Results and Discussion

3.1 HPMA Copolymer Preparation and Characterization

HPMA copolymers were easily prepared using free radical initiated polymerization as described in the literature. A series of HPMA copolymers were prepared with active ester content ranging from 5-20 mol % to test the ability to control active ester content by monomer feed ratio. Copolymer reactive side chain was typically within 2% of the target composition resulting from careful control of monomer feed ratios as shown in Table 1.2.1.

Table 1.2.1. Composition and molecular weight analysis of synthesized HPMA copolymers.

target mole% esters	actual mole % esters†	moles active esters/g copolymer (x 10^{-4})	approximate Mw (kDa)‡	average esters/polymer
5	4.9 ± 1.5	3.3 ± 0.9	18.2 ± 3.0	2.8
10	9.8 ± 1.6	6.1 ± 0.9	18.5 ± 1.0	5.6
15	13.2 ± 0.4	7.9 ± 0.2	16.6 ± 3.3	6.8
20	19.9 ± 0.2	11.5 ± 0.1	15.6 ± 1.7	9.7

† 5 mole % data represent 4 reactions analyzed 4 times each; 10 mole % data represent 3 reactions analyzed 4 times each; 15 and 20 mole % data represent one reaction analyzed 4 times.
‡ 5 and 10 mole % data represent 2 reactions analyzed 2 times each; 15 and 20 mole % data represent one reaction analyzed 2 times.

Analysis of poly(HPMA) by size exclusion chromatography showed formation of homogeneous polymer product of ~ 18 kDa molecular weight. A calibration curve using poly(HPMA) standards, and typical chromatogram of HPMA copolymer product are shown in Figure 1.2.6. The single peak at 22 min in Figure 1.2.6b indicates a

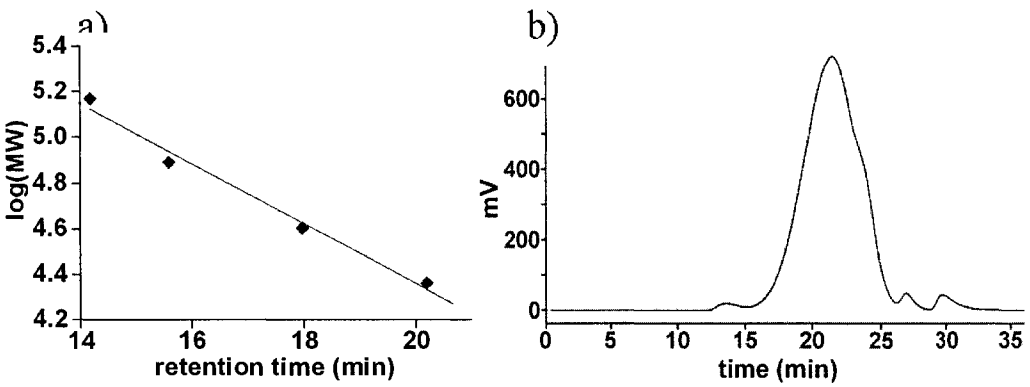

Figure 1.2.6. SEC analysis of poly(HPMA). a) column calibration with poly(HPMA) standards. b) Synthesized poly(HPMA) sample.

homogenous polymer product, with the small peak at 27 min most likely trace monomer. The small peak at 30 minutes was attributed to the carrier buffer eluting at the column dead volume.

Hydrazide functionality was readily achieved after reaction with hydrazine monohydrate in methanol. One concern with this reaction is crosslinking of polymer chains due to the dual functionality of the hydrazine nucleophile. This was prevented by slow addition of copolymer solution to concentrated hydrazine solution, maintaining hydrazine concentration in continuous excess. Analysis of HPMA copolymer by SEC after hydrazide derivatization showed a single peak at ~ 22 minutes, similar to that shown in Figure 1.2.6b, confirming that crosslinking did not occur under these conditions.

3.2 Optimization of TNBSA assay conditions

Previous work describing synthesis of hydrazide derivatized HPMA copolymers utilized the TNBSA assay to quantify conversion of active ester side chains to hydrazide groups using standard curves based on ethyl carbazate.[14] Initial attempts to quantify hydrazide groups on HPMA copolymers always resulted in a value higher than expected (~130-160% of the expected value). A comparison of MAGGH and ethyl carbazate standards is shown on Table 1.2.2.

Table 1.2.2. TNBSA assay hydrazide content analysis of poly(HPMA)-hydrazide using MAGGH and ethyl carbazate standards.

standard	mole ONP/g ($x 10^{-4}$)†	mole hydrazide/g ($x 10^{-4}$)‡	mole % hydrazide	% conversion
ethyl carbazate	3.0 ± 0.1	4.3 ± 1.2	6.6 ±1.5	143
MAGGH	3.0 ± 0.1	3.6 ± 0.9	5.1 ±1.0	120

† n = 4, ‡ n =18.

The poly(HPMA)-hydrazide TNBSA adduct differed in color from the ethyl carbazate TNBSA adduct, which appeared yellow-orange and red-orange respectively. It was suspected that the difference in structure between the two hydrazide-containing compounds affected the spectral properties of TNBSA-hydrazide adduct and thus the calculated hydrazide content in HPMA copolymers. To confirm this hypothesis, a hydrazide derivative that more closely matched poly(HPMA) reactive side chain chemistry (MAGGH) was synthesized from MAGGONP monomer (Figure 1.2.7).

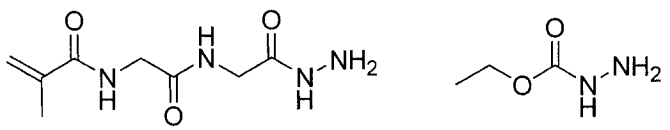

Figure 1.2.7. Structures of MAGGH and ethyl carbazate TNBSA assay standards used in this work.

The absorbance spectra of MAGGH and ethyl carbazate solutions after reaction with TNBSA for 4 hrs are shown in Figure 1.2.8.

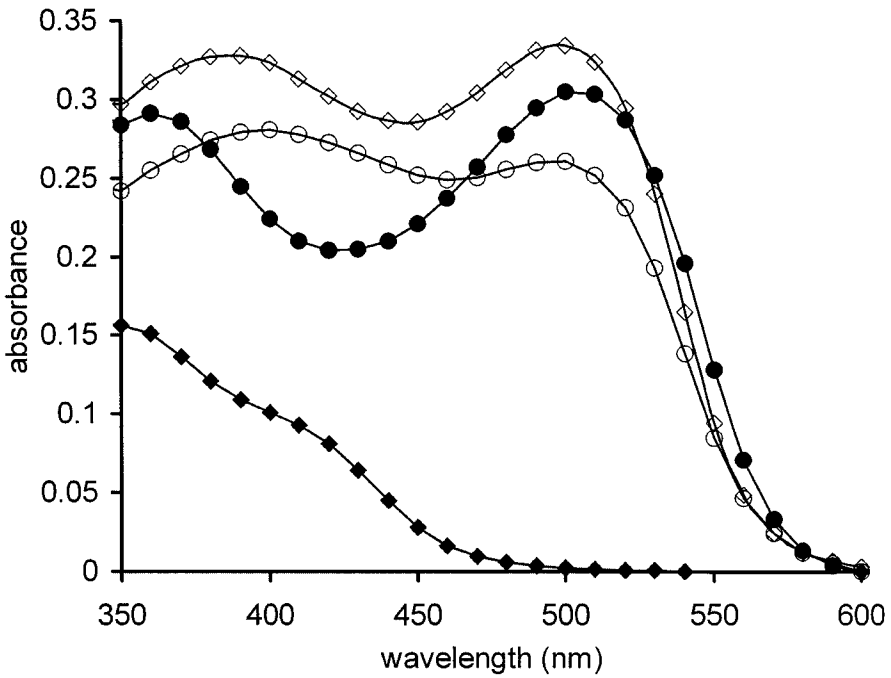

Figure 1.2.8. Absorbance spectra of hydrazide-containing samples with TNBSA for 4 hr in 0.1M $NaHCO_3$, pH 8.5.◇ 4 x 10^{-4} M MAGGH,○ ~ 4 x 10^{-4} M poly(HMPA)-hydrazide, ● 4.75 x 10^{-4} M ethyl carbazate,◆ TNBSA stock solution control.

As expected, the absorbance spectrum of MAGGH closely matched the absorbance spectrum of hydrazide-derivatized poly(HPMA). Additionally, the intensity of MAGGH-TNBSA absorbance at λ_{max} was found to be ~ 10% higher than the absorbance of the ethyl carbazate-TNBSA adduct at the same concentration. This was likely due to spectral overlap between the primary and secondary peaks in the absorbance spectrum, which is more substantial in MAGGH and poly(HPMA)-hydrazide than in ethyl carbazate. This difference in absorbance intensity could also be due to a difference in reactivity resulting from chemistries in proximity to hydrazide functionality. It is possible that increased electron withdrawing ability of the ester group in ethyl carbazate

may decrease the reactivity of the hydrazide group. If this is the case, longer incubation times of ethyl carbazate-TNBSA reactions may lead to more accurate hydrazide content estimation. To test this hypothesis standard curves of MAGGH and ethyl carbazate were incubated for various times ranging from 2-48 hours. Standard curves generated using MAGGH resulted in higher absorbance than ethyl carbazate at all times measured, with representative curves from 2 and 48 hours shown in Figure 1.2.9.

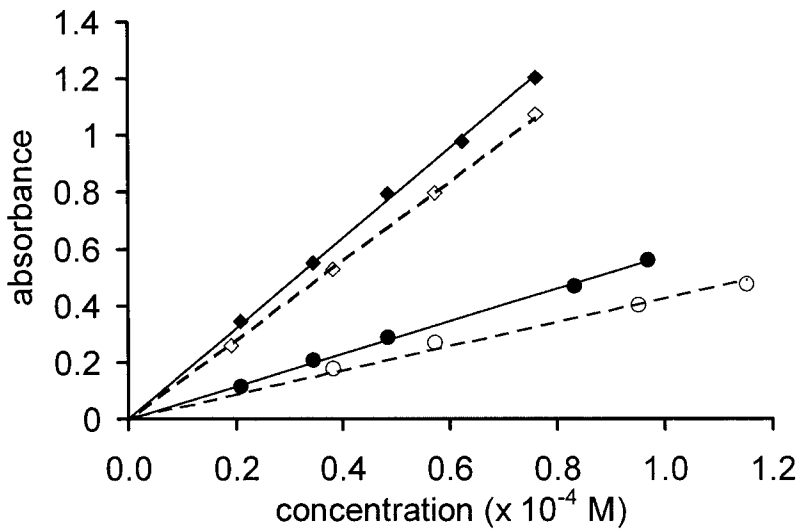

Figure 1.2.9. Comparison of MAGGH and ethyl carbazate TNBSA assay standards at 2 and 48 hr incubation. ● MAGGH, 24 hr incubation, ○ ethyl carbazate 24 hr, ◆ MAGGH 48 hr incubation, ◇ ethyl carbazate 48 hr incubation.

The observed increased absorbance of MAGGH standards compared to ethyl carbazate even after extended incubation prevents precise determination of hydrazide content in copolymer samples using ethyl carbazate standards. Spectral overlap of the primary and secondary peaks in TNBSA-amine adducts, not differences in reactivity, results in higher absorbance values in MAGGH and poly(HPMA) samples. However, use of ethyl carbazate as a standard may allow precise determination of hydrazide content

in future work. Close inspection of Figure 1.2.8 shows that the absorption spectra of MAGGH and ethyl carbazate cross at 520 nm. Further investigation of absorbance spectra of MAGGH and ethyl carbazate TNBSA adducts over a range of concentrations might show this wavelength to be an isosbestic point between the two standard-TNBSA adducts allowing use of ethyl carbazate as a precise standard for hydrazide content determination.

4 Conclusions

Reactive HPMA copolymers provide a starting point for the synthesis of complex copolymer systems for drug delivery application. Carefully designed strategies for subsequent derivatization allow incorporation of key chemistries as attachment sites for therapeutic drugs. Specific to this work, the hydrazide functionality allows subsequent attachment of ketone-containing molecules via a pH-labile hydrazone bond. Quantification of hydrazide functionality required use of standards for TNBSA analysis that closely match the chemistry contained on reactive poly(HPMA) side chains. The MAGGH standard prepared in this study allows accurate determination of hydrazide content and is in good agreement with original copolymer reactivity. However, future studies with ethyl carbazate standards and identification of an isosbestic point with MAGGH may allow use of ethyl carbazate standards as an inexpensive commercially available alternative.

References

1. Ringsdorf H. Structure and properties of pharmacologically active polymers. Journal of Polymer Science, Polymer Symposia 1975;51(Int. Symp. Macromol. Honor Professor Herman F. Mark):135-53.
2. Svenson S. Carrier-based drug delivery. Washington, DC [Oxford, England ; New York]: American Chemical Society ; Distributed by Oxford University Press; 2004.
3. Park K, Mrsny RJ, American Chemical Society. Meeting. Controlled drug delivery : designing technologies for the future. Washington, DC: American Chemical Society; 2000.
4. Wise DL. Handbook of pharmaceutical controlled release technology. New York: Marcel Dekker; 2000.
5. Mathiowitz E. Encyclopedia of controlled drug delivery. New York: Wiley; 1999.
6. Putnam D, Kopecek J. Polymer conjugates with anticancer activity. Biopolymers Ii 1995;122:55-123.
7. Vasey PA, Kaye SB, Morrison R, et al. Phase I clinical and pharmacokinetic study of PK1 [N-(2-hydroxypropyl)methacrylamide copolymer doxorubicin]: first member of a new class of chemotherapeutic agents-drug-polymer conjugates. Cancer Research Campaign Phase I/II Committee. Clin Cancer Res 1999;5(1):83-94.
8. Thanou M, Duncan R. Polymer-protein and polymer-drug conjugates in cancer therapy. Curr Opin Investig Drugs 2003;4(6):701-9.
9. Kopecek J, Rejmanova P, Chytry V. Polymers Containing Enzymatically Degradable Bonds .1. Chymotrypsin Catalyzed-Hydrolysis of Para-Nitroanilides of Phenylalanine and Tyrosine Attached to Side-Chains of Co-Polymers of N-(2-Hydroxypropyl)Methacrylamide. Makromol Chem Macromol Chem Phys 1981;182(3):799-809.
10. Rejmanova P, Obereigner B, Kopecek J. Polymers Containing Enzymatically Degradable Bonds .2. Poly "[N-(2-Hydroxypropyl)Methacrylamide] Chains Connected by Oligopeptide Sequences Cleavable by Chymotrypsin. Makromol Chem Macromol Chem Phys 1981;182(7):1899-915.
11. Ulbrich K, Strohalm J, Kopecek J. Polymers Containing Enzymatically Degradable Bonds .3. Poly[N-(2-Hydroxypropyl)Methacrylamide] Chains Connected by Oligopeptide Sequences Cleavable by Trypsin. Makromol Chem Macromol Chem Phys 1981;182(7):1917-28.
12. Kopecek J, Cifkova I, Rejmanova P, Strohalm J, Obereigner B, Ulbrich K. Polymers Containing Enzymatically Degradable Bonds .4. Preliminary Experiments Invivo. Makromol Chem-Macromol Chem Phys 1981;182(11):2941-9.
13. Rejmanova P, Kopecek J, Pohl J, Baudys M, Kostka V. Polymers Containing Enzymatically Degradable Bonds .8. Degradation of Oligopeptide Sequences in N-(2-Hydroxypropyl)Methacrylamide Co-Polymers by Bovine Spleen Cathepsin-B. Makromol Chem Macromol Chem Phys 1983;184(10):2009-20.
14. Etrych T, Chytil P, Jelinkova M, Rihova B, Ulbrich K. Synthesis of HPMA copolymers containing doxorubicin bound via a hydrazone linkage. Effect of spacer on drug release and in vitro cytotoxicity. Macromol Biosci 2002;2(1):43-52.

15. Etrych T, Jelinkova M, Rihova B, Ulbrich K. New HPMA copolymers containing doxorubicin bound via pH-sensitive linkage: synthesis and preliminary in vitro and in vivo biological properties. J Control Rel 2001;73(1):89-102.
16. Lu ZR, Kopeckova P, Wu ZC, Kopecek J. Functionalized semitelechelic poly[N-(2-hydroxypropyl)methacrylamide] for protein modification. Bioconj Chem 1998;9(6):793-804.
17. Kopecek J, Bazilova H. Poly[N-(2-Hydroxypropyl)Methacrylamide] .1. Radical Polymerization and Copolymerization. Eur Polym J 1973;9(1):7-14.
18. Subr V, Strohalm J, Ulbrich K, Duncan R, Hume IC. Polymers Containing Enzymatically Degradable Bonds .12. Effect of Spacer Structure on the Rate of Release of Daunomycin and Adriamycin from Poly[N-(2-Hydroxypropyl)-Methacrylamide] Copolymer Drug Carriers Invitro and Antitumor-Activity Measured Invivo. J Control Rel 1992;18(2):123-32.
19. Duncan R, Ulbrich K. Development of N-(2-Hydroxypropyl)Methacrylamide Copolymer Conjugates for Delivery of Cancer-Chemotherapy. Makromol Chem Macromolecular Symposia 1993;70-1:157-62.
20. Dvorak M, Kopeckova P, Kopecek J. High-molecular weight HPMA copolymer-adriamycin conjugates. J Control Rel 1999;60(2-3):321-32.
21. Kiessling F, Heilmann M, Lammers T, et al. Synthesis and characterization of HE-24.8: A polymeric contrast agent for magnetic resonance angiography. Bioconj Chem 2006;17(1):42-51.
22. Wang LX, Kristensen J, Ruffner DE. Delivery of antisense oligonucleotides using HPMA polymer: Synthesis of a thiol polymer and its conjugation to water-soluble molecules. Bioconj Chem. 1998;9(6):749-57.
23. Wroblewski S, Kopeckova P, Rihova B, Kopecek J. Lectin-HPMA copolymer conjugates: potential oral drug carriers for targeting diseased tissues. Macromol Chem Phys 1998;199(11):2601-8.
24. Lu ZR, Gao SQ, Kopeckova P, Kopecek J. Synthesis of bioadhesive lectin-HPMA copolymer- cyclosporin conjugates. Bioconj Chem. 2000;11(1):3-7.
25. Omelyanenko V, Kopeckova P, Prakash RK, Ebert CD, Kopecek J. Biorecognition of HPMA copolymer-adriamycin conjugates by lymphocytes mediated by synthetic receptor binding epitopes. Pharm Res 1999;16(7):1010-9.
26. David A, Kopeckova P, Rubinstein A, Kopecek J. Enhanced-biorecognition and internalization of HPMA copolymers containing multiple or multivalent carbohydrate side-chains by human hepatocarcinoma cells. Bioconj Chem 2001;12(6):890-9.
27. Omelyanenko V, Kopeckova P, Gentry C, Kopecek J. Targetable HPMA copolymer-adriamycin conjugates. Recognition, internalization, and subcellular fate. J Control Rel 1998;53(1-3):25-37.
28. Omelyanenko V, Kopeckova P, Gentry C, Shiah JG, Kopecek J. HPMA copolymer-anticancer drug-OV-TL16 antibody conjugates .1. Influence of the method of synthesis on the binding affinity to OVCAR-3 ovarian carcinoma cells in vitro. J Drug Targ 1996;3(5):357-73.
29. Nori A, Jensen KD, Tijerina M, Kopeckova P, Kopecek J. Tat-conjugated synthetic macromolecules facilitate cytoplasmic drug delivery to human ovarian carcinoma cells. Bioconj Chem 2003;14(1):44-50.

30. Kopecek J, Kopeckova P, Minko T, Lu Z. HPMA copolymer-anticancer drug conjugates: design, activity, and mechanism of action. Eur J Pharm Biopharm 2000;50(1):61-81.
31. Kopecek J, Kopeckova P, Minko T, Lu ZR, Peterson CM. Water soluble polymers in tumor targeted delivery. Journal of Control.led Release 2001;74(1-3):147-58.
32. Stevens MP. Polymer chemistry : an introduction. 3rd ed. New York: Oxford University Press; 1999.
33. Jensen KD, Kopeckova P, Bridge JHB, Kopecek J. The cytoplasmic escape and nuclear accumulation of endocytosed and microinjected HPMA copolymers and a basic kinetic study in Hep G2 cells. Aaps Pharmsci 2001;3(4):-.
34. Godwin A, Hartenstein M, Muller AHE, Brocchini S. Narrow molecular weight distribution precursors for polymer-drug conjugates. Ang. Chem. Int. Ed. 2001;40(3):594-7.
35. Skoog DA, West DM, Holler FJ. Fundamentals of analytical chemistry. 7th ed. Fort Worth: Saunders College Pub. 1996.
36. Habeeb AFS. Determination of Free Amino Groups in Proteins by Trinitrobenzenesulfonic Acid. Anal. Biochem. 1966;14(3):328-&.
37. Sashidhar RB, Capoor AK, Ramana D. Quantitation of Epsilon-Amino Group Using Amino-Acids as Reference-Standards by Trinitrobenzene Sulfonic-Acid - a Simple Spectrophotometric Method for the Estimation of Hapten to Carrier Protein Ratio. J. Immun. Methods 1994;167(1-2):121-7.
38. Hermanson GT. Bioconjugate techniques. San Diego: Academic Press; 1996.
39. Endo N, Umemoto N, Kato Y, Takeda Y, Hara T. A novel covalent modification of antibodies at their amino groups with retention of antigen-binding activity. J Immunol Methods 1987;104(1-2):253-8.
40. Morcol T, Subramanian A, Velander WH. Dot-blot analysis of the degree of covalent modification of proteins and antibodies at amino groups. J Immunol Methods 1997;203(1):45-53.
41. Bubnis WA, Ofner CM, 3rd. The determination of epsilon-amino groups in soluble and poorly soluble proteinaceous materials by a spectrophotometric method using trinitrobenzenesulfonic acid. Anal Biochem 1992;207(1):129-33.
42. Ulbrich K, Subr V, Strohalm J, Plocova D, Jelinkova M, Rihova B. Polymeric drugs based on conjugates of synthetic and natural macromolecules I. Synthesis and physico-chemical characterisation. J Control Rel 2000;64(1-3):63-79.
43. Kopecek J. Reactive Copolymers of N-(2-Hydroxypropyl)Methacrylamide with N-Methacryloylated Derivatives of L-Leucine and L-Phenylalanine .1. Preparation, Characterization, and Reactions with Diamines. Makromol Chem Macromol Chem Phys 1977;178(8):2169-83.
44. Drobnik J, Kopecek J, Labsky J, et al. Enzymatic Cleavage of Side-Chains of Synthetic Water-Soluble Polymers. Makromol Chem Macromol Chem and Phys 1976;177(10):2833-48.

CHAPTER III

SYNTHESIS AND SUB-CELLULAR TRAFFICKING OF A TAT PEPTIDE-MASKED CONJUGATE WITH A WATER-SOLUBLE POLYMER

This dissertation chapter contains a manuscript of a full paper in preparation for submission to the Journal of Controlled Release written by R. James Christie and edited by David W. Grainger. The observation of initial lysosomal trafficking and subsequent selective transport of Tat-PEG released from the polymer carrier provides insight to the currently misunderstood activity of cell-penetrating peptides.

Synthesis and Sub-cellular Trafficking of a Tat Peptide-Masked Conjugate with a Water-Soluble Polymer

R. James Christie, D.W. Grainger

Abstract

Cell penetrating peptides facilitate cytoplasmic entry of endocytosed molecules that otherwise remain entrapped in endosome/lysosome intracellular compartments. These short cationic peptides have the potential to enhance efficacy of many intracellular therapeutics that have limited potential due to their current inability to reach therapeutic targets once internalized. This work describes design, synthesis, and subcellular trafficking of a Tat conjugate in which the Tat peptide is buried within a macromolecular carrier and cargo, with release of the Tat peptide and cargo from the carrier following hydrolysis of a hydrazone bond within the acidic lysosomal environment. The construct exploited hydrazide-derivatized poly[N-(2-hydroxypropyl) methacrylamide] as the macromolecular carrier, with attachment of cysteine-containing Tat peptide and hydrazone formation both achieved using a novel aldehyde- and maleimide- containing heterobifunctional crosslinker. Poly(ethylene)glycol (Mw = 2000 Da) attached to the Tat peptide N-terminus served as a model therapeutic agent, and also to sterically interfere with Tat non-specific cell surface interactions. Dual fluorescent labeling of poly(HPMA) with Oregon Green® 488 and Tat peptide side chain with tetramethylrhodamine allowed independent tracking of the construct within RAW murine macrophage cells in vitro. The construct was sequestered within lysosomes during short incubation times, with

cytoplasmic entry and nuclear accumulation observed following extended (24 hr) incubation. Cytoplasmic entry was observed for the Tat-PEG conjugate, while poly(HPMA) remained entrapped within lysosomes suggesting endosomal uptake of the construct from culture media, then selective transport of Tat-conjugated molecules across the lysosome membrane. Direct conjugation of Tat to drug cargo is required to allow lysosomal membrane interaction and subsequent selective release into the cytosol.

Introduction

Cell penetrating peptides, or membrane translocating peptides have received much attention for drug delivery application due to their unusual ability to transport attached cargo into the cytoplasm of cells. These peptides have been identified from natural sources such as HIV-1(Tat), Drosophila (AntP), and herpes virus (vp22), with the conserved feature being a short sequence containing several charged arginine and lysine residues within the portion of the native protein responsible for membrane translocating activity. Excellent reviews summarizing the field are available.[1-7]

The Tat cell-penetrating peptide (CPP) comprising the basic residues 48-60 (and slightly shorter sequences) of the native HIV-1 Tat peptide has been shown to deliver a variety of cargo chemistries and sizes into the cytoplasm of cells including beta-galactosidase, gold and iron nanoparticles, poly(HPMA), siRNA, chelated paramagnetic cations.[8-19] The Tat peptide has also been shown to deliver antibodies into mammalian cells, GFP and RFP into monocot and dicot plant cells, and has been shown to penetrate various strains of pathogenic fungi where it exert some antifungal activity.[9, 19] Translocating activity is retained with inverted sequences or when non native D

isomer or β amino acids are used.[20-25] However, arginine residues are crucial for the activity of the peptide.[22, 26] Development of drug delivery vehicles employing Tat and analogous CPPs has progressed for some time, however, with the exact mechanism of cytoplasmic entry unknown.

Two general hypotheses have been proposed to account for the cytoplasmic entry behavior ascribed to Tat peptide conjugates: 1) direct transport across the exterior cell membrane, and 2) internalization by endocytosis, followed by lysosome escape. Early work with Tat peptide conjugates showed that cytoplasmic delivery was achieved at 4°C, and in the presence of metabolic inhibitors.[27, 28] This led to speculation that cellular entry occurred via a non-endocytotic, energy-independent pathway. However, later work showed that these observations could be artifacts of incomplete removal of surface-bound peptide, allowing Tat conjugates to leak into the cytoplasm following cell fixation.[29] However, unusually rapid cytoplasmic entry occurs has recently been observed in NIH 3T3 fibroblast cells with intact membranes, with $t_{1/2} \sim 1.8$ min to label the entire cell population.[30] This may further support a non-traditional uptake mechanism, but endocytotic uptake was not absolutely excluded in this study either.

Current hypotheses assert that Tat conjugates must first enter cells by lipid-raft mediated macropinocytosis (a non-specific form of endocytosis), with cytoplasmic entry gained by lysosome escape. This proposal results from recent experiments showing that cellular uptake is inhibited in the presence of the endocytotic inhibitors azide, amiloride, cytochalasin D and low temperature, as well as direct observation of punctate vesicles (endosomes or lysosomes) at early time points after incubation with Tat conjugates.[21, 24, 29, 31-35] Removal of cholesterol from the cell membrane with β-cyclodextrin also

inhibits Tat peptide uptake.[32] Even with inhibition of endocytosis, Tat peptide is still observed bound to cell surfaces. Furthermore, studies of fluorescently-labeled Tat peptide show that inhibition of lysosome acidification with ammonium chloride prevents cytoplasmic entry, with Tat peptide remaining sequestered within lysosomes, suggesting that endocytosis and acidification of the lysosome compartment is necessary for cytoplasmic entry of Tat conjugates.[32] This lysosome escape mechanism may be inefficient, as cytoplasmic entry is increased upon incubation of Tat conjugates with the known lysosome membrane destabilizer, chloroquine, as well as coupling Tat to a fusogenic peptide [31, 34, 36, 37]. Finally, internalization mechanisms may be confounded by influences of laser-based microscopy techniques where redistribution of cell-penetrating peptides from endosomes to the cytoplasm is observed following laser excitation in the presence of high CPP peptide concentrations (20-30μM, 2-3 hr incubations).[38]

Cytoplasmic entry may be different for Tat than other CPPs, as no secondary structure is observed upon interaction of Tat with negatively charged membranes, or polyanions, as observed for AntP and VP22.[39-43] However, other work reports that Tat secondary structure is predicted, with improved activity observed for synthetic analogs that strengthen alpha-helix formation, or impart secondary structure by formation of a cyclic fused peptide sequences.[44, 45] Regardless of the internalization mechanism, Tat-conjugates have a high affinity for cell surfaces, producing efficient internalization by non-specific endocytosis. Surface association may require cell-surface proteoglycans such as heparin sulfate (HS) [26] as removal of cell-surface HS, and addition of HS to Tat-containing media inhibits cellular uptake. However, Tat peptide

uptake is still observed in mutated cells not expressing heparin sulfate.[46] It is likely that proteoglycans are responsible for specific cell surface interactions that lead to increased uptake by non-specific endocytosis.

These findings have inspired in-depth studies into the physical interactions of the Tat peptide with negatively-charged biologically relevant components. Quantitative thermodynamic data has recently been reported for interactions of Tat peptide with negatively charged POPG and POPG/POPC lipid vesicles (~30-100 nm), heparin sulfate, heparin, and chondroitin sulfate.[47, 48] Affinity of Tat peptide for glycosaminoglycans was found to be approximately one order of magnitude higher than affinity for POPG vesicles ($\sim 10^5$ M^{-1} vs $\sim 10^3$-10^4 M^{-1}). Interestingly, binding of Tat peptide to dye-loaded micelles resulted in no dye leakage, or micelle disruption. Although this observation occurred in a synthetic lipid system different that natural membranes and may not directly translate into analogous biological activity, it may be that Tat peptide conjugates transport out of lysosomes without disrupting the vesicle, that is, has an escape mechanism distinct from that of traditional lysosomotropic agents such as chloroquine, poly(histidine)s, or poly(acrylic acid)s. This assertion is further supported by recent findings showing the inability of Tat peptide to induce hemolysis at concentrations up to 25 μM.[19] The higher observed binding constants for glycosaminoglycans may explain strong cell-surface association of Tat to cell surfaces, where direct interaction with the cellular lipid bilayer is unlikely.

Tat-mediated delivery of therapeutics into cells is a rapidly developing field and current approaches have recently been reviewed.[3] Intraperitoneal injection of a Tat-fluoroscein conjugate shows accumulation in all tissues upon examination with confocal

microscopy, association with 100% of cells isolated from circulation, and a Tat-β-galactosidase conjugate was able to cross the blood-brain barrier and accumulate in all regions of the brain.[49] Systemic targeted delivery of Tat-conjugated therapeutics may be limited as intravenous administration leads to increased clearance rate, abolishing the known tumor targeting ability of scFv(L19 antibody), with the majority of Tat-antibody found in the liver, kidney and spleen at early time points.[25] Similarly, conjugation of Tat-peptide to dextran-coated iron nanoparticles resulted in >10 fold decrease in circulation half life compared to non-conjugated nanoparticles, with the majority of injected dose accumulating in the liver, lymph node and spleen following intravenous injection.[11] Conjugation of Tat to [^{125}I]-labeled Fab antibody results in different biodistribution from Fab lacking the Tat peptide following intravenous administration in rats, with higher retention in organs.[50] ^{125}I labeled Fab lacking Tat peptide was found in the thyroid, gastrointestinal contents, renal cortex, and skin, while Tat conjugation resulted in additional accumulation in the liver, spleen, and adrenal gland.[50] At later time points, Tat conjugates were found, in levels similar to FAB fragments lacking the peptide, in all organs examined.[50] A similar trend was observed in non-targeted Tat-biotin-streptavidin conjugates, with rapid clearance following intravenous injection in rats, presumably due to rapid peptide conjugate sequestration in peripheral tissue following injection.[51] Additionally, Tat peptide has been shown to interact with serum albumin, rapidly decreasing bioavailable conjugate concentrations following intravenous administration.[34] These observations suggest limited practical application of Tat conjugates in systemic macromolecular drug delivery systems that utilize active (antibody) or passive (EPR effect) mechanisms to target specific sites, and which require

extended circulation times to be effective. Systemic delivery of Tat-conjugates may be improved if non-specific Tat interactions could be blocked until the reaching a desired therapeutic site.

We describe the design, synthesis, and preliminary *in vitro* trafficking for a novel macromolecular construct designed to study sub-cellular distribution of the Tat peptide and attached cargo. The approach exploits a Tat-masked macromolecular conjugate to observe subcellular trafficking of the Tat peptide and attached cargo, as well as its macromolecular carrier independently using confocal microscopy. The Tat peptide is sandwiched between two macromolecules: 1) the carrier (poly[N-(2-hydroxypropyl)methacrylamide] (HPMA)), and a model therapeutic (PEG, Mw 2000 Da). In this construct, the Tat peptide is conjugated to poly(HPMA) reversibly using a labile hydrazone bond, and irreversibly to PEG_{2000} via a stable amide bond. In vitro analysis of this HPMA-Tat-PEG conjugate in highly endocytotic murine macrophage cell cultures shows initial endocytotic uptake of the conjugate followed by cytoplasmic entry of Tat-PEG, but not the polymer carrier at extended incubation times.

Experimental

Materials.

All solvents were ACS grade and were purchased from Fisher Scientific (Fair Lawn, NJ). Glycylglycine (99+%), DL-1-amino-2-propanol (99+%), 4-nitrophenol (99+%), and dicyclohexyl carbodiimide (DCC, 99%) were obtained from Acros Organics (Geel, Belgium). Methacryloyl chloride (97%), 2,2'-azobisisobutyronitrile (98%), hydrazine monohydrate (97%), trinitrobenzene sulfonic acid (5% w/v solution in methanol) (TNBSA), 3-amino-1-propanol (99+%), triethyl amine (99.5%), oxalyl chloride (99+%), diidopropylethylamine (99.5%), anisole (99%), triisopropylsilane (99%), trifluoroacetic acid (99%), 4-(aminomethyl)cyclohexane carboxylic acid (97%), maleic anhydride (98+%), acetic anhydride (98+%) and glacial acetic acid, were purchased from Sigma Aldrich (St. Louis, MO). 1,2 ethanedithiol (95%) was purchased from Lancaster Synthesis (Pelham, NH). 5(6) - Tetramethylrhodamine-succinimidyl ester (TAMRA-NHS) was obtained from AnaSpec (San Jose, CA). Oregon Green™ 488 cadaverine was purchased from Molecular Probes (Eugene, OR). Methoxy PEG succinimidyl ester Mw 2000, and methoxy PEG amine Mw 2000 were purchased from Nektar (Huntsville, AL). Dimethyl sulfoxide-d_6 containing 0.05% w/v tetramethylsilane was purchased from Cambridge Isotope Laboratories, Inc. (Andover, MA). Spectra/Por 1, 3500 and 1000 Da molecular weight cutt-off dialysis tubing was obtained from Spectrum Laboratories, Inc. (Rancho Dominguez, CA). Tat peptide NH_2-[AHX]-Lys(TAMRA)-Gly-Gly-Tyr(Tbu)-Gly-Arg(Pbf)-Arg(Pbf)-Arg(Pbf)-Gln(Trt)-Arg(Pbf)-Lys(Boc)-Lys(Boc)-Arg(Pbf)-Gly-Cys(Trt) comprising residues 48-57 was purchased on-

resin from Global Peptide (Ft. Collins, CO). Poly(HPMA) molecular weight standards were a gift from Dr. P. Kopeckova at the Univ. of Utah. All NMR spectra were recordered on a Magnex Scientific Inova 400 MHz instrument in dimethyl sulfoxide-d_6 containing 0.05% w/v tetramethylsilane as an internal standard. Absorbance measurements were obtained using a Varian Carey 500 Scan instrument. MALDI-ToF mass spectroscopy analysis was performed by Global Peptide (Ft. Collins, CO).

Synthesis of poly[N-(2-hydroxypropyl)methacrylamide] copolymer.

Monomers N-2-hydroxypropyl methacrylamide (HPMA) and methacryloyl glycylglycine nitrophenyl ester (MAGGONP) were prepared using a previously described procedure.[52, 53] HPMA copolymers were prepared by free radical-initiated polymerization as previously described using 12.5% (w/v) monomer and 0.6% 2,2'-azobisisobutyronitrile (AIBN) initiator in freshly distilled acetone.[54] AIBN was recrystallized 3 times from methanol and dried under vacuum prior to use. Copolymer reactive side chain content was controlled by MAGGONP monomer feed ratio with 5 mol% reactive side chain content targeted. A typical procedure for synthesis of a HPMA copolymer with 95 mole % HPMA units and 5 mole % MAGGONP units is as follows; HPMA monomer (3.35 g, 23.4 mmol), MAGGONP (0.40 g, 1.2 mmol), and AIBN (0.18 g, 1.1 mmol) were added to 26 mL of acetone in a chemglass 50 mL pressure flask containing a magnetic stirbar. The solution was degassed by sonication under N_2 flow for 5 minutes, then capped and stirred until all solids dissolved (~ 30 minutes), then the reaction flask was placed in a 60 $^{\circ}$C hot water bath and stirred for 24 hr. After complete reaction, solids were collected by filtration and washed with cold acetone to yield a

cream colored powder. Solids were dissolved in 35 mL 90:10 CH_2Cl_2/MeOH, then precipitated into a 10-fold excess of cold acetone. The precipitate was allowed to settle and excess acetone was carefully decanted. Solids were washed 3 times with 100 mL cold acetone, once with 100 ml ether, and solids were dried under vacuum. Typical yield: ~ 2.2 g, 56%. Reactive ester content was determined by incubation of polymer samples in 0.5M NaOH , 37°C for 3 hr, then measuring released p-nitrophenolate ion using spectrophotometry at 400 nm ($\varepsilon = 1.8 \times 10^4\ M^{-1}cm^{-1}$). Reactive ester content was found to be 4.00 mole %, 2.66×10^{-4} mole ester/g polymer.

Molecular weight of synthesized poly(HPMA) copolymer was estimated by size exclusion chromatography (SEC) following displacement of reactive ester groups with 1-amino-2-propanol using an HP1050 HPLC system equipped with an HP1040A refractive index detector and Biosil 125 column. The instrument was calibrated with poly(HPMA) samples of known molecular weight (gift of P. Kopechekova). Sodium phosphate buffer (0.05 M, pH 7.4) mobile phase, 100 uL sample injection, and 0.5 mL/min flow rate was used for each analysis. Poly(HPMA) molecular weight was found to be ~ 18,200 Da.

Labeling poly(HPMA) with Oregon Green 488.

Poly(HPMA) was fluorescently labeled by covalent attachment of Oregon Green 488 cadaverine to a fraction of reactive esters present on the HPMA copolymer. The following procedure represents labeling of approximately 0.7 dye molecules/poly(HPMA): 0.4300 g poly(HPMA) (1.15×10^{-4} mol ester, 1 eq) was dissolved in 4 mL DMF and stirred until all solids dissolved (10 minutes). In a separate flask, 10 mg Oregon Green 488 cadaverine (2×10^{-5} mol, 0.17 eq) was dissolved in 2 mL DMF.

Oregon Green 488 solution was dripped into the poly(HPMA) solution, and stirred for 30 minutes at room temperature in the dark. After 30 minutes, 7.0uL diisopropylethylamine (DIPEA, $4.0x10^{-5}$ mol, 0.35 eq) was added, and the reaction was stirred an additional 6 hrs at room temperature in the dark. The reaction was halted by addition of 80 mL cold 50:50 acetone/diethyl ether. Excess solvent was carefully decanted, and solids were washed with 25 mL cold 50:50 acetone/diethyl ether, then 25 mL cold ether. Yield = 0.400 g, 93%. Oregon Green content in the labeled polymer product was found to be ~ 60 nmol/mg conjugate by measuring the absorbance of isolated product at 496 nm, using an extinction coefficient of $1.8x10^4$ $M^{-1}cm^{-1}$ determined for Oregon Green 488 cadaverine in water. This value represents labeling of 23% of the total available reactive sites and complete reaction of Oregon Green 488 with reactive esters on the polymer.

Incorporation of hydrazide groups into poly(HPMA).

Hydrazide functionality was incorporated into poly(HPMA) by displacement of remaining nitrophenol ester groups after Oregon Green 488 labeling in the presence of excess hydrazine monohydrate. This approach to incorporate hydrazide groups into poly(HPMA) side chains has been previously described.[55, 56] Oregon Green-labeled poly(HPMA) (0.200 g , ~ $4.5x10^{-5}$ mole esters, 1eq) was dissolved in 10mL methanol and slowly dripped into hydrazine monohydrate (21μL $5.3x10^{-4}$ mol, 10 eq) in 2mL methanol. The reaction mixture turned dark yellow indicating reaction of ester groups and formation of the p-nitrophenolate anion. The reaction was stirred for 4 hr at room temperature in the dark, then dripped into 20 mL cold water, placed in dialysis tubing (SpectraPore 3500 MWCO), and dialyzed against water for 2 days with frequent water

changes. Product was isolated by lyophilization. Yield = 0.142 g, 71%. Conversion of esters to hydrazide functional groups on poly(HPMA) was estimated using a modified trinitrobenzene sulfonic acid (TNBSA) assay, and ethyl carbazate standards as previously described.[55, 56] First, a 5.725 x 10^{-4} M stock solution of ethyl carbazate was prepared by dissolving 5.96 mg in 100 mL 0.1 M $NaHCO_3$, pH 8.5. An ethyl carbazate standard curve over a concentration range of ~ 0.2 – 0.03 mM was generated by serial dilution of this stock solution. A 0.01% w/v stock solution of TNBSA was prepared by diluting 20uL of 5% w/v TNBSA in methanol (Pierce), with 9.98 mL 0.1 M $NaHCO_3$. Poly(HPMA) samples were dissolved 0.1 M $NaHCO_3$ to a final concentration of 0.4-0.6 mg/mL. For each analysis, 1 mL of ethyl carbazate standard solution, or polymer sample solution was combined with 0.5 mL 0.01% w/v TNBSA solution. The samples were stirred for 4 hr at 37 °C. After incubation, the samples were placed on ice, and absorbance at 505 nm was measured. Hydrazide content was estimated to be ~ 3.8 x 10^{-4} mol hydrazide/g poly(HPMA), a 140% conversion. Higher values than expected were typically obtained from standard curves generated with ethyl carbazate.

Synthesis of Oregon Green 488 poly(HPMA) control.

Remaining nitrophenol esters after Oregon Green labeling were reacted with 1-amino-2-propanol to generate a polymer that closely resembled native poly(HPMA) for use as an *in vitro* control. Oregon Green-labeled poly(HPMA) (0.150 g, ~4x10^{-5} mol active esters) was dissolved in 2.0 mL DMF and 10μL 1-amino-2-propanol (1.3x10^{-4} mol, 3 eq) was added, stirred for 4 hrs at room temperature in the dark, then diluted to 30 mL with water. The resulting solution was dialyzed against water for 2 days

(SpectraPore, 3500 MWCO). Product was isolated by lyophilization. Yield = 0.100 g , 67%.

Synthesis of TAMRA-labeled PEG control.

A TAMRA-labeled PEG (Mw~2000 Da) control was prepared according to a previously described procedure.[57] Methoxy-PEG-amine (57.0 mg ~$2.8x10^{-5}$ mol, 1 eq) was dissolved in 1 mL DMF, followed by addition of 15 mg TAMRA-NHS ($2.8x10^{-5}$ mol, 1eq). The reaction was stirred for 30 minutes in the dark, then 14.8 μL diisopropylethylamine ($8.5x10^{-5}$ mol, 3.0 eq) was added, stirred an additional 4hrs, then diluted to 25 mL with water. The resulting solution was dialyzed (MWCO 1000 Da) against water for two days and product isolated by lyophilization. Yield = 34.0 mg, ~ 60%.

Synthesis of 4-(N-maleimidomethyl) cyclohexane carboxylic acid, MCCA

4-(aminomethyl) cyclohexane carboxylic acid (40.71 g, 0.259 mol, 1eq) was dissolved in dimethyl acetamide (DMAc, 100 mL). A solution of maleic anhydride (25.20 g, 0.257 mol, 0.99 eq) was prepared in DMAc (50 mL), then added dropwise to the 4-(aminomethyl) cyclohexane carboxylic acid solution dropwise while stirring. The reaction vessel was purged with nitrogen, capped and stirred for 24 hr at room temperature. After 24 hr, sodium acetate (5.00 g, 0.061 mol, 0.24 eq) and acetic anhydride (43 mL, 0.455 mol, 1.75 eq) were added and the reaction was continued for an additional 24 hrs. After 24 hrs, the reaction was heated to 65 °C and stirred for 5 hrs, then concentrated to ~ 125 mL under vacuum and poured into 1L cold water while

stirring. The light brown precipitate was collected by filtration and dried under vacuum. The aqueous portion was extracted twice with methylene chloride (500 mL), and product was isolated after evaporation of solvent. Both solid portions were combined and dissolved in methylene chloride (500 mL) then silica gel (5 g) was added to the solution, and the suspension was stirred for 30 min. The resulting colorless solution was filtered and solid product was obtained by evaporation of solvent under vacuum. Crude product was further purified by crystallization from ethyl acetate to yield a white solid. Yield: 14.70 g, 24 %, white solid. ^{1}H NMR, δ ppm: 0.926 (dd, 2H), 1.22 (dd, 2H), 1.517 (m, 1H), 1.6165 (d, 2H), 1.869 (d, 2H), 2.109 (m, 1H), 3.2355 (d, 2H), 7.012 (s, 2H), 12.010 (s, 1H). ^{13}C NMR, δ ppm: 27.932, 29.112, 36.013, 42.105, 42.861, 134.273, 171.549, 176.497. FAB-MS m/z = 238.1085 $[M+H]^{+}$(calculated m/z = 238.1079 $[M+H]^{+}$)

Synthesis of N-(1-propanol)-4-(N-maleimidomethyl) cyclohexane-1-amide

MCCA (3.00 g, .0126 mol, 1eq) was dissolved in methylene chloride (75 mL), purged with nitrogen, capped, and cooled to –15 °C. A suspension of NHS was prepared (1.454g, 0.0126 mol, 1eq) in methylene chloride (25 mL), then cooled to –15 °C. Next, a solution of DCC was prepared (2.8688g, 0.0139 mol, 1.1 eq) in methylene chloride (25 mL) and cooled to –15 °C. The DCC solution was added to the MCCA solution, followed by addition of the NHS suspension. The reaction flask was purged with nitrogen and stirred at –15 °C for 24 hr and then filtered to remove dicyclohexylurea (DCU). The filtrate was retained and 3-amino-1-propanol (1.982 mL, 0.025 mol, 2eq) was added dropwise. The reaction was purged with nitrogen, capped, and stirred at room temperature for 3 hr. After 3 hr, the reaction mixture was filtered to remove liberated

NHS and the filtrate was concentrated to ~2/3 original volume under vacuum, cooled to –20 °C, then refiltered. The resulting filtrate volume was doubled by addition of diethyl ether to form a precipitate, which was isolated by filtration. The solid product was further purified by silica gel chromatography (10 x 40 cm, 90/10 methylene chloride/methanol mobile phase) and isolated by evaporation of solvent under vacuum. Yield: 1.91 g, 51.6%, white solid. ^{1}H NMR, δ ppm: 0.886 (dd, 2H), 1.265 (dd, 2H), 1.508 (q, 3H), 1.618 (d, 2H), 1.682 (d, 2H), 1.998 (m, 1H), 2.5 (solvent overlap), 3.047 (q, 2H), 3.234 (d, 2H), 3.372 (q, 2H), 4.399 (t, 1H), 7.013 (s, 2H), 7.652 (t, 1H). ^{13}C NMR , δ ppm: 28.488, 29.349, 32.386, 35.423, 36.060, 42.980, 43.704, 58.307, 134.277, 171.188, 174.825. FAB-MS m/z = 295.1654 $[M+H]^{+}$(calculated m/z = 295.1657 $[M+H]^{+}$).

Synthesis of N-(1-propanal)-4-(N-maleimidomethyl) cyclohexane-1-amide, PMCA

Synthesis of N-(1-propanal)-4-(N-maleimidomethyl) cyclohexane-1-amide (PMCA) was prepared using the Swern procedure for oxidation of an alcohol to an aldehyde.[58] N-(1-propanol)-4-(N-maleimidomethyl) cyclohexane-1-amide (500 mg, 1.72 mmol, 1 eq) was dissolved in freshly distilled methylene chloride (20 mL) and cooled to –80 °C. An activated dimethyl sulfoxide (DMSO) solution was prepared by combining DMSO (295 uL, 4.13 mmol, 2.4 eq) and oxalyl chloride (0.950 mL of 2 M solution in methylene chloride, 1.89 mmol, 1.1 eq) in methylene chloride (1.5 mL) at –80 °C. The alcohol solution was slowly added to the activated DMSO solution over 5 minutes. The reaction proceeded for 15 minutes at –80 °C, followed by addition of triethylamine (1.2 mL, 8.5 mmol, 5 eq). The reaction was equillibrated to room temperature then water (15 mL) was added and the mixture was stirred for 10 minutes.

The organic layer was separated, and the aqueous portion was re-extracted with 2 x 10 mL methylene chloride then combined with the first organic portion. The combined organic portions were washed with 1M HCL, dilute $NaHCO_3$, and 2 x 20 mL H_2O, then dried with Na_2SO_4. Product was isolated after removal of Na_2SO_4 and evaporation of solvent. Yield: 0.350g, 66%, white powder. ^1H NMR, δ ppm: 0.878 (dd, 2H), 1.232 (dd, 2H), 1.507 (m, 1H), 1.636 (m, 2H), 1.976 (m, 1H), 2.502, (solvent overlap) 3.23 (d, 2H), 3.284 (q, 2H), 7.011 (s, 1H), 7.796 (t, 1H), 9.604 (t, 1H). ^{13}C NMR, δ ppm: 28.378, 29.286, 32.393, 36.037, 42.957, 43.265, 43.566, 134.274, 171.185, 174.958, 202.195. MS-FAB m/z = 293.1507 $[M+H]^+$(calculated m/z = 293.1501$[M+H]^+$).

Conjugation of PMCA to Oregon Green-labeled, hydrazide-derivatized poly(HPMA)

Oregon Green-labeled poly(HPMA)-hydrazide (86.0 mg, ~ 3.3 x 10^{-5} mol reactive sites) was dissolved in 1.0 mL methanol. PMCA was suspended in 0.5 mL MeOH, then added to the poly(HPMA) solution followed by addition of 4 uL acetic acid. This reaction was stirred at room temperature in the dark for 3 hr, then 100 μL DMSO was added to solubilize undissolved crosslinker, followed by reaction for an additional 5 hr. The reaction was stopped by addition of 9 mL diethyl ether. The solids were allowed to settle and excess solvent was carefully decanted. The solids were washed with 3x10 mL diethyl ether, then dried under vacuum. Yield: 80 mg, ~86%. This same reaction was conducted with hydrazide-derivatized poly(HPMA) lacking the Oregon Green dye to determine the efficiency of crosslinker conjugation. Product absorbance was measured at 297 nm and coupling efficiency was determined to be ~140% using an extinction coefficient of 5.53x10^2 $M^{-1}cm^{-1}$ for PMCA determined in water. TNBSA analysis of the

poly(HPMA-PMCA) conjugate showed less than 10% of the hydrazide groups remained on poly(HPMA) after coupling with PMCA using the procedure described above.

Synthesis of Tat-PEG

Tat-PEG was synthesized on resin with all amino acid side groups protected with Fmoc chemistry. Tat peptide resin (0.1 g) was suspended in 10 mL 50:50 CH_2Cl_2/DMF and allowed to swell for 2 hrs. Methoxy-PEG-NHS (Mw ~ 2000 Da, 0.150 g, ~75 μmol) was dissolved in 10 mL 50:50 CH_2Cl_2/DMF, then added to the Tat peptide resin suspension. The reaction was purged with N_2, capped, and stirred at room temperature in the dark. After 30 minutes, 35 μL (20 mmol) diisopropyl ethylamine was added, and the reaction proceeded with stirring for an additional 9 hrs. Unreacted PEG was then removed by centrifugation of the resin and careful removal of excess solvent. The resin was washed 3x with reaction solvent, then dried under vacuum overnight after the final rinse. The Tat-PEG conjugate was cleaved from the resin by incubation for 3 hr at room temperature in 5 mL of a cleavage cocktail (92% trifluoroacetic acid, 2% water, 2% anisole, 2% triisopropylsilane, 2% ethanedithiol). Cleaved Tat-PEG conjugate was removed from resin material by filtration through a porcelain frit. The filtrate was added to 80 mL cold diethyl ether and a precipitate formed. Solids were collected by centrifugation, and the pellet was washed with 2x10 mL diethyl ether. Solids were redissolved in 10 mL water, dialyzed (MWCO 3500) against water for 96 hrs, and isolated by lyophilization. Yield 19.1 mg. MALDI-TOF mass spectrometry: Mw found ~ 4595.58 Da (M+H, broad), calculated ~4489.41.

Tat-PEG Coupling to HPMA copolymer

Tat-PEG was coupled to poly(HPMA) by reaction of cysteine thiols to the maleimide functional groups on poly(HPMA). Tat-PEG (11.0 mg, ~2.4 μmol) was first reduced by incubation for 1 hr in 1.0 mL of degassed 10 mM DTT in 0.1M sodium phosphate buffer containing 0.5 mmol EDTA, pH 7.2. After disulfide reduction, the Tat-PEG solution was separated from DTT using a Sephadex G-25 column (1x13 cm) and eluted with the phosphate/EDTA buffer described above. Reduced Tat-PEG was collected (~5 mL) and combined with a solution of 10 mg Oregon Green-labeled, crosslinker-derivatized, maleimide-containing poly(HPMA) in 1.0 mL degassed phosphate/EDTA buffer. The reaction was purged with N_2, capped, stirred for 12 hrs in the dark at room temperature, fractionated using a Sephadex G-100 column (1x15 cm), and the poly(HPMA)-Tat-PEG conjugate was collected as the first orange/green band eluting from the column under UV illumination. This fraction was further purified and concentrated using NanoSep 10K OMEGA centrifugation membrane devices (10,000 MWCO, 13,000 rpm, 10 minutes). The resulting pellet on top of the membrane was washed 3x with water followed by concentration using the NanoSep centrifugation device. The final product was isolated using a speed-vac. Yield: 10 mg. The purified conjugate was analyzed by SEC using an HP1050A HPLC system equipped with a Biosil 125 column, monitoring 550 nm and 496 nm using diode array detection. An injection volume of 100 μL, 0.5 mL/min 0.1 M sodium phosphate buffer, pH 7.2, and sample concentrations of ~ 10 mg/ml were used for each analysis. The poly(HPMA)-Tat-PEG conjugate eluted after 13 minutes under these conditions. Tat-PEG content in the isolated poly(HPMA)-Tat-PEG conjugate was estimated to be 16.2 nmol/mg conjugate by

measuring the absorbance at 554 nm in water using an extinction coefficient of $6.4x10^4$ $M^{-1}cm^{-1}$ found for TAMRA-NHS in water. This value corresponds to ~ 8 % Tat-Peg by mass and ~ 11 mole % coupling efficiency.

Cell Culture

RAW 264.7 murine monocyte-macrophage cells were obtained from the American Type Culture Collection (Manassas, VA) and cultured in RPMI 1640 (Mediatech) supplemented with 10% fetal bovine serum (FBS, HyClone, Inc.) and 1% penicillin-streptomycin (Life Technologies). Cultures were maintained in T-175 TCPS flasks (Nunc™) under standard conditions: incubation at 37 °C, 98% humidity and 5% CO_2 and dissociated from culture flasks by incubation with Ca^{2+}- and Mg^{2+}- free cell culture grade Hank's balanced salt solution (HBSS, Life Technologies). After harvest from stock flasks, cells were seeded into Nunc Labtek II 0.5 coverglass chambers at a density of $1x10^5$ cells per chamber, and allowed to adhere for 24 hrs in RPMI 1640 media containing 10% FBS. Cells were then incubated for 1hr with poly(HPMA)-Tat-PEG (3.5 mg/mL, ~ 57 μM Tat peptide), or control solutions of Oregon Green-labeled poly(HPMA) (1 mg/mL, ~ 30 μM), or PEG-TAMRA (1 mg/mL, ~ 200 μM) conjugate dissolved in RPMI 1640 media. After incubation, cells were rinsed with RPMI and further incubated for various lengths of time preceding analysis by laser scanning confocal microscopy.

Confocal Microscopy

Live cells were imaged using an Olympus IX71 inverted microscope and Olympus FV 300 confocal scanner equipped with an Olympus UPLAPO60XW3/IR 60x water immersion objective, NA 1.2. Dual excitation was achieved using argon and He-Ne lasers passed through an Olympus FV-FCBGR 488/543/633 beam splitter cube. Simultaneous detection of Oregon Green and tetramethylrhodamine fluorescence was accomplished using a dichroic mirror that allows light below 570 nm to pass through to channel 1, and reflects wavelengths greater than 570 nm to channel 2. Signal from both channels were detected using photomultiplier tubes (PMTs) after passage through 510 long pass and 530 nm short pass barrier filters (channel 1), or through a 575-635 nm band pass filter (channel 2). In addition to fluorescence images, transmitted light images were obtained using differential interference contrast and PMT detection. Images from all three channels were obtained simultaneously, using a confocal aperture of 150 μm, and Kalman average of 4 images used for each confocal plane. Images were processed using FLUOVIEW software (v. 4.2).

Results and Discussion

Synthesis of poly(HPMA)-Tat-PEG.

Synthesis of the target synthetic polymer construct is shown in Scheme 1.3.1, with key components for activity and analysis represented in Figure 1.3.1. Poly(HPMA) was chosen as the macromolecular carrier molecule because of its long history as a polymeric drug carrier known to remain intracellularly sequestered primarily in lysosome/endosome compartments.[59-61] Synthesis of poly(HPMA) and subsequent

hydrazide derivatization was readily achieved as previously described.[55, 56, 62, 63] Polydispersity of the polymer products was not determined, however, typical values for HPMA copolymers prepared in similar fashion are found to be ~1.3-2.3.[55, 56, 64-66] Reactive nitrophenol ester groups on the poly(HPMA) backbone provided the starting point for subsequent grafting of desired

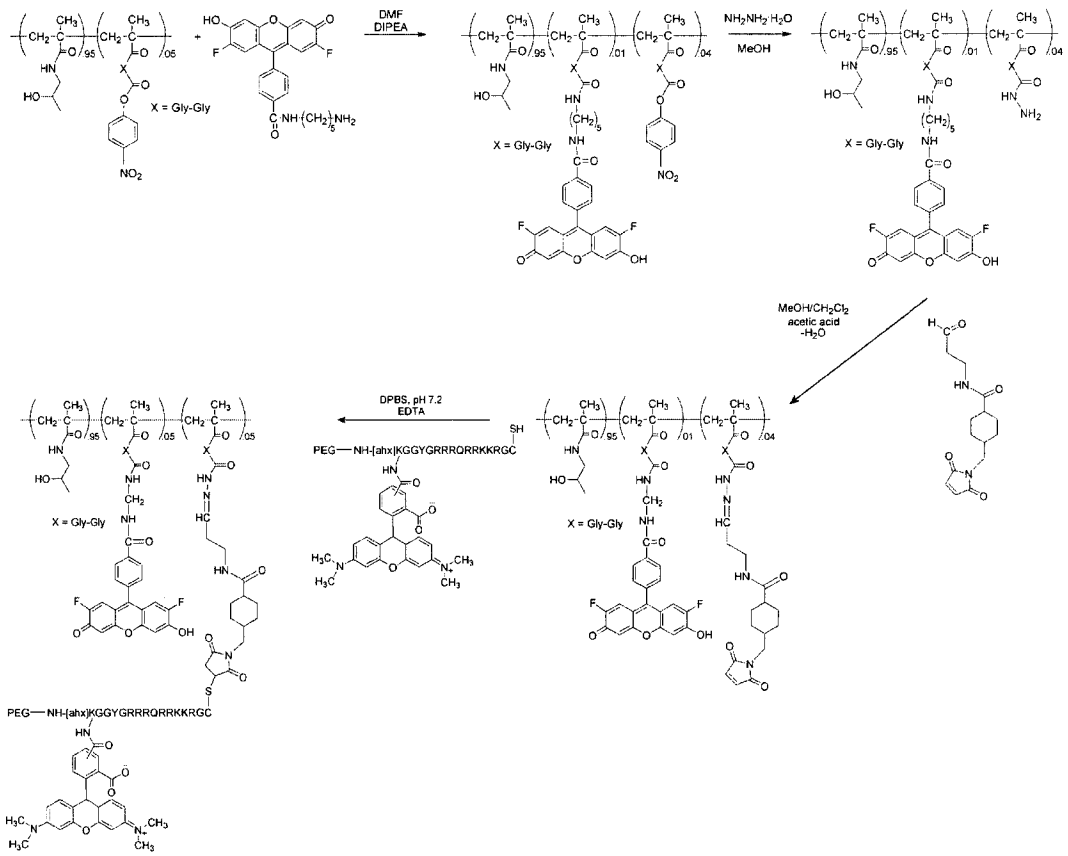

Scheme 1.3.1. Synthesis of poly(HPMA)-Tat-PEG.

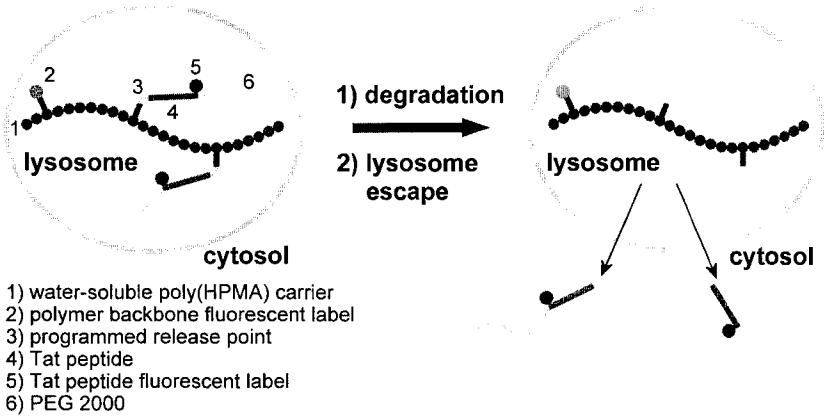

Figure 1.3.1. Target synthetic construct and proposed mechanism of action.

components onto the polymer. A portion of the total reactive side chains were labeled with Oregon Green 488 cadaverine before hydrazide derivatization, allowing labeling of the polymer backbone via a stable amide linkage and tracking of the polymer carrier backbone once internalized into live cells. Coupling of the heterobifunctional crosslinker 4-(maleimidomethyl) cyclohexane carboxylic acid (3-propanal) amide (PMCA) to poly(HPMA) was confirmed by ^{1}H NMR, shown in Figure 1.3.2.

Observation of the maleimide peak at 7.013 ppm, and disappearance of the aldehyde peak at 9.604 ppm in the poly(HPMA) conjugate shows reaction of aldheyde end of the crosslinker with hydrazide groups and successful conjugation. Other significant proton peaks in the spectrum were obscured by broad peaks of poly(HPMA). Although PMCA coupling efficiency was not directly measured on the Oregon Green-labeled product, analysis of unlabeled poly(HPMA)-PMCA analog products under identical conditions showed coupling to be very efficient, with complete conversion of

hydrazide groups determined by crosslinker optical absorbance (e = $5.53x10^2$ $M^{-1}cm^{-1}$, 297 nm) and measurement of remaining hydrazide functionality using the TNBSA assay

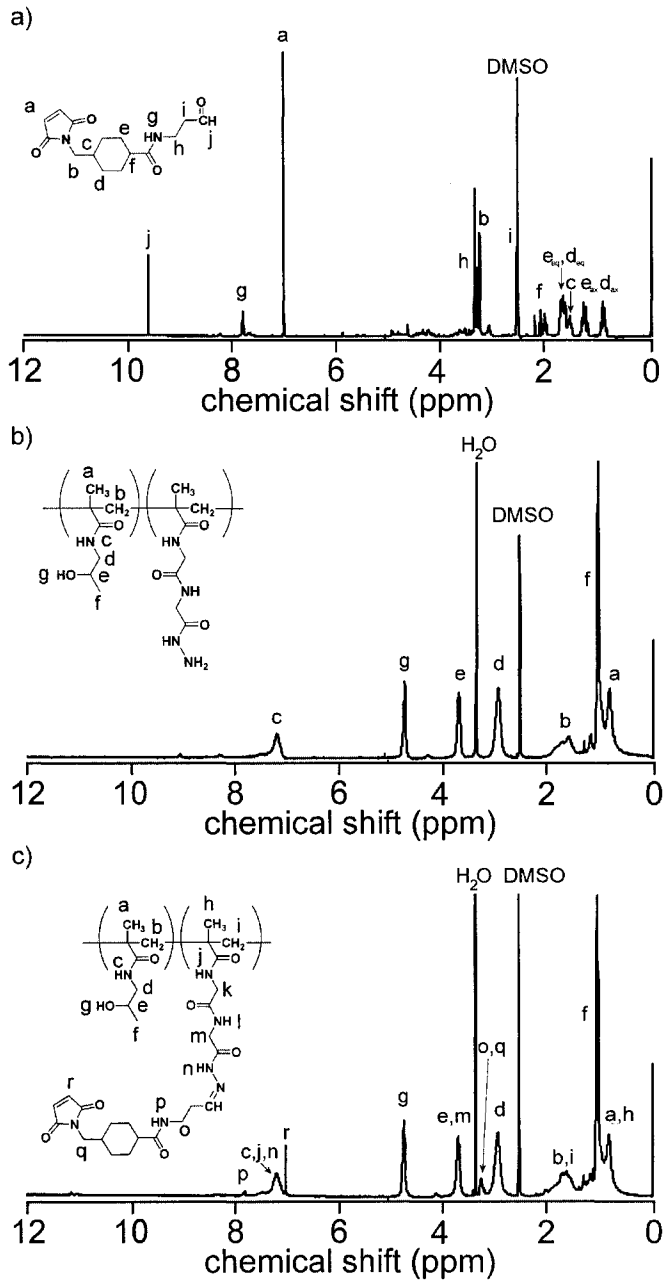

Figure 1.3.2. ^1H NMR spectra of a) PMCA hetero-bifunctional crosslinker, 2) hydrazide-derivatized poly(HPMA), and 3) PMCA-conjugated poly(HPMA). All spectra recorded at 400 mHz in d_6-DMSO.

after coupling. Less than 10% of the original hydrazide groups remain after the crosslinker coupling reaction. No crosslinking of poly(HPMA) was observed (e.g., gel formation) after hydrazide or crosslinker coupling (data not shown).

Synthesis of Tat-PEG was achieved on resin with protected side chains using the Tat peptide (residues 48-57) containing the following non-native features; 1) an aminohexanoic acid spacer at the N-terminus, 2) a cysteine residue at the C-terminus for maleimide coupling to poly(HPMA), and 3) a tetramethylrhodamine dye to allow for fluorescence detection in cells.

This amino acid sequence containing a glycine and tyrosine residue after residue 57 in the Tat peptide has shown to be able to deliver chelated metal ions into the cytoplasm of HeLa cells.[15] The aminohexanoic acid spacer at the N-terminus of the peptide allowed for single-point attachment of NHS-activated PEG to the fully protected Tat peptide via a stable amide linkage, avoiding attachment to lysine side-chains that would likely inhibit peptide bioactivity. Another present approach to synthesize a Tat conjugate on-resin used a single lysine residue containing a 1-(4,4-dimethyl-2,6-dioxocyclohexylidene)ethyl (Dde) protecting group, made reactive by deprotection with 2% hydrazine solution.[15] PEG was chosen as the model macromolecule therapeutic agent because of its neutral charge, generally does not interact with biological components, and is commercially available in reactive forms. Other works describe preparation of therapeutically relevant DNA and siRNA Tat-conjugates through single-point attachment, with great lengths taken to prevent aggregation of the negatively charged cargo with the positively charged peptide. In these cases, while stoichiometric product formation is shown, aggregation likely occurs upon solvation of the construct in

physiologically relevant buffered solutions via electrostatic interaction. Strategies allowing single-point attachment of a poly(anionic) payload to the Tat peptide and prevention of aggregation include: 1) binding the Tat peptide to an anionic resin, 2) conducting the coupling reaction in mixed acetonitrile/aqueous solvent sytems, or 3) using high concentrations of urea or salts in aqueous buffers.[67-70] One group reported aggregation and precipitation between covalent Tat and oligonucleotide conjugates, although stoichiometric product was observed by MALDI-TOF mass spectrometry.[69] Various covalent strategies for preparation of Tat conjugates are described including: disulfide formation by displacement of pyridine sulfonyl groups, reaction of thiol-containing Tat with vinyl sulfone groups, avidin/streptavidin cassettes, heterobifunctional amine and sulfhydryl-reactive crosslinkers, as well as expression of fusion proteins after expression in bacterial systems.[17, 51, 67, 69-75] Disulfide conjugation strategies may enhance the drug delivery effectiveness by release of the cargo molecule from the Tat carrier by endogenous dithiolreductase activity once in the cytoplasm.[74, 76]

Purification of the Tat-PEG conjugate resulted in a rather low yield (~ 0.2 mg/mg resin), resulting from tendency of the Tat-PEG conjugate to bind to materials used for purification, as well as glassware as previously described.[69, 77] Tat-PEG adhered strongly to both dialysis membranes and Sephadex column materials, and was partially recovered. Synthesis of the desired PEGylated Tat-peptide was confirmed by MALD-TOF mass spectrometry as shown in Figure 1.3.3. The broad peak centered at 4595.58 m/z is approximately 2000 Da higher than the unconjugated Tat peptide (m/z =2489.41 Da) showing successful conjugation, with peak broadening due to PEG polydispersity. No free Tat peptide was observed at m/z = 2489.41 Da.

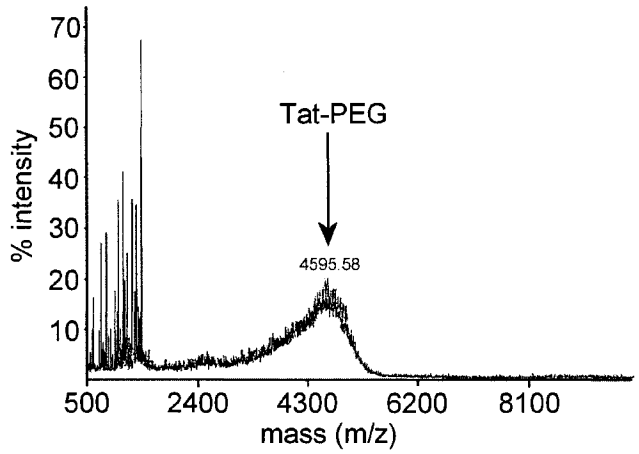

Figure 1.3.3. MALDI-TOF mass spectrum of Tat-PEG.

Coupling Tat-peptide to poly(HPMA) was achieved by Michael addition of Tat-PEG thiol groups to maleimide groups on the polymer backbone in aqueous conditions as previously described.[78] Independent fluorescent dye-labeling of both the poly(HPMA) backbone and the Tat peptide allowed convenient detection of both species during analysis by size exclusion chromatography (SEC) using diode array detection set to λ_{max} for each chromophore. However, detection slit widths must be kept small (< 10 nm), as fluorescence from Oregon Green 488 can decrease TAMRA signal. Figure 1.3.4a shows the SEC trace of PMCA-derivatized poly(HPMA); the polymer backbone is easily detected at 496 nm, with essentially no signal observed at 550 nm. Successful conjugation of the Tat-peptide is observed by the increase in signal at 550 nm, and the shift of the poly(HPMA) peak to a shorter retention time as shown in Figure 1.3.4b. The poly(HPMA) peak did not completely shift to the higher retention time, and an underlying native poly(HPMA) peak is observed, showing incomplete coupling to the polymer backbone. No attempt was made to further fractionate the product mixture and remove unconjugated poly(HPMA). Free Tat-PEG elutes from this column at 38 minutes

(Figure 4c), and was not detected in the purified poly(HPMA) conjugate, showing complete removal of unconjugated Tat-PEG that could interfere with subsequent *in vitro* analysis. Free Tat-PEG physically interacted with the column matrix used for SEC analysis, causing extensive peak broadening as shown by the broad peak in Figure 1.3.4c at 38 minutes, leading to Tat-PEG elution after the buffer peak at 30 minutes under these conditions. Conjugation of Tat-PEG to poly(HPMA) did not result in broadening of the native poly(HPMA) SEC trace, and did not retard elution of the conjugate by physical interaction with the column. This shows that burying the Tat peptide between two macromolecules can reduce its non-specific interactions. This may have implications for the development of long-circulating drugs delivery systems utilizing Tat.

Degradation of the poly(HPMA)-Tat-PEG conjugate was observed following incubation in acidified PBS buffer (pH 3.0, 37°C, 16 hr). Hydrazones are known to be pH-labile, however pH-dependence of hydrolysis is less pronounced for hydrazones formed with aldehyde functional groups.[79, 80] Free Tat-PEG is shown in Figure 1.3.4c, as the broad peak observed at ~ 38 minutes, indicating that free Tat-PEG is released under acidic conditions, also encountered upon trafficking of the conjugate to lysosome compartments within cells following internalization. Further analysis of the PMCA crosslinker used to couple Tat-PEG to poly(HPMA) showed slow degradation (data not shown) at both pH 7.4 and 5.0 at nearly the same rate ($t_{1/2}$ ~ 20 hr). Thus, short incubation times for *in vitro* analysis of poly(HPMA)-Tat-PEG were used to minimize degradation of the construct before internalization into cells. A more detailed analysis and discussion of hydrazone-forming crosslinkers for HPMA conjugation is forthcoming (Christie et al, manuscript in preparation).

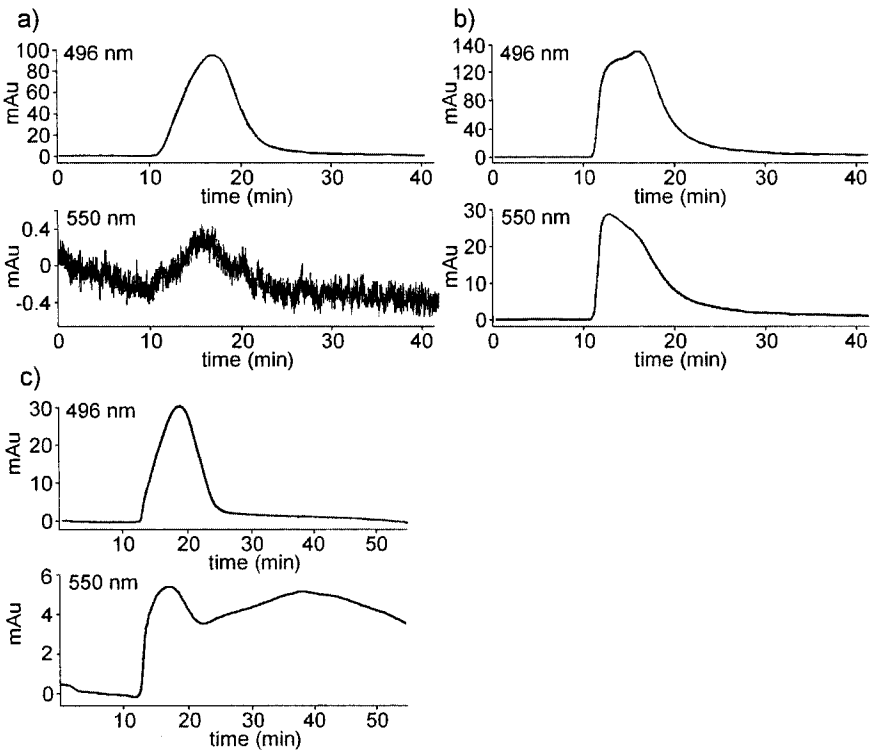

Figure 1.3.4. Size exclusion chromatography trace of poly(HPMA) before and HPMA-Tat-PEG conjugates monitored at 496 nm (Oregon Green, poly(HPMA) backbone) and 550 nm (TAMRA, Tat-PEG). (a) poly(HPMA) before Tat-PEG conjugation, (b) poly(HPMA) after Tat-PEG conjugation, and (c) poly(HPMA)-Tat-PEG after incubation for 16 hr at pH 3.0, 37°C. All chromatograms were recorded on an HP 1050A HPLC system using a BioSil 125 column and 0.1 M sodium phosphate buffer, 0.05 M NaCl, pH 7.2 as the elution buffer.

Subcellular Trafficking of HPMA-Tat-PEG

Incubation of cells with HPMA-Tat-PEG resulted in different subcellular localization of released Tat-PEG than unconjugated PEG, or poly(HPMA) alone. Highly endocytotic RAW murine macrophage cells were chosen for this study, and efficient internalization was observed after short incubation times (15 minutes) with labeled polymer solutions (data not shown). All cells were imaged live in phosphate buffer, so to alleviate artifacts

previously described following cell fixation.[29] Subcellular trafficking of free TAMRA-labeled PEG 2000, and Oregon-Green labeled poly(HPMA) controls lacking the Tat peptide resulted in these species sequestered into lysosome compartments even at long incubations (24 hr). This was indicated by lysosome-bound punctuate fluorescence in the microscopy images shown in Figure 1.3.5a. This type of lysosomal entrapment is expected, as these large, polar molecules require endocytotic or pinocytotic transport across the cell membrane and cannot escape the subcellular compartments.[81] Subcellular trafficking of HPMA-Tat-PEG was indicated by endocytotic uptake at early time points as shown in Figure 1.3.5b. Tat-PEG most likely has not been released from the poly(HPMA) backbone by hydrolysis of the hydrozone bond after this incubation period, preventing direct interaction of Tat with membrane components. Increased chase times following incubation with poly(HPMA)-Tat-PEG supports cytoplasmic entry of Tat-PEG, as shown in Figure 1.3.5c-e. Interestingly, while cytoplasmic entry and nuclear accumulation of Tat-PEG was observed in some cells, poly(HPMA) remained sequestered primarily in lysosomes. This result implies that the Tat peptide must be exposed to allow escape from lysosomal compartments, and cargo intented for cytoplasmic delivery must be covalently attached to the Tat peptide to be translocated across this membrane. To our knowledge, this type of selective transport has not previously been observed. It is possible that peptide fragments containing TAMRA dye, or TAMRA dye itself resulting from lysosomal degradation of the peptide portion of the construct are being released.

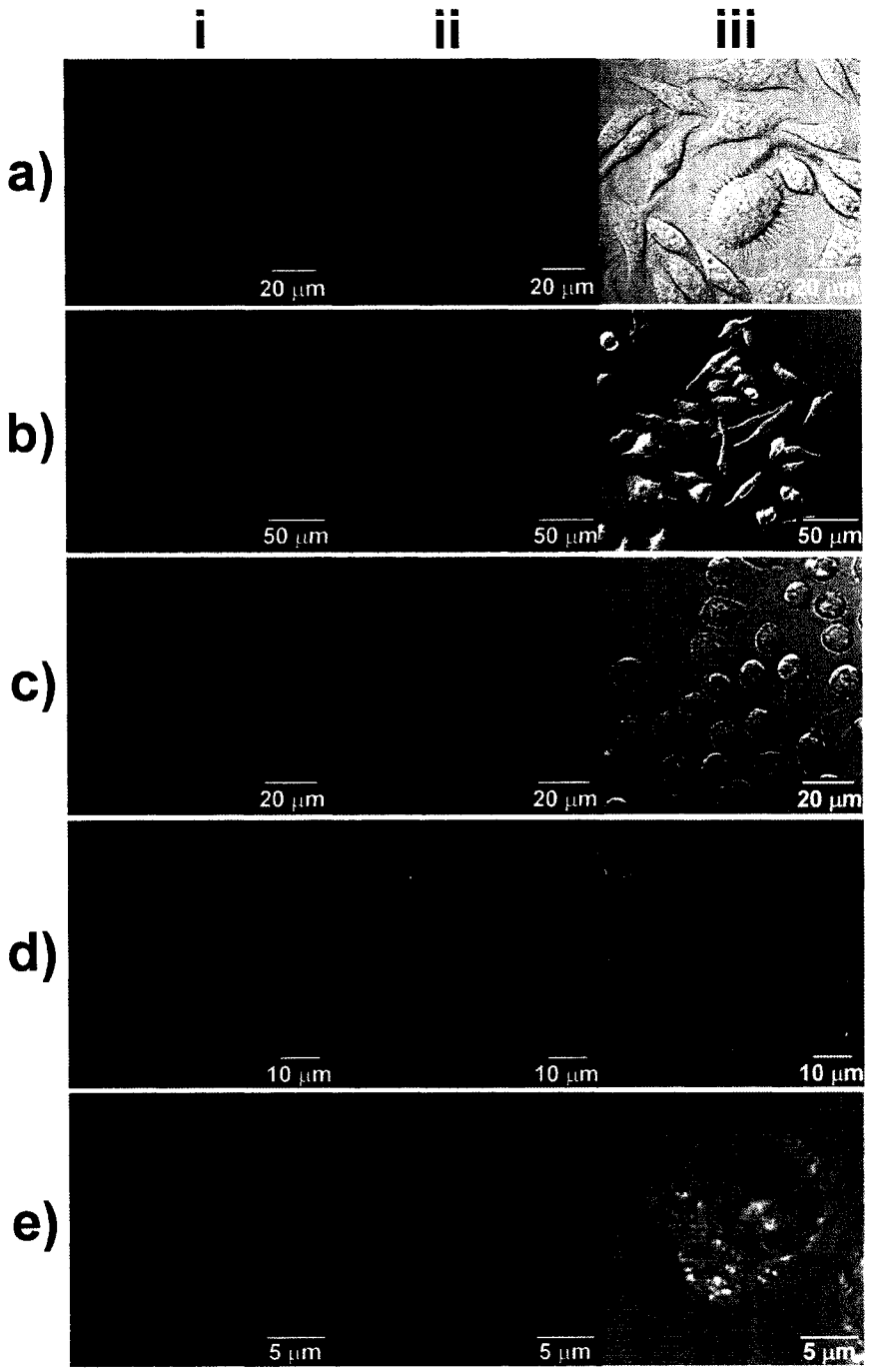

Figure 1.3.5. Confocal microscopy images of RAW 265.7 murine macrophage cells with a) co-incubation with poly(HPMA) and PEG 2000-TAMRA control, b) poly(HPMA)-Tat-PEG, 1hr incubation, 4 hr chase with label-free media, c,d,e) poly(HPMA)-Tat-PEG, 2 hr incubation, 24 hr chase with label-free media. For all images: i) Oregon Green channel, ii) TAMRA channel, iii) transmitted DIC image. All images recorded at 60x using a UPlanApo objective, all zoomed images were obtained digitally.

However, a previous study showed that for incubation of cells with trypsin-digested fluorescein-Tat peptide, cytoplasmic localization was not observed.[28] It is also possible that the Tat peptide and attached cargo is actively transported out of lysosome compartments by a specific transporter, as are known to exist for the amino acids lysine and arginine.[82, 83] The necessity to directly attach cargo to Tat is not clear based on findings from covalently conjugated constructs designed to deliver therapeutically relevant RNA or oligonucleotides. The problem with this approach arises from Tat interaction with negatively charged groups, preventing Tat peptides from associating with the membrane. Aggregation has been shown to occur, even though MALDI-TOF mass spectrometry shows that stoichiometric product has been formed.[69] However, some studies report antisense efficacy is increased with Tat under the assertion that Tat does not complex with nucleotide charges and affect activity.[70, 72] Others report modest siRNA activity for covalent siRNA-Tat conjugates, but less effective than Lipofectamine™ at similar concentrations.[75] Another report describes the inability of Tat-conjugated 2'-O-methyl, and locked nucleic acids, to block luciferase activity, with fluorescently labeled constructs observed bound in punctuate vesicles (presumably lysosomes) after 24 hrs.[71] However, increased transfection efficiency was observed in a branched Tat-oligonucleotide delivery construct, but only at high Tat/DNA charge ratios (1:8), perhaps indicating that some free, uncomplexed Tat is necessary to aid in lysosome escape, and thus increase transfection efficiency.[84] Tat oligomer-DNA electrostatic complexes have been shown to facilitate gene delivery, but efficiency was increased by pre-complexing with PEI first, with increased efficiency due to increased lysosomal escape claimed to result from PEI's proton sponge effect.[85] Again, the

observed increase in transfection ability could be due to free, exposed Tat sequences resulting from incomplete complexation with DNA in competition with PEI. Generally, free, unconjugated Tat peptide co-incubated with siRNA or DNA shows little or no desired activity.[71, 75, 86, 87] Reports of Tat-PAMAM –siRNA and Tat-PEG-PEI-DNA delivery constructs in which Tat peptide is bound to the carrier and not to the therapeutic agent do not increase delivery efficiency, supporting the possibility that direct covalent attachment of the Tat peptide is necessary for cargo to gain cytoplasmic entry.[73, 88] Interestingly, lower activity observed in vitro did not correlate to decreased activity in vivo for the Tat-PEG-PEI-DNA delivery construct, with reporter gene expressed in target bronchial and alveolar tissue.[73] Additionally, increased activity for Tat conjugates is observed by attachment to lipids, co-incubation with cationic lipids, or attachment of hydrophobic stearyl groups, perhaps illuminating a new cooperative pathway for conjugates to gain cytoplasmic entry.[37, 71, 87, 89, 90]

Tat cytoplasmic entry is also reported to be inefficient, as cytoplasmic entry is increased with the known lysosomotropic agent, chloroquine, and incorporation of a fusogenic peptide sequence, in addition to native Tat.[31] The construct described here does not allow direct determination of the efficiency of Tat escape, since the release rate of free Tat-PEG within lysosome compartments in unknown. Complete cytoplasmic entry of Tat-PEG was not observed in all cells after 24hr incubation, with much punctuate intracellular fluorescence still observed, This could also be due to Tat-PEG remaining covalently attached to the poly(HPMA) carrier. Quantification of subcellular localization of this construct may be realized using different dye-labeling approaches in conjunction with fluorescence microscopy techniques recently described.[91, 92]

Conclusions

In summary, we present a method to prepare a novel Tat conjugate as a tool to study subcellular trafficking of the Tat peptide by fluorescence microscopy. Utilization of a benign PEG model cargo allows stoichiometric attachment to the Tat peptide, avoiding undesirable electrostatic interactions that may skew membrane translocation ability. This degradable poly(HPMA)-Tat-PEG conjugate allows observation of subcellular trafficking of both the carrier and Tat-attached cargo independently using different fluorescent markers. Initial findings show that the HPMA-Tat-PEG construct containing masked Tat peptide is internalized within endocytotic vesicles. Extended incubation of HPMA-Tat-PEG results in cytoplasmic entry of Tat-PEG after degradation of the hydrazone linkage between the peptide and poly(HPMA) carrier, while species lacking the Tat peptide (poly(HPMA)) remain sequestered within lysosome compartments during the same time frame. This finding shows the importance for covalent attachment of potential therapeutic agents directly to the Tat peptide. These findings may allow for design of more effective Tat conjugates in which the Tat peptide is masked until the site of activity where cytoplasmic entry is desired, allowing for design of long-circulating conjugates. Future studies with this Tat-masked construct and further optimization of the reversible chemistries (rapidly, lysosome-specific degrading chemistries) used to attach Tat and cargo to the polymer carrier may result in a model therapeutic construct to accurately assess the efficiency with which Tat-mediated transport can occur. Additionally, studies involving metabolic inhibitors (deoxyglucose and azide), or agents known to prevent lysosome acidification (ammonium chloride), as

well as lysosome disrupting agents (chloroquine) could all lead to a better elucidation of this little-understood transport process.

Acknowledgements: The Authors thank G. Barisas for access to confocal microscopy facilities and helpful discussion, and G. Hagen for assistance with microscopy. We also thank D. Findley and E. Kaiser for excellent laboratory assistance.

References

[1] J.S. Wadia, S.F. Dowdy, Protein transduction technology. Current Opinion in Biotechnology 13(1) (2002) 52-56.
[2] B. Gupta, T.S. Levchenko, V.P. Torchilin, Intracellular delivery of large molecules and small particles by cell-penetrating proteins and peptides. Advanced Drug Delivery Reviews 57(4) (2005) 637-651.
[3] J.S. Wadia, S.F. Dowdy, Transmembrane delivery of protein and peptide drugs by TAT-mediated transduction in the treatment of cancer. Advanced Drug Delivery Reviews 57(4) (2005) 579-596.
[4] E. Vives, Present and future of cell-penetrating peptide mediated delivery systems: "is the Trojan horse too wild to go only to Troy?" J Control Release 109(1-3) (2005) 77-85.
[5] H. Brooks, B. Lebleu, E. Vives, Tat peptide-mediated cellular delivery: back to basics. Adv Drug Deliv Rev 57(4) (2005) 559-577.
[6] A.R. Thierry, S. Abes, S. Resina, A. Travo, J.P. Richard, P. Prevot, B. Lebleu, Comparison of basic peptides- and lipid-based strategies for the delivery of splice correcting oligonucleotides. Biochim Biophys Acta 1758(3) (2006) 364-374.
[7] E.L. Snyder, S.F. Dowdy, Cell penetrating peptides in drug delivery. Pharmaceutical Research 21(3) (2004) 389-393.
[8] S. Fawell, J. Seery, Y. Daikh, C. Moore, L.L. Chen, B. Pepinsky, J. Barsoum, Tat-mediated delivery of heterologous proteins into cells. Proc Natl Acad Sci U S A 91(2) (1994) 664-668.
[9] M. Chang, J.C. Chou, H.J. Lee, Cellular internalization of fluorescent proteins via arginine-rich intracellular delivery peptide in plant cells. Plant Cell Physiol 46(3) (2005) 482-488.
[10] E. Vives, P. Charneau, J. van Rietschoten, H. Rochat, E. Bahraoui, Effects of the Tat basic domain on human immunodeficiency virus type 1 transactivation, using chemically synthesized Tat protein and Tat peptides. J Virol 68(5) (1994) 3343-3353.
[11] P. Wunderbaldinger, L. Josephson, R. Weissleder, Tat peptide directs enhanced clearance and hepatic permeability of magnetic nanoparticles. Bioconjug Chem 13(2) (2002) 264-268.
[12] M. Zhao, M.F. Kircher, L. Josephson, R. Weissleder, Differential conjugation of tat peptide to superparamagnetic nanoparticles and its effect on cellular uptake. Bioconjug Chem 13(4) (2002) 840-844.
[13] A. Nori, K.D. Jensen, M. Tijerina, P. Kopeckova, J. Kopecek, Subcellular trafficking of HPMA copolymer-Tat conjugates in human ovarian carcinoma cells. Journal of Controlled Release 91(1-2) (2003) 53-59.
[14] A. Nori, K.D. Jensen, M. Tijerina, P. Kopeckova, J. Kopecek, Tat-conjugated synthetic macromolecules facilitate cytoplasmic drug delivery to human ovarian carcinoma cells. Bioconjugate Chemistry 14(1) (2003) 44-50.
[15] R. Bhorade, R. Weissleder, T. Nakakoshi, A. Moore, C.H. Tung, Macrocyclic chelators with paramagnetic cations are internalized into mammalian cells via a HIV-tat derived membrane translocation peptide. Bioconjug Chem 11(3) (2000) 301-305.

[16] M. Lewin, N. Carlesso, C.H. Tung, X.W. Tang, D. Cory, D.T. Scadden, R. Weissleder, Tat peptide-derivatized magnetic nanoparticles allow in vivo tracking and recovery of progenitor cells. Nat Biotechnol 18(4) (2000) 410-414.
[17] M. Mie, F. Takahashi, H. Funabashi, Y. Yanagida, M. Aizawa, E. Kobatake, Intracellular delivery of antibodies using TAT fusion protein A. Biochemical and Biophysical Research Communications 310(3) (2003) 730-734.
[18] J.M. de la Fuente, C.C. Berry, Tat peptide as an efficient molecule to translocate gold nanoparticles into the cell nucleus. Bioconjug Chem 16(5) (2005) 1176-1180.
[19] H.J. Jung, Y. Park, K.S. Hahm, D.G. Lee, Biological activity of Tat (47-58) peptide on human pathogenic fungi. Biochem Biophys Res Commun 345(1) (2006) 222-228.
[20] E.L. Snyder, B.R. Meade, C.C. Saenz, S.F. Dowdy, Treatment of terminal peritoneal carcinomatosis by a transducible p53-activating peptide. PLoS Biol 2(2) (2004) E36.
[21] T.B. Potocky, A.K. Menon, S.H. Gellman, Cytoplasmic and nuclear delivery of a TAT-derived peptide and a beta-peptide after endocytic uptake into HeLa cells. J Biol Chem 278(50) (2003) 50188-50194.
[22] P.A. Wender, D.J. Mitchell, K. Pattabiraman, E.T. Pelkey, L. Steinman, J.B. Rothbard, The design, synthesis, and evaluation of molecules that enable or enhance cellular uptake: peptoid molecular transporters. Proc Natl Acad Sci U S A 97(24) (2000) 13003-13008.
[23] S. Futaki, T. Suzuki, W. Ohashi, T. Yagami, S. Tanaka, K. Ueda, Y. Sugiura, Arginine-rich peptides - An abundant source of membrane-permeable peptides having potential as carriers for intracellular protein delivery. Journal of Biological Chemistry 276(8) (2001) 5836-5840.
[24] H. Xia, Q. Mao, B.L. Davidson, The HIV Tat protein transduction domain improves the biodistribution of beta-glucuronidase expressed from recombinant viral vectors. Nat Biotechnol 19(7) (2001) 640-644.
[25] U. Niesner, C. Halin, L. Lozzi, M. Gunthert, P. Neri, H. Wunderli-Allenspach, L. Zardi, D. Neri, Quantitation of the tumor-targeting properties of antibody fragments conjugated to cell-permeating HIV-1 TAT peptides. Bioconjug Chem 13(4) (2002) 729-736.
[26] M. Tyagi, M. Rusnati, M. Presta, M. Giacca, Internalization of HIV-1 tat requires cell surface heparan sulfate proteoglycans. J Biol Chem 276(5) (2001) 3254-3261.
[27] A.D. Frankel, C.O. Pabo, Cellular uptake of the tat protein from human immunodeficiency virus. Cell 55(6) (1988) 1189-1193.
[28] E. Vives, P. Brodin, B. Lebleu, A truncated HIV-1 Tat protein basic domain rapidly translocates through the plasma membrane and accumulates in the cell nucleus. J Biol Chem 272(25) (1997) 16010-16017.
[29] J.P. Richard, K. Melikov, E. Vives, C. Ramos, B. Verbeure, M.J. Gait, L.V. Chernomordik, B. Lebleu, Cell-penetrating peptides. A reevaluation of the mechanism of cellular uptake. J Biol Chem 278(1) (2003) 585-590.
[30] A. Ziegler, P. Nervi, M. Durrenberger, J. Seelig, The cationic cell-penetrating peptide CPP(TAT) derived from the HIV-1 protein TAT is rapidly transported into living fibroblasts: optical, biophysical, and metabolic evidence. Biochemistry 44(1) (2005) 138-148.

[31] J.S. Wadia, R.V. Stan, S.F. Dowdy, Transducible TAT-HA fusogenic peptide enhances escape of TAT-fusion proteins after lipid raft macropinocytosis. Nature Medicine 10(3) (2004) 310-315.
[32] I.M. Kaplan, J.S. Wadia, S.F. Dowdy, Cationic TAT peptide transduction domain enters cells by macropinocytosis. Journal of Controlled Release 102(1) (2005) 247-253.
[33] J.P. Richard, K. Melikov, H. Brooks, P. Prevot, B. Lebleu, L.V. Chernomordik, Cellular uptake of unconjugated TAT peptide involves clathrin-dependent endocytosis and heparan sulfate receptors. J Biol Chem 280(15) (2005) 15300-15306.
[34] I.A. Ignatovich, E.B. Dizhe, A.V. Pavlotskaya, B.N. Akifiev, S.V. Burov, S.V. Orlov, A.P. Perevozchikov, Complexes of plasmid DNA with basic domain 47-57 of the HIV-1 Tat protein are transferred to mammalian cells by endocytosis-mediated pathways. J Biol Chem 278(43) (2003) 42625-42636.
[35] M.M. Fretz, G.A. Koning, A. Mastrobattista, W. Jiskoot, G. Storm, OVCAR-3 cells internalize TAT-peptide modified liposomes by endocytosis. Biochimica Et Biophysica Acta-Biomembranes 1665(1-2) (2004) 48-56.
[36] D. Soundara Manickam, H.S. Bisht, L. Wan, G. Mao, D. Oupicky, Influence of TAT-peptide polymerization on properties and transfection activity of TAT/DNA polyplexes. J Control Release 102(1) (2005) 293-306.
[37] L. Hyndman, J.L. Lemoine, L. Huang, D.J. Porteous, A.C. Boyd, X.S. Nan, HIV-1 Tat protein transduction domain peptide facilitates gene transfer in combination with cationic liposomes. Journal of Controlled Release 99(3) (2004) 435-444.
[38] J.R. Maiolo, 3rd, E.A. Ottinger, M. Ferrer, Specific redistribution of cell-penetrating peptides from endosomes to the cytoplasm and nucleus upon laser illumination. J Am Chem Soc 126(47) (2004) 15376-15377.
[39] G. Drin, H. Demene, J. Temsamani, R. Brasseur, Translocation of the pAntp peptide and its amphipathic analogue AP-2AL. Biochemistry 40(6) (2001) 1824-1834.
[40] D. Persson, P.E. Thoren, M. Herner, P. Lincoln, B. Norden, Application of a novel analysis to measure the binding of the membrane-translocating peptide penetratin to negatively charged liposomes. Biochemistry 42(2) (2003) 421-429.
[41] D. Persson, P.E. Thoren, P. Lincoln, B. Norden, Vesicle membrane interactions of penetratin analogues. Biochemistry 43(34) (2004) 11045-11055.
[42] L.A. Kueltzo, N. Normand, P. O'Hare, C.R. Middaugh, Conformational lability of herpesvirus protein VP22. J Biol Chem 275(43) (2000) 33213-33221.
[43] M. Mano, A. Henriques, A. Paiva, M. Prieto, F. Gavilanes, S. Simoes, M.C. Pedroso de Lima, Cellular uptake of S4(13)-PV peptide occurs upon conformational changes induced by peptide-membrane interactions. Biochim Biophys Acta 1758(3) (2006) 336-346.
[44] A. Ho, S.R. Schwarze, S.J. Mermelstein, G. Waksman, S.F. Dowdy, Synthetic protein transduction domains: enhanced transduction potential in vitro and in vivo. Cancer Res 61(2) (2001) 474-477.
[45] A. Friedler, D. Friedler, N.W. Luedtke, Y. Tor, A. Loyter, C. Gilon, Development of a functional backbone cyclic mimetic of the HTV-1 Tat arginine-rich motif. Journal of Biological Chemistry 275(31) (2000) 23783-23789.
[46] M. Silhol, M. Tyagi, M. Giacca, B. Lebleu, E. Vives, Different mechanisms for cellular internalization of the HIV-1 Tat-derived cell penetrating peptide and recombinant proteins fused to Tat. Eur J Biochem 269(2) (2002) 494-501.

[47] A. Ziegler, X.L. Blatter, A. Seelig, J. Seelig, Protein transduction domains of HIV-1 and SIV TAT interact with charged lipid vesicles. Binding mechanism and thermodynamic analysis. Biochemistry 42(30) (2003) 9185-9194.
[48] A. Ziegler, J. Seelig, Interaction of the protein transduction domain of HIV-1 TAT with heparan sulfate: binding mechanism and thermodynamic parameters. Biophys J 86(1 Pt 1) (2004) 254-263.
[49] S.R. Schwarze, A. Ho, A. Vocero-Akbani, S.F. Dowdy, In vivo protein transduction: delivery of a biologically active protein into the mouse. Science 285(5433) (1999) 1569-1572.
[50] S. Kameyama, M. Horie, T. Kikuchi, T. Omura, T. Takeuchi, I. Nakase, Y. Sugiura, S. Futaki, Effects of cell-permeating peptide binding on the distribution of 125I-labeled fab fragment in rats. Bioconjug Chem 17(3) (2006) 597-602.
[51] H.J. Lee, W.M. Pardridge, Pharmacokinetics and delivery of tat and tat-protein conjugates to tissues in vivo. Bioconjug Chem 12(6) (2001) 995-999.
[52] K. Ulbrich, V. Subr, J. Strohalm, D. Plocova, M. Jelinkova, B. Rihova, Polymeric drugs based on conjugates of synthetic and natural macromolecules. I. Synthesis and physico-chemical characterisation. J Control Release 64(1-3) (2000) 63-79.
[53] J. Drobnik, J. Kopecek, J. Labsky, P. Rejmanova, J. Exner, V. Saudek, J. Kalal, Enzymatic Cleavage of Side-Chains of Synthetic Water-Soluble Polymers. Makromolekulare Chemie-Macromolecular Chemistry and Physics 177(10) (1976) 2833-2848.
[54] P. Rejmanova, J. Kopecek, J. Pohl, M. Baudys, V. Kostka, Polymers Containing Enzymatically Degradable Bonds .8. Degradation of Oligopeptide Sequences in N-(2-Hydroxypropyl)Methacrylamide Co-Polymers by Bovine Spleen Cathepsin-B. Makromolekulare Chemie-Macromolecular Chemistry and Physics 184(10) (1983) 2009-2020.
[55] T. Etrych, M. Jelinkova, B. Rihova, K. Ulbrich, New HPMA copolymers containing doxorubicin bound via pH-sensitive linkage: synthesis and preliminary in vitro and in vivo biological properties. Journal of Controlled Release 73(1) (2001) 89-102.
[56] T. Etrych, P. Chytil, M. Jelinkova, B. Rihova, K. Ulbrich, Synthesis of HPMA copolymers containing doxorubicin bound via a hydrazone linkage. Effect of spacer on drug release and in vitro cytotoxicity. Macromolecular Bioscience 2(1) (2002) 43-52.
[57] D.B. Rozema, K. Ekena, D.L. Lewis, A.G. Loomis, J.A. Wolff, Endosomolysis by masking of a membrane-active agent (EMMA) for cytoplasmic release of macromolecules. Bioconjug Chem 14(1) (2003) 51-57.
[58] K. Omura, D. Swern, Oxidation of alcohols by "activated" dimethyl sulfoxide. a preparative steric and mechanistic study. Tetrahedron 34 (1978) 1651-1660.
[59] D. Putnam, J. Kopecek, Polymer conjugates with anticancer activity. Biopolymers Ii 122 (1995) 55-123.
[60] A. Nori, J. Kopecek, Intracellular targeting of polymer-bound drugs for cancer chemotherapy. Adv Drug Deliv Rev 57(4) (2005) 609-636.
[61] K.D. Jensen, A. Nori, M. Tijerina, P. Kopeckova, J. Kopecek, Cytoplasmic delivery and nuclear targeting of synthetic macromolecules. Journal of Controlled Release 87(1-3) (2003) 89-105.
[62] J. Kopecek, H. Bazilova, Poly[N-(2-Hydroxypropyl)Methacrylamide] .1. Radical Polymerization and Copolymerization. European Polymer Journal 9(1) (1973) 7-14.

[63] J. Kopecek, Reactive Copolymers of N-(2-Hydroxypropyl)Methacrylamide with N-Methacryloylated Derivatives of L-Leucine and L-Phenylalanine .1. Preparation, Characterization, and Reactions with Diamines. Makromolekulare Chemie-Macromolecular Chemistry and Physics 178(8) (1977) 2169-2183.
[64] R. Duncan, K. Ulbrich, Development of N-(2-Hydroxypropyl)Methacrylamide Copolymer Conjugates for Delivery of Cancer-Chemotherapy. Makromolekulare Chemie-Macromolecular Symposia 70-1 (1993) 157-162.
[65] S. Wroblewski, P. Kopeckova, B. Rihova, J. Kopecek, Lectin-HPMA copolymer conjugates: potential oral drug carriers for targeting diseased tissues. Macromolecular Chemistry and Physics 199(11) (1998) 2601-2608.
[66] K.D. Jensen, P. Kopeckova, J.H.B. Bridge, J. Kopecek, The cytoplasmic escape and nuclear accumulation of endocytosed and microinjected HPMA copolymers and a basic kinetic study in Hep G2 cells. Aaps Pharmsci 3(4) (2001) -.
[67] F. Maurel, F. Debart, F. Cavelier, A.R. Thierry, B. Lebleu, J.J. Vasseur, E. Vives, Toward high yield synthesis of peptide-oligonucleotide chimera through a disulfide bridge: a simplified method for oligonucleotide activation. Bioorg Med Chem Lett 15(22) (2005) 5084-5087.
[68] E. Vives, B. Lebleu, Selective coupling of a highly basic peptide to an oligonucleotide. Tetrahedron Letters 38(7) (1997) 1183-1186.
[69] C.E. Prater, P.S. Miller, 3'-methylphosphonate-modified oligo-2'-O-methylribonucleotides and their Tat peptide conjugates: uptake and stability in mouse fibroblasts in culture. Bioconjug Chem 15(3) (2004) 498-507.
[70] A. Astriab-Fisher, D. Sergueev, M. Fisher, B.R. Shaw, R.L. Juliano, Conjugates of antisense oligonucleotides with the Tat and antennapedia cell-penetrating peptides: effects on cellular uptake, binding to target sequences, and biologic actions. Pharm Res 19(6) (2002) 744-754.
[71] J.J. Turner, A.A. Arzumanov, M.J. Gait, Synthesis, cellular uptake and HIV-1 Tat-dependent trans-activation inhibition activity of oligonucleotide analogues disulphide-conjugated to cell-penetrating peptides. Nucleic Acids Research 33(1) (2005) 27-42.
[72] A. Astriab-Fisher, D.S. Sergueev, M. Fisher, B.R. Shaw, R.L. Juliano, Antisense inhibition of P-glycoprotein expression using peptide-oligonucleotide conjugates. Biochem Pharmacol 60(1) (2000) 83-90.
[73] E. Kleemann, M. Neu, N. Jekel, L. Fink, T. Schmehl, T. Gessler, W. Seeger, T. Kissel, Nano-carriers for DNA delivery to the lung based upon a TAT-derived peptide covalently coupled to PEG-PEI. Journal of Controlled Release 109(1-3) (2005) 299-316.
[74] N. Nitin, P.J. Santangelo, G. Kim, S. Nie, G. Bao, Peptide-linked molecular beacons for efficient delivery and rapid mRNA detection in living cells. Nucleic Acids Res 32(6) (2004) e58.
[75] Y.L. Chiu, A. Ali, C.Y. Chu, H. Cao, T.M. Rana, Visualizing a correlation between siRNA localization, cellular uptake, and RNAi in living cells. Chem Biol 11(8) (2004) 1165-1175.
[76] E.P. Feener, W.C. Shen, H.J. Ryser, Cleavage of disulfide bonds in endocytosed macromolecules. A processing not associated with lysosomes or endosomes. J Biol Chem 265(31) (1990) 18780-18785.

[77] D.E. Chico, R.L. Given, B.T. Miller, Binding of cationic cell-permeable peptides to plastic and glass. Peptides 24(1) (2003) 3-9.
[78] G.T. Hermanson, Bioconjugate techniques, Academic Press, San Diego, 1996.
[79] F. Kratz, U. Beyer, M.T. Schutte, Drug-polymer conjugates containing acid-cleavable bonds. Critical Reviews in Therapeutic Drug Carrier Systems 16(3) (1999) 245-288.
[80] K.R. West, S. Otto, Reversible covalent chemistry in drug delivery. Curr Drug Discov Technol 2(3) (2005) 123-160.
[81] J.B. Lloyd, Lysosome membrane permeability: implications for drug delivery. Adv Drug Deliv Rev 41(2) (2000) 189-200.
[82] R.L. Pisoni, J.G. Thoene, H.N. Christensen, Detection and characterization of carrier-mediated cationic amino acid transport in lysosomes of normal and cystinotic human fibroblasts. Role in therapeutic cystine removal? J Biol Chem 260(8) (1985) 4791-4798.
[83] R.L. Pisoni, G.Y. Park, V.Q. Velilla, J.G. Thoene, Detection and characterization of a transport system mediating cysteamine entry into human fibroblast lysosomes. Specificity for aminoethylthiol and aminoethylsulfide derivatives. J Biol Chem 270(3) (1995) 1179-1184.
[84] I. Hellgren, J. Gorman, C. Sylven, Factors controlling the efficiency of Tat-mediated plasmid DNA transfer. Journal of Drug Targeting 12(1) (2004) 39-47.
[85] C. Rudolph, C. Plank, J. Lausier, U. Schillinger, R.H. Muller, J. Rosenecker, Oligomers of the arginine-rich motif of the HIV-1 TAT protein are capable of transferring plasmid DNA into cells. J Biol Chem 278(13) (2003) 11411-11418.
[86] Z. Siprashvili, F.A. Scholl, S.F. Oliver, A. Adams, C.H. Contag, P.A. Wender, P.A. Khavari, Gene transfer via reversible plasmid condensation with cysteine-flanked, internally spaced arginine-rich peptides. Human Gene Therapy 14(13) (2003) 1225-1233.
[87] S. Futaki, W. Ohashi, T. Suzuki, M. Niwa, S. Tanaka, K. Ueda, H. Harashima, Y. Sugiura, Stearylated arginine-rich peptides: A new class of transfection systems. Bioconjugate Chemistry 12(6) (2001) 1005-1011.
[88] H.M. Kang, R. DeLong, M.H. Fisher, R.L. Juliano, Tat-conjugated PAMAM dendrimers as delivery agents for antisense and siRNA oligonucleotides. Pharmaceutical Research 22(12) (2005) 2099-2106.
[89] V.P. Torchilin, T.S. Levchenko, R. Rammohan, N. Volodina, B. Papahadjopoulos-Sternberg, G.G.M. D'Souza, Cell transfection in vitro and in vivo with nontoxic TAT peptide-liposome-DNA complexes. Proceedings of the National Academy of Sciences of the United States of America 100(4) (2003) 1972-1977.
[90] V.P. Torchilin, R. Rammohan, V. Weissig, T.S. Levchenko, TAT peptide on the surface of liposomes affords their efficient intracellular delivery even at low temperature and in the presence of metabolic inhibitors. Proc Natl Acad Sci U S A 98(15) (2001) 8786-8791.
[91] H. Akita, R. Ito, H. Kamiya, H. Harashima, Semi-quantitative analysis of the intracellular trafficking of plasmid DNA with confocal laser scanning microscopy. Molecular Therapy 7(5) (2003) S214-S214.
[92] H. Akita, R. Ito, I.A. Khalil, S. Futaki, H. Harashima, Quantitative three-dimensional analysis of the intracellular trafficking of plasmid DNA transfected by a

nonviral gene delivery system using confocal laser scanning microscopy. Molecular Therapy 9(3) (2004) 443-451.

CHAPTER IV

PREPARATION AND OPTICAL PROPERTIES OF A NOVEL THIOL-CONTAINING TETRAMETHYLRHODAMINE DYE

This dissertation chapter contains the manuscript of a communication intended for publication in *Bioconjugate Chemistry* written by R. James Christie and edited by David W. Grainger. The finding of unique spectral properties resulting from oxidization and dimer formation of thiol-modified tetramethylrhodamine provides a new analytical tool for the study of redox processes in addition for use as a reactive dye for studies described in Chapter 5 of this dissertation section.

Preparation and Optical Properties of a Novel Thiol-Containing Tetramethylrhodamine Dye

R. James Christie, Constantino Tadiello, David W. Grainger

Abstract

A novel thiolated fluorescent dye was synthesized by reaction of 5(6)-succinimidyl tetramethylrhodamine with cystamine hydrochloride. The resulting TAMRA disulfide dimer exhibited a hypsochromic shift of 34 nm relative to the reduced monomer species, and an isosbestic point at 532 nm between reduced monomeric and oxidized dimeric forms. Molar extinction coefficients of the monomer and dimer relative to moles of TAMRA were similar ($6.4x10^4$ $M^{-1}cm^{-1}$ and $6.1x10^{-4}M^{-1}cm^{-1}$, respectively). However, fluorescence emission was altered, with > 93% of fluorescence quenched upon dimer formation in phosphate buffered saline. The resulting disulfide dye was easily reduced using both soluble and agarose gel immobilized tris(2-carboxyethyl) phosphine. Absorbance intensity ratios at 554 and 520 nm were used to determine the half-life of a $1.2x10^{-5}$ M solution of reduced TAMRA, to be ~50 hr at 22°C. The free thiol dye was further reacted with maleimide derivatized poly(HPMA) to form the dye-labeled polymer conjugate. This dye derivative should prove useful as a dithiol reductase-sensitive

fluorescent probe in cellular tracking systems as well as a thiol-based dye-labeling reagent.

Communication

Reactive fluorescent dyes have many applications from biological assay reporters to tracking molecules *in vitro* and *in vivo*.(*1-4*) A number of reactive fluorescent dyes are commercially available, containing functional groups such as NHS esters, isothiocyanates, maleimides, or iodoacetamides to match naturally occurring reactive amine and thiol functional groups on proteins.(*5*) However, only one thiol-containing dye is commercially available. This fluorescein-based dye (SAMSA, Invitrogen) contains an acetyl-protected thiol group that must be deprotected in basic conditions to generate free thiol. This product is known to be pH sensitive, with quantum yield decreasing by ~70-80% upon acidification and formation of the neutral molecule.(*6, 7*) Observing such fluorescein-labeled molecules within cells that are trafficked to lysosomes is difficult due to decreased fluorescein signal within these acidic subcellular compartments. Synthesis of a non-exotic, thiol-containing, pH-insensitive, reactive fluorescent dye reagent with minimal synthetic steps motivated this work. Tetramethylrhodamine (TAMRA) was chosen for this study because of its excellent stability, and unaffected quantum yield at acidic pH.(*8*) In fact, several intracellular pH estimates have been described based on the ratio of fluorescence from fluorescein and TAMRA.(*9-11*)

Thiol groups were incorporated into TAMRA by reacting commercially supplied 5-(and-6)-carboxytetramethylrhodamine, succinimidyl ester (5(6) TAMRA-NHS,

AnaSpec) with cystamine hydrochloride activated with diisopropylethylamine (DIPEA) as shown in Scheme 1.4.1. In a typical experiment, 9.6 mg cystamine hydrochloride (0.085 mmol, 0.9 eq. amines) was activated in 2.5 mL dimethylformamide (DMF) containing 30 μL DIPEA (0.17 mmol, 1.8 eq). This solution was then added to a solution of 50.0 mg TAMRA-NHS (0.095mmol, 1.0 eq) in 1.5 mL DMF and stirred at room temperature for 30 minutes. Then 15 μL (0.086 mmol, 1.0 eq) of DIPEA was added and the reaction stirred

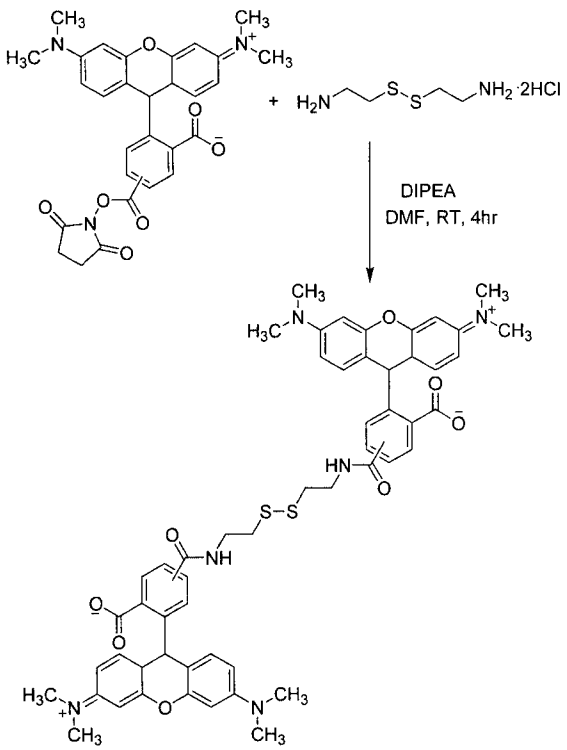

Scheme 1.4.1. Synthesis of ssTAMRA dimer

for an additional hour. Product was then precipitated by addition of 50 mL cold diethyl ether, washed several times with diethyl ether and dried under vacuum overnight. Solids were further purified by repeated precipitation from methanol into cold ether. Product was recovered in excellent yields, usually > 80%. Characterization of product by mass

spectrometry showed that the desired product was obtained (M[H+], FAB, calculated = 977.336, found = 977.334), and ^{1}H NMR analysis confirmed formation of the new amide bonds, with four relevant peaks observed corresponding to combinations of 5 and 6 TAMRA isomers (8.58, 8.91, 9.00, 9.07 ppm, triplets, total integration = 2H, d_6 DMSO). A similar synthetic approach has recently been described to produce a thiol-containing carboxy-x-rhodamine to observe light harvesting ability of a phenylene/ethynylene polymer, as well as synthesis of a self-quenching fluorescein-methyl red reporter molecule.(*12, 13*) However thiolated carboxy-x-rhodamine was prepared using mercaptoethylamine·HCl instead of cystamine. This same approach was attempted to produce monomeric thiolated TAMRA, with the majority of product isolated as disulfide. Thus subsequent experiments utilized dimerized starting material based on the cystamine product. Reduction of the disulfide was readily achieved after 30 min incubation in 10mM tris(2-carboxyethyl) phosphine hydrochloride (TCEP·HCl), with no increase in 554 nm TAMRASH monomer absorbance after this time indicating complete reduction.

Preparation of dimeric fluorescent reporter molecules has received much attention due to the different spectral properties of these molecules in monomeric and dimeric forms.(*13-15*) Spectral properties of the reduced monomeric (sTAMRA) and oxidized dimeric thiolated TAMRA (ssTAMRA) are summarized in Table 1.4.1.

Table 1.4.1. Spectral properties of oxidized and reduced sTAMRA.

	λ_{max} absorbance (nm)	ε ($M^{-1}cm^{-1}$)	554/521 ratio	521/554 ratio	λ_{max} emission (nm)	Relative fluorescence[b]
Reduced sTAMRA	520	6.4×10^{4}[a]	2.37	0.42	578	1.00
Oxidized ssTAMRA	554	6.1×10^{4}	0.38	2.64	578	.061

[a] expressed relative to moles TAMRA
[b] excitation at isosbestic point, 532 nm

Oxidized ssTAMRA exhibits a hypsochromic shift of 34 nm relative to the reduced sTAMRA absorption maximum, close to native TAMRA (Fig. 1.4.1a, Table 1.4.1). This phenomenon has been observed for concentrated aqueous solutions of rhodamine B with the formation of non-covalent dimers prominent at mM concentrations with a dissociation constant of $6.8\text{x}10^{-4}$M.(*16, 17*) This hypsochromic shift has also been used to study conformation and subunit exchange of *E. coli* ribosomal protein L7/L12, and configuration of the muscle protein, titin, labeled with tetramethylrhodamine iodoacetamide to label thiol groups on cysteine residues.(*18, 19*) These studies utilized the ratio of non-covalent dimer absorbance at 518 nm to monomer absorbance at 555 nm to determine proximity of TAMRA labels on the protein, with a 518/554 absorbance ratio of 1-1.3 reported for non-covalent dimeric TAMRA.(*18*) Additionally, a 519/550 ratio for an analogous covalent TAMRA dimer linked by thiourea bonds and an ethylene spacer has been reported to be 1.5.(*20*) Results for ssTAMRA show a 520/554 ratio of 2.64 for the covalent disulfide dimer, exceeding ratios previously described indicating that the disulfide 4-carbon spacer used in this study is perhaps more capable of producing

a completely dimeric TAMRA system. This ratio may be further increased by using pure starting material, instead of mixed 5 and 6 TAMRA-NHS isomers as reported here. Dimer formation had no affect on optical absorption of attached TAMRA, molar extinction coefficients determined for reduced and oxidized species are nearly identical. However, fluorescence emission was nearly extinguished, with fluorescence intensity reduced by > 93% upon dimer formation in ssTAMRA when excited at the isosbestic point (532 nm). This is likely due to self-quenching resulting from stacking of the xanthene rings as previously described for analogous rhodamine B, rhodamine 6G, and TAMRA covalent dimers in aqueous solution.(*17, 21, 22*) Stacking proximity of a folded covalent TAMRA dimer containing an ethylenediamine spacer has been estimated as 0.9 nm.(*20*) Fluorescence quenching of rhodamine dimers appears to be solvent dependent, with no quenching observed in mixed water/organic solvent systems, but observed in aqueous buffered systems as also described here.(*19-22*) The small amount of fluorescence emission observed in the current ssTAMRA dimer system was most likely due to residual monomer, or possibly extended dimers, as the fluorescence emission intensity relative to the monomer intensity increased from 2.4 to 12.7% upon excitation of the dimer at 521, 532, and 554 nm (λ_{max} of monomer). Additionally, the fluorescence emission peak was centered at 578 nm for dimer and monomer solutions, an unusually large Stokes shift of 58 nm for the dimer species. The reversibility of disulfide reduction/oxidation was determined following complete reduction of the disulfide with agarose gel-immobilized TCEP (Pierce) in buffer (0.1 M sodium phosphate, 0.15 M NaCl, 10 mM EDTA, pH 7.2). Upon removal of reducing agent by filtration, the resulting sTAMRA solution ($1.2x10^{-5}$ M) was maintained in the dark at room temperature

(22 °C), and the absorbance spectrum was recorded at various times. These absorbance spectra are shown in Figure 1.4.1a, showing the isosbestic point at 532 nm. The rate of reformation of the disulfide was determined by plotting the 554/520 absorption ratios as shown in Figure 1.4.1b. The reduced dye is relatively stable at μM concentrations in this buffer system for several days ($t_{1/2}$ ~ 50 hr).

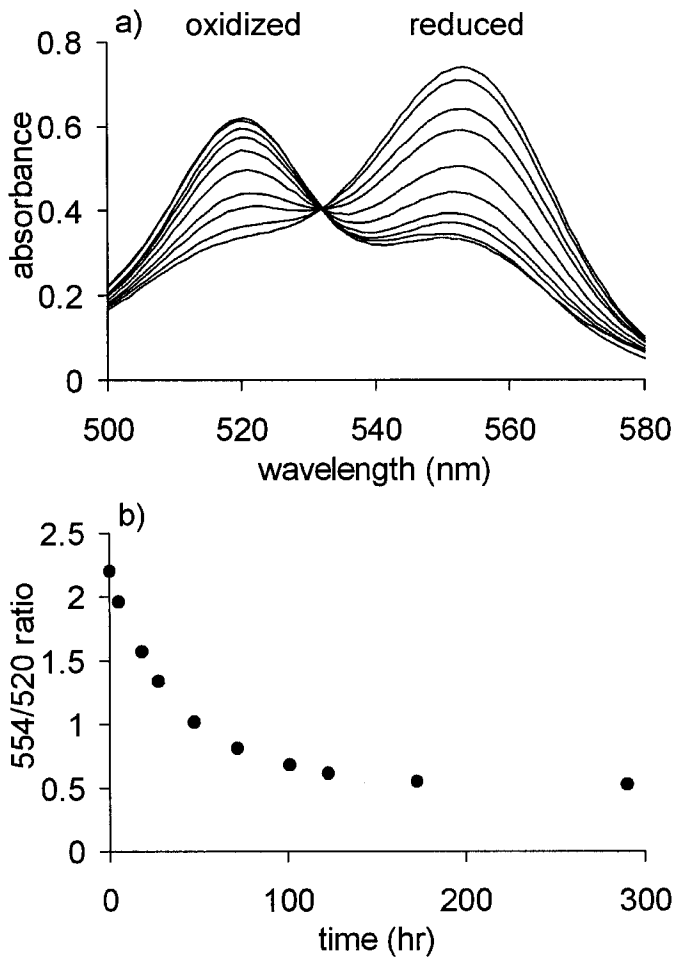

Figure 1.4.1. Oxidation of sTAMRA monomer in 0.1 M sodium phosphate, 0.15 M NaCl, 10 mM EDTA, pH 7.2 . a) absorbance spectra of $1.2x10^{-5}$ M sTAMRA at various times. b) 554/520 ratio of absorbance spectra showing disulfide formation rate.

Practical application of sTAMRA was realized by covalent reaction with Oregon Green®- labeled, maleimide derivatized, poly[N-(2-hydroxypropyl)methacrylamide] (HPMA). Maleimide functional groups are well-known to be thiol-reactive, forming thioethers by Michael addition of sulfur to the electron-deficient double bond.(*23*) This dual-labeled water-soluble polymer allowed dual observation of the Oregon Green® backbone and reacted sTAMRA using diode array detection at absorption wavelengths for Oregon Green® 488 (496 nm) and TAMRASH (554 nm). ssTAMRA dimer (7.0 mg, 1.6 μmol) was reduced using TCEP reducing gel (2.5 mL slurry/μmol ssTAMRA dimer) for 45 minutes, following removal of the reducing agent by filtration through a 0.2 μm filter. Reduced sTAMRA was allowed to react with maleimide-derivatized poly(HPMA) (40.45 mg, 1.60×10^{-6} mol maleimide groups) for 8 hr in 0.1M sodium phosphate, 0.15M NaCl, 10 mM EDTA, pH 7.2, then remaining maleimide groups were quenched by addition of 2 μL β-mercaptoethanol. The labeled poly(HPMA) product was separated from free sTAMRA dye and desalted using size exclusion chromatography (SEC) (Sephadex G-25, 15x1cm, H_2O mobile phase) then isolated using a speed-vac. Formation of the polymer-TAMRA conjugate was confirmed by analytical SEC (BioSilect 125 column, 0.5 mL/min 0.1M sodium phosphate, 0.15M NaCl, 10 mM EDTA, pH 7.2) with TAMRA eluting with the polymer fraction at 12-22 min as shown in Figure 1.4.2 (free dye elutes from this column after 30 minutes under these conditions). The small amount of free dye observed after the polymer peak is a characteristic of the degradable crosslinker used to incorporate maleimide groups into poly(HPMA).

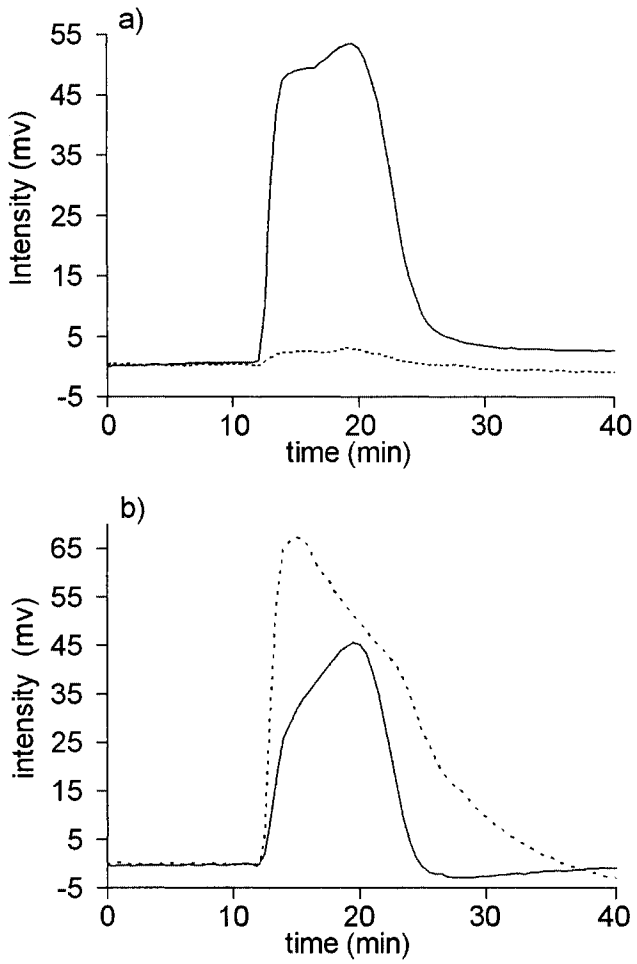

Figure 1.4.2. Size exclusion chromatography trace of dual-labeled poly(HPMA) in 0.1 M sodium phosphate, 0.15 M NaCl, 10 mM EDTA, pH 7.2 before (a) and after (b) sTAMRA conjugation. Detection at 496 nm (solid) corresponds to polymer backbone (Oregon Green®), and 554 nm detection (dashed) corresponds to sTAMRA.

In summary a simple synthesis of reactive thiolated TAMRA-based fluorescent dye is described that is inexpensive, and convenient. The resulting covalent ssTAMRA dimer exhibits unique spectral properties useful in the study of disulfide exchange, enzymatic processes or redox processes by either absorbance shifts or increases in fluorescence emission after generation of monomeric sTAMRA. Reduction of ssTAMRA dimers is readily achieved using TCEP, with reduced sTAMRA being reactive to maleimide functionality. Conjugation of this reduced sTAMRA to polymers,

proteins, or other targets is shown to be feasible for applications in fluorescence assays and imaging.

Acknowledgements. The Authors thank Dr. George Barisas for helpful discussion. This work was supported by NIH grant EB000894.

References

(1) Slavík, J. (1994) *Fluorescent probes in cellular and molecular biology*, CRC Press, Boca Raton.

(2) Andersson-Engels, S., Klinteberg, C., Svanberg, K., and Svanberg, S. (1997) In vivo fluorescence imaging for tissue diagnostics. *Phys Med Biol 42*, 815-24.

(3) Hassan, M., and Klaunberg, B. A. (2004) Biomedical applications of fluorescence imaging in vivo. *Comp Med 54*, 635-44.

(4) Rudin, M., and Weissleder, R. (2003) Molecular imaging in drug discovery and development. *Nat Rev Drug Discov 2*, 123-31.

(5) Haugland, R. P. (2002) *Handbook of fluorescent probes and research products*, 9th ed., Molecular Probes, Inc., Eugene, Or.

(6) Martin, M. M., and Lindqvist, L. (1975) Ph-Dependence of Fluorescein Fluorescence. *Journal Luminesce 10*, 381-390.

(7) Yguerabide, J., Talavera, E., Alvarez, J. M., and Quintero, B. (1994) Steady-state fluorescence method for evaluating excited state proton reactions: application to fluorescein. *Photochemistry and Photobiology 60*, 435-441.

(8) Geisow, M. J. (1984) Fluorescein Conjugates as Indicators of Subcellular Ph - a Critical-Evaluation. *Experimental Cell Research 150*, 29-35.

(9) Ichimura, T., Hatae, T., and Ishida, T. (1997) Direct measurement of endosomal pH in living cells of the rat yolk sac epithelium by laser confocal microscopy. *Eur J Cell Biol 74*, 41-8.

(10) McNamara, K. P., Nguyen, T., Dumitrascu, G., Ji, J., Rosenzweig, N., and Rosenzweig, Z. (2001) Synthesis, characterization, and application of fluorescence sensing lipobeads for intracellular pH measurements. *Analytical Chemistry 73*, 3240-3246.

(11) Chen, Y., and Arriaga, E. A. (2006) Individual acidic organelle pH measurements by capillary electrophoresis. *Analytical Chemistry 78*, 820-826.

(12) Bailey, G. C., and Swager, T. M. (2006) Masked michael acceptors in poly(phenyleneethynylene)s for facile conjugation. *Macromolecules 39*, 2815-2818.

(13) Wang, C., Leffler, S., Thompson, D. H., and Hrycyna, C. A. (2005) A general fluorescence-based coupled assay for S-adenosylmethionine-dependent methyltransferases. *Biochem Biophys Res Commun 331*, 351-6.

(14) Johansson, M. K., Fidder, H., Dick, D., and Cook, R. M. (2002) Intramolecular dimers: a new strategy to fluorescence quenching in dual-labeled oligonucleotide probes. *J Am Chem Soc 124*, 6950-6.

(15) Galande, A. K., Weissleder, R., and Tung, C. H. (2006) Fluorescence probe with a pH-sensitive trigger. *Bioconj Chem 17*, 255-7.

(16) Selwyn, J. E., and Steinfeld, J. I. (1972) Aggregation Equilibria of Xanthene Dyes. *J Physl Chem 76*, 762-774.

(17) Lopez Arbeloa, I., and Ruiz Ojeda, P. (1982) Dimeric States of Rhodamine B. *Cheml Phys Lett 87*, 556-560.

(18) Hamman, B. D., Oleinikov, A. V., Jokhadze, G. G., Bochkariov, D. E., Traut, R. R., and Jameson, D. M. (1996) Tetramethylrhodamine dimer formation as a

spectroscopic probe of the conformation of Escherichia coli ribosomal protein L7/L12 dimers. *J Biol Chem 271*, 7568-73.

(19) Grama, L., Somogyi, B., and Kellermayer, M. S. Z. (2001) Global configuration of single titin molecules observed through chain-associated rhodamine dimers. *Proc Natl Acad Sci 98*, 14362-14367.

(20) Hernando, J., van der Schaaf, M., van Dijk, E. M. H. P., Sauer, M., Garcia-Parajo, M. F., and van Hulst, N. F. (2003) Excitonic behavior of rhodamine dimers: A single-molecule study. *J Phys Chem A 107*, 43-52.

(21) Ilich, P., Mishra, P. K., Macura, S., and Burghardt, T. P. (1996) Direct observation of rhodamine dimer structures in water. *Spectrochimica Acta Part a-Mol Biomol Spectrosc 52*, 1323-1330.

(22) Burghardt, T. P., Lyke, J. E., and Ajtai, K. (1996) Fluorescence emission and anisotropy from rhodamine dimers. *Biophys Chem 59*, 119-131.

(23) Hermanson, G. T. (1996) *Bioconjugate techniques*, Academic Press, San Diego.

CHAPTER V

COMPARISON OF ACID-CLEAVABLE HETEROBIFUNCTIONAL CROSSLINKERS FOR CONJUGATING THIOL-CONTAINING MOLECULES TO AMINES

This dissertation chapter contains a full manuscript in preparation to be submitted to *Macromolecular Bioscience* written by R. James Christie and edited by David W. Grainger. This chapter presents how chemistries involved with hydrazone formation affect reactivity and stability for attachment to water-soluble carriers and subsequent release. Two novel heterobifunctional crosslinkers synthesized to contain aldehyde or methyl ketone functional groups in addition to maleimide functionality are presented.

Comparison of Acid-Cleavable Heterobifunctional Crosslinkers for Conjugating Thiol-Containing Molecules to Amines

R. James Christie, Emily J. Kaiser, Diana J. Findley, David W. Grainger

ABSTRACT

Reversible covalent chemistries that allow site- and condition-specific degradation are attractive components in nanotechnologies, bioconjugation methods, and drug delivery systems. Three heterobifunctional crosslinkers containing both thiol-and amine-reactive groups were assessed in their capabilities to form pH-labile hydrazones with hydrazide derivatives of the water-soluble polymer, poly[N-(2-hydroxypropyl methacrylamide)] (HPMA), while also coupling thiol-containing molecules via maleimide addition to the crosslinker. Two crosslinkers were prepared from the popular heterobifunctional crosslinker succinimidyl-4-(N-maleimidomethyl) cyclohexane-1-carboxylate (SMCC) modified to contain aldehyde (N-(1-propanal)-4-(N-maleimidomethyl) cyclohexane-1-amide, PMCA) or methylketone (N-(2-butanone)-4-(N-maleimidomethyl) cyclohexane-1-amide, BMCA) groups, while the third was the commercially available N-4-acetylphenyl maleimide (APM). PMCA and BMCA exhibited excellent reactivity towards hydrazide-derivatized poly(HPMA) with essentially complete conjugation to polymer reactive sites, while APM coupled only ~

60% of available reactive sites on the polymer. All polymer conjugates were then shown to further react with thiol-terminated tetramethylrhodamine (TAMRA), confirming crosslinker maleimide reactivity after polymer conjugation. Incubation of dye-labeled polymer conjugates in physiologically relevant buffers at 37 °C showed that hydrazones resulting from APM exhibited the best stability (least dye release) at pH 7.4, while hydrazones formed with BMCA resulted in the most rapid release at pH 5.0, and the PMCA crossliner showed little difference in release rates at pH 7.4 or 5.0.

Introduction

Recent developments in molecular building blocks for nanomaterials, biotechnology and advanced drug delivery systems have prompted innovation of new methods to attach components together with new conjugation techniques. For polymer-based therapeutics in particular, the benefits of conjugating drugs to water-soluble polymers are well known and include: increased circulation half-life, reduced non-specific activity, enhanced targeting ability, and physiological solubility.[1] While these benefits provide strong incentives for use of polymers in drug delivery, methods to couple therapeutic agents to polymer carriers have been frequently inflexible and performance-limiting. Yet, the chemistry used to couple therapeutic agent to polymer carrier is crucial to therapeutic potential. Most therapeutic agents must be released from the carrier at the desired physiological site of drug activity in order to be effective, while retaining stability in circulation until the construct reaches its therapeutic target. Many cleverly designed crosslinkers have therefore been developed that allow covalent

attachment to form stable or reversible linkage chemistries to carriers and targeting moieties.[2-4]

Strategies for site-specific macromolecular drug delivery often utilize the cell endocytotic pathway to specifically release drug into the cellular cytoplasm.[5] Polymer constructs internalized into cells by endocytosis are transported to lysosomes, membrane-bound organelles more acidic (pH ~ 5.0) than normal physiological conditions containing a host of specific enzymes.[6] Drugs targeting intracellular features beyond the lysosome (i.e., most drugs) must achieve lysosomal release without adverse side effects. For these reasons, polymer-drug conjugation chemistry is often designed to degrade via cleavage by lysosome-specific enzymes, as well as non-specific pH-dependent mechanisms. The Gly-Phe-Lys-Gly (GFLG) peptide sequence has been shown to degrade specifically by the lysosome enzyme cathepsin B and is a component in the poly[N-(2-hydroxypropyl) methacrylamide] (poly(HPMA)) copolymer-doxorubicin anticancer drug PK1, currently in clinical trials.[7-10] Non-specific pH driven degradation has been shown for a variety of coupling chemistries including hydrazone, acetal, carbamate and cis-aconityl moieties.[11-14]

More specifically, hydrazone bonds have been successfully employed to generate a variety of pH-sensitive conjugates of the anticancer drug doxorubicin with various polymers, particles, micelles, and antibodies by reaction with hydrazide-derivatized carriers or crosslinkers with the 13-keto position of this drug.[12, 13, 15-20] Hydrazone bonds are formed by condensation of hydrazides with aldehydes or ketones after elimination of the carbonyl oxygen as water resulting in an imine bond. This reaction can be performed under aqueous conditions with careful control of pH and reaction stoichiometry, but is

most often performed under organic conditions with an acid catalyst such as acetic acid or trifluoroacetic acid to facilitate dehydration and formation of the hydrazone bond.[16, 21, 22] While certain types of hydrazone linkages are known to be stable at pH 7.4 and degrade at low pH (ie. < 5.0), chemistries adjacent to both hydrazide and ketone functionality greatly affect stability, hence, specific substituents can be used to achieve different cleavage rates and pH sensitivities.[12, 13] This chemistry can also be tailored to present other functional groups useful for other conjugation strategies.

This work evaluates the performance of three crosslinkers designed to couple thiol-containing molecules to hydrozone derivatized poly(HPMA) carriers that exhibit a long history of use.[9, 10, 23] Efficiency of crosslinker coupling to reactive sites on the polymer backbone, and their subsequent stability at pH 7.4 and 5.0 were investigated. While either the polymer or crosslinker can be designed to bear the hydrazide functionality, we placed this functional group on the polymer carrier as previously described.[16, 17] The crosslinkers investigated contain ketone or aldehyde functionality on one terminus for reaction with these poly(HPMA) hydrazides and a maleimide functionality at the other terminus to react with sulfhydryl groups on a different adduct via a 1,4-Michael addition reaction.[16, 17] This type of coupling strategy is beneficial for coupling unmodified proteins/peptides lacking aldehyde/ketone functionality or other thiol-containing molecules to hydrazide derivatized poly(HPMA). Two crosslinkers investigated, N-(1-propanal)-4-(N-maleimidomethyl) cyclohexane-1-amide, and N-(2-butanone)-4-(N-maleimidomethyl) cyclohexane-1-amide were prepared from the popular heterobifunctional crosslinker succinimidyl-4-(N-maleimidomethyl)cyclohexane-1-

carboxylate (SMCC), while the third was a commercially available benzene derivative, N-4-acetylphenyl maleimide.

Experimental

Materials

All solvents were ACS certified grade purchased from Fisher Scientific (Fair Lawn, NJ) and used without further purification unless otherwise noted. Trinitrobenzene sulfonic acid (5% w/v solution in methanol) (TNBSA), cystamine hydrochloride (98%), diisopropylethylamine (DIPEA), ethyl carbazate (97%), N-hydroxysuccinamide (NHS) (98%), 4-(aminomethyl)cyclohexane carboxylic acid (97%), maleic anhydride (98+%), acetic anhydride, dicyclohexanecarbodiimide (DCC) (99%), hydrazine monohydrate (98%), 3-amino-1-propanol (99+%), triethyl amine (99.5%), oxalyl chloride (99+%) and glacial acetic acid, were all purchased from Aldrich (St. Louis, MO). N-4-(acetylphenyl) maleimide (APM) (98+%) was purchased from Lancaster Synthesis (Pelham, NH). 4-Amino-2-butanol (98%) ws purchased from Acros Organics, (Geel, Belgium). Reducing gel with immobilized tris(2-carboxyethyl)phosphine hydrochloride (TCEP) was purchased from Pierce (Rockford, IL). Spectra/Por 1, 6-8 kDa molecular weight cutt-off dialysis tubing was obtained from Spectrum Laboratories, Inc. (Rancho Dominguez, CA). Sephadex G-25 and LH-20 size exclusion chromatography gel was purchased from Amersham Biosciences (Uppsala, Sweden). Dimethyl sulfoxide-d_6 containing 0.05% w/v tetramethylsilane was purchased from Cambridge Isotope Laboratories, Inc. (Andover, MA). 5(6)- Tetramethylrhodamine-succinimidyl ester (TAMRA-NHS) was obtained from AnaSpec (San Jose, CA). Poly(HPMA) molecular weight standards were a gift

from Dr. P. Kopeckova, Univ. Utah, USA. Water eas Millipore-filtered ASTM Type I quality. All NMR spectra were recorded on a Magnex Scientific Inova 400 MHz instrument in DMSO-d_6 containing 5% w/v tetramethylsilane as an internal standard. Absorbance measurements were obtained on a Varian Carey 500 Scan instrument.

Synthesis of 4-(N-maleimidomethyl) cyclohexane carboxylic acid, MCCA

4-(Aminomethyl) cyclohexane carboxylic acid (40.71 g, 0.259 mol, 1eq) was dissolved in dimethyl acetamide (DMAc, 100 mL). A solution of maleic anhydride (25.20 g, 0.257 mol, 0.99 eq) was prepared in DMAc (50 mL), then added dropwise to the 4-(aminomethyl) cyclohexane carboxylic acid solution dropwise while stirring. The reaction vessel was purged with nitrogen, capped and stirred for 24 hr at room temperature. After 24 hr, sodium acetate (5.00 g, 0.061 mol, 0.24 eq) and acetic anhydride (43 mL, 0.455 mol, 1.75 eq) were added and the reaction was continued for an additional 24 hrs. After 24 hrs, the reaction was heated to 65 ^{o}C and stirred for 5 hrs, then concentrated to ~ 125 mL under vacuum and poured into 1L cold water while stirring. The light-brown precipitate was collected by filtration and dried under vacuum. The aqueous portion was extracted twice with methylene chloride (500 mL), and product was isolated after evaporation of solvent. Both solid portions were combined and dissolved in methylene chloride (500 mL) then silica gel (5 g) was added to the solution, and the suspension was stirred for 30 min. The resulting colorless solution was filtered and solid product was obtained by evaporation of solvent under vacuum. Crude product was further purified by crystallization from ethyl acetate to yield a white solid. Yield: 14.70 g, 24 %, white solid. ^{1}H NMR, δ ppm: 0.926 (dd, 2H), 1.22 (dd, 2H), 1.517 (m, 1H), 1.6165 (d, 2H), 1.869 (d, 2H), 2.109 (m, 1H), 3.2355 (d, 2H), 7.012 (s, 2H), 12.010

(s, 1H). ^{13}C NMR, δ ppm: 27.932, 29.112, 36.013, 42.105, 42.861, 134.273, 171.549, 176.497. FAB-MS m/z = 238.108 $[M+H]^+$(calculated m/z = 238.107 $[M+H]^+$)

Synthesis of N-(1-propanol)-4-(N-maleimidomethyl) cyclohexane-1-amide

MCCA (3.00 g, .0126 mol, 1eq) was dissolved in methylene chloride (75 mL), purged with nitrogen, capped, and cooled to –15 °C. A suspension of NHS was prepared (1.454g, 0.0126 mol, 1eq) in methylene chloride (25 mL), then cooled to –15 °C. Next, a solution of DCC was prepared (2.8688g, 0.0139 mol, 1.1 eq) in methylene chloride (25 mL) and cooled to –15 °C. The DCC solution was added to the MCCA solution, followed by addition of the NHS suspension. The reaction flask was purged with nitrogen and stirred at –15 °C for 24 hr and then filtered to remove dicyclohexylurea (DCU). The filtrate was retained and 3-amino-1-propanol (1.982 mL, 0.025 mol, 2eq) was added dropwise. The reaction was purged with nitrogen, capped, and stirred at room temperature for 3 hr. After 3 hr, the reaction mixture was filtered to remove liberated NHS and the filtrate was concentrated to ~2/3 original volume under vacuum, cooled to –20°C, then refiltered. The resulting filtrate volume was doubled by addition of diethyl ether to form a precipitate, which was isolated by filtration. The solid product was further purified by silica gel chromatography (10 x 40 cm, 90/10 methylene chloride/methanol mobile phase) and isolated by evaporation of solvent under vacuum. Yield: 1.91 g, 51.6%, white solid. ^1H NMR, δ ppm: 0.886 (dd, 2H), 1.265 (dd, 2H), 1.508 (q, 3H), 1.618 (d, 2H), 1.682 (d, 2H), 1.998 (m, 1H), 2.5 (solvent overlap), 3.047 (q, 2H), 3.234 (d, 2H), 3.372 (q, 2H), 4.399 (t, 1H), 7.013 (s, 2H), 7.652 (t, 1H). ^{13}C NMR , δ ppm: 28.488, 29.349, 32.386, 35.423, 36.060, 42.980, 43.704, 58.307, 134.277, 171.188, 174.825. FAB-MS m/z = 295.1654 $[M+H]^+$(calculated m/z = 295.1657 $[M+H]^+$).

Synthesis of N-(1-propanal)-4-(N-maleimidomethyl) cyclohexane-1-amide (PMCA)

Synthesis of N-(1-propanal)-4-(N-maleimidomethyl) cyclohexane-1-amide (PMCA) was prepared using the Swern procedure for oxidation of an alcohol to aldehyde.[24] N-(1-propanol)-4-(N-maleimidomethyl) cyclohexane-1-amide (500 mg, 1.72 mmol, 1 eq) was dissolved in freshly distilled methylene chloride (20 mL) and cooled to –80 °C. An activated dimethyl sulfoxide (DMSO) solution was prepared by combining DMSO (295 uL, 4.13 mmol, 2.4 eq) and oxalyl chloride (0.950 mL of 2M solution in methylene chloride, 1.89 mmol, 1.1 eq) in methylene chloride (1.5 mL) at –80 °C. The alcohol solution was slowly added to the activated DMSO solution over 5 minutes. The reaction was let proceed for 15 minutes at –80 °C, followed by addition of triethylamine (1.2 mL, 8.5 mmol, 5 eq). The reaction was equillibrated to room temperature then water (15 mL) was added and the mixture was stirred for 10 minutes. The organic layer was separated, and the aqueous portion was re-extracted with 2 x 10 mL methylene chloride which were then combined with the first organic portion. The combined organic portions were washed with 1M HCL, dilute $NaHCO_3$, and 2 x 20 mL H_2O, then dried with Na_2SO_4. Product was isolated after removal of Na_2SO_4 and evaporation of solvent. Yield: 0.350g, 66%, white powder. ^1H NMR, δ ppm: 0.878 (dd, 2H), 1.232 (dd, 2H), 1.507 (m, 1H), 1.636 (m, 2H), 1.976 (m, 1H), 2.502, (solvent overlap) 3.23 (d, 2H), 3.284 (q, 2H), 7.011 (s, 1H), 7.796 (t, 1H), 9.604 (t, 1H). ^{13}C NMR, δ ppm: 28.378, 29.286, 32.393, 36.037, 42.957, 43.265, 43.566, 134.274, 171.185, 174.958, 202.195. MS-FAB m/z = 293.1507 $[M+H]^+$(calculated m/z = 293.1501 $[M+H]^+$).

Synthesis of N-(2-butanol)-4-(N-maleimidomethyl) cyclohexane-1-amide

This product was obtained by an analogous procedure used to synthesize N-(1-propanol)-4-(N-maleimidomethyl) cyclohexane-1-amide (vida infra) with the only difference being the use of 4-amino-2-butanol (1.65 mL, 17.3 mmol, 1.1 eq) in methylene chloride (30 mL) as the amidation reagent. Yield: 2.88 g, 60%, white powder. ^{1}H NMR, δ ppm: 0.887 (dd, 2H), 1.036 (d, 3H), 1.267 (dd, 2H), 1.521 (m, 1H), 1.620 (d, 2H), 1.686 (d, 2H), 1.998, (m, 1H), 3.065 (q, 2H), 3.240 (d, 2H), 3.585 (septet, 1H), 4.443 (d, 1H), 7.018 (s, 2H), 7.645 (t, 1H). ^{13}C NMR, δ ppm: 23.509, 28.459, 29.334, 35.489, 36.046, 38.719, 42.966, 43.694, 63.628, 134.267, 171.168, 174.776. MS-FAB m/z = 309.1819 $[M+H]^{+}$(calculated m/z = 309.1814 $[M+H]^{+}$).

Synthesis of N-(2-butanone)-4-(N-maleimidomethyl) cyclohexane-1-amide (BMCA)

N-(2-butanone)-4-(N-maleimidomethyl) cyclohexane-1-amide (BMCA) was prepared analogously to PMCA. N-(2-butanol)-4-(N-maleimidomethyl) cyclohexane-1-amide. (2.00 g, 6.49 mmol, 1.0 eq) was dissolved in freshly distilled methylene chloride (125 mL) and cooled to –80 °C. An activated DMSO solution was prepared by combining DMSO (1.105 mL, 15.58 mmol, 2.4 eq) with oxalyl chloride (3.57 mL of 2M in methylene chloride, 7.14 mmol, 1.1 eq) under nitrogen, at –80 °C. This solution was stirred at –80°C for 10 minutes followed by dropwise addition of N-(2-butanol)-4-(N-maleimidomethyl) cyclohexane-1-amide. After complete addition, the reaction was stirred for 15 minutes, followed by addition of triethylamine (4.56 mL, 32.45 mmol, 5 eq). After the reaction was removed from the –80 °C bath and allowed to reach room temperature, water (100 mL) was added and the mixture was stirred for 30 minutes. The

organic layer was separated and re-extracted with 2 x 100 mL methylene chloride. The organic layers were combined and washed with 0.5M HCl (100 mL), 0.5M NaOH (100 mL), and water (100 mL). The organic layer was dried with Na_2SO_4 and product was recovered after filtration solvent evaporation and further purified by recrystylization from ethyl acetate. Yield: 1.34 g, 68%, white powder. ^{1}H NMR, δ ppm: 0.875 (q, 2H), 1.243 (q, 2H), 1.511 (m, 1H), 1.511 (m, 1H), 1.638 (m, 4H), 1.975 (m, 1H), 2.070 (s, 3H), 2.545 (t, 2H), 3.180 (q, 2H), 3.228 (d, 2H), 7.011 (s, 2H), 7.677 (t, 1H). ^{13}C NMR, δ ppm: 28.407, 29.305, 29.752, 33.626, 36.043, 42.620, 42.962, 43.548, 134.273, 171.179, 174.796, 207.179. MS-FAB m/z = 307.1657 $[M+H]^+$(calculated m/z = 307.1657 $[M+H]^+$)

Reaction of heterofunctional crosslinkers with model ethyl carbazate

PMCA

PMCA (100 mg, 0.342 mmol, 1.0 eq) was dissolved in 50/50 methylene chloride/Methanol (2mL), followed by addition of Na_2SO_4 (100 mg, 0.70 mmol, 2.5 eq). Ethyl carbazate (35.6 mg, 0.342 mmol, 1.0 eq) was dissolved in 2 mL 50/50 methylene chloride/methanol (2 mL) and added to the PMCA solution dropwise. After 30 minutes acetic acid (5.0 uL, 0.087 mmol, 0.25 eq) was added and the reaction was stirred for 12 hrs under nitrogen and periodically monitored by TLC. After 12 hrs, the reaction mixture was filtered through a 0.2 μm filter, then washed with 0.1 M $NaHCO_3$. The organic layer was retained, dried with Na_2SO_4 and product was obtained after evaporation of solvent. Yield: 116.2 mg, 89.8%, white powder. ^{1}H NMR, δ ppm: 0.882 (q, 3H), 1.175 (t, 3H), 1.243 (q, 3H), 1.506 (m, 1H), 1.603 (d, 2H), 1.679 (2, 2H), 1.980 (m, 1H), 2.251 (q, 2H),

3.153 (q, 2H), 3.232 (d, 2H), 4.059 (q, CH2), 7.014 (s, 2H), 7.214 (s, 1H), 7.760 (t, 1H), 10.681 (s, 1H). 13C NMR, δ ppm: 14.516, 28.422, 29.336, 32.341, 35.698, 36.095, 42.984, 43.724, 60.021, 134.298, 145.493, 153.287, 171.211, 174.839. MS-FAB m/z = 379.1976 $[M+H]^+$(calculated m/z = 379.1981 $[M+H]^+$). Product was further analyzed by UV-Vis spectroscopy and a molar extinction coefficient was calculated using dilutions in methanol.

BMCA

BMCA (100 mg, 0.326 mmol, 1.0 eq) was dissolved in 50/50 methylene chloride/methanol (2 mL), followed by addition of Na_2SO_4 (100 mg, 0.70 mmol, 2.2 eq). Ethyl carbazate (33.9 mg, 0.326 mmol, 1.0 eq) was dissolved in 50/50 methylene chloride/methanol (2 mL) and added to the BMCA solution dropwise through a septum. After 30 minutes acetic acid (5.0 uL, 0.087 mmol, 0.27 eq) was added and the reaction was allowed to proceed for 12 hrs. After 12 hrs the reaction mixture was filtered through a 0.2 μm filter, then washed with 0.1 M $NaHCO_3$. The organic layer was retained, dried with Na_2SO_4, and product was obtained after evaporation of solvent. Yield: 116.1 mg, 91.0%, white solid. ^1H NMR, δ ppm: 0.873 (q, 2H), 1.193 (t, 3H), 1.232 (m, 2H), 1.501 (m, 1H), 1.595 (d, 2H), 1.673 (d, 2H), 1.777 (s, 3H), 1.963 (m, 1H), 2.250 (t, 2H), 3.190 (q, 2H), 3.228 (d, 2H), 4.083 (q, 2H), 7.015 (s, 2H), 7.669 (t, 1H), 9.653 (s, 1H). ^{13}C NMR δ ppm: 14.565, 15.917, 28.408, 29.345, 33.292, 36.080, 36.623, 42.980, 43.757, 60.245, 134.290, 154.058, 156.534, 171.194, 174.704. MS-ESI m/z = 393.2135 $[M+H]^+$(calculated m/z = 393.2137 $[M+H]^+$). Product was further analyzed by UV-Vis

spectroscopy and a molar extinction coefficient was calculated using dilutions in methanol.

N-4-(acetylphenyl) maleimide (APM)

APM (400.0 mg, 1.86 mmol, 1.0 eq) was dissolved in 50/50 methylene chloride/methanol (2 mL), followed by addition of Na_2SO_4 (528 mg, 3.72 mmol, 2.2 eq). Ethyl carbazate (176.0 mg, 1.69 mmol, 0.91 eq) was dissolved in 50/50 methylene chloride/methanol (2 mL) and added to the APM solution dropwise with stirring. After 30 minutes acetic acid (5.0 μL, 0.174 mmol, 0.1 eq) was added and the reaction was continued for 12 hrs at room temperature. After 12 hrs the reaction mixture was filtered through a 0.2 μm filter and washed with 0.1 M $NaHCO_3$. The organic layer was retained, dried with Na_2SO_4, and crude product was obtained after evaporation of solvent. Product was further purified by silica gel chromatography (50/50 methylene chloride/ethyl acetate mobile phase). Yield: 0.150 g, 27%, yellow solid. ^{1}H NMR, δ ppm: 1.262 (d, 3H), 2.234 (s, 3H), 4.177 (q, 2H), 7.197 (s, 2H), 7.368 (m, 2H), 7.827 (m, 2H), 10.173 (s, 1H). ^{13}C NMR, δ ppm: 13.782,14.545, 60.509, 126.246, 126.356, 131.830, 134.676, 137.458, 147.997, 154.097,169.744. MS-FAB m/z = 302.1137 $[M+H]^+$(calculated m/z = 302.1140 $[M+H]^+$). Product was further analyzed by UV-Vis spectroscopy, and the molar extinction coefficient was calculated using dilutions in methanol.

Synthesis of poly(HPMA)

Poly(HPMA) was synthesized to contain 5 mol% reactive nitrophenol ester terminated, non-degradable glycylglycine side chains using previously described procedures.[25-27] N-(2-hydroxypropyl) methacrylamide and methacryloyl glycylglycine nitrophenol ester (MAGGONP) monomers were prepared in house and confirmed with NMR and mass spectrometry. The number of active esters in the resulting copolymer was estimated to be 2.55 x 10^{-4} mol/g polymer, 3.8 mol % by measuring the absorbance of released p-nitrophenolate anion at 400 nm (ε = 1.74 x 10^4 $M^{-1}cm^{-1}$) following hydrolysis of ester bonds in 0.05 M sodium hydroxide. Copolymer molecular weight was estimated to be 18,200 Da by size exclusion chromatography using a HP1050A HPLC equipped with a HP1047A refractive index detector and BioSil 125 column calibrated with poly(HPMA) samples of known molecular weight. Samples were eluted at 0.5 mL/min with 0.1 M sodium phosphate, 0.05 M NaCl, pH 7.4.

HPMA copolymer was further modified to contain hydrazide-terminated side chains by reaction of p-nitrophenol ester terminated MAGGONP side chains with excess hydrazine monohydrate using methods previously described.[16, 17] Briefly, 2.0 g p-nitrophenol activated poly(HPMA) (2.0 g, 0.51 mmol, 1 eq) was dissolved in methanol (25 mL). After preparing a solution of hydrazine monohydrate (0.267 mL, 5.5 mmol, 10.8 eq) in methanol (25 mL), the poly(HPMA) solution was added dropwise. The reaction was purged with nitrogen, capped, and stirred for 3 hr at room temperature. The reaction solution turned dark yellow indicating reaction of active ester groups and release of p-nitrophenol. After complete reaction, the reaction mixture was dripped into cold water (50 mL) and low molecular weight byproducts were removed by dialysis

(SpectraPore, 6-8 kDa molecular weight cut-off, 2 days). Polymer product was isolated by lyophilization. Yield: 0.120 g, 60%, white powder. Hydrazide content: 2.63×10^{-4} mol/g, ~100.5% conversion.

Analysis of poly(HPMA) hydrazide content

Hydrazide content was estimated using a modified trinitrobenzene sulfonic acid (TNBSA) assay and methacryloyl glycylglycine hydrazide (MAGGH) standards. MAGGH was synthesized by reaction of MAGGONP with hydrazine monohydrate. MAGGONP (750 mg, 2.33 mmol, 1 eq) was dissolved in methanol (90 mL), dripped into a solution of hydrazine monohydrate (567 uL, 11.7 mmol, 5 eq) and stirred for 5 hr at room temperature under nitrogen. Solvent was removed under vacuum to yield crude solids that were then dissolved in 90/10 methylene chloride/methanol (40 mL), filtered, and loaded onto a silica gel column (2.5 x 17.5 cm) equilibrated with 90/10 methylene chloride/methanol. After the sample was loaded onto the column, the elution solvent was changed to Methanol and MAGGH eluted after the visible yellow p-nitophenol band. Yield: 0.156 g, 31%, white powder. ^{1}H NMR, δ ppm: 1.836 (s, 1H), 3.619 (d, 2H), 3.712 (d, 2H), 4.165 (d, 2H), 5.341 (d, 1H), 5.698 (d, 1H), 8.048 (t, 1H), 8.131 (t, 1H), 8.907 (s, 1H). ^{13}C NMR, δ ppm: 18.479, 40.779, 42.402, 119.752, 139.356, 167.597, 168.011, 169.204. MS-FAB m/z = 215.1147 $[M+H]^{+}$(calculated m/z = 215.1144 $[M+H]^{+}$)..

For each poly(HPMA) hydrazide content analysis, stock solutions of 0.1% w/v TNBSA and ~ 2×10^{-4} M MAGGH were prepared in 0.1 M $NaHCO_3$, pH 8.5. The MAGGH solution was further diluted with 0.1 M $NaHCO_3$ to generate standards in the range of ~0.3-2 x 10^{-4} M. Next, hydrazide-derivatized HPMA copolymers were dissolved

in 0.1 M $NaHCO_3$ at a concentration of 0.2-0.4 mg/mL for samples prior to crosslinker reactions, and 1-2 mg/mL for crosslinker-reacted samples. TNBSA stock solution (0.5 mL) was combined with MAGGH standard or HPMA copolymer solution (1.0 mL) and incubated for 1.5 hr at 37°C. After incubation, sample absorbance was measured at 505 nm and hydrazide content was estimated from the MAGGH standard curve.

Reaction of hydrazide derivatized poly(HPMA) with crosslinkers.

Hydrazide derivatized poly(HPMA) (0.20 g, 5.22×10^{-5} mol hydrazide, 1 eq) was dissolved in 50/50 methylene chloride/methanol (2 mL), and 100 mg Na_2SO_4 was added. Crosslinker solutions (PMCA: 46.0 mg, BMCA: 48.0 mg, APM: 34.0 mg, 1.57×10^{-4} mol, 3 eq) were prepared in 50/50 methylene chloride/methanol (2 mL) and then added to the poly(HPMA) solution dropwise. After complete addition, acetic acid (5 μL of 34% v/v solution in Methylene chloride, 29.7 μmol, 0.57 eq) was added and the reaction was stirred under nitrogen at room temperature for 24 hr. The reaction was terminated by precipitation of poly(HPMA) product into ether. Product was further purified by size exclusion chromatography (Sephadex LH-20, 1 x 15 cm, Methanol mobile phase). Yield: poly(HPMA)-PMCA, 116.1 mg 59%; poly(HPMA)-BMCA, 122.17 mg, 61%; poly(HPMA)-APM, 126.5 mg, 63%, white powders. Hydrazide content post-conjugation was determined using a TNBSA assay, as described above. Crosslinker content was determined by an absorbance measurement at λ_{max} and using molar extinction coefficients of corresponding ethyl carbazate-crosslinker hydrazone derivatives (vida infra). Polymer-crosslinker conjugates were analyzed by ^1H NMR to confirm the presence of maleimide functionality on the polymer backbone.

Synthesis of Thiol-Containing Tetramethylrhodamine

Thiolated tetramethylrhodamine was prepared by reaction of TAMRA-NHS with cystamine hydrochloride activated with diisopropylethylamine (DIPEA) to form the TAMRA disulfide dimer (ssTAMRA). Cystamine hydrochloride (9.6 mg, 0.085 mmol, 0.9 eq. amines) was activated in dimethylformamide (DMF, 2.5 mL) containing DIPEA (30 μL, 0.17 mmol, 1.8 eq). This solution was added to TAMRA-NHS (50.0 mg, 0.095mmol, 1.0 eq) in DMF (1.5 mL) and stirred at room temperature in the dark for 30 minutes followed by addition of DIPEA (15 μL ,0.086 mmol, 1.0 eq) and reaction for an additional hour. Product was precipitated by addition of 50 mL cold diethyl ether, washed five times, and dried under vacuum overnight. Further purification was achieved by repeat precipitation from methanol into cold ether. Yield: 24.81 mg, 54%, dark red solid. MS, FAB m/z = $M[H^+]$ 977.3348, calculated $M[H^+]$ = 977.3366.

Coupling of thiolated TAMRA to maleimide-activated poly(HPMA)

Dimeric TAMRA disulfide was reduced using TCEP - immobilized gel immediately prior to reaction with crosslinker-derivatized poly(HPMA). Disulfide TAMRA dimer (17.46 mg, 0.036 mmol, 1 eq) was dissolved in 1 mL DMSO and dripped into an immobilized TCEP gel suspension (5 mL gel, ~ 0.04 mmol TCEP, ~1.1 eq) in 12.0 mL phosphate buffer (0.1M sodium phosphate, 0.05 M NaCl, 2.5 mM EDTA, pH 7.0). The reduction reaction was allowed to proceed for 1.25 hr, followed by removal of TCEP gel by centrifugation. The gel material was washed with 6 mL buffer (pH 7.0, 2.5 mM EDTA), centrifuged, and the supernatant was retained and combined with the first fraction.

Reduced ssTAMRA solution (3 mL, ~ 5.9 μmol, ~ 1.1 eq) was added to crosslinker conjugated poly(HPMA) (20.0 mg, ~5.3 μmol, 1eq). The reaction was degassed, purged with nitrogen, capped, and stirred at room temperature in the dark for 3 hr and terminated by separation of unreacted TAMRA thiol after passage through an SEC column (Sephadex, G-25, 2 x 20 cm, aqueous mobile phase). The polymer conjugate fraction was collected as the first red band eluting from the column and lyophilized. Yield: HPMA-PMCA, 15.35 mg, HPMA-BMCA, 19.23 mg, HPMA-MBA, 19.42 mg.

Acid-induced release of TAMRA from poly(HPMA)

Release of free TAMRA dye from poly(HPMA) was monitored at pH 5.0 (0.1 M sodium acetate buffer) and pH 7.4 (0.1 M sodium phosphate buffer containing 0.05 M NaCl). TAMRA-conjugated poly(HPMA) samples (1.5-2.5 mg) were dissolved in the appropriate buffer (8.5 mL) and incubated at 37°C in the dark while stirring. At various time points, 750 μL of polymer solution was withdrawn and free TAMRA was separated from polymer using a sephadex G-25 SEC column (1 x 13 cm, H_2O mobile phase). The two resulting bands were collected and water was evaporated. The samples were then dissolved in 500 μL water and % free TAMRA was determined by the ratio of absorbance at 554 nm of the two fractions. For APM-derivatized poly(HPMA), TAMRA release was also determined after acidification (pH 3.0) of a sample incubated for 72 hrs at pH 7.4.

RESULTS AND DISCUSSION

Synthesis of SMCC-based heterobifunctional crosslinkers

Figure 1.5.1a shows the general approach and desired objective of this crosslinking strategy, and chemical structures of all heterobifunctional crosslinkers shown in Figure 1.5.1b. While several heterobifunctional crosslinkers are commercially available that form hydrazone bonds and also contain thiol reactivity, most are synthesized to contain hydrazide groups that react with synthetic ketone-containing drugs such as doxorubicin or oxidized sugar moieties present on biomolecules. We know of only one commercially available crosslinker that contains ketone and maleimide functionality, since hydrazide groups are not a common target for reaction with

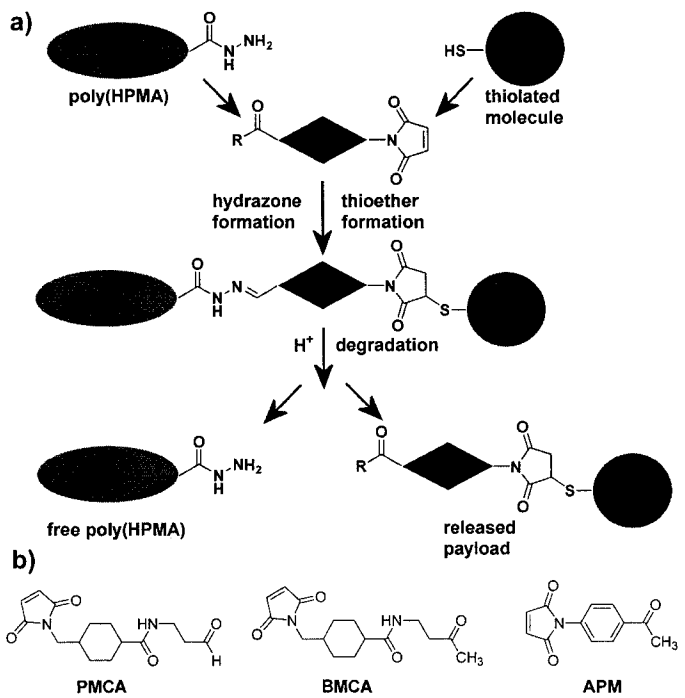

Figure 1.5.1. a) Strategy for reversible attachment of thiol-containing moleucules with hydrazide derivatized poly(HPMA). b) Chemical structures of crosslinkers utilized in this study.

biomolecules or synthetic drugs.

Synthesis of the aldehyde or methyl ketone SMCC-based heterobifunctional crosslinkers is shown in Scheme 1.5.1. The SMCC core was chosen due to known increased stability of the maleimide group by the cyclohexane bridge.[2] Early attempts to synthesize these crosslinkers involved direct modification of commercially available SMCC, but synthesis of SMCC precursors in-house allowed inexpensive scale-up. Synthesis of the corresponding alcohols of SMCC was performed in a one-pot reaction after activation of carboxylic acid with NHS using well-known carbodiimide chemistry.[2] Direct coupling of amines to 4-(N-maleimidomethyl) cyclohexane carboxylic acid following DCC activation without NHS led to a mixture of products, presumably due to addition of alcohol groups to the highly reactive DCC activated carboxylic acid. The choice of methylene chloride as the solvent aided in product purification due to the limited solubility of NHS by-product, which precipitated from solution and was easily removed by filtration after concentration and cooling. Residual NHS was removed by aqueous extraction for BMCA synthesis, but this purification strategy for PMCA resulted in reduced yields due to higher water solubility. Chromatographic purification resulted in markedly increased yields.

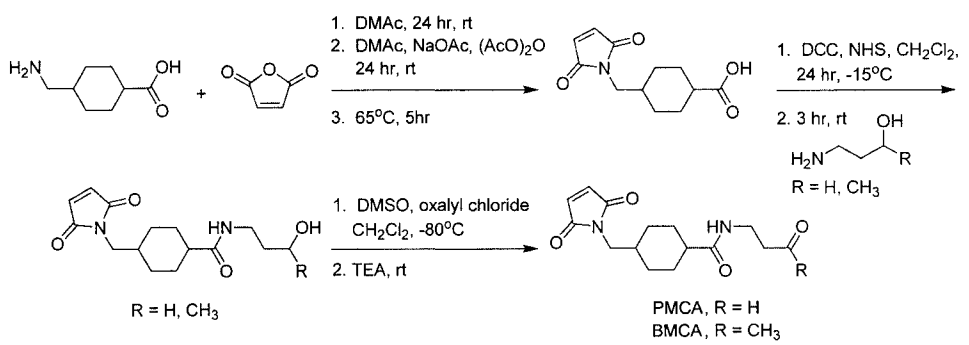

Scheme 1.5.1. Synthesis of SMCC-based crosslinkers PMCA and BMCA

Oxidation of alcohol groups in PMCA and BMCA alcohol precursors was readily achieved using the mild oxidation conditions of the Swern procedure to yield the corresponding aldehyde and methylketone containing reactive crosslinkers. No side reactions were observed with other functional groups in the molecule. Other attempts to oxidize the alcohol functional groups using pyridinium chlorochromate resulted in oxidation of alcohol groups, but removal of chromium salt by-products was difficult, resulting in low yields (data not shown).

Model reactions of crosslinkers with ethyl carbazate

The ability of each crosslinker to form hydrazone linkages was modeled with the hydrazide-containing small molecule ethyl carbazate, with confirmation of hydrazone formation being more analytically straightforward than with a small percentage of reactive sites in a polymer conjugate. For PMCA and BMCA, rapid, stoichiometric conversion to hydrazone product was obtained, with only a simple purification procedure needed to isolate pure hydrazone product. However, reaction of APM with ethyl carbazate resulted in formation of several products and purification required a separation procedure for isolation, which resulted in a lower overall yield. Although extensive analysis of reaction by-products was not performed, one by-product of the APM reaction with ethyl carbazate did show loss of maleimide functionality by ^{1}H NMR analysis.

The spectroscopic properties of hydrazones formed from crosslinker reaction with ethyl carbazate are summarized in Table 1.5.1.

Table 1.5.1. Spectral properties of crosslinkers and correspoding hydrazones formed with ethyl carbazate

Crosslinker	λ_{max} (nm)	λ_{max} of hydrazone (nm)	ε ($M^{-1}cm^{-1}$) of hydrazone
PMCA	299	297	5.53×10^2
BMCA	297	299	5.66×10^2
APM	268	288	1.90×10^4

Spectral properties of crosslinkers before and after hydrazone formation were nearly identical, preventing simple analysis of hydrazone formation or degradation by simple absorbance measurements. The absorbance of PMCA and BMCA at 297 nm is due to the maleimide functional group, while the more intense and red-shifted APM absorbance results from the conjugated π system. The relatively high molar extinction coefficient of APM provides a convenient analytical tool for determination of the degree of conjugation, even at low concentrations.

Crosslinker Coupling to poly(HPMA)

Synthesis of hydrazide derivatived poly(HPMA) was easily achieved by reaction of active nitrophenyl esters on pendant side chains with hydrazine monohydrate as previously described.[16, 17] This construct has been previously utilized to couple doxorubicin via a hydrazone bond to allow pH dependent release.[16, 17] The number of reactive hydrazide sites in poly(HPMA) was controlled by monomer feed ratio in the free radical initiated polymerization reaction to produce poly(HPMA). Formation of hydrazone bonds has been reported for doxorubicin conjugates with poly(HPMA) and poly(ethylene glycol) when methanol was used as the solvent, and acetic acid as the catalyst.[16, 17] Since the hydrophobic crosslinkers used in this study were only minimally

soluble in methanol with more hydrophilic poly(HPMA) minimally soluble in solvents ideal for crosslinker solvation. The best methanol-based solvent system for optimal crosslinker/polymer solubility was found to be 50/50 methanol/methylene chloride. Poly(HPMA)-crosslinker reactions showing conjugation efficiency are summarized in Table 1.5.2.

Table 1.5.2. Summary of poly(HPMA) conjugation reactions.

	crosslinker content (μmol/g)	% conversion[b]	remaining hydrazide (μmol/g)	% conversion[b]	TAMRA content (μmol/g)	% conversion[c]
PMCA	373.0 ± 21.2	141.8 ± 8.1	19.5 ± 0.1	92.6 ± 4.3	105.2 ± 17.8	28.19 +/-4.8
BMCA	248.9 ± 8.1	94.6 ± 3.1	18.6 ± 0.1	92.9 ± 5.6	47.8 ± 3.7	19.28 +/-1.5
APM	166.7 ± 14.5	69.8 ± 6.1	90.9 ± .1	62.0 ± 1.9	23.5 ± 0.82	25.9 +/-7.2

Data represents an average of 4 experiments
a Determined using molar extinction coefficient of crosslinker relative to original hydrazide content
b Relative to original hydrazide content
c Relative to crosslinker content

Reaction of the crosslinkers PMCA and BMCA resulted in complete conversion of hydrazide groups to hydrazone conjugates as determined by crosslinker absorbance and determination of remaining hydrazide groups by TNBSA measurements. Optical absorption measurements of the poly(HPMA)-PMCA crosslinker product showed slightly more than 100% coupling indicative of the higher reactivity of aldehyde functional groups which may be reacting with a fraction of the alcohol groups on the polymer backbone. The methylketone group of BMCA reacted with poly(HPMA) hydrazide groups in a stoichiometric fashion, with absorbance and remaining hydrazide content

being in good agreement. This demonstrates that the less reactive methyl ketone functionality results in a more readily controlled conjugation The APM crosslinker did not stoichiometrically react with hydrazide-derivatized poly(HPMA) with only 60-70% conversion, which was expected from the lower hydrazone yields observed with APM in the ethyl carbazate model reactions. ^{1}H NMR analysis of each crosslinker-polymer conjugate also showed a convenient analytical signal to confirm conjugation due to the strong signal of the maleimide peak at 7.0-7.2 ppm (Figure 1.5.2).

For PMCA and BMCA, the maleimide peak appeared in an unobscured region of the NMR spectrum allowing easy detection. Additionally, conjugation of PMCA was confirmed by the disappearance of the aldehyde peak present in unreacted crosslinker at 9.6 ppm (data not shown). Although the maleimide signal overlapped with the polymer

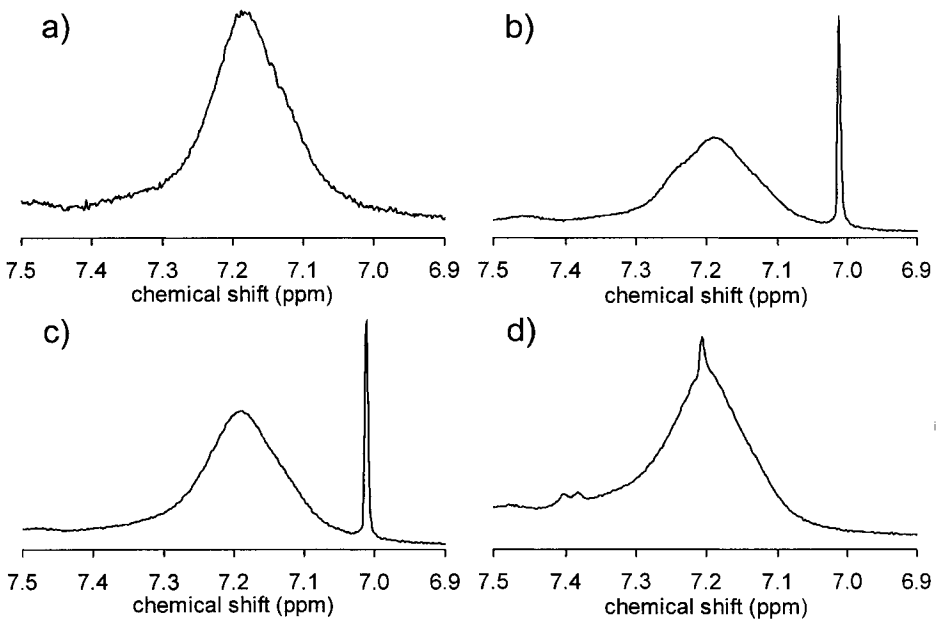

Figure 1.5.2. ^{1}H NMR spectra of poly(HPMA) and crosslinker conjugates. a) poly(HPMA)-hydrazide, b) poly(HPMA)-PMCA, c) poly(HPMA)-BMCA, d) poly(HPMA)-APM. All spectra recorded at 400 MHz in DMSO-d_6. Poly(HPMA) backbone amide signal is observed as the broad peak at 7.19 ppm. The sharp peak at 7.01 ppm (PMCA and BMCA) or 7.21 ppm (APM) shows crosslinker maleimide groups in polymer conjugates.

backbone signal for APM, it was still visible protruding above the broad amide peak.

Attachment of thiolated cargo to poly(HPMA) and subsequent release

Synthesis of the poly(HPMA)-crosslinker-TAMRA conjugate is shown in Scheme 1.5.2. Thiol-modified TAMRA was used as a model cargo compound to react with maleimide groups resulting from crosslinker conjugation to poly(HPMA). This model system was convenient, as TAMRA is fairly water-soluble, readily detected by simple absorbance measurements, and released dye is sufficiently smaller in size to allow rapid separation from the polymer-bound fraction using size exclusion chromatography.

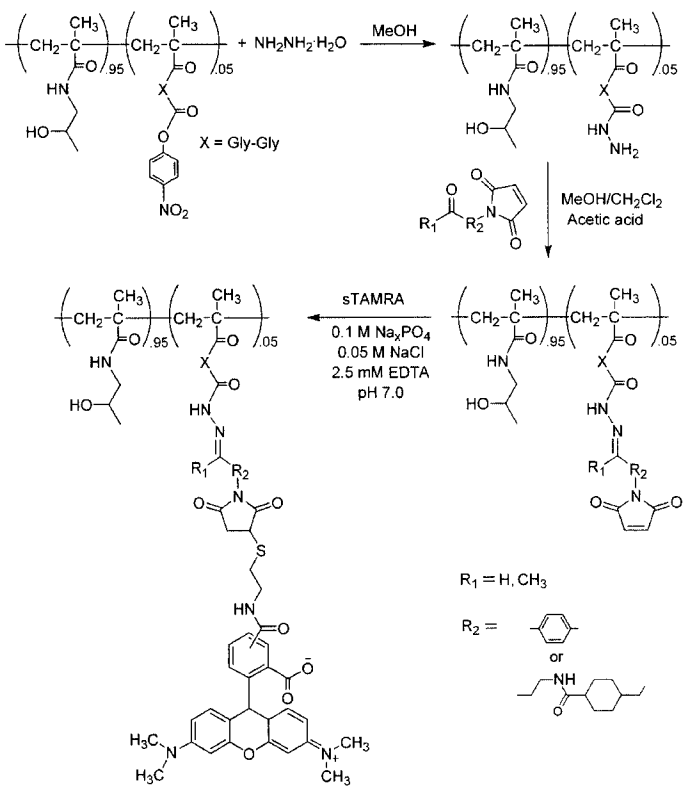

Scheme 1.5.2. Synthesis of poly(HPMA)-TAMRA conjugates linked with heterobifunctional crosslinkers.

Reduction of the TAMRA disulfide was performed with TCEP-immobilized gel which allowed easy separation of reducing agent. Free TCEP, DTT, or combinations of both resulted in lower conjugation of TAMRA to the polymer (data not shown). Although TCEP is generally believed to be unreactive towards maleimide functional groups, similar observations have been reported for the effects of free TCEP.[28, 29] Reaction times of TAMRA with crosslinker - derivatized poly(HPMA) were kept short in this study as degradation rates of these crosslinkers werre unknown. Maleimide coupling efficiency may increase with longer reaction times until crosslinker degradation and release from the polymer competes with TAMRA conjugation.

Release of conjugated TAMRA from the polymer backbone was affected by crosslinker structure as shown in Figure 1.5.3a. Release rates at both pH 7.4 and 5.0

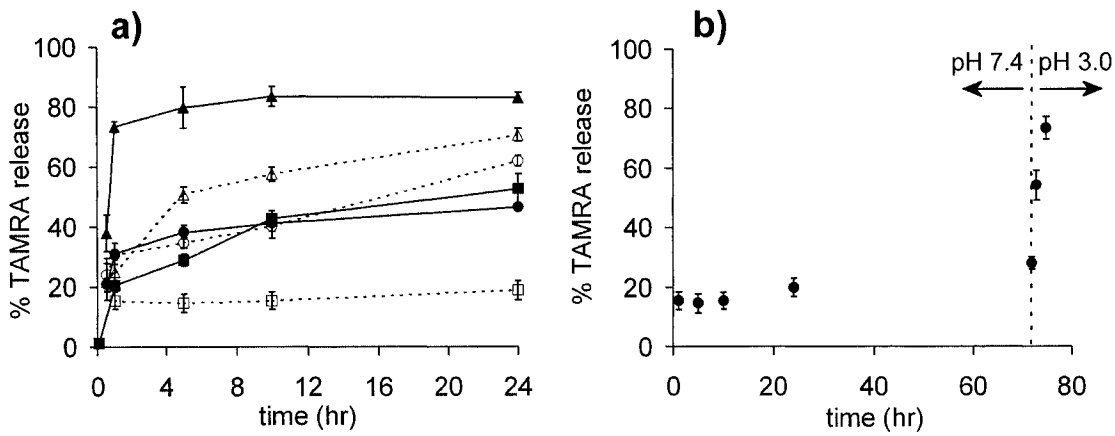

Figure 1.5.3. a) Release of TAMRA from poly(HPMA) at pH 7.4 and 5.0. Dashed/hollow, pH 7.4; ○ poly(HPMA)-PMCA, △ poly(HPMA)-BMCA, □ poly(HPMA)-APM. Solid/solid, pH 5.0; ● poly(HPMA)-PMCA, ▲ poly(HPMA)-BMCA, ■ poly(HPMA)-APM. b) Release of TAMRA from poly(HPMA)-APM after incubation at pH 7.4 for 72 hr followed by acidification to pH 3.0 with HCl. Buffers: 0.1 M NaP. 0.5 M NaCl (pH 7.4) and 0.1 M NaOAc (pH 5.0).

showed the same trend in stability based on the groups attached to the immine carbon atom participating in the hydrazone bond; aliphatic/CH_3 > aliphatic/H > phenyl/CH_3. This affect has been observed for other hydrazone systems has been recently reviewed

elsewhere.[12] Degradation of the stable hydrazone formed with poly(HPMA)-APM occurs rapidly upon acidification even after extended incubation at pH 7.4, as shown in Figure 1.5.3b.

The pH-dependent release mechanism for hydrazone hydrolysis involves protonation of the imine nitrogen, formation of a tetrahedral carbinolamine intermediate and nucleophilic attack of a water molecule. [12, 14, 30] The rate at which this hydrolysis occurs is influenced oppositely by substituents in the reactive aldehyde or ketone/aldehyde- containing parts and the hydrazide- containing group. In general, electron donating groups on the ketone/aldehyde- containing constituent increase the hydrolysis rate, while electron withdrawing groups on the hydrazide component increase hydrolysis rate, as was observed in this study.[12, 31, 32] This effect has also been observed with a poly(HPMA) conjugate containing phenyl hydrazide- derivatized reactive side chains which result in a less stable doxorubicin conjugate than that formed using glycylglycine hydazide reactive groups.[16] It is interesting to note that hydrozones formed with the 13 keto position of doxorubicin using this same glycylglycine hydrazide side chain chemistry on poly(HPMA) exhibit pH-dependent release and excellent stability at pH 7.4 even though the hydrazone is claimed to form with an aliphatic ketone.[16, 17] The hydroxyl functionality on adjacent carbons in doxorubicin may provide sufficient electron withdrawing strength to affect hydrozone stability. Additionally, the hydroxy group on the beta hydroxy ketone adjacent to the hydrazone bond in DOX conjugates can hydrogen bond with the hydrazone nitrogen to form a stable six-membered ring conformation. Glyoxylyl aldehydes prepared from N-terminal serine modified amino acids have also been recently used to form pH-sensitive hydrazones with acyl

hydrazides.[33] These observations suggest that further optimization of the SMCC-based crosslinker chemistries described here could be achieved by incorporation of electron withdrawing groups on carbon atoms adjacent to the reactive ketone functionality.

Conclusions

This work demonstates the feasibility of forming thiol-reactive poly(HPMA) conjugates via varying stability controlled with different crosslinker chemistries. Currently, the APM crosslinker is likely the best choice for *in vivo* application due to the high stability at pH 7.4, with desired degradation rate occurring in acidic conditions analogous to the lysosome environment within cells. Although APM shows desired release properties, this crosslinker has the inherent disadvantage of lower polymer coupling efficiency and formation of side-products. The heterobifunctional crosslinkers PMCA and BMCA may serve as highly efficient crosslinkers for formation of degradable bioconjugates where pH-dependent stability is not required. Alternatively, modifications of chemistry contained in hydrazide part of target macromolecules could result in conjugates with more stable hydrazone linkages formed with PMCA and BMCA.

Acknowledgements

We thank Andrew Higginbotham and Dr. Mark Kerr for helpful discussion with organic procedures. Partial support from NIH grant EB000894 is gratefully acknowledged.

References

1. Monfardini, C.; Veronese, F. M., Stabilization of substances in circulation. *Bioconjug Chem* **1998,** 9, (4), 418-50.
2. Hermanson, G. T., *Bioconjugate techniques*. Academic Press: San Diego, 1996; p xxv, 785 p.
3. Brinkley, M., A brief survey of methods for preparing protein conjugates with dyes, haptens, and cross-linking reagents. *Bioconjug Chem* **1992,** 3, (1), 2-13.
4. Mattson, G.; Conklin, E.; Desai, S.; Nielander, G.; Savage, M. D.; Morgensen, S., A practical approach to crosslinking. *Mol Biol Rep* **1993,** 17, (3), 167-83.
5. Asokan, A.; Cho, M. J., Exploitation of intracellular pH gradients in the cellular delivery of macromolecules. *J Pharm Sci* **2002,** 91, (4), 903-13.
6. Wattiaux, R.; Laurent, N.; Wattiaux-De Coninck, S.; Jadot, M., Endosomes, lysosomes: their implication in gene transfer. *Adv Drug Deliv Rev* **2000,** 41, (2), 201-8.
7. Satchi, R.; Connors, T. A.; Duncan, R., PDEPT: polymer-directed enzyme prodrug therapy. I. HPMA copolymer-cathepsin B and PK1 as a model combination. *Br J Cancer* **2001,** 85, (7), 1070-6.
8. Duncan, R.; Gac-Breton, S.; Keane, R.; Musila, R.; Sat, Y. N.; Satchi, R.; Searle, F., Polymer-drug conjugates, PDEPT and PELT: basic principles for design and transfer from the laboratory to clinic. *J Control Release* **2001,** 74, (1-3), 135-46.
9. Kopecek, J.; Kopeckova, P.; Minko, T.; Lu, Z. R.; Peterson, C. M., Water soluble polymers in tumor targeted delivery. *Journal of Controlled Release* **2001,** 74, (1-3), 147-158.
10. Putnam, D.; Kopecek, J., Polymer conjugates with anticancer activity. *Biopolymers Ii* **1995,** 122, 55-123.
11. Gillies, E. R.; Goodwin, A. P.; Frechet, J. M. J., Acetals as pH-sensitive linkages for drug delivery. *Bioconjugate Chemistry* **2004,** 15, (6), 1254-1263.
12. West, K. R.; Otto, S., Reversible covalent chemistry in drug delivery. *Curr Drug Discov Technol* **2005,** 2, (3), 123-60.
13. Kratz, F.; Beyer, U.; Schutte, M. T., Drug-polymer conjugates containing acid-cleavable bonds. *Critical Reviews in Therapeutic Drug Carrier Systems* **1999,** 16, (3), 245-288.
14. D'Souza, A. J.; Topp, E. M., Release from polymeric prodrugs: linkages and their degradation. *J Pharm Sci* **2004,** 93, (8), 1962-79.
15. Flenniken, M. L.; Liepold, L. O.; Crowley, B. E.; Willits, D. A.; Young, M. J.; Douglas, T., Selective attachment and release of a chemotherapeutic agent from the interior of a protein cage architecture. *Chemical Communications* **2005,** (4), 447-449.
16. Etrych, T.; Chytil, P.; Jelinkova, M.; Rihova, B.; Ulbrich, K., Synthesis of HPMA copolymers containing doxorubicin bound via a hydrazone linkage. Effect of spacer on drug release and in vitro cytotoxicity. *Macromolecular Bioscience* **2002,** 2, (1), 43-52.
17. Etrych, T.; Jelinkova, M.; Rihova, B.; Ulbrich, K., New HPMA copolymers containing doxorubicin bound via pH-sensitive linkage: synthesis and preliminary in vitro and in vivo biological properties. *Journal of Controlled Release* **2001,** 73, (1), 89-102.
18. King, H. D.; Dubowchik, G. M.; Mastalerz, H.; Willner, D.; Hofstead, S. J.; Firestone, R. A.; Lasch, S. J.; Trail, P. A., Monoclonal antibody conjugates of

doxorubicin prepared with branched peptide linkers: inhibition of aggregation by methoxytriethyleneglycol chains. *J Med Chem* **2002,** 45, (19), 4336-43.
19. Bae, Y.; Fukushima, S.; Harada, A.; Kataoka, K., Design of environment-sensitive supramolecular assemblies for intracellular drug delivery: Polymeric micelles that are responsive to intracellular pH change. *Angewandte Chemie-International Edition* **2003,** 42, (38), 4640-4643.
20. Rodrigues, P. C. A.; Beyer, U.; Schumacher, P.; Roth, T.; Fiebig, H. H.; Unger, C.; Messori, L.; Orioli, P.; Paper, D. H.; Mulhaupt, R.; Kratz, F., Acid-sensitive polyethylene glycol conjugates of doxorubicin: Preparation, in vitro efficacy and intracellular distribution. *Bioorganic & Medicinal Chemistry* **1999,** 7, (11), 2517-2524.
21. King, T. P.; Zhao, S. W.; Lam, T., Preparation of Protein Conjugates Via Intermolecular Hydrazone Linkage. *Biochemistry* **1986,** 25, (19), 5774-5779.
22. Kaneko, T.; Willner, D.; Monkovic, I.; Knipe, J. O.; Braslawsky, G. R.; Greenfield, R. S.; Vyas, D. M., New Hydrazone Derivatives of Adriamycin and Their Immunoconjugates - a Correlation between Acid Stability and Cytotoxicity. *Bioconjugate Chemistry* **1991,** 2, (3), 133-141.
23. Kopecek, J.; Kopeckova, P.; Minko, T.; Lu, Z., HPMA copolymer-anticancer drug conjugates: design, activity, and mechanism of action. *European Journal of Pharmaceutics & Biopharmaceutics* **2000,** 50, (1), 61-81.
24. Omura, K.; Swern, D., Oxidation of Alcohols by Activated Dimethyl-Sulfoxide - Preparative, Steric and Mechanistic Study. *Tetrahedron* **1978,** 34, (11), 1651-1660.
25. Kopecek, J., Reactive Copolymers of N-(2-Hydroxypropyl)Methacrylamide with N-Methacryloylated Derivatives of L-Leucine and L-Phenylalanine .1. Preparation, Characterization, and Reactions with Diamines. *Makromolekulare Chemie-Macromolecular Chemistry and Physics* **1977,** 178, (8), 2169-2183.
26. Drobnik, J.; Kopecek, J.; Labsky, J.; Rejmanova, P.; Exner, J.; Saudek, V.; Kalal, J., Enzymatic Cleavage of Side-Chains of Synthetic Water-Soluble Polymers. *Makromolekulare Chemie-Macromolecular Chemistry and Physics* **1976,** 177, (10), 2833-2848.
27. Ulbrich, K.; Subr, V.; Strohalm, J.; Plocova, D.; Jelinkova, M.; Rihova, B., Polymeric drugs based on conjugates of synthetic and natural macromolecules I. Synthesis and physico-chemical characterisation. *Journal of Controlled Release* **2000,** 64, (1-3), 63-79.
28. Getz, E. B.; Xiao, M.; Chakrabarty, T.; Cooke, R.; Selvin, P. R., A comparison between the sulfhydryl reductants tris(2-carboxyethyl)phosphine and dithiothreitol for use in protein biochemistry. *Analytical Biochemistry* **1999,** 273, (1), 73-80.
29. Shafer, D. E.; Inman, J. K.; Lees, A., Reaction of tris(2-carboxyethyl)phosphine (TCEP) with maleimide and alpha-haloacyl groups: Anomalous elution of TCEP by gel filtration. *Analytical Biochemistry* **2000,** 282, (1), 161-164.
30. Cordes, E. H.; Jencks, W. P., Mechanism of Hydrolysis of Schiff Bases Derived from Aliphatic Amines. *Journal of the American Chemical Society* **1963,** 85, (18), 2843-&.
31. Harnsberger, H. F.; Cochran, E. L.; Szmant, H. H., The Basicity of Hydrazones. *Journal of the American Chemical Society* **1955,** 77, (19), 5048-5050.
32. Nguyen, R.; Huc, I., Optimizing the reversibility of hydrazone formation for dynamic combinatorial chemistry. *Chemical Communications* **2003,** (8), 942-943.

33. Galande, A. K.; Weissleder, R.; Tung, C. H., Fluorescence probe with a pH-sensitive trigger. *Bioconjugate Chemistry* **2006,** 17, (2), 255-257.

CHAPTER VI

SUMMARY AND PROPOSED FUTURE WORK

This dissertation section focuses on improving the efficacy and utility of water-soluble polymeric drug delivery systems. Currently, reliable all site targeting, sub-cellular trafficking and requirements for efficient reversible covalent chemistries for carrier-drug attachment limit this approach. The ability of the Tat peptide to transport lysosome-sequestered molecules into the cytoplasm may provide opportunities for delivery of macromolecular therapeutic agents such as DNAs, siRNAs, proteins and enzymes. The mechanism of Tat peptide (and cell-penetrating peptides in general) mediated cytoplasmic entry is currently unknown with some groups proposing direct transport across exterior cell membranes and others suggesting endocytotic uptake followed by lysosome escape. The observation of endocytotic uptake following release from lysosome compartments is an important finding in this dissertation.

Studies investigating chemistries involved in forming pH-sensitive hydrazone bonds show that electron donating and withdrawing groups adjacent to the desired hydrazone affect both reactivity and stability. Degradation studies of poly(HPMA)-hydrazone conjugates showed that hydrazones formed from aliphatic carbonyls are too unstable for use in long circulating drug conjugates where long-term stability at pH 7.4 is

desired. This result will effect future design of cleavable crosslinkers that allow reversible attachment of thiol-containing synthetic- or biomolecules to polymer carriers. Combining existing technologies with a multi-disciplinary approach facilitates innovation of new drug delivery systems with improved potential for high efficacy.

In summary, sub-cellular trafficking studies with poly(HPMA) elucidated lysosome escape as one mechanism for Tat peptide cytoplasmic entry. Degradation studies of poly(HPMA)-hydrazone conjugates showed that hydrazone lability at pH 7.4 can be overcome by incorporation of electron withdrawing or π-conjugated chemistries adjacent to the carbonyl-containing hydrazone precursor.

Major accomplishments of this dissertation research:

1. HPMA copolymers were modified to contain both hydrazone and maleimide functionality for reversible attachment of thiol-containing molecules using a heterobifunctional crosslinker approach.
2. The effects of carbonyl chemistries on resulting hydrazone stability were identified.
3. A Tat-PEG model therapeutic compound was prepared with 1:1 Tat:PEG stoichiometry.
4. Subcellular distribution of HPMA-Tat-PEG was observed using scanning laser confocal fluorescence microscopy. Independent tracking of the HPMA copolymer backbone component and Tat-PEG component was achieved using a dual dye labeling approach.
5. The Tat peptide gained cytoplasmic entry after endocytotic uptake.

6. A novel thiol-containing tetramethylrhodamine dye was prepared and spectral properties were identified.

Proposed Future Work

1. Optimization of Heterobifunctional Crosslinker Chemistries

This dissertation work identifies the requirement of electron-withdrawing groups adjacent to the carbonyl reaction partner to generate a hydrazone linkage stable at pH 7.4, but degradable at pH 5.0. Optimal chemistries were not found in this work, but a recent study shows that hydrazones formed with acyl hydrazides and glyoxylyl groups results in excellent yields, desired stability at pH 7.4 and lability at pH 5.0[1]. Glyoxylyl groups are readily prepared from the amino acid, serine, using sodium periodate oxidation[2,3].

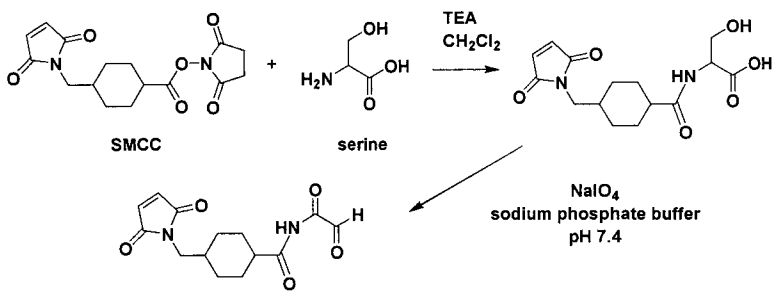

Scheme 1.6.1. Synthesis of glyoxylyl containing heterobifunctional crosslinker

1. Galande, A.K., Weissleder, R, Tung, C.H. (2006) *Bioconj. Chem. 17(2)*, 255-257.
2. Dixon, H.B.F., Weitkamp, L.R. (1962) *Biochem J.* 84, 462-468.
3. Geoghegan K. F., and Stroh, J. G. (1992) *Bioconj. Chem. 3*, 138-146.

2. Effect of cargo size on Tat-mediated lysosome escape.

This dissertation work shows the ability of Tat to transport 2000 g/mol poly(ethylene glycol) (PEG) out of lysosome compartments into the cytoplasm. A systematic study using PEGs of different molecular weights could provide insight to limitations of this drug delivery approach. PEGs containing NHS activated esters analogous to that used in this work are commercially available up to 20,000 g/mol, and Tat-PEG attachment could be performed using the same coupling strategy described in Chapter 3. The ability of the Tat peptide to transport entire proteins into the cytoplasm of cells using could also be observed by preparation of genetically engineered green fluorescent protein (GFP), containing the Tat peptide fused to the C or N terminus.

3. Effect of metabolic inhibitors on trafficking of HPMA-Tat-PEG.

Inhibiting certain metabolic processes could provide insight into the mechanism for cytoplasmic entry of Tat-attached cargo. Bafilomycin A and ammonium chloride could be used to prevent lysosome acidification, preventing pH-dependent hydrolysis of hydrazone bonds[1-3]. Observation of sub-cellular distribution of HPMA-Tat-PEG after co-incubation with compounds preventing lysosome acidification will confirm the requirement for Tat-PEG to be cleaved from the polymer carrier in order to gain cytoplasmic entry.

The efficacy of masking the Tat peptide between two macromolecules to block non-specific cell-surface interactions could be confirmed using metabolic inhibitors such as sodium azide and deoxyglucose[4,5]. Endocytosis is an energy-dependent process, and these two metabolites prevent ATP formation in cells, thus preventing endocytosis.

Demonstration of reduced cell-surface interactions of HPMA-Tat-PEG compared to Tat-PEG alone would show the potential for *in vivo* application, where strong cell-surface interactions result in rapid clearance of Tat conjugates where Tat is exposed.

The efficiency of Tat-PEG escape from lysosome compartments could be determined by co-incubation with chloroquine[6,7]. Chloroquine promotes rupture of lysosome compartments, resulting in release of entrapped components. If lysosome escape is inefficient, cytoplasmic accumulation of Tat-PEG will increase upon co-incubation with choroquine.

1. Bowman, E.J. et al. (1988) Proc. Natl. Acad. Sci. USA *85*, 7972-7976.
2. Palokangas, H., et al. (1998) Mol. Biol. Cell *8*, 3561-3578.
3. Gagliardi, S., et al. (1999) Curr. Med. Chem. *6*, 1197.
4. Wadia, J.S., et al. (2004) Nature Med *10(3)*, 310-315.
5. Kaplan, I.M. et al. (2005) J. Control. Rel. *102(1)* 247-253.
6. Ignatovich, I.A., et al. (2003) J Biol Chem *278(43)* 42625-42636.
7. Soundara Manickam,D., et al. (2005) J Control Rel *102(1)* 293-306.

4. Preparation of Tat-masked conjugates that degrade in the cytoplasm.

While this study shows that the Tat peptide can transport large molecules into the cytoplasm of cells, attachment of the Tat peptide to therapeutic agents could hinder their efficacy once transported into the cytoplasm. A sequentially degrading construct would allow release of the Tat peptide after cytoplasm entry occurs. A Tat-masked conjugate containing a pH-sensitive bond between Tat and the polymer carrier would allow release in the lysosome and subsequent cytoplasmic entry, and a peptide sequence specific to a known cytoplasmic enzyme between the therapeutic agent and the Tat peptide would allow release of the Tat peptide from the therapeutic following cleavage in the cytoplasm.

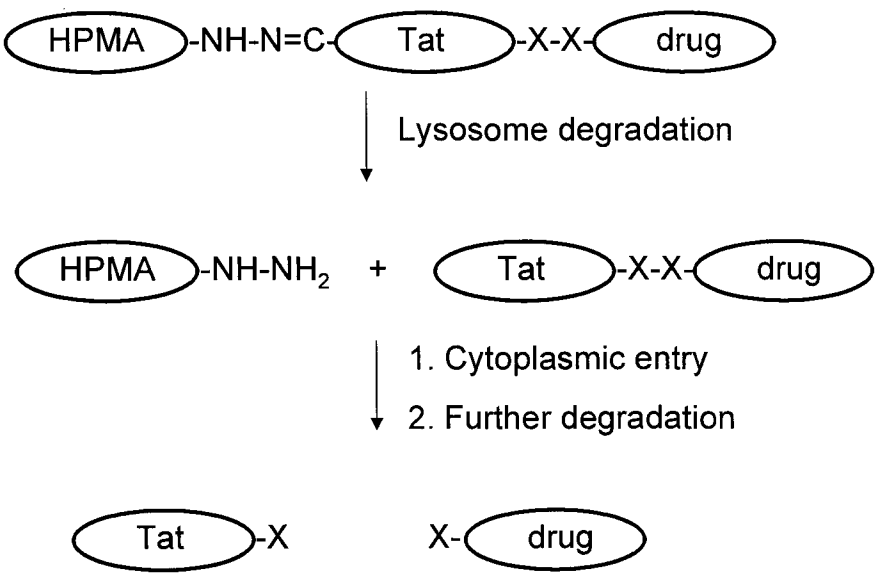

Figure 1.6.1. Design of a Polymer-Tat-Drug System for Sequential Degradation

PART 2

HYDROGEL ENCAPSULATION OF LIVE VACCINE FOR BALLISTIC DELIVERY

CHAPTER I

PHOTOPOLYMERIZED HYDROGEL CARRIERS FOR LIVE VACCINE BALLISTIC DELIVERY

Reprinted with permission from R. James Christie, Diana Findley, Matt Dunfee, Rick Hansen, Steve Olsen, and David Grainger, *Vaccine* 2006, 24, 1346-1353.

This dissertation chapter contains the manuscript of a full paper accepted by Vaccine. The manuscript was written by R. James Christie and edited by David W. Grainger. This chapter shows the utility of poly(ethylene) glycol hydrogels as an encapsulation matrix for delivery of live SRB51 vaccine to bison.

Photopolymerized Hydrogel Carriers for Live Vaccine Ballistic Delivery

R.J. Christie, D.J. Findley, M. Dunfee, R. Hansen, S.C. Olsen, D.W. Grainger

Abstract

Photopolymerized poly(ethylene glycol) (PEG) crosslinked hydrogels were assessed for their ability to serve as a payload vehicle to deliver a viable bacterial vaccine (*Brucella abortus* strain RB51 (RB51) to bison in Yellowstone National Park) ballistically using thermoplastic degradable Biobullets®. PEG modified with degradable glycolide or lactide oligomers capped with photopolymerizable methacrylate groups served to crosslink the hydrogel vaccine carrier inside commercial hydroxypropylcellulose Biobullets®. Release of 1-micron diameter model fluorescent particles from hydrogels followed known degradation trends for glycolide- and lactide-modified PEG hydrogels. All particles were released from PEG-co-glycolide hydrogels after ~10 days and PEG-co-lactide hydrogels after ~45 days following gel degradation. Minimal particle release was observed from pure PEG dimethacrylate hydrogels over 40 days. *P. aeruginosa* (strain PAO1) and RB51 live vaccines exhibit excellent viability following exposure to photopolymerization encapsulation within these gel matrices. Hydrogels photopolymerized into the payload chamber of Biobullets® exhibit similar ballistic

properties to commercially available Biobullets®, and penetrate and remain intact when fired intramuscularly into live elk for release of their gel payload in the host.

Introduction

Yellowstone National Park's interagency bison management plan provides an adaptive framework for long-term research and management of the indigenous free-ranging bison herd [1,2]. The high prevalence of *Brucella abortus* in resident free-ranging bison requires that the National Park Service produce vaccination options to mitigate *B. abortus* infection and transmission at minimal risk to both animals and park visitors [3,4]. Because infection of *B. abortus* results in late-stage abortion and reduced fertility in females, and orchitis, epididymitis, and sterility in males, high infection rates of *B. abortus* can have detrimental long-term effects on the bison populations from decreased calf recruitment [5-7]. Although transmission of this disease to domestic cattle is generally accepted to be minimal, it has been shown to occur, producing concern about shared rangelands for bison, elk and private cattle herds adjacent to the Park [8]. The Park's "leave no trace" environmental policy eliminates other known vaccination methods, such as darts, feedgrounds, or capture facilities within the park. This policy and the bison management plan demand development of new technology highly effective for vaccination of wild bison, while minimizing environmental impact and disturbance to native herd behavior.

The current commercial *B. abortus* bovine live microbial vaccine, *B. abortus* strain RB51 (RB51), exhibits some protective efficacy in bison vaccination [9-16]. This bacterial vaccine is currently used for domestic cattle, primarily administered by

parenteral injection. Preservation of protective cell-mediated immune response in bison requires delivery of live brucella vaccine at dosages of ~10^{10} CFUs i.m., with lyophilized RB51 formulations also shown to be effective when administered i.m. as either a powder or after aqueous reconstitution [17-18]. Rapid, immediate release of the live vaccine into the host is desirable, requiring a promptly degrading carrier since the delivered bacteria are large (~ 1-micron), non-motile, and slow diffusing. Utility of this vaccine in Yellowstone Park will also depend upon its impact on non-target species. Recent studies show minimal morbidity or mortality in ravens, ground squirrels, deer mice, or prairie voles following RB51 oral ingestion at 76-92% of the dose needed for bison inoculation [19]. Another non-target species, pronghorn antelope (*Antilocapra americana*) showed no adverse affects or abortion following injestion at bison inoculation doses [20].

Delivery of live vaccine to wildlife, and specifically to bison in the Park, requires a ballistics approach from a distance (> 30 m). Several modes have been reported for remote delivery to wildlife and domestic species, including feedgrounds, aerosols, darts, and other various projectiles [21-34]. Current technology also exists for remote delivery of various therapeutics to livestock via a biodegradable thermoplastically molded hydroxypropylcellulose Biobullet® fired from an air rifle charged to ~1200 psi [35]. In this case, the payload (i.e. vaccine dose) is loaded into the hollow Biobullet® chamber using powder compression, forming a hard pellet. While this works acceptably for modified live virus (MLV) vaccines and non-viable therapeutics, initial work with lyophilized RB51 vaccine compression loaded into Biobullets® demonstrates little bioactivity (i.e., immune response) following bison vaccination, likely due to low RB51 viability after dry compression and Biobullet® loading [34]. This observation has

prompted investigation of other payload and formulation methods to produce high vaccine viability in the Biobullet® payload, while maintaining the predictable and reliable ballistic properties of the delivery system.

We report application of known poly(ethylene glycol)-based (PEG) photopolymerized hydrogels to encapsulate live brucella vaccine bacteria within commercial biodegradable hydroxypropylcellulose bullets, ultimately intended for remote vaccine delivery to bison. PEG and photopolymerized PEG diacrylates are well-documented as benign biological encapsulation and delivery matrices with suitable properties for this application [36-39]. Furthermore, PEG hydrogel chemistries can be modified with known biodegradable components to produce degradation characteristics necessary for brucella vaccination in this context [40-43]. These PEG-based hydrogels exhibit tissue-like elastic properties, high water content, mild processing conditions, rapid fluid uptake, and controlled degradation, all useful properties for live cell encapsulation. Acceptable viability for several different cell types has been shown following encapsulation in several different photopolymerized PEG-based hydrogels [39, 43-48]. Because bacteria are frequently considered more robust than mammalian cells, recent successes for cell encapsulation imply reasonable feasibility as well for bacteria encapsulation.

Exploiting this approach for a ballistic-based wildlife vaccine depends on reliable post-processing viability of the vaccine within the bullet, the ability of the vaccine-carrying gel to survive firing from the remote delivery device, accurate impact/penetration into the tissue of the target animal, and release of the live vaccine in the host at dosing sufficient to provide immune response and protection. We report *in*

vitro analysis of release, viability, and ballistic properties for PEG hydrogel-loaded Biobullets®, and preliminary *in vivo* analysis of hydrogel-loaded Biobullet® performance. These RB51-loaded PEG hydrogels are currently in further in vivo testing in live bison models to assess the capability of remote brucellosis vaccination to produce requisite protective immune stimulus.

Experimental

Materials

PEG (mw 6000-7500) was obtained from J.T. Baker Chemical Co. (Phillipsburg, NJ) and purified by dissolution in methylene chloride followed by repeated precipitation into diethyl ether and hexane. Methacryloyl chloride (99%) and d,l-lactide (3,6-dimethyl-1,4-dioxane-2,5-dione (99+%)) were obtained from Aldrich (St. Louis, MO). Glycolide (1,4-dioxane-2,5-dione (99+%)) was purchased from Polysciences, Inc. (Warrington, PA). Irgacure®184 (1-hydroxy-cyclohexyl-phenyl-ketone) was obtained from Ciba Specialty Chemicals (Tarrytown, NY). Triethylamine, methylene chloride, diethyl ether, hexane, ethanol, and phosphate buffered saline (PBS) were all obtained from Fisher Scientific (Pittsburgh, PA). Methylene chloride-d_2 and tetramethylsilane were purchased from Cambridge Isotope Laboratories, Inc. (Andover, MA). Difco™ Tryptose agar, LB broth and agar (Miller) were purchased from Becton Dickinson (Sparks, MD). Fluorescent polystyrene microparticles (1-micron diameter, <5% CV) were obtained from Duke Scientific (Palo Alto, CA). Hydroxypropylcellulose Biobullets® and a SolidTech Delivery System air rifle were donated by SolidTech Animal Health, Inc. (Newcastle, OK). Cultured *P. aeruginosa* strain PAO1 (American Type

Culture Collection, Manassas, VA) was provided by Dr. H. Schweizer, Dept. of Microbiology, Colorado State University. Lyophilized *B. abortus* commercial vaccine (RB51) was obtained from Colorado Serum Co. (Denver, CO). Live wild elk (*Cervus elaphus*) quarantined for disease were provided by the Wyoming Game and Fish Department (Wheatland, WY).

Preparation of lactide- and glycolide- modified PEGs

PEG-co-glycolide and PEG-co-lactide were synthesized using a previously published procedure [40]. PEG was heated to 140 °C and dried under vacuum for 5 minutes. Glycolide or lactide (5 moles per mole of PEG) and tin(II) ethylhexanoate catalyst (0.092 moles per mole of PEG) were added to the flask and stirred at 200 °C for 1 hr, 150 °C for 8 hrs under vacuum, allowed to cool to room temperature, and diluted with CH_2Cl_2. The resulting turbid solution was centrifuged at ~ 10,000 rpm for 10 min. The resulting clear supernatant was decanted from the pellet and precipitated into diethylether. This solid product was collected by filtration and dried under vacuum. The solids were then dissolved in CH_2Cl_2 and precipitated into hexane and dried under vacuum, yielding a white product. Typical yield was ~ 80%. Product was analyzed using IR (Nicolet, Avatar 320 FT-IR) and ^1H NMR (Varian, 400 MHz) spectroscopy in d_2-methylene chloride with tetramethylsilane as an internal standard.

PEG methacrylation

Dimethacrylated PEG was prepared from pure PEG, PEG-lactide and PEG-glycolide according to a previously published procedure [40]. Briefly, PEG derivatives were added to dry CH_2Cl_2 to form 10% w/v solutions. The reaction flask was capped with a septum, purged with nitrogen and cooled to 0 °C. A three-fold molar excess (relative to PEG terminal-OH groups) each of triethylamine and methacryloyl chloride was added drop-wise through the septum under nitrogen. The reaction flask was stirred at 0 °C for 12 hrs, followed by reaction at room temperature for 12 hrs. After the reaction was complete, the PEG solution was concentrated under vacuum to ~ 1/2 original volume. Triethylamine hydrochloride crystals were removed by filtration. Filtrate was precipitated into a 10-fold excess of diethyl ether, isolated by filtration and dried under vacuum. Product was re-dissolved in dry CH_2Cl_2 and precipitated into a ten-fold excess of hexane. Solids were collected by filtration and dried to a constant mass under vacuum. Typical yield was > 90%. Methacrylation was confirmed by ^1H NMR spectroscopy (Varian, 400 MHz) in d_2-methylene chloride with tetramethylsilane as an internal standard.

Photopolymerization of methacrylated PEGs

A 35% w/w PEG solution was prepared by dissolving 350 mg of methacrylated PEG derivatives in 650 μL PBS buffer. A saturated Irgacure®184 solution in ethanol was prepared at room temperature (~ 4.0 M) and 6 μL of this solution was added to the PEG solution as a photoinitiator (benzophenone derivative). Photopolymerization was

performed in a "home-built" UV reactor with a Hannovia low pressure Hg lamp (Hanovia, 200 W) equipped with a quartz water-cooling jacket (20 mW/cm^2, 90 s).

2.5. Ballistic analysis of hydrogel-loaded Biobullets®

Hydrogels were photopolymerized into the payload chamber of pure hydroxypropyl cellulose Biobullets® (SolidTech Animal Health Inc., OK) using the procedure described in section 2.4. Figure 2.4.1 shows the commercial thermoplastic molded Biobullet® projectile (length = 1.6 cm) with its hollow payload compartment

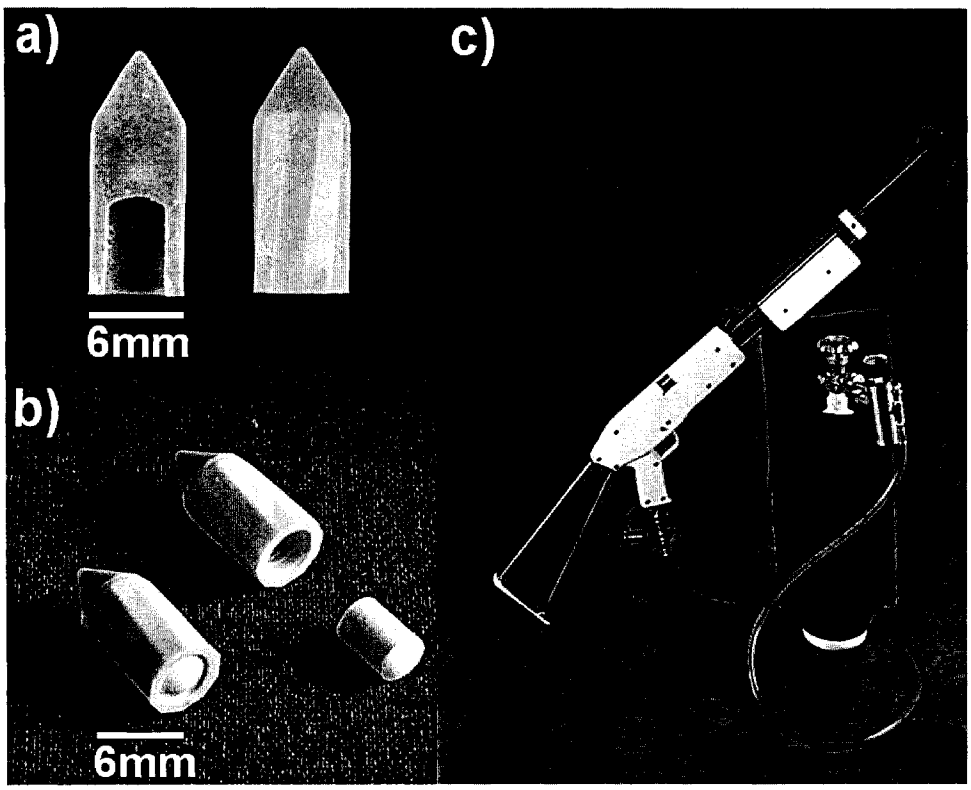

Figure 2.1.1. (a) Thermoplastic molded hydroxypropyl cellulose Biobullet®, 90 μL payload capacity (b) Thermoplastic molded hydroxypropyl cellulose Biobullet®, 90 μL payload capacity, showing commercially available molded pellet payload (c) SolidTech Delivery System air rifle and gas cylinder backpack.

(90 μL), the current commercial compression molded payload Biobullet®, and the air rifle device used in these experiments. PEG solution (90 μL) was loaded into the payload compartment of Biobullets® and photopolymerized for each analysis except when compressed solid payloads were used as controls. For ballistic kinetic energy and range assessments, Biobullets® were fired from an air rifle charged to ~ 1200 psi through a chronograph (Shooting Chrony®, Inc.) at various distances in open air. Accuracy measurements were determined with hydrogel-loaded Biobullets® fired into paper targets at a distance of 20 m.

Analysis of hydrogel-loaded Biobullets® fired into live penned wild elk

Pure thermoplastic degradable hydroxypropylcellulose Biobullets® (SolidTech Animal Health Inc., OK) with a 90 μL payload volume (length = 1.6 cm) were loaded with PEG dimethacrylate macromonomer, and Irgacure®184 solution and photopolymerized as in section 2.4 above. Hydrogel Biobullets ® were then fired from a compressed air rifle (SolidTech Animal Health Inc., OK) at a distance of 20 m into live penned and quarantined (diseased) adult wild elk. Hindquarter muscle was the desired target. After 24 hr, the animals were sacrificed and the bullets were recovered by necropsy, along with analysis of bullet tracts, resting locations and associated tissue trauma.

Release rate of 1-micron diameter fluorescent polymer particles from PEG gels

PEG hydrogels containing encapsulated 1-micron red fluorescent polymer microspheres were prepared by dissolving 350 mg PEG in 650 μL aqueous stock particle solution (1.8×10^{10} particles/mL). After addition of 6 μL saturated Irgacure® 184 in ethanol, the polymer-particle suspension was vortexed briefly, and air bubbles were

removed by brief centrifugation. This suspension (90 μL, ~ 1.62 x 10^9 total particles) was photopolymerized in the bottom of glass NMR tubes (inner diameter of commercial NMR tubes nearly identically matched the Biobullet® payload chamber diameter of 4 mm). Cured gel samples were recovered by fracturing the NMR tubes and placed in a porous plastic sample holder suspended in 10 mL PBS buffer. The sample was sealed from air, and incubated at 37 °C while being gently stirred. The fluorescent intensity of the buffer surrounding the gel was measured at various time points (λ_{ex} = 496 nm, λ_{em} = 575 nm, slits = 1 nm excitation, 10 nm emission, Spex Fluorolog-3, Horiba Jobin Yvon). Fluorescence intensity of known dilutions of fluorescent microparticle solutions was found to be linear over the release range of this experiment (data not shown). Control particle formulations were prepared with non-methacrylated, pure PEG, and exposed to UV light for identical amounts of time (90 s) as crosslinked samples to account for possible photobleaching of fluorescent microspheres following UV exposure. Hydrogel swelling was determined gravimetrically as a mass percent increase of original gel mass over time in PBS buffer at 24 °C. Gels were photopolymerized in NMR tubes, recovered, and cut into segments corresponding to the dimensions of the Biobullet® payload volume.

Post-hydrogel processing viability of P. aeruginosa and RB51 bacteria

Viability assessments included both *P. aeruginosa* (strain PAO1) as a model bacterium (biosafety level 1), and *B. abortus* (RB51, biosafety level 2) as the target vaccine organism. For PAO1, organisms were grown to stationary phase in LB broth and concentrated by centrifugation. The resulting pellet was then diluted with PBS to obtain a solution of 1x10^{10} viable organisms per 650 μL of solution (assessed by agar plate

culture). This PBS solution was then subjected to various processing conditions duplicating gel polymerization procedures including: 1) bacteria PBS solution subjected directly to UV exposure (as in section 2.4 for all viability experiments), 2) bacteria PBS solution prepared in 35% w/w PEG macromer solution exposed to UV light for 90 s, and 3) 6 μL Irgacure® 184 (as in section 2.4) photoinitiator solution added to 650 μL of bacteria PBS solution and subjected to identical UV exposure. Agar plate counting of viable organism colonies both before and after different model PEG polymerization procedures used serial dilutions of recovered organisms. For RB51 samples, lyophilized RB51 powder was suspended in PBS buffer to obtain ~$1x10^{10}$ viable organisms per 650 μL of solution. This solution was then subjected to the same photo processing conditions as for PAO1 above. The recovered RB51 samples were then courier shipped under refrigeration to Dr. Steve Olsen (USDA labs, Ames, IA) for viability assessment. Viability of RB51 samples were determined by serial dilution in 0.15 M phosphate buffered sodium chloride (pH 7.2) and inoculation onto tryptose agar plates containing 5% bovine serum. After incubation at 37 °C and 5% CO_2 for 3 days, standard plate counts were conducted. Isolates were confirmed as RB51 by colony morphology, growth characteristics, and resistance to rifampin [16].

Results and discussion

PEG end group modification and hydrogel formation

PEG end group modification with lactide and glycolide was readily achieved under neat conditions, with tin(II) ethylhexanoate catalyzing the trans-esterification reaction. This reaction has been performed using various conditions and catalysts

[40,41,49-54]. Formation of the desired product consistent with these reports was confirmed with IR spectroscopy (ester C=O stretch, 1700 cm^{-1}) and ^1H NMR spectroscopy (δ = 4.8 ppm, $C\underline{H}_2$, glycolide, δ =1.4ppm, $C\underline{H}_3$, lactide). The degree of end group modification was estimated by comparing ^1H NMR integral intensities for glycolide $C\underline{H}_2$ and lactide $C\underline{H}_3$ peaks to the PEG $C\underline{H}_2$ backbone integral intensity (δ = 3.6 ppm). ^1H NMR analysis showed the glycolide and lactide components of the PEG macromer to be between 4-4.5 mol per mol PEG (80-90% conversion). No unreacted glycolide or lactide was observed in each product, and the calculated incomplete conversion is most likely due to reagent PEG polydispersity. No affects on the solubility of the PEG macromer were observed with this ratio of lactide or glycolide to PEG. Further modification of terminal PEG groups to form a photopolymerizable PEG macromer is achieved by routine reaction with methacryloyl chloride under these conditions. Evidence for this reaction's success is indicated by the appearance of vinyl $C\underline{H}_2$ protons (δ = 5.6, 6.1ppm), characteristic of the methacrylate functional group. Photopolymerization of the methacrylated PEGs is easily performed using Irgacure®184 photo-initiator. Irgacure®184 was chosen for its history and known cytocompatability in this context [55]. Upon exposure to UV light (20 mW/cm^2) from a low-pressure mercury lamp, firm, elastic crosslinked PEG hydrogels were consistently formed from PEG aqueous solutions after 90 s. The relatively high concentration of PEG used in the aqueous macromer solution resulted in a gel with sufficient structural integrity to survive air-rifle firing and target impact.

Preparation of PEG hydrogel-loaded Biobullets®

Photopolymerizion of PEG derivative hydrogels into the hollow payload chamber of the thermoplastic Biobullets® maintains similar Biobullet® charisteristics as commercially available, compression-mold filled Biobullets®. Careful hand-loading of 90 μL PEG macromer solution into the Biobullet® payload chamber results in a Biobullet® which is only slightly lighter than compressed solid-loaded commercial Biobullets® due to the lower density PEG solution. Hand-loaded Biobullets® exhibit a similar mass of 0.753g (+/- 0.008g) compared to commercial compression-mold filled Biobullets® (0.780g +/- 0.009g). Reproducibility of hand-loading macromer solution into a Biobullet® is acceptable to achieve reliable ballistic properties.

Ballistic performance of hydrogel-loaded Biobullets®

Hydrogel-loaded Biobullets® performed very similarly to commercial Biobullets® loaded with molded thermoplastic pellet payloads in both accuracy and downrange kinetic energy. Figure 2.1.2 shows the chronograph-determined downrange energies of hydrogel-loaded Biobullets® versus commercial pellet-loaded Biobullets®. The slightly lower average mass of the hydrogel Biobullets® results in higher velocity at ranges less than 20 m, translating into slightly higher kinetic energy than commercial pellet-loaded Biobullets®. Increased kinetic energy at close range could result in slightly greater bullet penetration into the target animal. However, at distances greater than 20 m, (the most probable field scenario with wild bison) both Biobullet® formulations showed similar kinetic energy values.

Accuracy of the hand-loaded gel payload Biobullets® also proved to be acceptable for field use. When fired into a target at 20 m, 100% of shots can be placed within 13 cm of the target center, an area corresponding to a fraction of the desired target of bison hindquarter tissue. Accurate firing of hydrogel-loaded Biobullets® through the

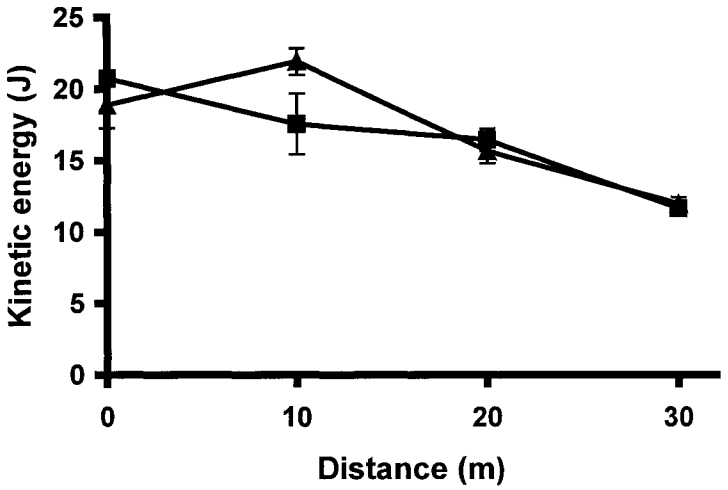

Figure 2.1.2. Down-range performance of hydrogel-loaded thermoplastic Biobullets® (n=4) using chronography. ▲= hydrogel-loaded Biobullet®, ■ = commercial pellet-loaded Biobullet®.

chronograph target area (8 cm x 34 cm x 38 cm trapezoid) was also reliable at 30 m. At extreme ranges of ~ 100 m (beyond recommended range of air-rifle delivery system), hydrogel-loaded Biobullets® drop ~ 1 m from target center, with left-to-right accuracy maintained fairly well. This implies that extended accuracy may be possible with calibrated scopes placed on the air-rifle to account for bullet drop if downfield energy allows for sufficient target penetration.

Hydrogel-loaded bullets fired into the hindquarters of live penned elk at 20 m remained intact after air rifle firing, producing visible bullet tracts into the target muscle and penetration deep into the hindquarter muscle tissue bed (penetration depth into the

muscle tissue averaged ~ 10 cm from skin exterior, non-linear tracking was observed). No bullets exited the animal and no bones were broken nor did animals exhibit any apparent excess morbidity from bullet entry. Figure 2.1.3 shows necropsy recovery of a

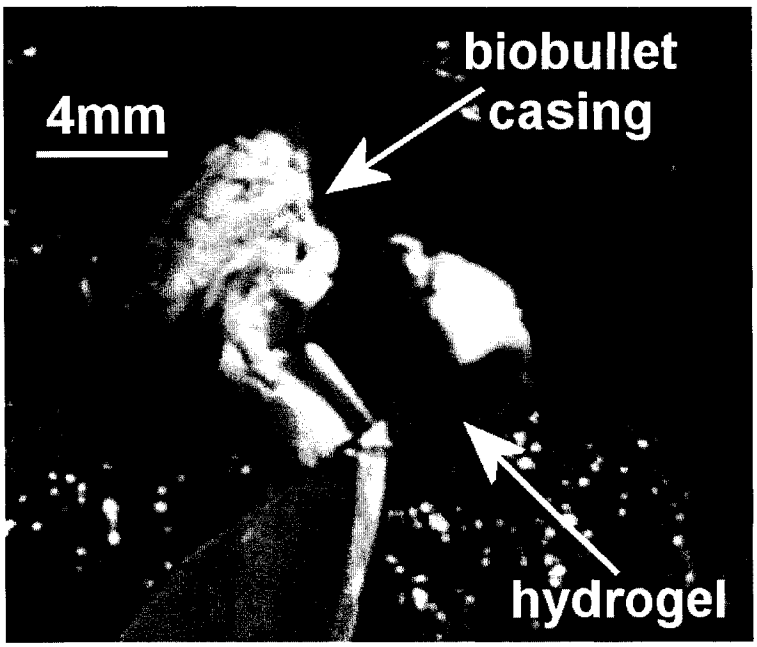

Figure 2.1.3. Necropsy-recovered hydrogel-loaded Biobullet® from elk hindquarter muscle bed 24 hr after firing into hindquarter tissue from 20 m. This bullet was found ~ 10 cm deep from elk exterior.

hydrogel-loaded Biobullet® 24 hr after entry into an elk hindquarter. In general, hydrogel-loaded Biobullets® softened rapidly *in vitro* and *in vivo* to release the swelling PEG gel payload as an integral swelling gel cylinder. Under the air-rifle air-pressure conditions and short range, only intramuscular placement was observed.

Fluorescent microsphere release from PEG hydrogels in vitro

Release of 1-micron fluorescent polymer particles from the PEG hydrogel carrier serves as a convenient approximation for release of non-motile brucella bacteria of

similar size from the Biobullet® without need for biosafety level 2 facilities. An initial burst of bacteria release is desirable for vaccination, with possible altered formulations including an additional slow release component to serve as a longer-term booster. With these considerations, crosslinked glycolide- and lactide-functionalized PEG hydrogels were analyzed for their ability to release particles from the gel matrix. These PEG end-group modifications have been utilized in numerous previous photopolymerized biodegradable gel systems. Figure 2.1.4 shows that release profiles of these 1-micron particles from the various PEG hydrogels closely follow published degradation profiles from similar formulations [40]. Release of these particles depends solely on degradation of the hydrogel since the particles are much larger than the predicted mesh size of the crosslinked gel matrix. Negligible particle release (< 2%) was observed in crosslinked pure PEG-dimethacrylate hydrogels with no incorporated degradation component over 45 days, emphasizing the importance of glycolide- and lactide-modification to produce degradation-controlled particle and microbial release.

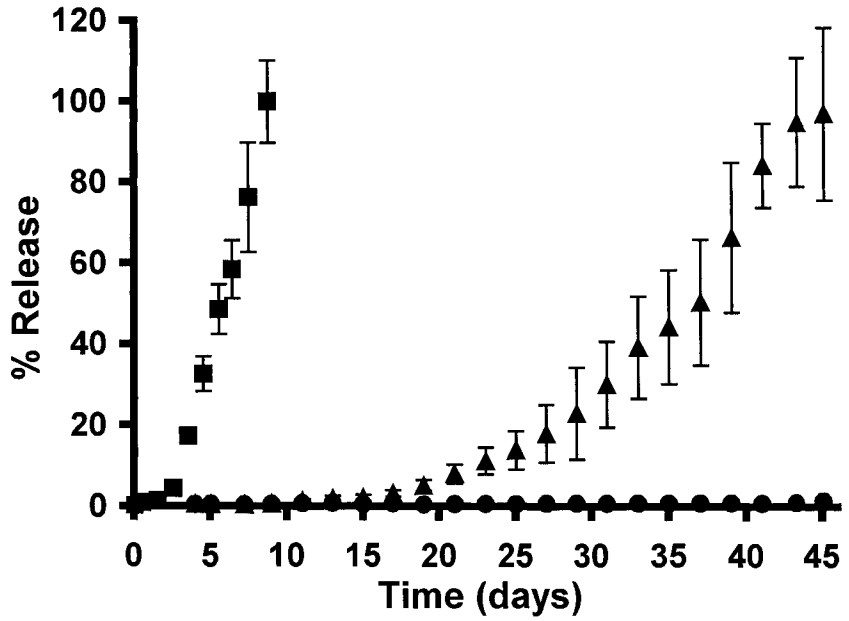

Figure 2.1.4. Release of 1-micron diameter fluorescent polymer particles from photopolymerized crosslinked PEG hydrogels (n = 4). ■ = PEG-co-glycolide hydrogel, ▲= PEG-co-lactide hydrogel, ● = PEG hydrogel.

A hydrogel formulation comprising crosslinked PEG (mw = 8000) with 5 lactide units on each end capped with acrylate groups has a reported mesh size of ~50 Å, calculated using the technique developed by Canal and Peppas [41,56]. Average gel pore size increased to ~ 130 Å over 100 hr due to swelling and degradation, well-below sizes needed to release 1-micron particles. This degradation-dependent swelling effect is clearly evidenced by the observed 15-day lag period before any particle release in PEG-co-lactide formulations. By contrast, glycolide-functionalized PEG matrices appear to be the optimal candidate for initial vaccination formulations, providing a burst of particle release more rapidly over ~ 9 days. Lactide-functionalized PEG matrices release polymer particles slowly over a period beginning at 15 days and spanning to 45 days, making this formulation appealing as a slow release vaccine booster matrix. While these results were

obtained under stirred but static incubating in vitro conditions, faster gel degradation and particle release could occur *in vivo* due to normal muscle mechanics aiding in the mechanical breakdown of the hydrogel matrix and vaccine release.

The current *B. abortus* vaccine comprises viable reconstituted RB51 organisms suspended in buffer, administered to bison or cattle by hand via parenteral injection at a dose of ~ 10^{10} viable organisms per animal. To our knowledge, no RB51 vaccine formulation has been designed specifically for controlled release versatility where dose is released at specific rates over time. The desired release kinetics could resemble the method of hand administration, that is, a burst of released bacteria, but this is not known. Booster requirements could mandate staged or pulsatile release, but little is known about this dosing either. The PGA crosslinked hydrogels produced the fastest release kinetics and further testing *in vivo* is required to determine if this is sufficient to generate the desired cellular immune response.

Hydrogel swelling studies show that equilibrium swelling is reached rapidly after ~ 4 hrs (250% mass increase by water uptake) for PEG-dimethacrylate hydrogels, further indicating that particle release is a degradation-dependent process.

Viability of P. aeruginosa PAO1 and RB51 bacteria after hydrogel photopolymerization processing

Post-processing viability of the photo-irradiated bacteria strains in PEG gel models was investigated for model *P. aeruginosa* (strain PAO1) and target vaccine RB51. Viability of both bacteria strains was determined in the presence of UV exposure only, UV exposure in the presence of PEG-dimethacrylate monomer, and UV exposure in

the presence of Irgacure® 184 initiator. Viability of 1 x 10^{10} CFU per device was assessed. These conditions resulted in a suitable non-crosslinked solution model that could easily be diluted and subjected to agar plate culture and assessment of viable colony (CFU) formation. Results shown in Figure 2.1.5 support sufficient bacteria viability maintained when bacteria are exposed to these relevant hydrogel- processing conditions. *P. aeruginosa* is apparently more robust to this photo-reactive encapsulation than RB51, but RB51 device loading can be increased to compensate for viability loss and achieve requisite dosing. Viability assessment under these conditions represents processing that is harsher than the actual conditions when a gel is formed and free radicals are scavenged from solution by the polymerization process. As a result, actual viabilities of live bacteria within photopolymerized gels are expected to be higher.

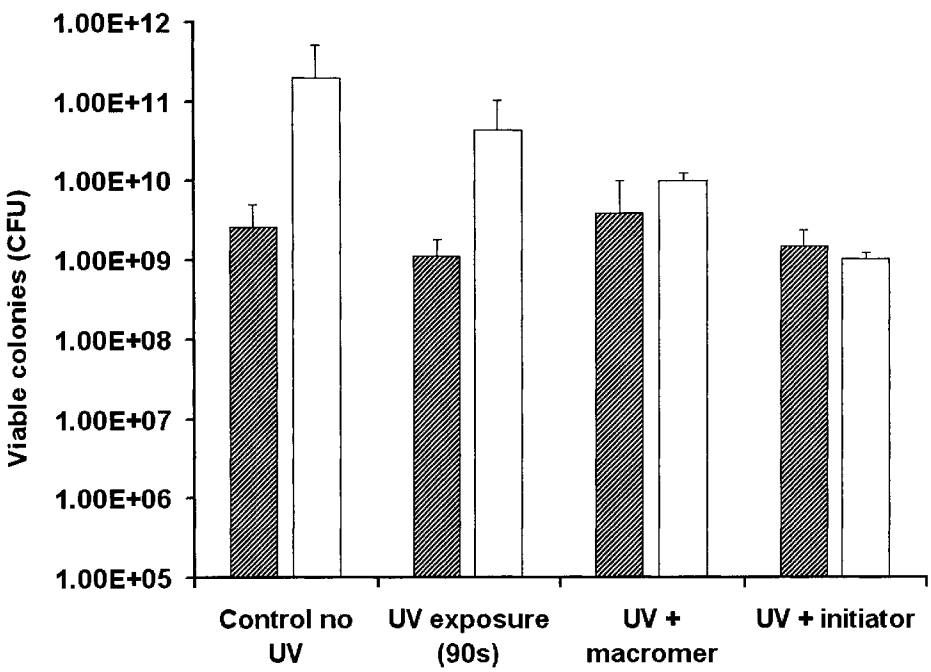

Figure 2.1.5. Post-hydrogel-processing viability of model bacteria *P. aeruginosa* and target vaccine RB51 organisms. ▨= PAO1, □= RB51.

Although no viability studies were performed on the RB51 vaccine organisms within the gels over time, previous work has shown that this vaccine exhibits excellent viability (less than ~ 10% viability loss) when stored in aqueous milieu at temperatures lower than 4 °C over a period of 12 weeks [57]. Considering that the hydrogel vaccine formulation is a suspension of RB51 containing a variety of stabilizing agents aimed at preserving viability in the commercial product following lyophilization, the hydrogel vaccine should also exhibit excellent viability when stored at low temperatures.

Conclusions

The ability to produce a degradable Biobullet® delivery vehicle that utilizes mild vaccine processing conditions is a current barrier for remote delivery of viable wildlife vaccines. This work illustrates the potential application of photopolymerized PEG hydrogels as a carrier for remote delivery of viable wildlife therapeutics. The resulting projectile has similar ballistic and tissue penetration characteristics to commercial bullets used for livestock vaccination, with the added utility of live vaccine encapsulation and subsequent reliable release. The expected viability loss in commercial RB51 upon encapsulation can easily be compensated by slight vaccine overdosing to achieve the desired $\sim 10^{10}$ CFU viable bacteria target needed for effective bison field vaccination in Yellowstone Park. In summary, these hydrogel-loaded Biobullets® represent attractive candidate vehicles to accurately deliver viable vaccine to target animals from a distance with completely degradability. On-going field trials are currently assessing cell-based immunity in penned bison cohorts.

Acknowledgements

This research was supported by the National Park Service contract 1200-99-009. The authors thank Rick Wallen, Bison Ecology Lab, Yellowstone National Park, for initiating and supporting this collaborative project. The authors also acknowledge Dr. Jack Rhyan, USDA National Wildlife Research Center, Fort Collins, CO for extending facilities to allow RB51 *in vitro* work and Terry Kreeger, Wyoming Game and Fish Dept., Wheatland, WY, for facilitating work with live quarantined elk. The authors also thank Ted Randolph and John Carpenter, University of Colorado, for technical discussions and Emily Kaiser for valuable technical contributions.

References

[1] Plumb G, Aune, K. The long term interagency bison management plan for Yellowstone National Park and the state of Montana. In: Kreeger TJ, editor. Brucellosis in Elk and Bison in the Greater Yellowstone Area. Cheyenne: Wyoming game and Fish Department; 2002. p. 136-45.

[2] U.S. Department of Interior and U. S. Department of Agriculture. Bison Management for the State of Montana and Yellowstone National Park: Final Environment Impact Statement, vol.1, Washington DC; 2000.

[3] Cheville NF, McCullough DR, Paulson LR. Brucellosis in the Greater Yellowstone Area. Washington DC: National Academy Press; 1998.

[4] Williams ES, Thorne ET, Anderson SL, Herriges JD. Brucellosis in free-ranging bison (*Bison bison*) from Teton County, Wyoming. J Wildl Dis 1993;29(1):118-22.

[5] Smith LD, Ficht TA. In: O'Leary WM, editor. Critical Reviews of Microbiology. Boca Raton: CRC Press Inc.; 1990. p. 209-30.

[6] Enright FM. In: Nielsen K and Duncan JR, editors. Animal Brucellosis. Boca Raton: CRC Press Inc.; 1990. p.301-20.

[7] Rhyan JC, Quinn WJ, Stackhouse LS, Henderson JJ, Ewalt DR, Payeur JB, Johnson, M, Meagher M. Abortion caused by *Brucella abortus* biovar 1 in a free-ranging bison (*Bison bison*) from Yellowstone National Park. J Wildl Dis 1994;30(3):445-46.

[8] David DS, Templeton JW, Ficht TA, Williams JD, Kopec JD, Adams LG. *Brucella abortus* in captive bison. I. Serology, bacteriology, pathogenesis, and transmission to cattle. J Wildl Dis 1990;26(3):360-71.

[9] Cheville NF. Development, testing and commercialization of a new brucellosis vaccine for cattle. Ann NY Acad Sci 2000;916:147-53.

[10] Roffe TJ, Olsen SC, Gidlewski T, Jensen AE, Palmer MV, Huber R, Biosafety of parenteral *Brucella abortus* strain RB51 vaccine in bison calves. J Wildl Manag 1999;63:950-55.

[11] Elzer PH, Edmonds MD, Hagius SD, Walker JV, Gilsdorf MJ, Davis, DS. Safety of *Brucella abortus* strain RB51 in Bison. J Wildl Dis 1998;34(4):825-29.

[12] Davis DS, Elzer, PH. Brucella vaccines in wildlife. Vet Microbiol 2002;90(1-4):533-44.

[13] Olsen SC, Cheville NF, Kunkle RA, Palmer MV, Jensen AE. Bacterial survival, lymph node changes, and immunologic response of bison (*Bison bison*) vaccinated with *Brucella abortus* strain RB51 or strain 19. J Wildl Dis 1997;33:146-51.

[14] Olsen SC, Holland SD. Safety of revaccination of pregnant bison with *Brucella abortus* strain RB51. J Wildl Dis 2003;39(4):824-29.

[15] Olsen SC, Jensen AE, Stoffregen WC, Palmer MV. Efficacy of calfhood vaccination with *Brucella abortus* strain RB51 in protecting bison against brucellosis. Res Vet Sci 2003;74(1):17-22.

[16] Olsen SC, Jensen AE, Palmer MV, Stevens MG. Evaluation of serologic responses, lymphocyte proliferative responses, and clearance from lymphatic organs after vaccination of bison with *Brucella abortus* strain RB51. Am J Vet Res 1998;59(4):410-15.

[17] Capsel RL, Olsen SC, Cheville NF, Thoen CO, Survival of *Brucella abortus* strain RB51 lyophilized and as a liquid under different storage conditions. Biologicals 2000;28(4):209-15.
[18] Olsen SC, Rhyan JC, Gidlewski T, Stoffregen WC. Immunologic responses of bison to vaccination with fresh or lyophilized *Brucella abortus* strain RB51. J Wildl Dis (Submitted).
[19] Januszewski MC, Olsen SC, McLean RG, Clark L, Rhyan JC. Experimental infection of nontarget species of rodents and birds with *Brucella abortus* RB51 vaccine. J Wildl Dis 2001;37(3):532-37.
[20] Elzer PH, Smith J, Roffe T, Kreeger T, Edwards J, Davis D. Evaluation of *Brucella abortus* strain RB51 and strain 19 in pronghorn antelope. Ann NY Acad Sci 2002;969:102-5.
[21] Bradley MP, Eade J, Penhale J, Bird P. Vaccines for fertility regulation of wild and domestic species. J Biotechnol 1999;73(2-3):91-101.
[22] Elzer PH, Colby FM, Hagius SD, Walker JV, Fatemi M. Protection against infection and abortion induced by virulent challenge exposure after oral vaccination of cattle with *Brucella abortus* strain RB51. Am J Vet Res 1998;59(12):1575-78.
[23] Corner LAL, Buddle BM, Pfeiffer DU, Morris RS. Vaccination of the brushtail possum (*Trichosurus vulpecula*) against Mycobacterium bovis infection with Bacilli Calmette-Guerin: the response to multiple doses. Vet Microbiol 2002;84(4):327-36.
[24] Denicola AJ, Kesler DJ, Swihart RK. Ballistics of a biobullet delivery system. Wildl Soc Bull 1996;24:301-5.
[25] Jacobsen NK, Jessup DA, Kesler DJ. Contraception of captive black-tailed deer by remotely delivered norgestomet ballistic implants. Wildl Soc Bull 1995;23:718-22.
[26] Kesler DJ, Favero RJ. Estrous synchronization and fertility enhancement in cattle with ballistically administered pharmaceutical agents. Proceedings of the 16th International Symposium on the Controlled Release of Bioactive Materials; 1989 Aug 6-11; Chicago, USA. Controlled Release Society; 1989.
[27] DeNicola AJ, Kesler DJ, Swihart RK. Dose determination and efficacy of remotely delivered norgestomet implants on contraception of white-tailed deer. Zoo Biol 1997;16 :31-37.
[28] DeNicola AJ, Swihart RK, Kesler DJ. The effect of remotely delivered gonadotropin formulations on reproductive function of white-tailed deer. Drug Development and Industrial Pharmacy 1996;22(8):847-850.
[29] Kirkpatrick JF, Turner JW, Liu IK, Fayrer-Hosken R Application of pig zona pellucida immunocontraception to wildlife fertility control. J Reprod Fert Supp 1996;50:183-189.
[30] Turner JW, Liu IK, Kirkpatrick JF. Remotely delivered immunocontraception in free-roaming feral burros (*Equus asinus*). J Reprod Fert 1996;107(1):31-35.
[31] Shideler SE, Stoops MA, Gee NA, Howell JA, Lasley BL. Use of porcine zona pelucida (PZP) vaccine as a contraceptive agent in free-ranging tule elk (*Cervus elaphus nannodes*). Reprod Supp 2002;60:169-176.
[32] Van de Widjen GP. Development and assessment of mini projectiles as drug carriers. J Control Release 2002;85(1-3):145-162.

[33] Drew ML, Waldrup K, Kreeger TJ, Craigmill AL, Wetzlich SE, Mackintosh C. Pharmacokinetics of ceftiofur in red deer (*Cervus elaphus*). J Vet Pharmacol Ther 2004; 27:7-11.
[34] Olsen SC, Kreeger TJ, Schultz W. Immune responses of bison to ballistic or hand vaccination with *Brucella abortus* strain RB51. J. Wildl. Dis. 2002;38(4):738-745.
[35] Hansen R. Medicament Dosing Ballistic Implant of improved accuracy, U.S. Patent 6,375,971, 2002 Apr 23.
[36] Working PK, Newman MS, Johnson J, Cornacoff JB. Safety of poly(ethylene glycol) derivatives. In: Harris JM, S. Zalipsky S, editors. Poly(ethylene glycol) Chemistry and Biological Applications. ACS Symposium Series, vol. 680. Washington DC: American Chemical Society; 1997. p. 45-57.
[37] Poshusta AK, Anseth KS. Photopolymerized biomaterials for application in the temporomandibular joint. Cells Tissues Organs 2001;169(3):272-78.
[38] Lyman M, Melanson D, Sawhney A. Characterization of the formation interfacially photopolymerized thin hydrogels in contact with arterial tissue. Biomaterials 1996;17:359-64.
[39] Bryant SJ, Anseth KS, The effects of scaffold thickness on tissue engineered cartilage in photocrosslinked poly(ethylene oxide) hydrogels. Biomaterials 2001;22(6):619-26.
[40] Sawhney AS, Pathak CP, Hubbell JA. Bioerodible hydrogels based on photopolymerized poly(ethylene glycol)-co-poly(α-hydroxy acid) diacrylate macromers. Macromolecules 1993;26(4):581-87.
[41] Lu S, Anseth KS. Release behavior of high molecular weight solutes from poly(ethylene glycol)-based degradable networks. Macromolecules 2000;33:2509-15.
[42] Sawhney AS, Handrashekhar CP, van Rensburg JJ, Randall DC, Hubbell JA. Optimization of photopolymerized bioerodible hydrogel properties for adhesion prevention. J Biomed Mat Res 1994;28(7):831-38.
[43] Hubbell J, Hill-West JL, Pathak CP, Sawhney AS. In: Roseman TJ, N.A. Peppas NA, Gabelnick HL, editors. PEG-based gels for the release of proteins and the encapsulation of cells. Proceedings of the 20th International Symposium on the Controlled Release of Bioactive Materials; 1993 Jul 25-28; Washington DC, USA. Deerfield: Controlled Release Society; 1993.
[44] Cruise GM, Hegre OD, Lamberti FV, Hager SR, Hill R, Scharp DS, Hubbell JA. In vitro and in vivo performance of porcine islets encapsulated in interfacially photopolymerized poly(ethylene glycol) diacrylate membranes. Cell Transplantation 1999;8(3):293-306.
[45] Nguyen KT, West JL. Photopolymerizable hydrogels for tissue engineering applications. Biomaterials 2002;23(22):4307-14.
[46] Koh WG, Revzin A, Pishko MK. Poly(ethylene glycol) hydrogel microstructures encapsulating living cells. Langmuir 2002;18:2459-62.
[47] Bryant SJ, Anseth KS. Hydrogel properties influence ECM production by chondrocytes photoencapsulated in poly(ethylene glycol) hydrogels. J Biomed Mater Res 2002;59(1): 63-72.

[48] Rice MA, Anseth KS, Encapsulating chondrocytes in copolymer gels: Bimodal degradation kinetics influence cell phenotype and extracellular matrix development. J Biomed Mater Res 2004;70A(4):560-68.
[49] Du YJ, Lemstra PJ, Nijenhuis AJ, van Aert HAM, Bastiaansent C. ABA type copolymers of lactide with poly(ethylene glycol). Kinetic, mechanistic, and model studies. Macromolecules 1995;28:2124-32.
[50] Chung YM, Simmons KL, Gutowska A, Jeong B. Sol-gel transition temperature of PLGA-g-PEG aqueous solutions. Biomacromolecules 2002;3:511-16.
[51] Li S, Vert M. Synthesis, characterization, and stereocomplex-induced gelation of block copolymers prepared by ring-opening polymerization of l(d)-lactide in the presence of poly(ethylene glycol). Macromolecules 2003;36:8008-14.
[52] Chan-Park MB, Zhu AP, Shen JY, Fan AL. Novel photopolymerizable biodegradable triblock polymers for tissue engineering scaffolds: Synthesis and characterization. Macromol Biosci 2004;4:665-73.
[53] Farnia SMF, Mohammadi-Rovshandeh J, Sarbolouki MN. Synthesis and characterization of novel biodegradable triblock copolymers from L-lactide, glycolide, and PPG. J Appl Polym Sci 1999;73:633-37.
[54] Mohammadi-Rovshandeh J, Farnia SMF, Sarbolouki MN. Synthesis and characterization of novel ABA triblock copolymers from l-lactide, glycolide, and PEG. J Appl Polym Sci 1999;74:2004-9.
[55] Bryant SJ, Nuttelman CR, Anseth KS. Cytocompatibility of UV and visible light photoinitiating systems on cultured NIH/3T3 fibroblasts in vitro. J Biomat Sci Polym Ed 2000;11(5):439-57.
[56] Canal T, Peppas NA. Correlation between mesh size and equilibrium degree of swelling of polymer networks. J Biomed Mater Res 1989;23:1183-93.
[57] Capsel, RL, Olsen, SC, Cheville, NF, Thoen, CO. Survival of *Brucella abortus* strain RB51 lyophilized as a liquid vaccine under different storage conditions. Biologicals 2000;28:209-215.

CHAPTER II

IMMUNOLOGIC RESPONSES OF BISON TO VACCINATION WITH BRUCELLA ABORTUS STRAIN RB51: COMPARISON OF PARENTERAL TO BALLISTIC DELIVERY VIA COMPRESSED PELLETS OR PHOTOPOLYMERIZED HYDROGELS

Steven C. Olsen, R.J. Christie, D.W. Grainger, and W.S. Stoffregen

Reprinted with permission from: S. C. Olsen, R.J. Christie, D.W. Grainger, and W.S. Stoffregen, *Vaccine* 2006, 24, 1346-1353.

This dissertation contains the manuscript of a full paper published in Vaccine. The manuscript was written by Steven Olsen with contributions from R.J. Christie, D.W. Grainger, and W.S. Stoffregen. This chapter shows that hydrogel encapsulated SRB51 vaccine when ballistically administered to bison generates an immune response greater than traditional compression loaded formulations and comparable to hand vaccination. Serological studies were performed by Steven Olsen and William Stoffregen at the National Animal Disease Center, United States Department of Agriculture, Ames, Iowa 50010, USA.

Immunologic Response of Bison to Vaccination with Brucella Abortus Strain RB51: Comparison of Parenteral to Ballistic Delivery via Compressed Pellets or Photopolymerized Hydrogels

Steven C. Olsen, R.J. Christie, D.W. Grainger, and W.S. Stoffregen

Abstract

This study compared responses of bison calves to 1010 CFU *Brucella abortus* strain RB51 (SRB51) delivered by parenteral or ballistic methods. Two types of biobullet payloads were evaluated; compacted SRB51 pellets or SRB51 encapsulated in photopolymerized poly(ethylene glycol) hydrogels. Bison were vaccinated with saline, parenteral SRB51 alone, or in combination with Spirovac^{TM}, or ballistically with compressed SRB51 or hydrogel biobullets. Bison parenterally vaccinated with SRB51 had greater ($P < 0.05$) immunologic responses when compared to control bison. Co-administration of Spirovac^{TM} as an adjuvant did not influence immunologic responses. As compared to compressed SRB51 biobullets, ballistic vaccination with hydrogel biobullets increased cellular immune responses at some sampling times. Our data suggest that hydrogel formulations of SRB51 may be a superior alternative to compressed SRB51 tablets for ballistic vaccination of bison. Although preliminary, data suggest that immunologic response of bison to SRB51 hydrogel bullets are similar to response after parenteral vaccination with SRB51.

Introduction

The Brucellosis Eradication Program in the United States is close to its goal of elimination of *Brucella abortus* infections in cattle. The investment in this program has been extensive, with approximately 11 billion dollars spent over the last 70 years and continued spending of approximately $30 million dollars per year for surveillance. The persistence of wildlife reservoirs of *Brucella abortus* in the United States and the potential for transmission of brucellosis from wildlife to livestock remains a concern for regulatory personnel and producers. Within the last several years, a number of *Brucella*-infected cattle herds have been identified in Wyoming and Idaho [1,2] in which the source of infection was presumed to be free-ranging elk (*Cervus elaphus nelsoni*). The free-ranging bison (*Bison bison*) within Yellowstone National Park have a high seroprevalence for brucellosis [3,4] and management of brucellosis in this reservoir has high public visibility. The current Interagency Bison Management plan for the Greater Yellowstone area requires the development of a safe and effective remotely delivered vaccine for full implementation [5].

Strong cellular immune responses with associated high levels of γ-interferon (γ-IFN) are believed to be important for long-term protection against intracellular pathogens such as *Brucella* [6]. We have previously demonstrated that parenteral vaccination of bison with 10^{10} colony-forming units (CFU) of *Brucella abortus* strain RB51 (SRB51) is safe and induces antigen-specific proliferative responses and γ-IFN production [7,8]. When evaluated using standard methodology, parenteral vaccination with SRB51 protects bison against abortion and fetal or mammary infection after experimental challenge [9]. However, when evaluating a remote delivery system, bison parenterally vaccinated with

SRB51 had greater immunologic responses when compared to bison ballistically vaccinated with a bullet containing a compressed solid powdered SRB51 pellet [10].

In the study reported here, we evaluate the use of a recently described photopolymerized poly(ethylene glycol)-based hydrogels as a payload vehicle for more effective delivery of SRB51 in ballistic bullets [11]. As antigen-specific nitric oxide production has been demonstrated to differ between cattle vaccinated with *Mycobacterium bovis* bacillus Calmette-Guérin (BCG) and nonvaccinated cattle [12], we evaluated this assay for differentiation of SRB51-vaccinated and nonvaccinated bison. Also a commercially available vaccine that induces strong cellular immune responses in cattle was co-administered with SRB51 to determine if it would boost protective immune responses to brucellosis vaccination.

Materials and methods

Brucella abortus culture

A master seed stock of SRB51 was obtained from G. Schurig (Virginia Tech, Blacksburg, Virginia, USA), and after one passage on tryptose agar (Difco Laboratories, Detroit, Michigan, USA), was designated as the ARS/1 seed stock of SRB51. For experimental use, SRB51 bacteria from the ARS/1 seed stock were grown on tryptose agar for 48 hr at 37 °C. For the dot-blot assay, SRB51 suspensions ($1.3x10^{12}$ CFU/ml) were inactivated by γ-irradiation ($1.4x10^{6}$ rads). Following irradiation, suspensions were washed in 0.15M sodium chloride (saline) and stored in 1 ml aliquots at -70 °C.

Hand Vaccine

For hand vaccination of bison, a commercially prepared SRB51 product (Colorado Serum Company, Denver, Colorado, USA) derived from the ARS/1 seed stock was utilized. The lyophilized vaccine was diluted in saline to approximately 10^{10} CFU based upon standard plate counts on other vials with the same lot number. In an effort to booster cell-mediated immune responses to hand vaccination with SRB51, one group of bison received co-administrations of a commercial vaccine (Spirovac^{TM}, Pfizer Animal Health, Exton, PA, USA) that induces strong cellular immune responses in cattle against *Leptospira borgpetersenii* serovar hardjo type hardjo-bovis [13].

Compressed Ballistic Bullets

For ballistic vaccination of bison, the lyophilized commercial strain RB51 product was pelleted via compression (Eureka tablet machine, Stokes Pennwalt, Warminster, PA), and incorporated into a 0.25 caliber, hydroxypropyl cellulose Biobullet^{R} payload compartment (Solidtech Animal Health, Newcastle, OK, USA).

Hydrogel SRB51 Ballistic bullets

Poly(ethylene glycol) macromers (MW ~ 7000 g/mol) containing photopolymerizable methacrylate endgroups, and PEG macromers containing co-polymerized degradable lactide or glycolide segments (5 mol lactide or glycolide/mol PEG) terminated with methacrylate groups were prepared using a previously published procedure [14]. PEG macromer solutions were dissolved in PBS (pH 7.4) to form a 35% w/w solution. Irgacure 184^{TM} (Ciba Specialty Chemicals, Tarrytown, NY, USA)

saturated in ethanol (6 µl) was added to this solution to serve as a photoinitiator. Lyophilized SRB51 (Colorado Serum Company, Denver, CO, USA) was then suspended in PEG macromer solutions at a concentration of ~ $1x10^{11}$ CFU/mL, using the SRB51 viability provided by the manufacturer. PEG macromer solution containing suspended SRB51 (90 µL) was transferred to hydroxypropyl cellulose biobullet payload compartments (SolidTech Animal Health, Oklahoma City, OK, USA), then photopolymerized using a low pressure Hg lamp (Hanovia, 20 mW/cm^2, 90 s). Post-photopolymerization viability was determined after homogenization of gels followed by serial dilution and plating on tryptose agar containing 5% heat inactivated bovine serum.

Animals and inoculation

Thirty-two, 7-9-mo-old bison heifers (*Bison bison*) were obtained from brucellosis-free herds. After acclimation for 4 wk, bison were randomly assigned to treatments: control (n=5), hand SRB51 vaccination (n=6), hand SRB51 combined with Spirovac™ (n=6), compressed SRB51 bullet (n=6), and SRB51 hydrogel bullets (PEG, PEG L5, PEG G5; n=3/trt). Bison in the hand SRB51 treatment were inoculated subcutaneously (SQ) in the left cervical region with a 2 ml volume of the SRB51 reconstituted suspension. Bison in the hand SRB51 + Spirovac™ treatment were inoculated with SRB51 in a similar manner and received a co-administration of Spirovac™ (2 ml, SQ) in the left cervical region. Bison in this treatment received an additional Spirovac™ vaccination at 6 weeks after initial vaccination. Bison in the compressed or hydrogel bullet treatments were ballistically inoculated into the left hip region using an air-powered rifle system (SolidTech Animal Health, Newcastle, OK,

USA). The concentration of inoculum in the hand SRB51, compressed bullet, and hydrogel bullet treatments were determined by standard plate counts.

Serologic evaluation

Blood samples were collected by jugular venipuncture prior to vaccination, and at 4, 8, 12, 16, 20, and 24 wk post-inoculation. Blood was allowed to clot for 12 hr at 4 °C and centrifuged. Serum was divided into 1 ml aliquots, frozen, and stored at -70 °C.

Antibody titers to *Brucella* were determined by a previously described antibody dot-blot assay in which γ-irradiated SRB51 is used as antigen [15].

Lymphocyte proliferation assays

At 4, 8, 12, 16, 20, and 24 wk after vaccination, blood was obtained from the jugular vein of all bison and placed into an acid-citrate dextrose solution. Peripheral blood mononuclear cells (PBMC) were enriched by density centrifugation using a Ficoll-sodium diatrizoate gradient (Sigma Diagnostics, Inc., St. Louis, Missouri, USA). Peripheral blood mononuclear cells were diluted in RPMI 1640 medium to 1×10^7 viable cells per ml as determined by trypan blue dye exclusion.

Fifty μl of each cell suspension, containing 5×10^5 cells, was added to each of two separate flat-bottom wells of 96-well microtiter plates that contained 100 μl of RPMI 1640 medium only, or 1640 medium containing γ-irradiated SRB51 (10^5 to 10^9 bacteria per well). Microtiter plates were prepared prior to initiation of the study and maintained at -70 °C until use. Cell cultures were incubated for 7 days at 37 C in 5% CO_2. After 7 days incubation, cell cultures were pulsed with 1.0 μCi of [^{3}H]thymidine per well for 18

hr. Cells were harvested onto glass filter mats and counted for radioactivity in a liquid scintillation counter.

γ-IFN Production

In conjunction with proliferation assays, 50 μl of cell suspensions (5 x 10^5 cells) from each bison at each sampling time were added to separate flat-bottom wells of 96-well microtiter plates that contained 150 μl of RPMI 1640 medium only, or RPMI 1640 medium containing γ-irradiated SRB51 (10^8 or 10^6 bacteria per well). At 72 hr after initiation of culture, 100 ul of supernatant was removed from wells containing 10^8 or 10^6 SRB51 or RPMI alone. Data from previous studies demonstrated that bison PBMC produce more γ-IFN at 72 hr incubation, as compared to 24 or 48 hr incubations. Supernatants were frozen at -70 °C until assayed for γ-IFN using a commercial kit (Bovigam, CSL Limited, Victoria, Australia) in accordance with manufacturer's instructions. Standard dilutions of a purified bovine γ-IFN of known quantity (108 to 0.211 ng/ml) were included on each microtiter plate. Optical density measurements at 450 nm were made using an ELISA plate reader (Molecular Devices, Sunnyvale, CA, USA). Samples with optical densities outside the standard curve were diluted and assayed again. Linear regression analysis was conducted on standards and used to calculate γ-IFN concentrations within individual samples.

Nitric oxide (NO) Production

In conjunction with proliferation and γ-IFN assays, 50 μl of cell suspensions (5 x 10^5 cells) from each bison at each sampling time were added to each of three separate flat-bottom wells of 96-well microtiter plates that contained 150 μl of RPMI 1640 medium only, or RPMI 1640 medium containing γ-irradiated SRB51 (10^8 bacteria per well). At 24, 48 and 72 hr after initiation of culture, 100 μl of supernatant was removed from wells containing SRB51 and RPMI alone and placed in separate wells in a microtiter plate. Concentrations of nitrite, the stable oxidation product of nitric oxide, were assayed as described previously [12,16]. Standard dilutions of $NaNO_2$ (2500 to 39 ng/ml) were included on each plate. After addition of 100 ul of Griess Reageant (Sigma, St. Louis, MO) to each well, the microtiter plate was allowed to incubate for 15 min at room temperature. Following centrifugation (5 min at 400 x g) to remove any bubbles in wells, optical densities for each well were determined at 562 nm on a ELISA plate reader. Linear regression analysis was conducted on standards and used to calculate NO concentrations within individual samples.

Statistical analysis

For γ-IFN production, data were analyzed as the difference in γ-IFN concentration between paired wells with or without SRB51 antigen. In a similar manner, NO data were analyzed as both NO in wells with or without SRB51 antigen, and as net NO (NO in wells with SRB51 minus NO in paired wells without antigen). Serologic, proliferation, NO, and γ-IFN data were analyzed as logarithms of their values. Serologic data were compared over all times using a general linear model procedure (SAS Institute Inc. Cary,

North Carolina, USA), whereas proliferation, NO, and γ-IFN production to response to γ-irradiated SRB51 bacteria were analyzed by sampling time. Means for individual treatments were separated by use of a least significant difference procedure ($P<0.05$).

Data were initially analyzed across all treatments with all three hydrogel formulations (PEG, PEG-co-lactide, PEG-co-glycolide) combined as one general hydrogel treatment. A second analysis was conducted in which individual hydrogel formulations were compared to responses of nonvaccinated bison.

Results

Vaccine dosages

Standard plate counts indicated that average dosages in hand SRB51, dry compressed SRB51 biobullet, and hydrogel SRB51 biobullet treatments were 3.2×10^{10}, 6×10^{9}, and 1.5×10^{11} CFU of SRB51, respectively.

Serologic evaluation

Mean antibody titers to SRB51 did not differ ($P>0.05$) between treatments prior to vaccination (Figure 2.2.1). Bison hand vaccinated with SRB51 alone, or combined with the Spirovac™ vaccine, had greater mean titers ($P<0.05$) than control bison at 4, 8 and 12 weeks after vaccination. Mean titers of bison ballistically vaccinated with with biobullets containing SRB51 as a compressed pellet, or incorporated into hydrogels were greater ($P<0.05$) than control bison only at 4 weeks after vaccination. In a similar manner, mean titers of bison vaccinated with hydrogel SRB51 bullets only differed from control bison

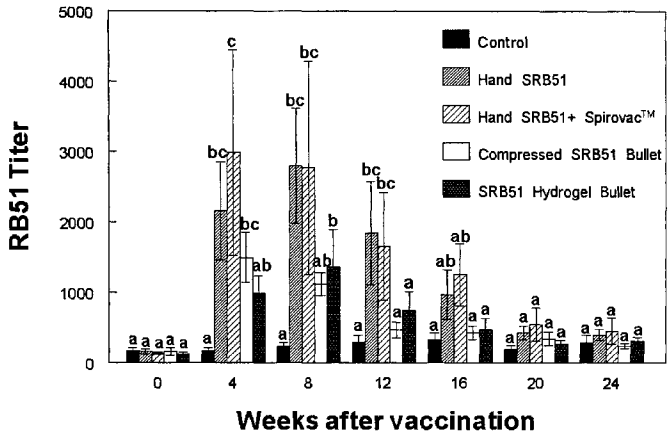

Figure 2.2.1. Serologic responses of control or SRB51-vaccinated bison to γ-irradiated SRB51 in a dot blot assay. Bison were ballistically vaccinated with SRB51 in a hydrogel (10^{11} CFU; n=9) or as a compressed pellet (6 x 10^{9} CFU; n=6), or parenterally vaccinated with 10^{10} CFU of SRB51 alone, or in combination with Spirovac™ (n=6/trt). Control bison received SQ inoculation with saline (n=5). Bison in the SRB51 + Spriovac™ treatment were booster vaccinated with Spirovac™ at 6 weeks after initial inoculation. Responses are presented as mean antibody titer ± SEM. Means with different superscripts are statistically different ($P<0.05$).

at 8 weeks after vaccination. By 16 weeks after vaccination, mean titers of all parenteral and ballistic vaccination treatments did not differ ($P>0.05$) from the control treatment. With the exception of both ballistic treatments at 12 weeks, and the ballistic hydrogel treatment at 4 weeks, mean titer of parenteral vaccination treatments did not did not differ ($P>0.05$) from ballistic vaccination treatments throughout the study.

Mean titers of bison vaccinated with the PEG hydrogel payload bullet formulations were greater than control bison at 4, 8, and 12 weeks after vaccination (Figure 2.2.2). Bison vaccinated with the PEG co-glycolide hydrogel had greater mean

titers than control bison at 4 and 8 weeks after vaccination. Whereas mean titers of bison the PEG-co-lactide hydrogel treatment were greater than the control treatment only at 4

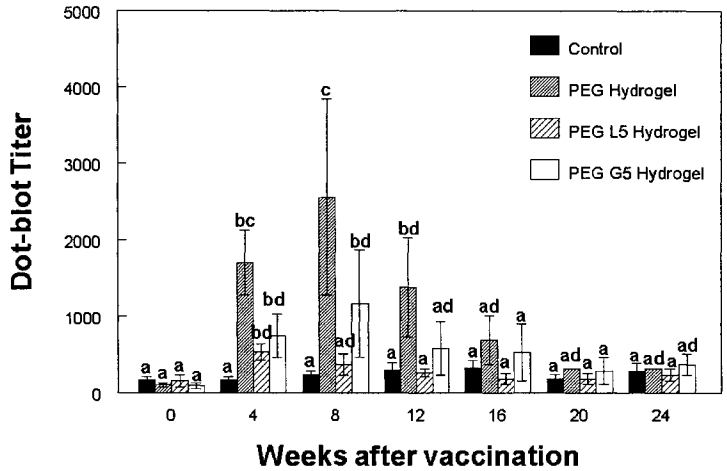

Figure 2.2.2. Serologic responses of control or bison ballistically vaccinated with SRB51 hydrogel bullets to γ-irradiated SRB51 in a dot blot assay. Bison were SQ inoculated with saline (control; n=5) or were ballistically vaccinated with 10^{11} CFU of SRB51 in three types of hydrogels (PEG; PEG-co-lactide (PEG L5); or PEG-co-glycolide (PEG G5); n=3/trt). Responses are presented as mean antibody titer ± SEM. Means with different superscripts are statistically different ($P<0.05$).

weeks after vaccination. Although only greater ($P<0.05$) at 8 weeks after vaccination, there was a tendency for the PEG treatment to induce greater mean titers when compared to the other hydrogel treatments.

Lymphocyte proliferation assays

Proliferative responses to SRB51 of PBMC from bison in all vaccination treatments did not differ ($P>0.05$) from responses of control bison at 4 weeks after vaccination (representative data in Figure 2.2.3). Peripheral blood mononuclear cells

obtained from bison hand vaccinated with SRB51 alone produced greater (P<0.05) proliferative responses to killed SRB51 at 8, 12, and 20 weeks after vaccination when compared to responses of PBMC from control bison. When Spirovac™ was combined

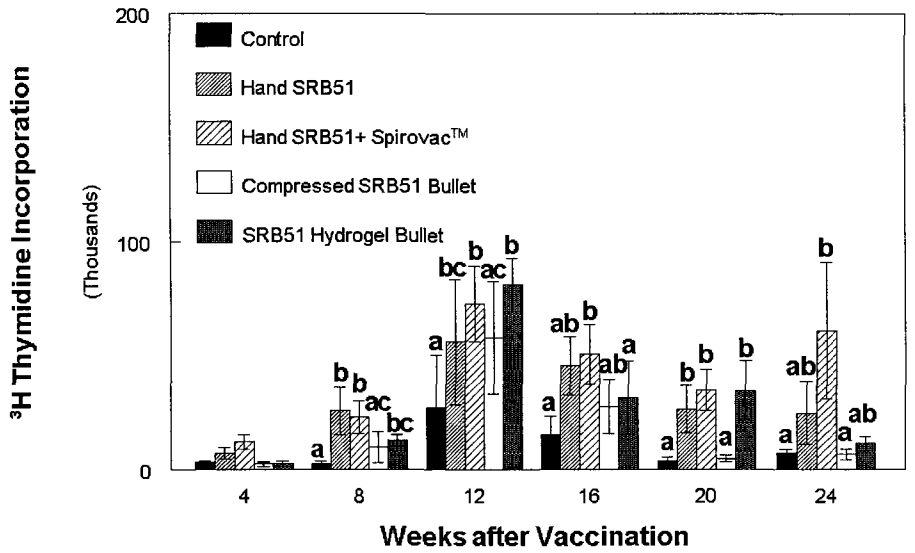

Figure 2.2.3. Proliferative responses of peripheral blood mononuclear cells from control or SRB51-vaccinated bison to 10^8 CFU of γ-irradiated SRB51. Bison were ballistically vaccinated with SRB51 in a hydrogel (10^{11} CFU; n=9) or as a compressed pellet (6 x 10^9 CFU; n=6), or parenterally vaccinated with 10^{10} CFU of SRB51 alone, or in combination with Spirovac™ (n=6/trt). Control bison received SQ inoculation with saline (n=5). Bison in the SRB51 + Spriovac™ treatment were booster vaccinated with Spirovac™ at 6 weeks after initial inoculation. Cells were incubated at 37 C in 5% CO_2 for 7 days and pulsed for 18 hrs with [^{3}H]thymidine. Results are expressed as mean stimulation indexes. Means within a sampling time with different superscripts are statistically different (P<0.05).

with SRB51 vaccination, proliferative responses by PBMC to SRB51 antigens were greater at 8, 12, 16, 20, and 24 weeks after vaccination. SRB51-specific proliferative responses of PBMC from bison parenterally vaccinated with SRB51 alone, or in combination with Spirovac™, did not differ (P<0.05) at any sampling time. When

compared to responses of nonvaccinates, proliferative responses of PBMC from bison ballistically inoculated with a compressed lyophilized SRB51 bullet did not differ at any sampling time. However, PBMC from bison ballistically inoculated with SRB51 PEG hydrogels exhibited greater ($P<0.05$) proliferative responses to killed SRB51 at 8, 12, and 20 weeks after vaccination. When both ballistic treatments were compared, PBMC from bison inoculated with SRB51 PEG hydrogel bullets had greater ($P<0.05$) SRB51-specific proliferative responses to at 12 and 20 weeks after vaccination when compared to proliferative responses of bison inoculated with compressed lyophilized SRB51 bullets.

Proliferative responses to killed SRB51 by PBMC from bison in the three SRB51 PEG hydrogel treatments did not differ ($P>0.05$) at any sampling time (representative data in Figure 2.2.4).

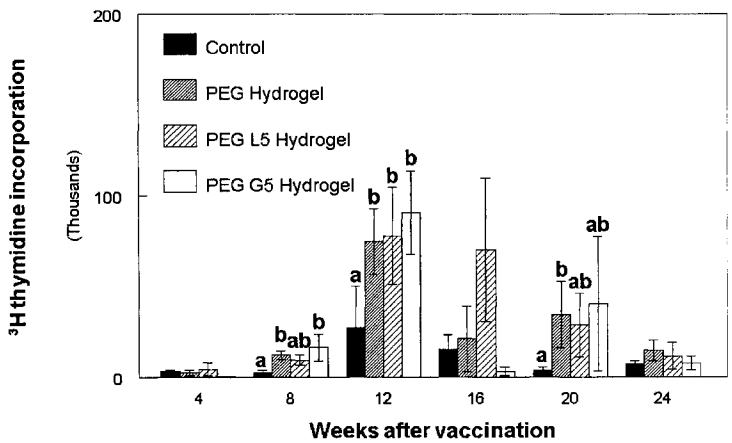

Figure 2.2.4. Proliferative responses to 10^8 CFU of γ-irradiated SRB51 by peripheral blood mononuclear cells from bison inoculated with saline (control; n=5) or ballistically vaccinated with hydrogel bullets. Ballistically vaccinated bison received 10^{11} CFU of SRB51 in three types of hydrogels (PEG; PEG-co-lactide (PEG L5); or PEG-co-glycolide (PEG G5); n=3/trt) Cells were incubated at 37 C in 5% CO_2 for 7 days and pulsed for 18 hrs with [^{3}H]thymidine. Results are expressed as mean stimulation indexes. Means within a sampling time with different superscripts are statistically different ($P<0.05$).

However, proliferative responses of bison vaccinated with PEG hydrogel treatments did differ from responses of nonvaccinated bison at various sampling times. In bison ballistically inoculated with bullets containing SRB51 in PEG hydrogel payloads, PBMC had greater SRB51-specific proliferative responses at 8, 12, and 20 weeks after vaccination when compared to responses of nonvaccinated bison. In a similar manner, PBMC from bison ballistically vaccinated with SRB51 in PEG-co-glycolide hydrogels prompted greater proliferative responses at 8 and 12 weeks after vaccination as compared to responses of nonvaccinates. Proliferative responses of bison receiving bullets containing SRB51 in PEG-co-lactide hydrogels were greater than responses of control bison only at 12 weeks after vaccination.

Interferon Production

Production of γ-IFN in response to killed SRB51 did not differ ($P>0.05$) between treatments at 4 weeks after vaccination (Figure 2.2.5). Bison hand vaccinated with SRB51 alone exhibited greater ($P<0.05$) mean γ-IFN responses to SRB51 at 8, 12, and 20 weeks after vaccination when compared to nonvaccinated bison. In bison vaccinated with both SRB51 and Spirovac™, mean γ-IFN production to SRB51 was greater ($P<0.05$) than nonvaccinated bison at 12 and 20 weeks after vaccination. In bison vaccinated with PEG hydrogel SRB51 bullets, mean γ-IFN production to SRB51 was greater ($P<0.05$) than nonvaccinated bison at 8, 12, and 20 weeks after vaccination. Bison ballistically inoculated with compressed lyophilized SRB51 did not differ ($P>0.05$) from controls at any sampling time in mean γ-IFN production. In 4 of 5 sampling times

between 8 and 24 weeks after vaccination, bison vaccinated with PEG hydrogel SRB51 bullets had greater

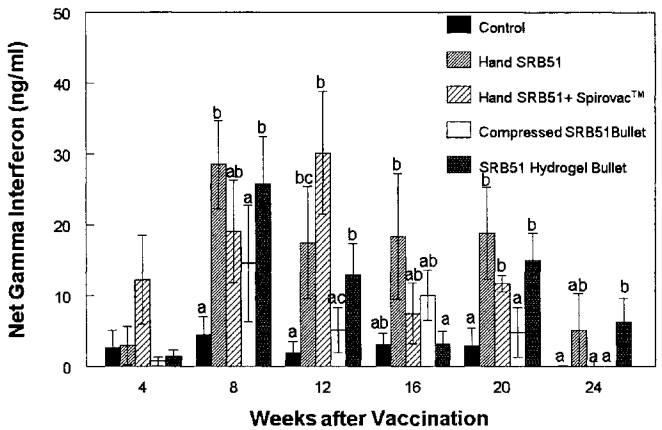

Figure 2.2.5. Production of γ-IFN from peripheral blood mononuclear cells of control or SRB51-vaccinated Bison were ballistically vaccinated with SRB51 in a hydrogel (10^{11} CFU; n=9) or as a compressed pellet (6 x 10^9 CFU; n=6), or parenterally vaccinated with 10^{10} CFU of SRB51 alone, or in combination with Spirovac™ (n=6/trt). Control bison received SQ inoculation with saline (n=5). Bison in the SRB51 + Spriovac™ treatment were booster vaccinated with Spirovac™ at 6 weeks after initial inoculation. Cells were incubated at 37 C in 5% CO_2 for 72 in the absence of antigen, or with 10^8 CFU/well of γ-irradiated SRB51. Data is presented as mean net γ-IFN (wells with SRB51 - wells without antigen) ± SEM.. Means within a sampling time with different superscripts are statistically different (P<0.05).

(P<0.05) mean γ-IFN production to SRB51 when compared to bison vaccinated with compressed lyophilized SRB51 bullets.

When responses of bison vaccinated with individual PEG hydrogel formulations were compared to responses of nonvaccinated bison, the PEG hydrogels produced greater (P<0.05) mean γ-IFN production to SRB51 at 8, 12, and 20 weeks after vaccination (Figure 2.2.6). In comparison, bison ballistically vaccinated with PEG-co-lactide hydrogels produced greater (P<0.05) mean γ-IFN production at 20 and 24 weeks after vaccination when compared to responses of nonvaccinated bison. Bison vaccinated with

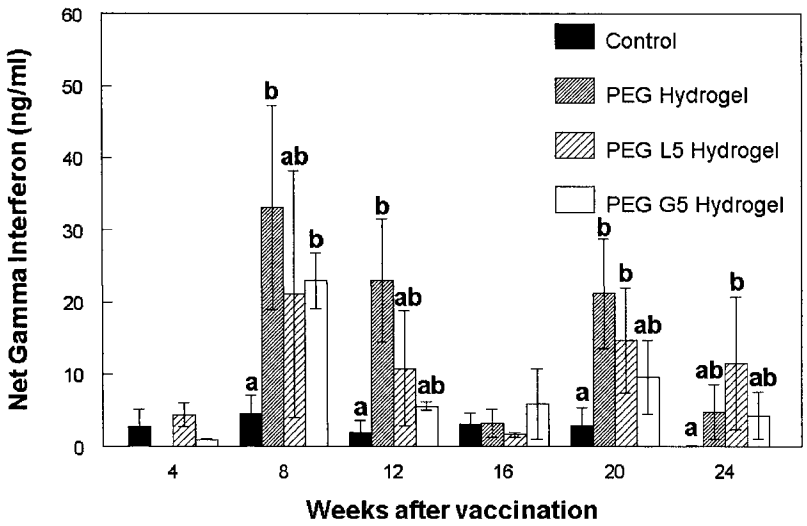

Figure 2.2.6. Production of γ-IFN by peripheral blood mononuclear cells from bison inoculated with saline (control; n=5) or ballistically vaccinated with hydrogel bullets. Ballistically vaccinated bison received 10^{11} CFU of SRB51 in three types of hydrogels (PEG; PEG-co-lactide (PEG L5); or PEG-co-glycolide (PEG G5); n=3/trt) control or SRB51-vaccinated. Cells were incubated at 37 C in 5% CO_2 for 72 in the absence of antigen, or with 10^8 CFU/well of γ-irradiated SRB51. Data is presented as mean net γ-IFN (wells with SRB51 - wells without antigen) ± SEM.. Means within a sampling time with different superscripts are statistically different ($P<0.05$).
the PEG-co-glycolide hydrogels had greater ($P<0.05$) mean γ-IFN production to SRB51 only at 8 weeks after vaccination. Although not statistically different at any sampling time ($P>0.05$), bison vaccinated with the PEG hydrogels tended to promote the greatest mean γ-IFN production when compared to PEG-co-lactide and PEG-co-glycolide hydrogel formulations.

Nitric Oxide Production

Across all times, incubations, and treatments, PBMC incubation with SRB51 antigen induced greater NO than paired wells containing cells incubated in the absence of antigen (data not shown). However, mean NO concentration in wells containing SRB51 antigen did not differ between treatments across various sampling times or incubations. In a similar manner, mean net nitric oxide production by PBMC to γ-irradiated SRB51

did not differ ($P>0.05$) between treatments for all incubations at all sampling times (data not shown). Hydrogel formulations evaluated in the current study did not influence NO production by PBMC to SRB51 antigens at any sampling time.

Discussion

Previous studies have demonstrated that ballistic vaccination of bison with a bullet containing a compressed lyophilized SRB51 pellet reduces immunologic responses when compared to parenteral delivery [10]. Results of the current study suggest that encapsulation of SRB51 in photopolymerized PEG hydrogels for delivery via ballistic payloads may enhance immunologic responses of bison when compared to responses of bison vaccinated with a bullet containing a compressed lyophilized SRB51 pellet. This could be due to high post-processing viability of the photopolymerized hydrogel formulations, which is typically greater than 90% (data not shown). If increases in antigen-specific γ-IFN production correlate to increased protection against *Brucella*, our data suggest that vaccination of bison with SRB51 hydrogel bullets may produce greater efficacy than currently used bullets containing compressed lyophilized vaccine pellets. However, unpublished data from our laboratory suggests that even though *in vitro* assays demonstrated reduced immunologic responses in bison vaccinated with bullets containing a compressed SRB51 pellet, data from paired efficacy experiments suggest that protection against *Brucella* is only slightly reduced when compared to parenteral vaccination (Olsen, unpublished data). Therefore, efficacy studies will have to be conducted before definitive conclusions can be made in regards to protective

immunologic responses induced by ballistic vaccination of bison with SRB51 encapsulated within PEG hydrogel payloads.

The PEG hydrogel formulations are designed to degrade by hydrolysis and were shown to release particles at different rates when hydrated [11]. Previous work studying the release of 1 μm diameter fluorescent beads from hydrogels show that PEG-co-glycolide hydrogels release all beads over a period of nine days, PEG-co-lactide hydrogels release all beads over a period of 45 days, and PEG hydrogels with no degradable component release less than 1% of encapsulated particles over 45 days [11]. Although these experiments were performed in buffer, they should serve to approximate gel degradation and vaccine relese in vivo once in bison. Other factors that could influence the actual release rate in a biobullet formulation in vivo include dissolution of the hydroxpropyl cellulose biobullet casing, and possible gel mechanical agitation and break-up due to host muscle contractions.

Data indicate little correlation to immune responses based on specific PEG hydrogel formulations used. It is possible that the high concentration of SRB51 (~ 10^{11}/bullet) used within PEG hydrogels for these experiments alters the controlled release behavior observed for 1 μm fluorescent particles (~10^{8}/bullet) [11]. Figures 1,3, and 5 represent all hydrogel formulations combined as one data point (n=9). Non-degradable PEG biobullets exhibit comparable (or slightly higher) immune responses, suggesting factors other than hydrogel hydrolysis alone may contribute to release of SRB51 into the host. Biobullet placement in the host may produce effects on hydrogel degradation and release SRB51 in vivo not readily duplicated *in vitro*.

Hydrogel formulations offer several advantages for preparation of ballistic bullets as compared to the previously used compressed SRB51 dry tablet. When lyophilized SRB51 is compressed into a pellet, we have noted viability losses of approximately 80% (Olsen, unpublished data). Current data suggests that loss of viability during preparation of SRB51 hydrogels is far less (< 10%) when compared to preparation of compressed pellets. An additional benefit of hydrogels is that the process is less labor intensive and appears to be more readily scalable for production of larger numbers of bullets. One disadvantage of these PEG hydrogel-based biobullets is their tendency to soften the hydroxypropyl cellulose bullet casing over time, reducing the structural integrity and firing reliability of the biobullet. We are currently investigating use of lyophilized PEG hydrogels as vaccine carriers to for biobullets that can easily be prepared and stored for extended lengths of time.

We had expected a beneficial effect by co-administration of Spirovac^{TM} with parenteral SRB51. If Spirovac^{TM} induces cytokines associated with TH-1 immune responses [17], it was hypothesized that co-administration might also enhance protective TH-1 immune responses to SRB51. However, in general, our data suggest that co-administration of Spirovac^{TM} had no effect on *Brucella*-specific immunologic responses. One hypothesis may be that brucellosis vaccination provides maximal stimulation of cell-mediated immune responses in bison. Others have found that heat killed *B. abortus* induces strong TH1 responses in human monocytes and mice [18-20]. As we did not see a reduction in immune responses to SRB51 by co-administration of Spirovac^{TM}, the hypothesis of immune overload does not seem to be applicable. However, others have noted that combining foot and mouth disease and vesicular stomatitis live virus vaccines

[21], or rinderpest and contagious bovine pleuropneumonia vaccines to cattle [22] reduced immune responses to a least one vaccine when compared to responses in cattle receiving only one vaccine. In the study using rinderpest and contagious bovine pleuropneumonia vaccines [22], serologic responses of cattle receiving both vaccines simultaneously did not differ from responses of cattle receiving single vaccinations. However, protection against bovine pleuropneumonia was reduced after experimental challenge in cattle vaccinated simulataneously with both vaccines as compared to cattle vaccinated with only the bovine pleuropneumonia vaccine.

Our data also suggest that bison PBMC incubated with SRB51 induce greater NO production than paired wells incubated without antigen. This observation concurs with others who noted significant NO production when J774-A1 macrophage cells were infected with rough, but not smooth strains of *B. suis* or *B. melitensis* [23]. However, NO production in response to SRB51 appears to be an inate, rather than adaptive, immune response, as it did not differ between SRB51-vaccinated and control bison. Although NO production may have diagnostic implications in regards to *Mycobacterium bovis* infection or vaccination [12], our data suggest that this assay has no diagnostic value for detecting SRB51-vaccinated bison.

In summary, our data suggests that hydrogel formulations of SRB51 may be a superior alternative to compressed lyophilized SRB51 tablets for ballistic vaccination of bison. Although preliminary, data suggest that immunologic responses to SRB51 hydrogel bullets are similar to responses after parenteral vaccination with SRB51. At the present time, immunologic correlates of protective immunity against *Brucella* are not characterized in bison, and the limited data on induction of γ-IFN production by RB51

vaccination of bison has not been correlated to protection against experimental challenge with *B. abortus*. Therefore, additional studies evaluating efficacy will be required before the influence of SRB51 hydrogel biobullets on protective immunity against brucellosis can be definitely determined.

Acknowledgements

The authors thank D. Buffington, A. Duit, A. Jensen, D. Pringle, D. Robinson, L. Wright, D. Findley, and D. Weuve for their technical assistance.

Names are necessary to report factually on available data; however, the USDA neither guarantees nor warrants the standard of the product, and the use of the name by USDA implies no approval of the product to the exclusion of others that may also be suitable.

References

[1] Hillman B. Brucellosis in eastern Idaho. 2002. p. 189-92.

[2] Holland SD. Report of the Committee on Brucellosis. Proceedings of the United States animal Health Association. 2004.

[3] Pac HI, Frey K. Some population characteristics of the Northern Yellowstone Bison Herd during the winter of 1988-1989. Montana Department of Fish, Wildlife, and Parks. 1991.

[4] Rhyan JC, Gidlewski T, Roeffe TJ, Aune K, Philo LM, Ewalt DR. Pathology of brucellosis in bison from Yellowstone National Park. J Wildl Dis 2001;37: 101-109

[5] Interagency Bison Management Plan for the State of Montana. Helena, MT, USA: Montana Department of Livestock; 2000. p. 5-8.

[6] Tizard IR. Veterinary immunology, an introduction. Philadelphia, PA, USA: Saunders; 2000. p. 250.

[7] Olsen, SC, Cheville NF, Kunkle RA, Palmer MV, Jensen AE. Bacterial survival, lymph node changes, and immunologic responses of bison (*Bison bison*) vaccinated with *Brucella abortus* strain RB51. J Wild Dis 1997;33:146-51.

[8] Olsen SC, Jensen AE, Palmer MV, Stevens, MG. Vaccination of bison with *Brucella abortus* strain RB51: serology, lymphocyte proliferative resonses, clearance, and biosafety. Am J Vet Res 1998;59:410-15.

[9] Olsen SC, Jensen AE, Stoffregen WC, Palmer MV. Efficacy of calf-hood vaccination with *Brucella abortus* strain RB51 in protecting bison against brucellosis. Res Vet Sci 2003;74:17-22.

[10] Olsen SC, Kreeger TJ, Schultz W. Immune responses of bison to ballistic or hand vaccination with *Brucella abortus* strain RB51. J Wildl Dis 2002;38:738-45.

[11] Christie RJ, Findley DJ, Dunfee M, Hansen R, Olsen SC, Grainger DW. Photopolymerized hydrogel carriers for live ballistic delivery. Vaccine 2006;24:1462-69.

[12] Nonnecke BJ, Waters WR, Foote MR, Palmer MV, Miller BL, Johnson TE, et al. Development of an adult-like cell-mediated immune response in calves after early vaccination with *Mycobacterium bovis* bacillis Calmette-Guerin. J Dairy Sci 2005;88:195-210.

[13] Naimen BM, Alt D, Bolin CA, Zuerner R, Baldwin CA. Protective killed *Leptospira borgpetersenii* vaccine induces potent Th1 immunity comprising responses by CD4 and γδ T lymphocytes. Inect Immun 2001;69:7550-58.

[14] Sahwney AS, Pathack CP, Hubbell JA. Bioerodible hydrogels based on photopolymerized poly(ethylene glycol)-co-poly(α-hydroxy acid) diacrylate monomers. Macromolecules 1993;26(4):581-87.

[15] Olsen SC, Stevens MG, Cheville NF, Schurig GG. Experimental use of a dot-blot assay to measure serologic responses of cattle vaccinated with Brucella abortus strain RB51. J Vet Diagn Invest 1997;9:363-67.

[16] Rajaraman V, Nonnecke BJ, Franklin ST, Hammell DC, Horst RL. Effect of vitamins A and E on nitric oxide production by blood mononuclear leukocytes from neonatal calves fed milk replacer. J Dairy Sci 1998;3278-85.

[17] Brown RA, Blummerman S, Gay C, Bolin C, Duby R, Baldwin CA. Comparison of three different leptospiral vaccines for induction of a type 1 immune response to *Leptospira borgpetersenii* serova Hardjo. Vaccine 2003;21:4448-58.

[18] Golding B, Zaitseva M, Golding H. The potential for recruiting immune resonses toward type 1 or type 2 cell help. Am J Trop Med Hyg 1994;50:33-40.

[19] Zaitseva M, Golding H, Manishewitz J, Webb D, Golding B. *Brucella abortus* as a potential vaccine candidate: induction of interleukin-12 secretion and enhanced B7.1 and B7.2 and intercellular adhesion molecule 1 surface expression in elutriated human monocytes stimulated by heat-inactivated *B. abortus*. Infect Immun 1996;64:3109-17.

[20] Agranovich I, Scott DE, Terle D, Lee K, Golding B. Down-regulation of Th2 responses by *Brucella abortus*, a strong Th2 stimulus correlates with alterations in the B7.2-CD28 pathway. Infect Immun 1999;67:4418-26.

[21] Castaneda J, Espinoza M, Bernal C, Jimenez J, Aguirre L. Simultaneous vaccination of cattle with foot and mouth disease and vesicular stomatitits live viral vaccines. Dev Biol Stand 1976;35:429-36.

[22] Jeggo MH, Wardley RC, Corteyn AH. A reassessment of the dual vaccine against rinderpest and contagious bovine pleuropneumonia. Vet Rec 1987;120:131-5.

[23] Jimenez de Bagues MP, Terraza A, Gross A, Dornard J. Different responses of macrophages to smooth and rough *Brucella* spp.: relationship to virulence. Infect Immun 2004;72:2429-33.

CHAPTER III

LYOPHILIZED POLY(ETHYLENE GLYCOL) HYDROGEL CARRIERS FOR BALLISTIC DELIVERY OF LIVE RB51 BRUCELLA VACCINE

This dissertation chapter contains the manuscript of a full paper to be submitted to Vaccine written by R. James Christie and edited by David W. Grainger. This chapter shows the utility of lyophilized poly(ethylene glycol) hydrogels as carriers of live RB51 vaccine. Ballistic properties of biobullets containing lyophilized hydrogels are compared to wet hydrogel and traditional pellet formulations. Viability of RB51 vaccine after encapsulation before and after lyophilization is shown.

Lyophilized Poly(ethylene glycol) Hydrogels Carriers for Ballistic Delivery of Live RB51 BrucellaVaccine

R.J. Christie, E. J. Kaiser, S.C. Olsen, D.W. Grainger

Abstract

Lyophilized poly(ethylene glycol) (PEG) crosslinked hydrogels were assessed as a payload vehicle to deliver a viable bacterial vaccine *Brucella abortus* strain RB51 (RB51), ballistically using thermoplastic degradable biobullets. Photopolymerized, swollen PEG hydrogel rods loaded with ~ 10^{10} CFU RB51were cut into appropriately sized segments and lyophilized, generating dense, glassy monoliths for insertion into thermoplastic biobullet payload chambers. Lyophilized hydrogels were secured within biobullet payload chambers using a hydroxypropylcelllulose paste or cyanoacrylate-based adhesive, with the latter superior at retaining the monolith within the bullet following ballistic penetration into bovine hindquarter. Biobullets with payload chambers loaded with lyophilized hydrogel pellets exhibit downrange ballistic properties similar to commercially available biobullets. Lyophilized hydrogels rehydrated rapidly by swelling in buffer, serum, and muscle tissue, with complete hydration observed after 5 hours in serum. Live RB51 vaccine exhibits excellent viability following both photopolymerization and lyophilization, at levels sufficient for vaccine dosing to bison.

These results warrant further investigation of lyophilized PEG hydrogel rods as carriers for remote vaccination of wildlife and other targets.

Introduction

The recent outbreak of *Brucella abortus* within Yellowstone National Park has initiated investigations of low-impact mechanisms for vaccination of free-ranging bison within the park and to minimize transfer of the disease to domestic cattle[1-5]. Surveys of the prevalence of the disease indicate that ~74% of bison are sereopositive for brucellosis antibodies[6]. Transfer of this disease from bison to cattle and elk has been observed under experimental conditions, and the possibility for disease spread to local domestic cattle herds has generated substantial concern[7]. Cattle raised in the areas surrounding Yellowstone (Wyoming, Montana, and Idaho) currently retain brucellosis class-free status, and the capability to maintain this status is of substantial economic importance.

Vaccination of cattle against brucellosis is achieved using the commercialized live vaccine, RB51, formulated as a lyophilized powder and administered subcutaneously to calves as a suspension preconstituted in buffer by hand in most applications[8, 9]. Strain RB51 has also been shown to be an effective vaccine in bison, generating host immune response and ultimately prevention of abortion at doses of ~10^{10} CFUs[10-16]. This strain also has the inherent diagnostic advantages of not producing antibodies that interfere with standard serological field tests for brucellosis, limiting false positives observed due to vaccination. This strain has also been shown to be innocuous to non-

target species including: field mice, elk, coyotes, antelope, ravens, ground squirrels, prairie voles bighorn sheep, moose, mule deer, and black bears[17-22].

While the use of RB51 vaccine has been shown effective when administered by hand in controlled experimental situations, administration of the vaccine to wild bison within the Park presents a significant challenge. Ideally, reliable bison vaccination will be achieved in a single dose without capture, handling, or direct contact between humans and animals, and minimal intervention to preserve the free-ranging nature of the population. Vaccination methods shown to be effective for other wildlife-related scenarios such as darts, aerosols, baits, and biobullets, are all currently being considered. The use of biobullets is especially attractive due to the ability to specifically target bison, and minimal environmental impact associated with these degradable vaccine carriers. Commercial biobullet technology utilizes hydroxypropylcellulose (HPC) bullet casings, with the vaccine payload loaded into a hollow chamber within the casing, and fired from an air-rifle charged to ~1200 psi [23]. Previous biobullet use as carriers of live RB51 vaccine to bison utilized dry, lyophilized RB51 vaccine compressed within HPC pellet payloads in biobullets[24]. These studies showed significant vaccine viability loss, with multiple bullets required to attain the target vaccine dose. Additionally, cell-mediated responses to RB51 compressed ballistic vaccinates were reduced compared to parenteral vaccinate controls.

We have recently demonstrated the use of poly(ethylene glycol) (PEG) hydrogels as a live-vaccine carrier when photopolymerized directly into the payload chamber of HPC biobullets[25, 26]. High dosing and dose viability of both live RB51 and a model *P. aeruginosa* were shown. Hydrogels formed from PEG utilize mild processing

conditions, are biologically benign, and have been used to encapsulate a variety of live cells[27-34]. Preliminary serological tests indicate that an immune response is generated against the RB51 vaccine organisms when administered ballistically using PEG hydrogels, but overall efficacy will be determined by reduced abortion rates when vaccinated animals are challenged with *Brucella abortus*. Although preliminary results are promising, the intrinsic high water content of the gels retained after photopolymerization softens the HPC biobullet casing over time in storage, leading to occasional misfires due to gun jamming[25]. Additionally, slow evaporation of water over time results in mass variability and potential ballistic accuracy issues. RB51 biobullets prepared by direct in-bullet photopolymerization are designed for immediate use with several advantages. Nonetheless, a biobullet formulation that could be prepared on a large scale, demonstrate shelf life and reliable formulation properties over time is desirable.

This study investigates the use of lyophilized hydrogel pellet (LHP)-loaded biobullets as a carrier of live RB51 vaccine for ballistic delivery. Exploiting this approach for a ballistic-based wildlife vaccine depends on reliable post-processing viability of the vaccine within the bullet, the ability of the vaccine-carrying gel to survive firing from the remote delivery device, accurate impact/penetration into the tissue of the target animal, and release of live vaccine within the host at dosing sufficient to provide immune response and protection. We report fabrication and rehydration of LHPs, ballistic properties for LHP-loaded biobullets, and post-processing viability of encapsulated RB51 vaccine. These RB51-loaded PEG hydrogels are currently in further

in vivo testing in live bison models to assess the capability of remote brucellosis vaccination to produce requisite protective immune stimuli.

Experimental Methods

Materials

PEG (molecular weight 6000-7500) was obtained from J.T. Baker Chemical Co. (Phillipsburg, NJ) and purified by dissolution in methylene chloride followed by repeated precipitation into diethyl ether and hexane. Methacryloyl chloride (99%) was obtained from Aldrich (St. Louis, MO). Irgacure®184 (1-hydroxy-cyclohexyl-phenyl-ketone) was obtained from Ciba Specialty Chemicals (Tarrytown, NY). Triethylamine, methylene chloride, diethyl ether, hexane, ethanol, and phosphate buffered saline (PBS) were all obtained from Fisher Scientific (Pittsburgh, PA). Difco™ Tryptose agar, LB broth and agar (Miller) were purchased from Becton Dickinson (Sparks, MD). Fluorescent polystyrene microparticles (1-micron diameter, <5% CV) were obtained from Duke Scientific (Palo Alto, CA). Fetal bovine serum was purchased from Hyclone (Logan, UT). Hydroxypropylcellulose Biobullets® (100 μL payload volume), tungsten-doped Hydroxypropylcellulose Biobullets® (100 μL payload volume), and a SolidTech Delivery System air rifle were donated by SolidTech Animal Health, Inc. (Newcastle, OK). Lyophilized *B. abortus* commercial vaccine (RB51) product was donated by Colorado Serum Co. (Denver, CO).

Photopolymerization of PEG Dimethacrylate

Synthesis of PEG dimethacrylate (molecular weight 6750) was achieved using a previously published procedure [34]. Photopolymerization was achieved from 35% w/w PEG macromer solutions prepared by dissolving 350 mg of PEG dimethacrylate in 650 μL PBS buffer. A saturated Irgacure®184 (benzophenone derivative) solution in ethanol was prepared at room temperature (~ 4.0 M) and 6 μL of this solution was added to the PEG solution as a photoinitiator. Photopolymerization was performed in a "home-built" UV reactor with a Hanovia low pressure Hg lamp (Hanovia, 200 W) equipped with a quartz water-cooling jacket (20 mW/cm^2, 90 s).

Lyophilized Hydrogel Pellet Preparation

Lyophilized PEG hydrogel pellets were designed to fit within the payload chamber of thermoplastic degradable hydroxypropylcellulose hollow biobullet (1.6 mm; Solid Tech, OK) with a 100 μL payload volume. Wet PEG hydrogels were photopolymerized in different diameter rod-shaped glass molds, and pellet segments (7.6 mm x 5.5 mm, length x diameter) were cut from the resulting wet gel after removal of the mold. Wet hydrogel pellets were rapidly frozen within plastic vials immersed in liquid nitrogen and then lyophilized to form dry, glassy hydrogel cylindrical pellets. Alternatively, hydrogel glasst rods were fabricated by allowing freshly prepared hydrogels to dry under ambient conditions (22°C, ~40% humidity). Drying characteristics were monitored and used to determine mold dimensions required to reliably produce a hydrogel pellet fitting the dimensions of the biobullet payload chamber.

Lyophilized Hydrogel Pellet Hydration

Lyophilized and wet hydrogel hydration (swelling) rates were determined gravimetrically in phosphate buffer, pH 7.4 (PBS) and in fetal bovine serum (FBS) over time. The effect of encapsulated particles on swelling was determined by encapsulating one-micron particles ($1.8x10^9$ particles/mL, $3.05x10^9$ total particles) into hydrogels, simulating the presence of vaccine organisms.[25]

Biobullet loading

Dried hydrogel rods were manually pressed into the biobullet payload chamber (standard HPC, or tungsten particle-doped HPC Biobullets®) after addition of 1 drop of commercial cyanoacrylate glue, or HPC paste within the payload chamber (made by dissolving 2 biobullets in 1.5 mL distilled water). Any remaining volume within the biobullet payload chamber after pellet insertion was filled with HPC paste (consistent with the type of biobullet loaded) and allowed to dry overnight. HPC paste was re-applied until a tight seal covering the entire back of the bullet was attained. Excess dry HPC material was removed from the back of the biobullet by manual sanding to leave a seamless rear seal.

Ballistic Analysis

For ballistic kinetic energy and range assessments, Biobullets® were fired from a commercial, specially designed air rifle charged to ~ 1200 psi through a chronograph (Shooting Chrony®, Inc.) at various distances in open air. Accuracy measurements were determined with lyophilized hydrogel-loaded Biobullets® fired into paper targets at a

distance of 20 m. LHP loaded biobullets were fired into sandbags at point-blank range, and then recovered to assess the effect of rifle discharge. Ability of hydrogel pellets to remain within the biobullet payload chamber following penetration into a target was monitored by shooting hydrogel-loaded biobullets into partially frozen bovine hindquarter. The bovine hindquarter was allowed to thaw to until factory HPC-loaded biobullets lodged firmly into the hide with the payload chamber still visible and without complete penetration into muscle bed, allowing individual bullet tracking upon target impact. Biobullets were recovered immediately and gel retention was noted.

Preparation of RB51-loaded Lyophilized Hydrogel Rods

RB51 suspensions were prepared by dissolving 6 vials of lyophilized RB51 vaccine (5-17x10^{10} CFU viable bacteria/vial) in 3.64 mL PBS. This suspension was vortexed briefly, followed by addition of 1.56 g PEG dimethacrylate and brief vortexing. Finally, 31 μL of Irgacure 184 solution (saturated in ethanol) was added and the solution vortexed briefly and transferred to a glass mold. Photopolymerization was achieved by mold end-on exposure to quartz-water jacket filtered UV light for 90s, followed by 30s irradiation on each side of the mold. Gels were then extracted from the molds. For lyophilization, segments were placed in plastic vials and frozen by immersing the vials in liquid nitrogen, then lyophilized for 30 hr at 7 μm Hg, 25° C.

Post-hydrogel processing viability of RB51 bacteria

Viability of target vaccine organism *B. abortus* (RB51, biosafety level 2) was conducted after both photopolymerization and gel lyophilization. Commercial lyophilized RB51 was photopolymerized into 30% w/v hydrogel rods, then cut into 7.6 mm x 5.5 mm segments as described above. Viability of RB51 samples was determined for RB51 following photoencapsulation and again after lyophilization. Gels were homogenized in 5 mL PBS and viability of RB51 samples were determined by serial dilution in PBS and inoculation onto tryptose agar plates containing 5% bovine serum. After incubation at 37 °C and 5% CO_2 for 3 days, standard plate counts were conducted. Isolates were confirmed as RB51 by colony morphology, growth characteristics, and resistance to rifampin[16].

Results and Discussion

Photopolymerization of PEG Dimethacrylate

Hydrogels formed rapidly upon exposure of PEG macromer solutions to UV light. Irgacure 184 was chosen as the photoinitiator due to its known cytocompatability with mammalian cell types[34]. Photopolymerization of PEG diacrylates to form rigid 3-dimensional gel matrices in aqueous mileu is well-documented. These types of gels are known to be biologically benign, have been used to encapsulate live mammalian cells and bacteria, and are well-suited for this application[25-27, 29-33, 35].

Lyophilized Hydrogel Rod Preparation

Lyophilization of PEG hydrogels yielded a dense, opaque, rigid glassy material (density =1.14 g/mL +/- 0.03). Pellet fabrication was easily achieved upon photopolymerization of hydrogel rods, followed by cutting appropriately sized gel segments and subsequent lyophilization. Wet hydrogels shrank upon drying, with the degree of shrinking of rod-shaped samples dependent on both length and diameter of the original wet hydrogel (data not shown). For 35% w/v PEG macromer solutions, a wet gel size of 7.6 mm x 5.5 mm (length x diameter) yielded dry gels of 5.9 mm x 4.1 mm (length x diameter), readily inserted into the biobullet payload chamber with mild pressure. Nearly isotropic shrinking was observed, with minor flaring occurring at the ends of some samples. Due to a tendency to crack when placed directly in liquid N_2, samples were placed within plastic vials and frozen with indirect contact to liquid N_2 prior to lyophilization.

Hydration of Lyophilized Hydrogel Rods

Lyophilized PEG hydrogels should optimally rehydrate in biological milieu following placement into a target host to facilitate RB51 vaccine release and proliferation. Rehydration of both as-polymerized and lyophilized hydrogels occurs rapidly as shown in Figure 2 . Rehydration of lyophilized hydrogels occurs at a rate similar to as-polymerized gels, with the rate unaffected by the presence of one-micron diameter polystyrene particles within the matrix (approximating ~30% of bacteria loaded in a full RB51 dose). Additionally, the rehydration rate of lyophilized gels in serum was nearly identical to rates of swelling in buffer (Fig. 2.3.1). Interestingly, while serum is a

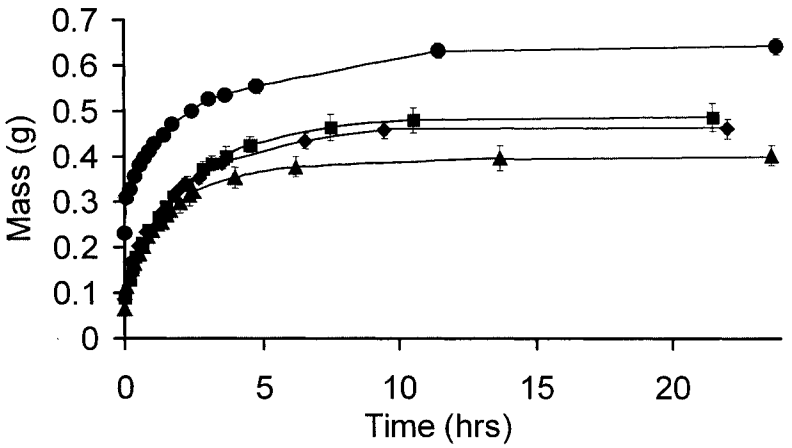

Figure 2.3.1. Rehydration of various PEG hydrogel formulations in buffer or serum. ● wet hydrogel in PBS buffer, ■ lyophilized hydrogel in PBS buffer, ▲ particle-loaded lyophilized hydrogel in PBS buffer, ◆ lyophilized hydrogel in serum. N = 4 for all measurements.

yellow color, gels fully swollen in serum remain transparent and colorless, reflecting the ability of the gel to "sieve" certain proteins. Lyophilized hydrogels never reached the same hydration maximum observed in as-polymerized hydrogels, presumably due to hysteresis from increased chain entanglement after gel shrinking during the lyophilization process.

Rapid rehydration of lyophilized gels in buffer and serum also translated into rapid swelling following insertion into harvested bovine muscle tissue. Figure 2.3.2 shows a partially hydrated lyophilized hydrogel pellet ~ 1hr after insertion into bovine muscle tissue. The peripheral outer portion of the payload pellet is hydrated (clear), while the dry center remains dry (opaque). Lyophilized gels were transparent upon full hydration in tissue, indicative of the sieving effect of these non-degradable hydrogels, presumably a pore size too small to sorb large molecules into the gel matrix as also

observed in serum rehydration [36]. Although PEG hydrogels used in this study were non-degradable, PEG

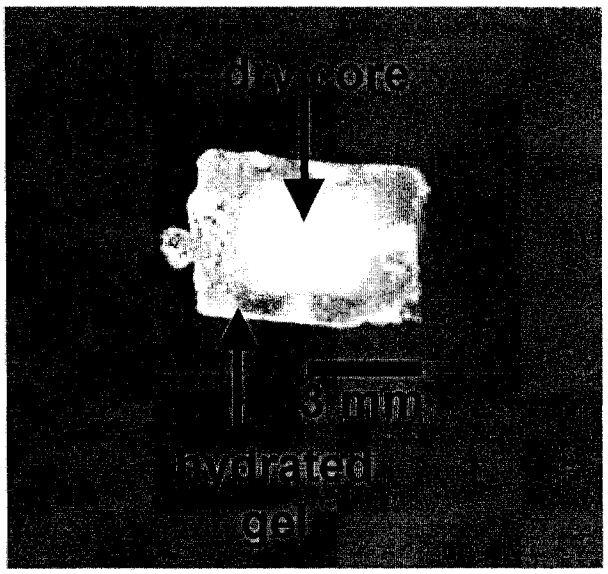

Figure 2.3.2 Partially rehydraded LHP after intramuscular placement into bovine hindquarter tissue for one hour.

macromer endgroup chemistries can be readily modified with degradable lactide or glycolide groups, shown previously to facilitate release of gel particles approximately the same size as RB51 bacteria [25, 35].

Biobullet loading

Biobullets loaded with LHPs were constructed as shown in Figure 2.3.3. Although the empty biobullets contain interior ridges with the payload chamber designed to hold molded HPC compressed pellet payloads within the payload chamber, additional adhesive measures were used to secure payload pellets within the biobullet chamber. Two approaches of drop-wise adhesive addition within the payload chamber were

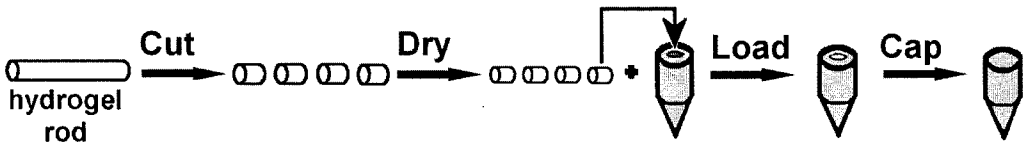

Figure 2.3.3. Fabrication of LHP-loaded biobullets.

utilized; 1) HPC paste, or 2) commercial cyanoacrylate glue prior to insertion of the payload pellet and sealing. Reproducibility of the biobullet fabrication process is shown in Table 2.3.1. Hand-loading of lyophilized pellets into the biobullet payload chamber produces a coefficient of variation of less than ~1%, which should provide reliable ballistics performance down-range.

Table 2.3.1. Characteristics of LHP-loaded biobullets

formulation	average mass (g)	standard deviation	coefficient of variation (%)
HPC hydrogel†	0.6633	0.0067	1.01
HPC compressed†	0.6799	0.0011	0.16
HPC/tungsten hydrogel‡	1.0351	0.0049	0.48
HPC/tungsten compressed‡	1.1734	0.0017	0.14

† n = 16
‡ n = 4

Ballistics performance

Figure 2.3.4 shows the chronograph-determined downrange energies of lyophilized hydrogel-loaded biobullets versus commercial compression HPC pellet-loaded biobullets. Lyophilized hydrogel-loaded biobullets performed similarly to commercial HPC pellet-loaded biobullets in terms of downrange kinetic energy, but accuracy was slightly less consistent than commercial formulations containing molded HPC thermoplastic pellet payloads. For commercial HPC biobullets, kinetic energies were nearly identical for both factory HPC pellet-loaded and lyophilized hydrogel pellet payloads. Substancial variation in kinetic energy was observed at 10m for lyophilized hydrogel pellet loaded bullets, presumably caused by the HPC cap at the back of the bullet cracking and partially disintegrating upon discharge from the air-rifle, causing temporary instability at short range. This effect was less noticeable farther downrange as bullets stabilized in flight.

Biobullets fired into sandbags at short range (< 5m) showed that all hydrogels remained intact (i.e., not ejected) within the payload chamber when either HPC paste or

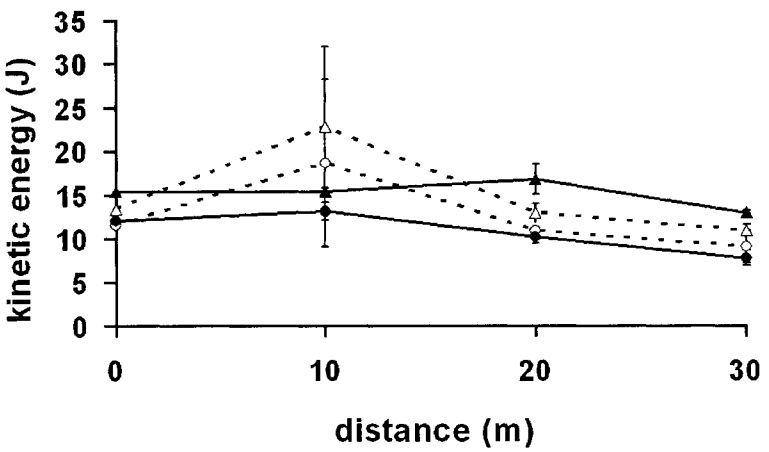

Figure 2.3.4. Downrange kinetic energy of biobullet formulations. ○= lyophilized hydrogel pellet-loaded HPC biobullet ●= HPC pellet loaded HPC biobullet, △= lyophilized hydrogel pellet-loaded tungsten-doped HPC biobullet, ▲= HPC pellet-loaded tungsten-doped biobullet. N = 4 for each data point.

cyanoacrylate glue was used to secure the biobullets within the payload chamber. The HPC cap was either absent, or partially disintegrated in all biobullets recovered from sandbags. LHP-loaded biobullets were also fired into partially frozen bovine hindquarter (through attached hide) to determine if LHPs remained within the biobullet payload chamber upon target impact. LHP-loaded biobullets using HPC paste as the sealant within the payload chamber resulted in a higher number of gels ejected from the payload chamber upon target impact (8/12). Cyanoacrylate glue was far superior at retaining gels within the payload upon target impact (14/14), demonstrating the need to strongly secure the LHPs within the biobullet payload chamber for reliable tissue penetration.

Post-hydrogel processing RB51 bacteria viability

Photoencapsulation of RB51 suspensions within PEG hydrogel matrices was readily achieved following 150 s exposure to UV light. Slightly more time was required to cure RB51-loaded PEG macromer suspensions compared to PEG-buffer only formulations due to the optical density of the cloudy solution. The resulting gels were uniformly dense and rigid, with no noticeable regions of incomplete curing after removal of the glass mold, and sectioning of the resulting hydrogel rod. For gels containing a full dose of 10^{10} CFU RB51, 30% PEG macromer solutions were required to maintain LHP dimensions for reliable, snug insertion into the biobullet payload chamber. Vaccine formulations prepared with 30% w/v PEG macromer were also easier to transfer and manipulate than higher w/w solutions. Figure 2.3.5 shows comparative photos of RB51 encapsulated within 30% w/w hydrogels before and after lyophilization.

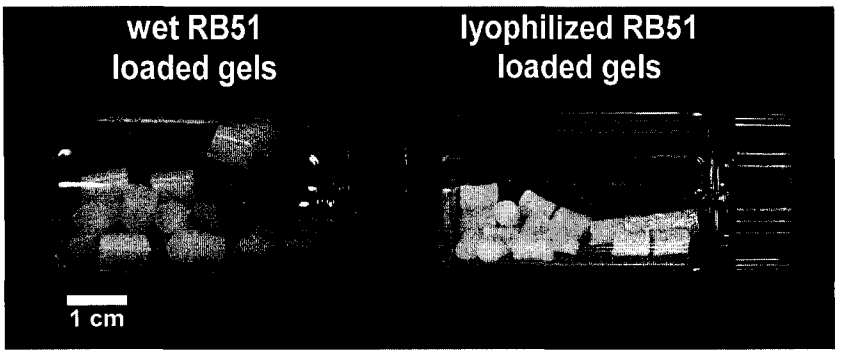

Figure 2.3.5. RB51-loaded PEG hydrogels before and after lyophilization.

Viability of RB51 vaccine was determined after photopolymerization within PEG gel matrices and after subsequent lyophilization. Previous work demonstrated viability for both RB51 and *P. aeruginosa* (strain PAO1) following exposure to various serial photopolymerization procedures, but viability following actual complete gel encapsulation was unknown[24]. Results shown in Figure 2.3.6 support sufficient RB51 viability maintained following photoencapsulation (dosing ~ 10^{10} CFU). Lyophilization

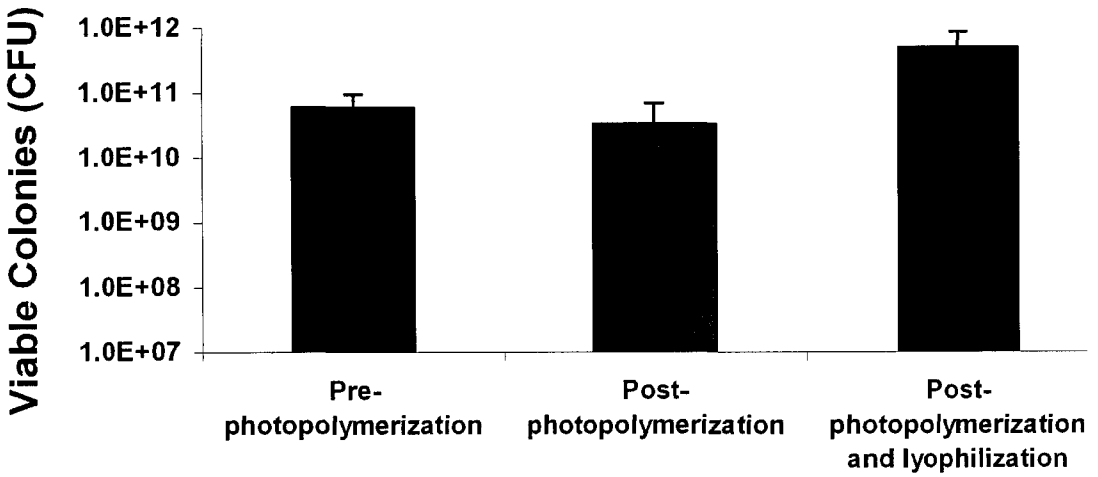

Figure 2.3.6. Post hydrogel-processing viability of RB51 (n=4).

has a minimal affect on RB51 viability, and sufficient viable organisms (> 10^{10} CFU per rod) are maintained for future vaccination. High bacteria viability is likely maintained due to the presence of proprietary cryopreservants found in the lyophilized commercial RB51 product and therefore present in the gel formulation. Although no viability studies were performed on RB51 vaccine organisms within LHPs over time, previous work has shown that this vaccine exhibits excellent viability (less than ~ 10% viability loss) following lyophilization, and reconstitution in aqueous milieu when stored at temperatures lower than 4 °C over a period of 12 weeks[37]. Considering that the hydrogel vaccine formulation is a commercially derived suspension of RB51 containing a variety of stabilizing agents aimed at preserving viability in the commercial product following lyophilization, the hydrogel vaccine should also be expected to exhibit excellent viability when carefully formulated and stored at low temperatures.

Conclusions

This work illustrates the properties and potential applications of lyophilized PEG hydrogels as a carrier for live organisms, and specifically for remote delivery of viable wildlife therapeutics. This lyophilized hydrogel approach yields a robust, glassy vaccine carrier with little residual water, thus eliminating adverse effects on the water-degradable HPC biobullet casing. These lyophilized hydrogel pellets swell rapidly in buffer, serum, and muscle tissue, which should facilitate rapid reconstitution and proliferation of the RB51 vaccine in target animals. LHP-loaded biobullets behave similarly to commercial biobullet ballistics in terms of accuracy and downfield energy, but a strong adhesive is required to prevent LHP payload ejection upon impact with a target animal. Vaccine

viability following photopolymerization and lyophilization procedures ensures that a payload dosing of ~10^{10} CFU is readily achieved. In summary, these LHP-loaded biobullets represent attractive candidate vehicles to accurately deliver viable vaccine to target animals from a distance. On-going field trials are currently assessing cell-based immunity in penned bison cohorts from such ballistic delivery.

Acknowledgements

This research was supported by the National Park Service contract 1200-99-009. The authors thank Rick Wallen, Bison Ecology Lab, Yellowstone National Park, for initiating and supporting this collaborative project, Rick Hansen, SolidTech Animal Health, and Colorado Serum Company for assistance with biobullet components and RB51 donation and discussions, respectively.

References

[1] Plumb G, Aune K. The long term interagency bison management plan for Yellowstone National Park and the state of Montana. In: Kreeger TJ, editor. Brucellosis in Elk and Bison in the Greater Yellowstone Area. Cheyenne, Wyoming Game and Fish Department, 2002: 136-45.
[2] Williams ES, Thorne ET, Anderson SL, Herriges JD. Brucellosis in Free-Ranging Bison (Bison-Bison) from Teton County, Wyoming. Journal of Wildlife Diseases 1993;29(1):118-22.
[3] bison management for the state of Montana and Yellowstone National Park: final environmental impact statement. Washington D.C.: U.S. Department of Interior U.S. Department of Agriculture
2000.
[4] Cheville NF, McCullough DR, Paulson LR, ebrary Inc. Brucellosis in the greater Yellowstone area. In. Washington, D.C., National Academy Press, 1998: xvi, 186 p.
[5] Meyer ME, Meagher M. Brucellosis in free-ranging bison (Bison bison) in Yellowstone, Grand Teton, and Wood Buffalo National Parks: a review. J Wildl Dis 1995;31(4):579-98.
[6] Rhyan JC, Gidlewski T, Roffe TJ, Aune K, Philo LM, Ewalt DR. Pathology of brucellosis in bison from Yellowstone National Park. J Wildl Dis 2001;37(1):101-9.
[7] Davis DS, Templeton JW, Ficht TA, Williams JD, Kopec JD, Adams LG. Brucella abortus in captive bison. I. Serology, bacteriology, pathogenesis, and transmission to cattle. J Wildl Dis 1990;26(3):360-71.
[8] Cheville NF, Jensen AE, Halling SM, Tatum FM, Morfitt DC, Hennager SG, et al. Bacterial survival, lymph node changes, and immunologic responses of cattle vaccinated with standard and mutant strains of Brucella abortus. Am J Vet Res 1992;53(10):1881-8.
[9] Cheville NF. Development, testing and commercialization of a new brucellosis vaccine for cattle. Ann N Y Acad Sci 2000;916:147-53.
[10] Roffe TJ, Olsen SC, Gidlewski T, Jensen AE, Palmer MV, Huber R. Biosafety of parenteral Brucella abortus RB51 vaccine in bison calves. Journal of Wildlife Management 1999;63(3):950-55.
[11] Elzer PH, Edmonds MD, Hagius SD, Walker JV, Gilsdorf MJ, Davis DS. Safety of Brucella abortus strain RB51 in Bison. J Wildl Dis 1998;34(4):825-9.
[12] Davis DS, Elzer PH. Brucella vaccines in wildlife. Vet Microbiol 2002;90(1-4):533-44.
[13] Olsen SC, Cheville NF, Kunkle RA, Palmer MV, Jensen AE. Bacterial survival, lymph node pathology, and serological responses of bison (Bison bison) vaccinated with Brucella abortus strain RB51 or strain 19. J Wildl Dis 1997;33(1):146-51.
[14] Olsen SC, Holland SD. Safety of revaccination of pregnant bison with Brucella abortus strain RB51. Journal of Wildlife Diseases 2003;39(4):824-29.
[15] Olsen SC, Jensen AE, Stoffregen WC, Palmer MV. Efficacy of calfhood vaccination with Brucella abortus strain RB51 in protecting bison against brucellosis. Res Vet Sci 2003;74(1):17-22.

[16] Olsen SC, Jensen AE, Palmer MV, Stevens MG. Evaluation of serologic responses, lymphocyte proliferative responses, and clearance from lymphatic organs after vaccination of bison with Brucella abortus strain RB51. Am J Vet Res 1998;59(4):410-5.
[17] Januszewski MC, Olsen SC, McLean RG, Clark L, Rhyan JC. Experimental infection of nontarget species of rodents and birds with Brucella abortus strain RB51 vaccine. J Wildl Dis 2001;37(3):532-7.
[18] Elzer PH, Smith J, Roffe T, Kreeger T, Edwards J, Davis D. Evaluation of Brucella abortus strain RB51 and strain 19 in pronghorn antelope. Ann N Y Acad Sci 2002;969:102-5.
[19] Kreeger TJ, DeLiberto TJ, Olsen SC, Edwards WH, Cook WE. Safety of Brucella abortus strain RB51 vaccine in non-target ungulates and coyotes. J Wildl Dis 2002;38(3):552-7.
[20] Cook WE, Williams ES, Thorne ET, Kreeger TJ, Stout GW, Schurig G, et al. Safety of Brucella abortus strain RB51 in bull elk. J Wildl Dis 2000;36(3):484-8.
[21] Cook WE, Williams ES, Thorne ET, Taylor SK, Anderson S. Safety of Brucella abortus strain RB51 in deer mice. J Wildl Dis 2001;37(3):621-5.
[22] Olsen SC, Rhyan J, Gidlewski T, Goff J, Stoffregen WC. Safety of Brucella abortus strain RB51 in black bears. J Wildl Dis 2004;40(3):429-33.
[23] Hansen RD, inventor (Ballistic Technologies, Inc., USA). assignee. Medicament dosing ballistic implant of improved accuracy. Application: US
US patent 2000-561224
6375971. 2002 20000428.
[24] Olsen SC, Kreeger TJ, Schultz W. Immune responses of bison to ballistic or hand vaccination with Brucella abortus strain RB51. J Wildl Dis 2002;38(4):738-45.
[25] Christie RJ, Findley DJ, Dunfee M, Hansen RD, Olsen SC, Grainger DW. Photopolymerized hydrogel carriers for live vaccine ballistic delivery. Vaccine 2006;24(9):1462-9.
[26] Olsen SC, Christie RJ, Grainger DW, Stoffregen WS. Immunologic responses of bison to vaccination with Brucella abortus strain RB51: comparison of parenteral to ballistic delivery via compressed pellets or photopolymerized hydrogels. Vaccine 2006;24(9):1346-53.
[27] Hubbell JA, Hill-West JL, Pathak CP, Sawhney AS. PEG-based gels for the release of proteins and the encapsulation of cells. Proc Int Symp Controlled Release Bioact Mater, 20th 1993:137-8.
[28] Working PK, Newman MS, Johnson J, Cornacoff JB. Safety of poly(ethylene glycol) and poly(ethylene glycol) derivatives. Poly(Ethylene Glycol) 1997;680:45-57.
[29] Poshusta AK, Anseth KS. Photopolymerized biomaterials for application in the temporomandibular joint. Cells Tissues Organs 2001;169(3):272-8.
[30] Lyman MD, Melanson D, Sawhney AS. Characterization of the formation of interfacially photopolymerized thin hydrogels in contact with arterial tissue. Biomaterials 1996;17(3):359-64.
[31] Bryant SJ, Anseth KS. The effects of scaffold thickness on tissue engineered cartilage in photocrosslinked poly(ethylene oxide) hydrogels. Biomaterials 2001;22(6):619-26.
[32] Itle LJ, Pishko MV. Cryopreservation of cell-containing poly(ethylene) glycol hydrogel microarrays. Biotechnol Prog 2005;21(3):1004-7.

[33] Liu VA, Bhatia SN. Three-dimensional photopatterning of hydrogels containing living cells. Biomedical Microdevices 2002;4(4):257-66.
[34] Nuttelman CR, Tripodi MC, Anseth KS. In vitro osteogenic differentiation of human mesenchymal stem cells photoencapsulated in PEG hydrogels. J Biomed Mater Res A 2004;68(4):773-82.
[35] Sawhney AS, Pathak CP, Hubbell JA. Bioerodible Hydrogels Based on Photopolymerized Poly(Ethylene Glycol)-Co-Poly(Alpha-Hydroxy Acid) Diacrylate Macromers. Macromolecules 1993;26(4):581-87.
[36] Canal T, Peppas NA. Correlation between mesh size and equilibrium degree of swelling of polymeric networks. J Biomed Mater Res 1989;23(10):1183-93.
[37] Capsel RL, Olsen SC, Cheville NF, Thoen CO. Survival of Brucella abortus strain RB51 lyophilized and as liquid vaccine under different storage conditions. Biologicals 2000;28(4):209-15.

CHAPTER IV

SUMMARY AND PROPOSED FUTURE WORK

The ability to produce a degradable Biobullet® delivery vehicle that utilizes mild vaccine processing conditions is a current barrier for remote delivery of viable wildlife vaccines. This work illustrates the potential application of photopolymerized PEG hydrogels as a carrier for remote delivery of viable wildlife therapeutics. The resulting projectile has similar ballistic and tissue penetration characteristics to commercial bullets used for livestock vaccination, with the added utility of live vaccine encapsulation and subsequent reliable release. The expected viability loss in commercial RB51 upon encapsulation can easily be compensated by slight vaccine overdosing to achieve the desired $\sim 10^{10}$ CFU viable bacteria target needed for effective bison field vaccination in Yellowstone Park. *In vivo* testing in penned bison while preliminary in a limited cohort of 32 animals, supports efficacy of the biobullet-delivered vaccine formulation equivalent to or better than hand vaccinated or lyophilized powder controls. Biomarkers including host antibody response, interferon gamma production and T-cell proliferative response

all support the ability of the encapsulated vaccine to stimulate host immune response effectively in field use in wild animals. In summary, these hydrogel-loaded Biobullets® represent attractive candidate vehicles to accurately deliver viable vaccine to target animals from a distance with completely degradability. On-going field trials are currently assessing cell-based immunity in penned bison cohorts. The collective results in this report represent a substantial increase in progress and productivity relative to the initial project outline and task agreement.

Improvements upon the wet hydrogel-loaded Biobullet® delivery approach were achieved after lyophilization of hydrogels to form pellets for insertion into the payload chamber. Preliminary results indicate that excellent vaccine viability is maintained after photopolymerization and lyophilization. The resulting dry pellets do not soften the biobullet casing as was observed with wet hydrogels, which causes jamming of the bullets in the barrel of the air-rifle delivery system. Lyophilized hydrogel payloads do not dry out when stored in open air, resulting in constant mass, necessary for reliable downrange energy and accuracy. Lyophilized hydrogel-loaded biobullets may provide a superior method for commercial scale-up due to increased biobullet stability.

Major accomplishments of this dissertation research

1. A novel approach to encapsulate and deliver live RB51 vaccine within poly(ethylene glycol) hydrogels and Biobullets® was developed.
2. Ballisic properties of hydrogel-loaded Biobullets® were found to be similar to the commercial compression molded pellet formulation. Hydrogel-loaded Biobullets®

maintain downrange energy and accuracy is maintained for both wet and lyophilized forms.

3. The photopolymerization proceedure used for hydrogel formation results in excellent RB51 vaccine viability. Viability is also maintained after lyophilization of RB51-encapsulted hydrogels.
4. Degradable endgroup chemistries were incorporated into PEG macromers used to form hydrogels, and release profiles of 1 μm particles from hydrogels show that RB51 organisms are released.
5. A bison immune response to hydrogel-encapsulated RB51 following ballistic Biobullet® delivery is observed, and persists for 24 weeks.
6. Degradable hydrogels are not required to generate an immune response to RB51 delivered within hydrogel-loaded biobullets.
7. A method to formulate lyophilized hydrogel vaccine carriers was developed, resulting in increased Biobullet® stability.

Proposed Future Work

1. RB51 Viability Assessments

Wet RB51-loaded hydrogels generate the desired immune response when delivered to live bison using Biobullets®. However, these wet-hydrogel Biobullets® dry out over time and soften the Biobullet® casing leading to unknown down-range energies, and gun jamming. One possible approach to overcome this problem is to store wet hydrogel-loaded Biobullets® frozen until needed. Determination of hydrogel-

encapsulated RB51 vaccine viability in frozen gels over time would show the validity of this approach.

Additional viability assessment of RB51 vaccine contained within lyophilized hydrogels is needed, as the current viability data set is small. Shelf-life studies of RB51 encapsulated within lyophilized hydrogels at different temperatures (room temperature (~22 °C), refridgerated (4 °C), and frozen (-20 °C) will identify the optimal storage conditions needed to maintain vaccine viability (i.e. efficacy) and the time-frame in which Biobullets® should be used after preparation.

2. Improvement of Lyophilized Hydrogel-Loaded Biobullets®

Lyophilized hydrogels have the inherent advantage of mass stability after complete removal of water from the gels. However, lyophilized gels have a tendency to be ejected from the Biobullet® payload chamber upon target impact. Initial attempts to glue lyophilized gels into the payload chamber using hydroxypropylcellulose paste did not solve this problem. Cyanoacrylate (superglue) adhesive decreased the occurrence of ejection, but 100% gel retention within Biobullets® after target impact was not achieved. Methods to retain the lyophilized gel within the payload chamber must be developed. One possible approach involved threading both the lyophilized gels and Biobullet® payload chamber allowing gels to be screwed into the payload chamber. This could decrease occurrence of ejection and result in a reliable Biobullet® delivery system.

Fabrication of threaded gels and biobullets could easily be performed using a commercially available tap-and-die tool. Gel retention within biobullet payload

chambers following firing into beef hindquarter (with skin attached) will allow easy assessment of gel retention.

3. Develop new two-stage vaccine releasing formulation: immediate bolus and delayed booster (t=0 + t=3 months?) within the new SolidTech enlarged payload degradable bullet containing tungsten ballast. This new bullet with a range of 60m has never been tested. This booster formulation could use a payload composite with RB51 encapsulated within degradable polymer microspheres and then embedded into the PEG hydrogel also containing fast-releasing live RB51 not residing in microspheres.

APPENDIX A

CALCULATIONS FOR SYNTHESIS OF HPMA COPOLYMER USING MATHCAD™

HPMA Copolymer Synthesis
95/5 (mole % HPMA/MAGGONP)

ORIGIN = 1

scale := 30 scale = total mass of system

acetone := .869·scale

monomer := .125·scale <--- total monomer content is 12.5 wt %

x := .01

f(x) := (143.18·.95·x) + 321.29·.05·x <----- equation to find monomer amount
143.18 = HPMA, 321.29 = MAGGONP

Given

f(x) = monomer <----- mathcad solve block to find x

monomer := Find(x)

monomer = 0.025

HPMA := monomer·143.18·.95

MAGGOnP := monomer·321.29·.05

AIBN := scale·.006

$$acetone\_volume := \frac{acetone}{.790}$$

Amounts of reagents to use:

acetone_volume = 33 mL

HPMA = 3.354 g

MAGGOnP = 0.396 g

AIBN = 0.18 g

mathcheck := acetone + HPMA + MAGGOnP + AIBN

mathcheck = 30

APPENDIX B

CALCULATION OF HPMA COPOLYMER ACTIVE ESTER CONTENT USING MATHCAD™

HPMA Copolymer Composition Analysis

Based on .008-.012g polymer dissolved in 100mL .05M NaOH

ORIGIN ≡ 1 $\quad i := 1..4$ absorbance measured @ 400 nm

$$mass := \begin{pmatrix} .01041 \\ .01056 \\ .01572 \\ .01220 \end{pmatrix} \quad abs := \begin{pmatrix} .878 \\ .890 \\ 1.27 \\ 1.01 \end{pmatrix} \quad molarity_i := \frac{abs_i}{1.74 \cdot 10^4} \quad molOnp_i := molarity_i \cdot .1$$

$$molarity = \begin{pmatrix} 5.046 \times 10^{-5} \\ 5.115 \times 10^{-5} \\ 7.299 \times 10^{-5} \\ 5.805 \times 10^{-5} \end{pmatrix} \quad molOnp = \begin{pmatrix} 5.046 \times 10^{-6} \\ 5.115 \times 10^{-6} \\ 7.299 \times 10^{-6} \\ 5.805 \times 10^{-6} \end{pmatrix}$$

$massOnp_i := molOnp_i \cdot 321.26$ $\quad massHPMA_i := mass_i - massOnp_i$

$$massOnp = \begin{pmatrix} 1.621 \times 10^{-3} \\ 1.643 \times 10^{-3} \\ 2.345 \times 10^{-3} \\ 1.865 \times 10^{-3} \end{pmatrix} \quad massHPMA = \begin{pmatrix} 8.789 \times 10^{-3} \\ 8.917 \times 10^{-3} \\ 0.013 \\ 0.01 \end{pmatrix}$$

$$molHPMA_i := \frac{massHPMA_i}{143.22} \quad molHPMA = \begin{pmatrix} 6.137 \times 10^{-5} \\ 6.226 \times 10^{-5} \\ 9.339 \times 10^{-5} \\ 7.216 \times 10^{-5} \end{pmatrix}$$

$$mol\%Onp_i := \frac{molOnp_i}{molOnp_i + molHPMA_i} \cdot 100$$

$mean(mol\%Onp) = 7.471$

$stdev(mol\%Onp) = 0.142$

$$mol\%Onp = \begin{pmatrix} 7.598 \\ 7.592 \\ 7.249 \\ 7.445 \end{pmatrix}$$

$$molpergram_i := \frac{molOnp_i}{mass_i}$$

$mean(molpergram) = 4.773 \times 10^{-4}$

$stdev(molpergram) = 8.311 \times 10^{-6}$

$$molpergram = \begin{pmatrix} 4.847 \times 10^{-4} \\ 4.844 \times 10^{-4} \\ 4.643 \times 10^{-4} \\ 4.758 \times 10^{-4} \end{pmatrix}$$

APPENDIX C

CALCULATION OF HYDRAZIDE CONTENT IN HPMA COPOLYMERS USING MATHCAD™

TNBSA Assay for Hydrazide Content

origin ≡ 1 i := 1.. 14

$$x := \begin{pmatrix} 1.225 \\ 1.184 \\ 1.019 \\ 1.089 \\ 1.073 \\ .971 \\ .913 \\ .893 \\ .780 \\ .530 \\ .528 \\ .369 \\ .224 \end{pmatrix} \qquad y := \begin{pmatrix} 1.35\cdot10^{-4} \\ 1.315\cdot10^{-4} \\ 1.246\cdot10^{-4} \\ 1.18\cdot10^{-4} \\ 1.108\cdot10^{-4} \\ 1.039\cdot10^{-4} \\ .969\cdot10^{-4} \\ .9\cdot10^{-4} \\ .831\cdot10^{-4} \\ .761\cdot10^{-4} \\ .485\cdot10^{-4} \\ .346\cdot10^{-4} \\ .208\cdot10^{-4} \end{pmatrix}$$

standard curve using MAGGH standards

z := 0, .01.. 1.3

m := slope(x, y) m = 1.118×10^{-4}

b := intercept(x, y) b = -2.587×10^{-6}

bestfit(z) := m·z + b

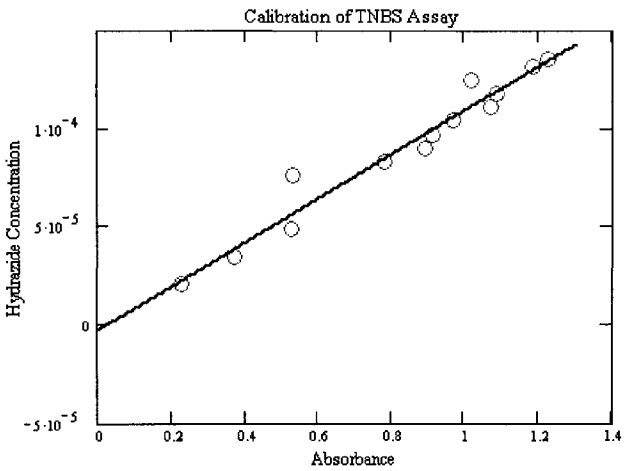

Analysis of HPMA Copolymer Samples

ORIGIN ≡ 1 **poly(HPMA)-hydrazide from 8/8/05**

$j := 1..4$

$$mass := \begin{pmatrix} .00327 \\ .00435 \\ .00396 \\ .00492 \end{pmatrix} \qquad abs := \begin{pmatrix} .498 \\ .680 \\ .609 \\ .728 \end{pmatrix}$$

$conc_j := m \cdot abs_j + b$

$$conc = \begin{pmatrix} 5.31 \times 10^{-5} \\ 7.345 \times 10^{-5} \\ 6.551 \times 10^{-5} \\ 7.882 \times 10^{-5} \end{pmatrix}$$

$concB4dilution_j := conc_j \cdot 1.5$

$volume := .015$

$molesNHNH2_j := concB4dilution_j \cdot volume$

$$molesNHNH2 = \begin{pmatrix} 1.195 \times 10^{-6} \\ 1.653 \times 10^{-6} \\ 1.474 \times 10^{-6} \\ 1.773 \times 10^{-6} \end{pmatrix}$$

$$molespergram_j := \frac{molesNHNH2_j}{mass_j}$$

$$molespergram = \begin{pmatrix} 3.654 \times 10^{-4} \\ 3.799 \times 10^{-4} \\ 3.722 \times 10^{-4} \\ 3.604 \times 10^{-4} \end{pmatrix}$$

$mean(molespergram) = 3.695 \times 10^{-4}$

$stdev(molespergram) = 7.331 \times 10^{-6}$

$massNHNH2_j := molesNHNH2_j \cdot 214.11$ $\qquad massHPMA_j := mass_j - massNHNH2_j$

$$massNHNH2 = \begin{pmatrix} 2.558 \times 10^{-4} \\ 3.538 \times 10^{-4} \\ 3.156 \times 10^{-4} \\ 3.797 \times 10^{-4} \end{pmatrix} \qquad massHPMA = \begin{pmatrix} 3.014 \times 10^{-3} \\ 3.996 \times 10^{-3} \\ 3.644 \times 10^{-3} \\ 4.54 \times 10^{-3} \end{pmatrix}$$

$$molHPMA_j := \frac{massHPMA_j}{143.18}$$

$$mol\%NHNH2_j := \frac{molesNHNH2_j}{molesNHNH2_j + molHPMA_j} \cdot 100$$

$$mol\%NHNH2 = \begin{pmatrix} 5.37 \\ 5.59 \\ 5.474 \\ 5.296 \end{pmatrix}$$

$mean(mol\%NHNH2) = 5.433$ $\qquad \frac{5.433}{4.552} = 1.194$

$stdev(mol\%NHNH2) = 0.111$

APPENDIX D

REACTION MECHANISMS

D.1 Hydrazone Hydrolysis

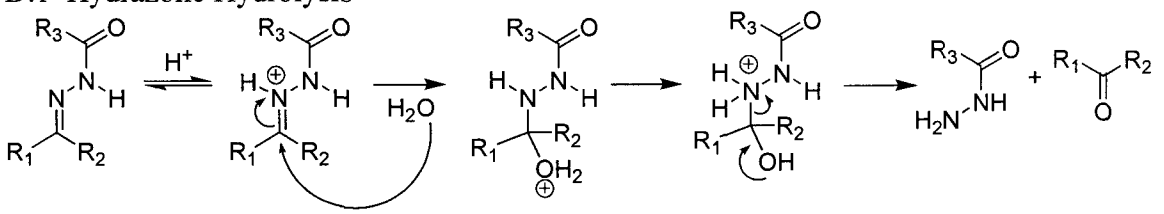

D.2 Dicyclohexylcarbodiimide-Mediated Ester Formation

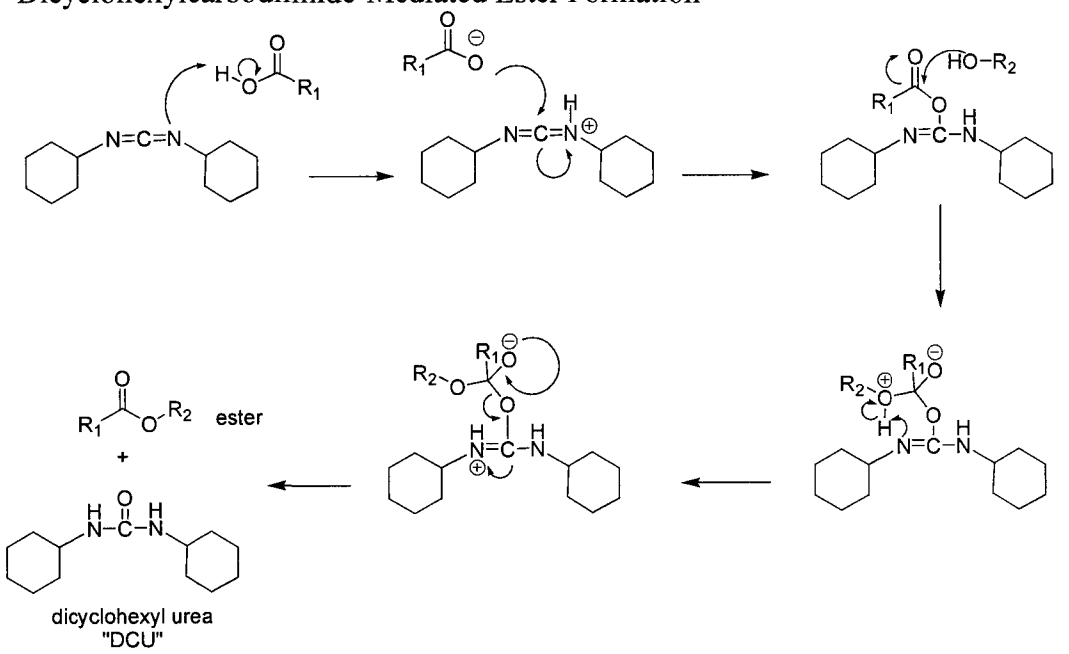

D.3 Swern Oxidation of Alcohols

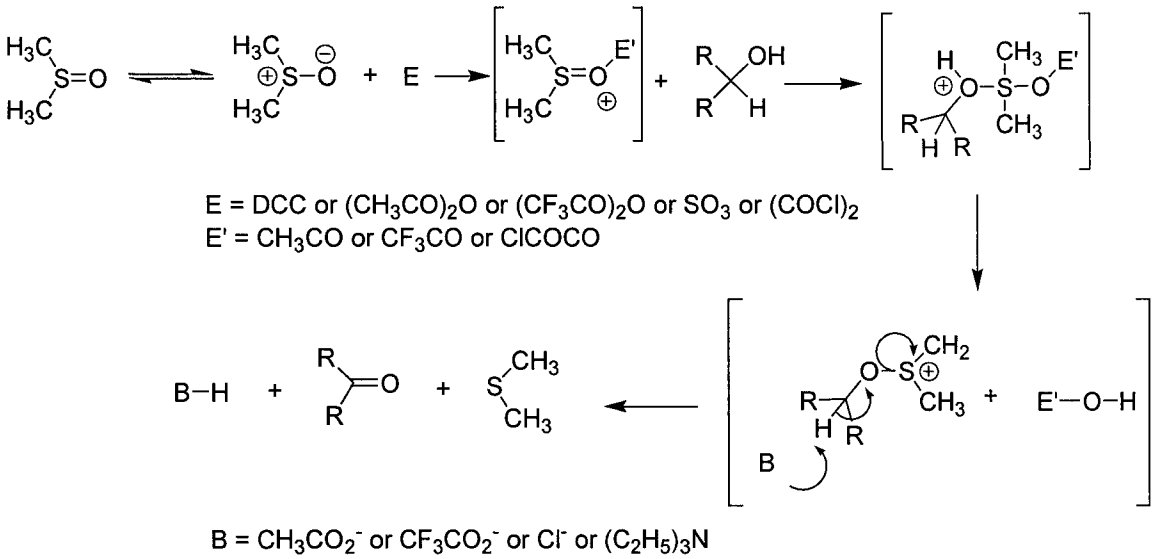

D.4 Tin Catalyzed Ring Opening Polymerization of Lactide

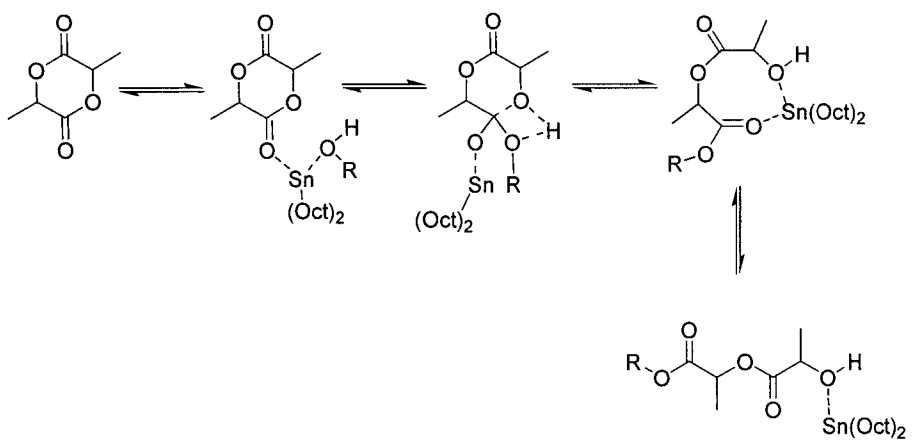

APPENDIX E

IRGACURE 184™

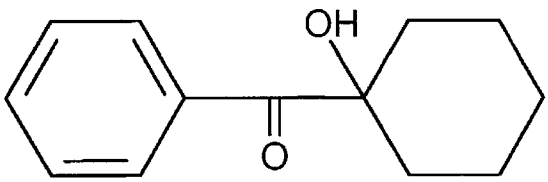

1-Hydroxy-cyclohexyl-phenyl-ketone
Molecular weight: 204.3 CAS No. 947-19-3

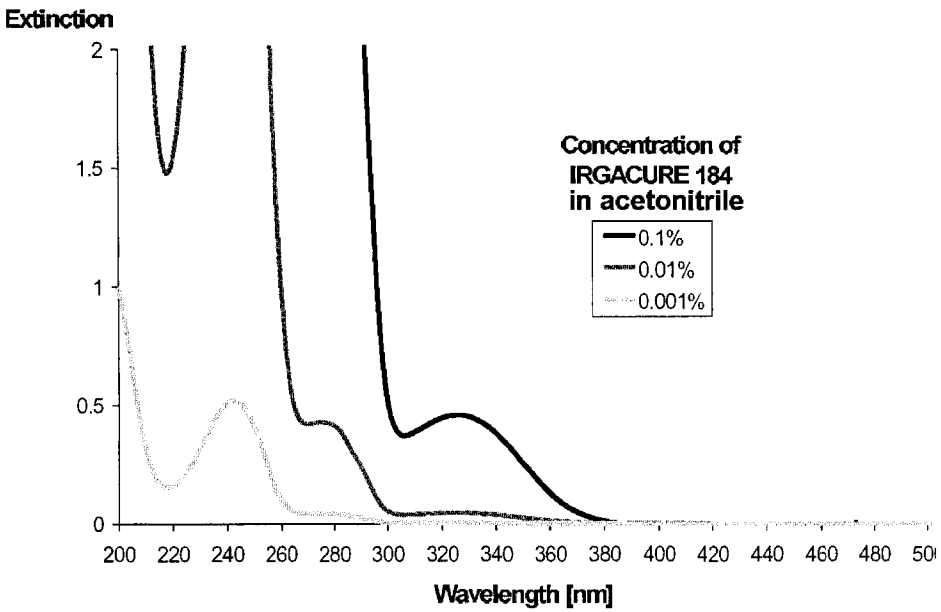

Source: CibaVision Specialty Chemicals

APPENDIX F

DETAILED ^{1}H NMR SPECTRUM OF 4-MALEIMIDOMETHYL CYLCLOHEXANE CARBOXILIC ACID: LOCKED RING CONFORMATION

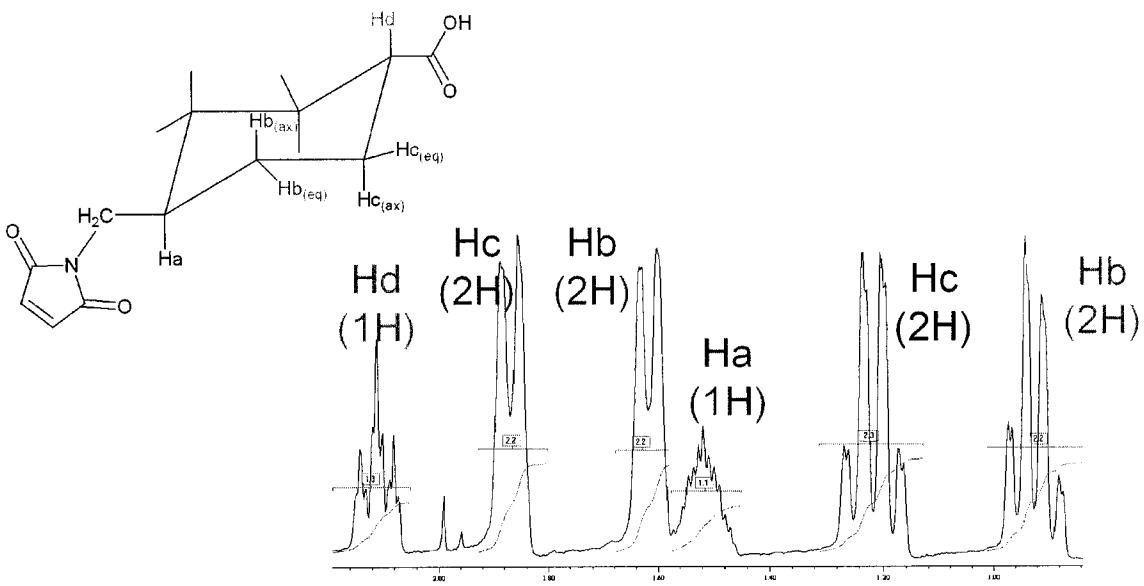

APPENDIX G

MICROSPHERE RELEASE FROM PEG HYDROGEL ASSAY